

**University of Southampton**

*“Investigation of the vortex phase diagram  
and dynamics in single crystalline samples  
of the high temperature superconductor  
 $YBa_2Cu_3O_{7-\delta}$ ”*

**by**

**STYLIANOS KOKKALIARIS**

*Thesis submitted for examination for the degree of  
Doctor of Philosophy*

**Department of Physics**

**January 2000**

UNIVERSITY OF SOUTHAMPTON

ABSTRACT

FACULTY OF SCIENCE

PHYSICS

Doctor of Philosophy

**INVESTIGATION OF THE VORTEX PHASE DIAGRAM AND  
DYNAMICS IN SINGLE CRYSTALLINE SAMPLES OF THE HIGH  
TEMPERATURE SUPERCONDUCTOR  $\text{YBa}_2\text{Cu}_3\text{O}_{7-\delta}$**

by Stylianos Kokkaliaris

The present thesis contains an extended experimental investigation of the hysteretic behaviour of the vortex system in pure  $\text{YBa}_2\text{Cu}_3\text{O}_{7-\delta}$  single crystals.

A method based on partial magnetization loops is used to study memory effects in pure  $\text{YBa}_2\text{Cu}_3\text{O}_{7-\delta}$  single crystals with various types and densities of pinning sites. For detwinned samples with low densities of point defects, our measurements reveal the transition from a dislocation-free Bragg glass to a disordered vortex phase. This boundary is mapped for the first time in the  $B - T$  phase diagram and is located in proximity to the onset of the second magnetization peak. The transition line is further found to be in accordance with theoretical predictions. For fields above this line, metastable topological disorder invades the vortex system leading to a pronounced dependence of the critical current on the formation history of the vortex lattice. The effect of decreasing oxygen stoichiometry is the shift of this boundary to lower fields, and its disappearance for high values of the oxygen deficiency in agreement with theory. We also study the influence of extended defects and find that a low density of twin boundaries does not affect the Bragg glass significantly. However, a high concentration of twins as well as even low densities of columnar defects suppress the transition and eliminate the memory effects.

Studies of the second magnetization peak in pure  $\text{YBa}_2\text{Cu}_3\text{O}_{7-\delta}$  reveal several new features, such as a non-monotonous temperature dependence of the peak position and the presence of a rather sharp peak near the melting line. These observations contradict conventional interpretations and support more realistic scenarios for the origin of this phenomenon. The effect of oxygen ordering on the magnetization peak is also investigated. Although for temperatures below 70 K the peak does not depend on the distribution of oxygen vacancies, above 70 K ordering effects become essential leading to the suppression of the peak for a more homogeneous distribution of oxygen defects. These results indicate that while at low temperatures pinning by individual oxygen vacancies is important, at elevated temperatures clusters mainly dominate the hysteresis.

Pinning of vortices for fields along the superconducting planes is also investigated. We show that the magnetization exhibits an oscillatory behaviour that can be fully accounted by considering the commensurability of the vortex lattice with the layered structure. The effect of varying point disorder is also studied. We demonstrate that the interplay between pinning and thermal fluctuations leads to a remarkable non-monotonous temperature dependence of the current at intermediate temperatures. Finally, from the oscillations we extract the anisotropy of this compound and study its dependence on the oxygen content.

# Contents

<b>Acknowledgments</b> .....	v
------------------------------	---

## Chapter 1

### *Introduction*

1.1 Superconductivity .....	1
1.2 Thesis outline .....	6
References .....	10

## Chapter 2

### *Vortices in type-II superconductors*

2.1 Elastic properties of the vortex lattice .....	11
2.2 Pinning of the vortex lattice .....	16
2.2.1 The critical state model .....	17
2.2.2 Collective pinning theory .....	19
2.2.3 Flux creep .....	22
2.2.4 Theory of collective flux creep .....	26
References .....	29

## Chapter 3

### *The high temperature superconductor $YBa_2Cu_3O_{7-\delta}$*

3.1 Structural properties .....	31
3.2 Effect of variations in the oxygen stoichiometry on the physical parameters of $YBa_2Cu_3O_{7-\delta}$ .....	37
3.3 Single crystals .....	41

3.3.1 Single crystal growth.....	42
3.3.2 Twin boundaries.....	43
3.3.3 Investigated samples.....	46
References.....	49

## Chapter 4

### *Experimental Techniques*

4.1 Vibrating sample magnetometer.....	53
4.1.1 Physical principles.....	53
4.1.2 Technical details.....	57
4.2 Torque magnetometer.....	61
4.2.1 Physical principles.....	61
4.2.2 Technical details.....	63
References.....	67

## Chapter 5

### *The vortex phase diagram of $YBa_2Cu_3O_{7-\delta}$*

5.1 Flux line lattice melting in high- $T_c$ superconductors.....	68
5.1.1 Theoretical approach.....	69
5.1.2 The melting transition.....	73
5.1.3 The vortex liquid phase.....	77
5.2 The vortex glass phase.....	79
5.3 The Bose glass phase.....	81
5.4 The Bragg glass phase.....	82
5.5 Evidence for a transition from elastic to plastic vortex phases in $YBa_2Cu_3O_{7-\delta}$ single crystals.....	85
5.5.1 Introduction.....	85
5.5.2 Experimental details.....	87
5.5.3 Results.....	89
5.5.4 Discussion.....	99

5.5.5 Summary.....	109
References .....	110

## Chapter 6

### *The peak effect in pure $YBa_2Cu_3O_{7-\delta}$ single crystals*

6.1 Introduction .....	117
6.2 Studies of the second magnetization peak in pure $YBa_2Cu_3O_{7-\delta}$ single crystals.....	120
6.2.1 Experimental details .....	122
6.2.2 Results and discussion.....	124
6.2.2.1 The second magnetization peak in pure $YBa_2Cu_3O_{7-\delta}$ single crystals.....	124
6.2.2.2 Peak effect and oxygen ordering in pure $YBa_2Cu_3O_{7-\delta}$ single crystals.....	134
6.2.3 Conclusions .....	143
References .....	144

## Chapter 7

### *Commensurability effects induced by the layered structure of $YBa_2Cu_3O_{7-\delta}$*

7.1 Vortices in layered superconductors.....	149
7.1.1 Theoretical approach .....	149
7.1.2 Josephson vortices.....	152
7.1.3 The lock-in transition .....	153
7.2 Signature of Josephson vortices in pure $YBa_2Cu_3O_{7-\delta}$ single crystals.....	158
7.2.1 Introduction .....	158
7.2.2 Experimental details .....	161
7.2.3 Results and Discussion.....	162
7.2.4 Summary.....	181

References .....	183
------------------	-----

## Chapter 8

### *Summary*

8.1	The vortex phase diagram of $\text{YBa}_2\text{Cu}_3\text{O}_{7-\delta}$ .....	187
8.2	The peak effect in pure $\text{YBa}_2\text{Cu}_3\text{O}_{7-\delta}$ single crystals .....	189
8.3	Commensurability effects induced by the layered structure of $\text{YBa}_2\text{Cu}_3\text{O}_{7-\delta}$ .....	190

# Acknowledgments

I would like to thank my supervisor *Peter de Groot* for giving me the chance to commence this study and for his assistance during the last three years towards completing it successfully. I am also grateful to the Research Fellows of our group, *Sergey Gordeev* and *Alexander Zhukov* for being always willing to answer any question and their critical, but positive stance to my ideas. The former is also acknowledged for teaching me the difference between having good results and having a paper. Many thanks should also go to *Luc Früchter*, *Darko Bracanovic* and *Maciej Sawicki* for helping me comprehend several experimental issues and fruitful collaboration. In addition, I would like to thank *Konstantinos Deligiannis* and *Steven Pinfeld* for their substantial support during my first year as well as their friendship.

My gratitude also goes to the pedagogues *Xenofon Aslanoglou*, *Theofilos* and *Georgios Filactos*, *Euaggelos Manesis*, *Alkiviadis Papastergiadis*, *Xristos Patias*, and *Maria Riga*. Their personal qualities and devotion to the undersupported task of teaching, helped and motivated me significantly at the early stages of my involvement in education. *Argirios Pantzios* is acknowledged for unconsciously turning on the spark of science in me. I would also like to thank the hundreds of people I met during my long employment in the Greek fruit markets. They have been the best University I have ever been to.

It would also be unfair to omit mentioning the contribution of people that all this time have decorated my life with the best of their feelings. My gratitude goes to *Kostas Manolas*, *Giorgos Karapostolis*, *Meghan Agresto*, and *Euthimios Karbelis* for being my friends. I am lucky to have been offered the exceptional fragrance and freshness of the undutchably sweet girl *Marije Smit* and *Daria Crippa*. I am grateful to *Daria* for her love and support during this period. I also thank *Adrián*, *Alexandra*, *Alistair*, *Azhar*, *Beda*, *Chris*, *Christos*, *Eva*, *George*, *Gilberto*, *Han*, *Jose*, *Lalita*, *Maan*, *Mary*, *Mphaka*, *Mustafa*, *Nacho*, *Öke*, *Panikos*, *Salem*, and *Steve* for the nice time we had together.

Finally, I would like to thank from the bottom of my heart those people that have always tried and given their best to me, so as to become a useful member of this society. These are my father *Dimitrios*, mother *Theano*, sister *Anna*, brother *Georgios* and my grandmother *Sultana*.

---

# Chapter 1

---

## Introduction

### 1.1 Superconductivity

The discovery of superconductivity by Heike Kamerlingh Onnes,<sup>1</sup> opened a new chapter in the field of condensed matter physics in general, which has still not been fully explored. Traditionally, there are two hallmarks characterizing the superconducting state that sets in below a critical temperature  $T_c$ . The first one is the vanishing electric resistivity of the material, i.e., perfect electric conductivity. The second feature is the complete expulsion of magnetic flux from the bulk of the specimen (i.e., perfect diamagnetism), irrespective of whether the magnetic field was applied after or before cooling the superconductor below  $T_c$ .<sup>2</sup> More precisely, the magnetic field is exponentially screened from the bulk of the superconductor with penetration depth  $\lambda$  that is typically of the order of only  $10^{-7}$  m.

The presence of perfect diamagnetism, that is also known as the Meissner – Ochsenfeld effect, cannot be explained by perfect conductivity alone,<sup>3</sup> and demonstrates that superconductivity is a true thermodynamic state. In addition, considering that holding the field out of the sample increases the energy of the superconducting state, this effect also implies that superconductivity will be destroyed when the applied magnetic field exceeds a finite critical value  $B_c$ .<sup>4,5</sup> This field can be estimated by equating the Gibbs free energies of the two phases at a certain temperature and is related to the superconducting condensation energy, i.e., the free energy difference between the normal and superconducting states in zero applied field (assuming that the normal state is non-magnetic).<sup>6-8</sup> It has been found experimentally that this thermodynamic critical field  $B_c(T)$  can be approximately given by a parabolic law,  $B_c(T) \approx B_c(0)[1-(T/T_c)^2]$ , as shown in Fig. 1.1 (a). For such a superconductor, the dependence of the magnetic flux,  $B$ , on the applied

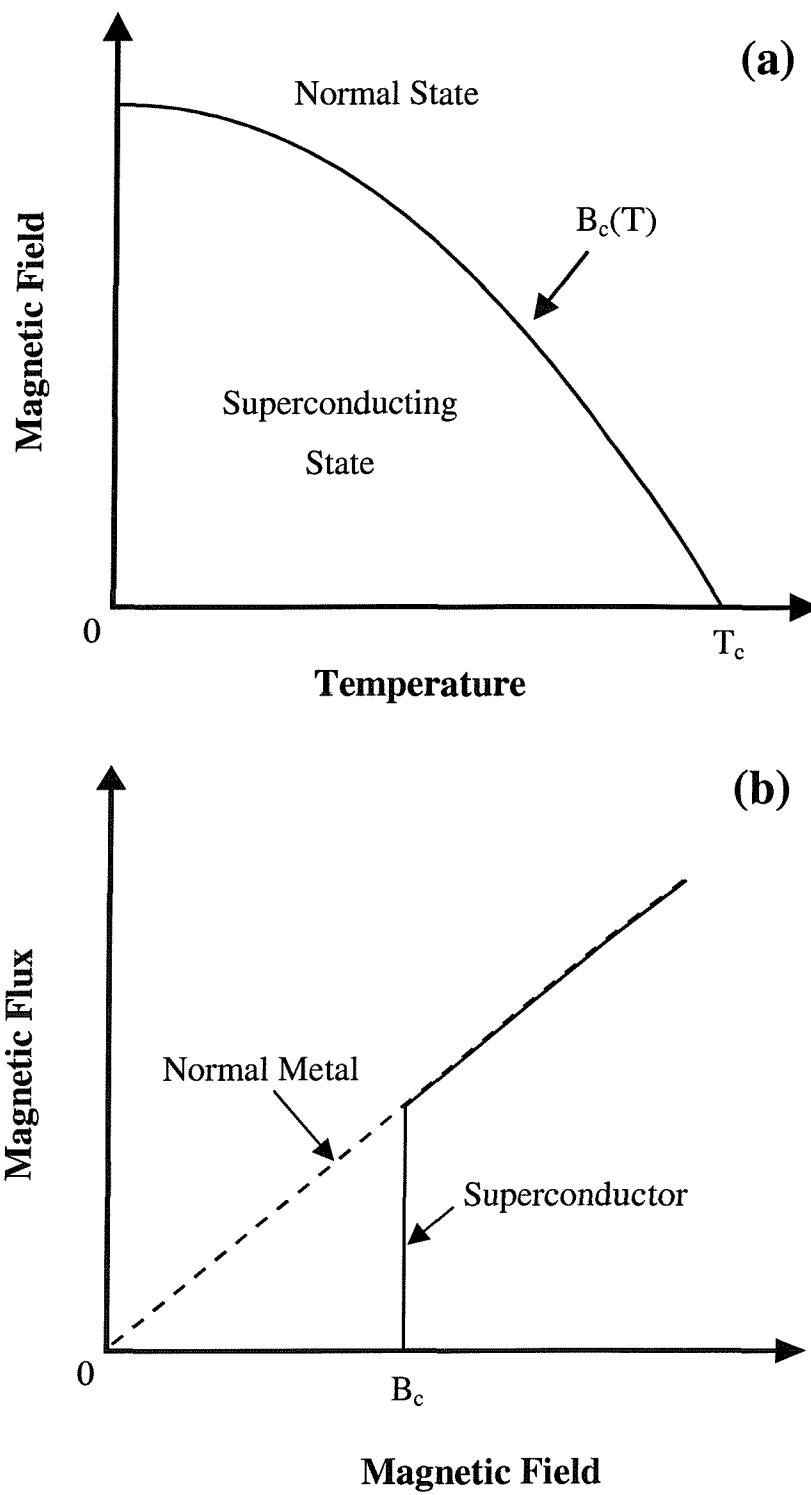


Fig. 1.1. (a) Traditional phase diagram of a (type-I) superconductor, illustrating the variation of the critical field  $B_c$  with temperature. (b) Magnetic response of the same superconductor. For comparison the behaviour of a normal metal is also shown as indicated on the graph.

magnetic field  $B_a$  is illustrated schematically in Fig. 1.1 (b).<sup>5</sup> Such a behaviour is mostly observed in the case of elemental superconductors (see Refs. 6-8 for more details). It is also noted that in zero field the superconducting transition at  $T_c$  is of second order, while in the presence of a magnetic field the transition becomes a first order one.<sup>6-8</sup>

The first successful attempt to describe the basic electrodynamic properties of the superconducting state was made by the brothers F. and H. London in 1935.<sup>9</sup> They formulated a phenomenological model where the microscopic electric and magnetic fields in the superconductor can be described by a set of two equations. The first of them accounts for perfect conductivity. Incorporating the second London equation with the Maxwell equations reveals that a magnetic field decays exponentially in the interior of the superconductor, penetrating only through a small distance  $\lambda$ , i.e., the Meissner – Ochsenfeld effect. The penetration depth was related to the density  $n_s$  of superconducting electrons and was shown to diverge as one approaches  $T_c$ .<sup>9</sup>

The applicability of the London theory is constrained by the fact that it cannot deal with situations where  $n_s$  varies in space as well as with non-linear effects of fields strong enough to change  $n_s$ . Such features can be accounted by a more general macroscopic phenomenological theory, introduced by Ginzburg and Landau in 1950,<sup>10</sup> which, however, retained the local approximation of the London electrodynamics. In this theory, the physical description of the system is based on a spatially varying complex order parameter  $\Psi(\mathbf{r})$ , that describes the superconducting electrons and is related to their local density as  $|\Psi(\mathbf{r})|^2 = n_s(\mathbf{r})$ . The Ginzburg – Landau (GL) theory also introduces a new length  $\xi$ , called the GL coherence length, which determines the scale of variations in the order parameter. The ratio  $\lambda/\xi$  defines the GL parameter  $\kappa$ . Since both  $\lambda$  and  $\xi$  diverge as  $(T_c - T)^{-1/2}$  near  $T_c$ ,<sup>6-8</sup>  $\kappa$  is approximately temperature independent.

Although both the London and GL models are rather useful and can describe satisfactorily the phenomenology of the superconducting state within their range of applicability, they are not able to provide with any information about the microscopic mechanism producing superconductivity. Such a microscopic description had not been developed until 1957, when Bardeen, Cooper and Schrieffer (BCS) published their pairing theory of superconductivity.<sup>11</sup> The BCS model demonstrated that the effect of even a weak attraction between electrons, such as that caused by the electron-phonon interaction, can bind them into pairs (called *Cooper* pairs), where electrons occupy states with equal and opposite momentum and spin. These pairs comprise the superconducting

charge carriers that were anticipated in the phenomenological theories described above. The BCS theory also provided with a quantitative explanation of the energy gap  $\Delta$  between the ground state and the quasi-particle excitations of the system observed in experiments (see for instance Ref. 12). It was predicted that the energy  $E_g(T) = 2\Delta(T)$  required to break a Cooper pair and create two quasi-particle excitations, increases from zero at  $T_c$  to a limiting value  $E_g = 3.528k_B T_c$  for  $T \ll T_c$ , in agreement with the experimental results. It is also mentioned that as was subsequently shown by Gor'kov,<sup>13</sup> the GL theory is a limiting form of the BCS theory for temperatures near  $T_c$  and not too rapid spatial variations of both  $\Psi$  and the vector potential  $\mathbf{A}$ . As a result, within the new framework,  $\Psi$  can be regarded as the wavefunction of the motion of the *Cooper* pairs' centre of mass.<sup>6-8</sup>

For a long time it was supposed that the behaviour illustrated in Fig. 1.1 was characteristic of all superconductors. However, in 1957 the work of Abrikosov revealed that there might be another class of superconductors with somewhat different properties.<sup>14</sup> Based on the GL theory, Abrikosov showed that the 'classic' field – temperature ( $B - T$ ) phase diagram of the superconducting state illustrated in Fig. 1.1 (a), is appropriate only for the limiting case of  $\kappa < 1/\sqrt{2}$ . On the other hand, if the relation  $\kappa > 1/\sqrt{2}$  holds, the  $B - T$  phase diagram is radically different and expected to have a more complicated structure as depicted characteristically in Fig. 1.2 (a). To distinguish between these two varieties, the superconductors with  $\kappa < 1/\sqrt{2}$  were called type-I as contrasted to type-II superconductors characterized by  $\kappa > 1/\sqrt{2}$ . As can be seen from Fig. 1.2 (a), for fields below a lower critical field  $B_{c1}$ ,<sup>5</sup> a type-II superconductor is in the superconducting state (or Meissner phase), i.e., the flux is expelled out of the bulk of the specimen. However, when the field is increased above  $B_{c1}$ , it is energetically more favorable for the magnetic flux to penetrate homogeneously the superconductor in the form of quantized units called vortex lines (or vortices or flux lines). Each vortex carries one quantum of magnetic flux  $\Phi_0 = h/2e = 2.07 \times 10^{-15}$  Wb,<sup>15</sup> and consists of a normal core with diameter  $\sim \xi$ , in the centre of which the superconducting order parameter vanishes. The core is surrounded by screening currents that decay exponentially over a distance  $\lambda$ , providing with the shielding of the magnetic field. Ideally, the vortex lines will form a regular lattice. Minimization of the energy of the system shows that the unit cell of this lattice must be triangular with the nearest neighbor distance being  $a = 1.075 \cdot (\Phi_0/B)^{1/2}$ . This state of

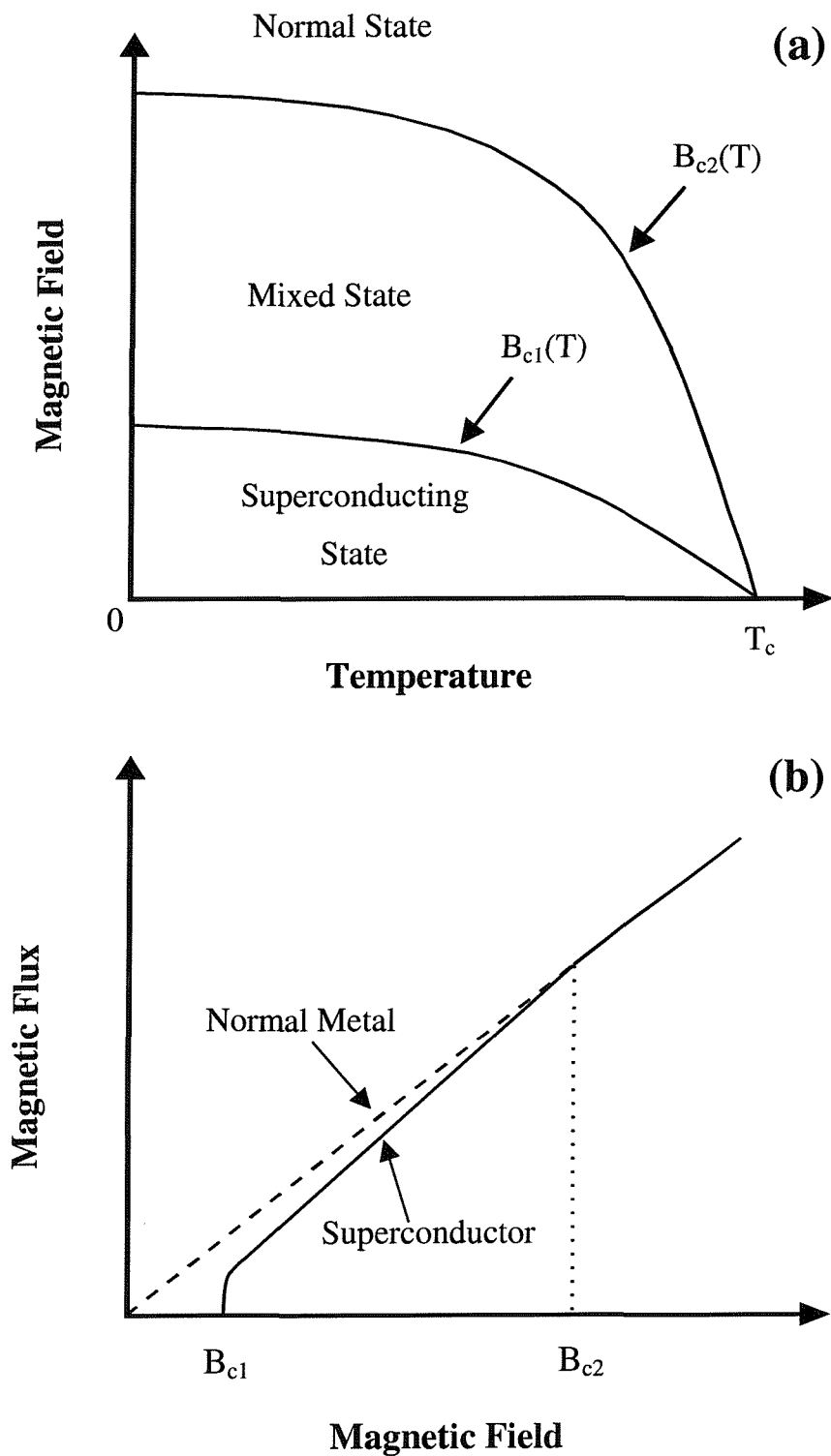


Fig. 1.2. (a)  $B - T$  phase diagram of a type-II superconductor. The indicated phases are discussed in the text. (b) Magnetic behaviour of a type-II superconductor (solid line). For comparison the response of a normal metal is also included (dashed line).

type-II superconductors is called the mixed state or Shubnikov phase, and persists until the upper critical field  $B_{c2} = \sqrt{2} \kappa B_c$  is reached,<sup>5</sup> where superconductivity is extinguished in the bulk of the specimen giving way to the normal state. The dependence of the magnetic induction on the applied field for such a superconductor is illustrated schematically in Fig. 1.2 (b).

The complete and satisfactory theoretical picture of the properties of the superconducting state outlined above, was up to a certain degree overturned by the discovery of the high temperature superconductors (HTSC) by Bednorz and Müller in 1986.<sup>16</sup> Thus a problem that was raised and remains still unresolved, regards the basic microscopic mechanism responsible for high temperature superconductivity. Although a two-electron pairing is most probably still involved, at the moment the nature of pairing is unclear. Recent experiments have supported d-wave symmetry,<sup>17</sup> as opposed to the s-wave symmetry assumed by the BCS theory. In addition, although the mixed state of these materials obeys the same general phenomenology with the conventional type-II superconductors, the strongly layered structure as well as the significantly increased influence of thermal fluctuations due to the small coherence lengths, large penetration depths, large anisotropy and high operating temperatures, result in a wealth of novel phenomena that can be accessible in experimental investigations. These include, for example, the possibility of quasi-two-dimensional behaviour and the appearance of a melting transition that leads to a vortex liquid phase, which occupies a large part of the B – T phase diagram.<sup>18</sup>

## 1.2 Thesis outline

The work presented in this thesis has been devoted to understanding the behaviour of the vortex system in pure single crystals of the high- $T_c$  superconductor  $YBa_2Cu_3O_{7-\delta}$ , in the part of the vortex phase diagram below the melting line. The thesis is organized as follows.

We start by reviewing in **Chapter 2** the phenomenology of vortices in type-II superconductors. Following a discussion of the elastic properties of the ideal vortex lattice, an overview is made of the pinning properties as well as the structure of the lattice in the presence of weak point disorder (collective pinning theory). Subsequently, the

effect of thermal fluctuations is discussed (flux creep), with special emphasis given to the case of the HTSC where flux creep is significantly enhanced. Finally, a brief reference is made to the improvements of the collective pinning theory, made in order to account for the influence of both quenched and thermal disorder (theory of collective flux creep).

**Chapter 3** contains a detailed description of the material properties of the high- $T_c$  superconductor  $\text{YBa}_2\text{Cu}_3\text{O}_{7-\delta}$ , as these have been determined in several recent investigations using a variety of techniques. The variation of the structural parameters of this compound with oxygen stoichiometry is also presented. However, changes in the oxygen content affect the physical parameters of this material as well. Hence, details regarding the variation of  $T_c$ , the out-of-plane anisotropy  $\gamma$ ,  $\xi$ , and  $\lambda$  with the oxygen concentration are also included. Subsequently, there follows an extended description of the single crystal growing procedure. Finally, the nature and mechanism leading to the formation of twin boundaries are discussed, together with a reference to the most commonly used detwinning processes.

The results presented in this thesis have been obtained using two different experimental techniques that are outlined in **Chapter 4**. These are vibrating sample and torque magnetometry. In this chapter we describe the physical principles upon which these techniques are based and specify the technical details of the experimental set-ups utilized in our studies.

At the beginning of **Chapter 5** we give an overview of the most recent theoretical and experimental results regarding the vortex phase diagram of the HTSC. Then our contribution to the elucidation of the structure of the phase diagram of  $\text{YBa}_2\text{Cu}_3\text{O}_{7-\delta}$  is presented. Using a partial magnetization loop technique we investigate history effects in the magnetic hysteresis of pure  $\text{YBa}_2\text{Cu}_3\text{O}_{7-\delta}$  single crystals with various types and densities of pinning sites. This allows the detection of the point where topological disorder first invades the vortex system thus revealing a phase transition in the mixed state of the superconductor that separates a dislocation-free Bragg glass from a highly disordered vortex phase. The transition line is mapped in the field-temperature phase diagram and found to lie in the vicinity of the onset of the second magnetization peak. The effect of variations in quenched disorder on the transition is also investigated, by studying samples with different concentrations of point as well as correlated pinning centres, such as twin planes and columns.

In **Chapter 6**, we present a thorough investigation of the second magnetization peak in high quality  $\text{YBa}_2\text{Cu}_3\text{O}_{7-\delta}$  single crystals. Following an introduction to this topic, we demonstrate that in pure crystals the peak shows several new features that are absent in more disordered samples. Thus we find that the peak position depends non-monotonously on temperature. In addition, at high temperatures the peak becomes extremely sharp and is located close to the melting line. Possible correlations with the transport peak effect are also discussed. The magnetization peak is moreover influenced strongly by variations in the density of oxygen vacancies, shifting to higher field values with increasing oxygen content. These results reject mechanisms that were previously proposed in order to account for the origin of this phenomenon, and suggest other more realistic scenarios.

We also study the effect of oxygen ordering on the magnetization peak by comparing samples with different distributions of oxygen vacancies, as succeeded by low (1 bar) and high (100 bar) oxygen pressure annealing. It is demonstrated that for temperatures below 70 K the peak is independent of the distribution of oxygen defects. However, we find that for  $T > 70$  K oxygen ordering effects become important leading to the suppression of the peak for the high pressure annealed samples. These observations illustrate that although at low temperatures pinning of vortices by clusters or a more homogeneous distribution of oxygen vacancies is similar, at high temperatures, thermally-induced smearing of the pinning potential is more significant in the latter case, leading to the absence of the peak and lower critical currents.

After discussing the theoretical description of the vortex state for fields parallel to the superconducting layers and the lock-in transition, **Chapter 7** presents in detail our results concerning the effect of the layered structure on the hysteretic response of  $\text{YBa}_2\text{Cu}_3\text{O}_{7-\delta}$  single crystals. We show that for fields along the ab-plane, the magnetic hysteresis curves show an oscillatory behaviour that is found to be periodic in  $B^{-1/2}$ . A full accord of the mechanism that produces these oscillations (called the lock-in oscillations) is given. The effect of varying temperature for this field configuration is also studied and reveals a remarkable non-monotonic temperature dependence of the current density that is in qualitative agreement with theory. The influence of variations in the oxygen stoichiometry on the lock-in oscillations in the region near optimal doping is also investigated. This additionally allows to study the dependence of the out-of-plane anisotropy of  $\text{YBa}_2\text{Cu}_3\text{O}_{7-\delta}$ , as this is estimated from the period of the lock-in oscillations,

on the oxygen concentration. The obtained anisotropy values are compared with the ones found using other techniques such as transport and equilibrium torque magnetometry on similar samples, pointing out a possible temperature dependence of the anisotropy.

Finally, the overall contribution of this work to the field of high temperature superconductivity is summarized in **Chapter 8**.

---

## References

---

- <sup>1</sup> H. Kamerlingh Onnes, Leiden Comm. 120b, 122b, 124c (1911)
- <sup>2</sup> W. Meissner and R. Ochsenfeld, *Naturwissenschaften* 21, 787 (1933)
- <sup>3</sup> Note that although a perfect conductor would exclude a field applied after cooling below  $T_c$  from entering the specimen, it would tend to trap in magnetic flux if the field was applied in the normal state.
- <sup>4</sup> For simplicity in the present description we ignore the influence of demagnetizing effects.
- <sup>5</sup> In this thesis the notation  $B_a = \mu_0 H_a$ ,  $B_c = \mu_0 H_c$ ,  $B_{c1} = \mu_0 H_{c1}$  and  $B_{c2} = \mu_0 H_{c2}$  will be used.
- <sup>6</sup> A. C. Rose-Innes and E. H. Rhoderick, *Introduction to Superconductivity*, (Pergamon Press, 1978)
- <sup>7</sup> D. R. Tilley and J. Tilley, *Superfluidity and Superconductivity*, (A. Hilger, Bristol, 1990)
- <sup>8</sup> M. Tinkham, *Introduction to Superconductivity*, (McGraw-Hill, Singapore, 1996)
- <sup>9</sup> F. and H. London, *Proc. Roy. Soc. (London)* A149, 71 (1935)
- <sup>10</sup> V. L. Ginzburg and L. D. Landau, *Zh. Eksperim. i Teor. Fiz.* 20, 1064, (1950)
- <sup>11</sup> J. Bardeen, L. N. Cooper, and J. R. Schrieffer, *Phys. Rev.* 108, 1175, (1957)
- <sup>12</sup> R. E. Glover and M. Tinkham, *Phys. Rev.* 104, 844 (1956); 108, 243 (1957) and references therein.
- <sup>13</sup> L. P. Gor'kov, *Zh. Eksperim. i Teor. Fiz.* 36, 1918 (1959) [JETP 9, 1364 (1959)]
- <sup>14</sup> A. A. Abrikosov, *Zh. Eksperim. i Teor. Fiz.* 32, 1442 (1957) [JETP 5, 1174 (1957)]
- <sup>15</sup> A. A. Abrikosov, *Phys. Chem. Solids* 2, 199 (1957)
- <sup>16</sup> J. G. Bednorz and K. A. Muller, *Z. Phys. B* 64, 189, (1986)
- <sup>17</sup> D. A. Brawner and H. R. Ott, *Phys. Rev. B* 50, 6530 (1994) and references therein.
- <sup>18</sup> G. Blatter, M. V. Feigel'man, V. B. Geshkenbein, A. I. Larkin and V. M. Vinokur, *Rev. Mod. Phys.* 66, 1125 (1994) and references therein.

---

# Chapter 2

---

## Vortices in type-II superconductors

### 2.1 Elastic properties of the vortex lattice

As discussed in the previous chapter, fields greater than  $B_{c1}$  penetrate a type-II superconductor in the form of quantized units called vortices. Ideally, in a homogeneous material a triangular lattice is formed. Nevertheless, in practice vortices are usually displaced from their ideal positions for several reasons:<sup>1</sup> The exertion of pinning forces by inhomogeneities or structural defects in the sample, thermal fluctuations, gradients in the material parameters, or finally currents. If such distortions are small, the resulting change in the free energy of the system can be conveniently calculated from linear elasticity theory.<sup>2, 3</sup> In this case the energy changes are determined by three elastic moduli:<sup>2</sup> The modulus for uniaxial compression  $c_{11}$ , the tilt modulus  $c_{44}$  and the shear modulus  $c_{66}$ , whose physical meaning has as follows.  $c_{11}$  reflects the rigidity of the flux line lattice against compression,  $c_{44}$  is a measure of the easiness with which vortices can be tilted away from the magnetic field and finally,  $c_{66}$  describes the resistance of the vortex lattice against shearing.

As shown for the first time by Brandt,<sup>2</sup> within the continuum description and for non-uniform deformations of the vortex lattice, in isotropic superconductors the elastic response is nonlocal. In other words,  $c_{11}$  and  $c_{44}$  are dispersive i.e., they depend on  $k$ , the modulus of the wave vector of the force field that generates the distortion.<sup>2-4</sup> On the other hand,  $c_{66}$  is essentially nondispersive.<sup>2</sup> The dispersion of the two elastic moduli is due to the fact that the range of the vortex interaction  $\lambda$ , typically exceeds the vortex spacing  $a_0$  and as a consequence the elastic energy caused by a local distortion is contained into a sphere with radius of several  $\lambda$ .<sup>5</sup>

Within the continuum approximation, theory predicts that for isotropic superconductors in a field  $B > B_{c1}$  along the  $z$  direction,  $\kappa = \lambda/\xi \gg 1$ ,  $b = B/B_{c2} < 0.25$  (London limit) and  $k_{\perp} = (k_x^2 + k_y^2)^{1/2} \ll k_{\text{BZ}} = (4\pi B/\Phi_0)^{1/2}$  ( $k_{\text{BZ}}$  is the radius of the first Brillouin zone) the elastic moduli can be given by:<sup>6,7</sup>

$$c_{11}(k) \approx \frac{B^2}{\mu_0} \frac{1}{1 + k^2 \lambda^2} \quad (2.1)$$

$$c_{44}(k) = c_{44}^{(0)}(k) + c_{44}^{\text{corr}}(k) = \frac{B^2}{\mu_0} \left[ \frac{1}{1 + k^2 \lambda^2} + \frac{\tilde{\kappa}}{k_{\text{BZ}}^2 \lambda^2} \right] \quad (2.2)$$

$$\text{with } \tilde{\kappa} = \left( \frac{1 + \kappa^2 + k_z^2 \lambda^2}{1 + b\kappa^2 + k_z^2 \lambda^2} \right)^{1/2}$$

$$\text{and } c_{66} \approx \frac{B\Phi_0}{16\pi \mu_0 \lambda^2}. \quad (2.3)$$

The correction term  $c_{44}^{\text{corr}}(k)$  in eq. (2.2) is introduced in order to account for the isolated vortex contribution that becomes significant for  $B \rightarrow 0$  or  $k \approx k_{\text{BZ}}$ .<sup>5, 8</sup> It is also mentioned that although the tilt component  $k_z$  can in principle attain arbitrarily large values, in practice it is limited by the vortex core radius. As a consequence, the shortest excited tilt waves should have  $k_z \leq 1/\xi$ .<sup>7</sup>

A direct implication of the dispersive nature of  $c_{11}$  and  $c_{44}$  is that the flux line lattice is much softer for short-wavelength compression or tilt than it is for uniform compression or tilt.<sup>2-9</sup> Indeed, as can be seen from eqs. (2.1) and (2.2), for large enough  $k$  a suppression factor  $(k\lambda)^2$  is obtained as compared to the value at  $k = 0$  that corresponds to uniform distortion.<sup>9</sup>

At very small values of the induction [ $B < (B_{c1}/\ln\kappa)$ ], the compression and shear moduli become exponentially small, whereas the tilt modulus attains values

corresponding to the single vortex regime as given by  $c_{44}^{\text{corr}}(k)$  [see eq. (2.2)]. More specifically in this case  $c_{11} = 3c_{66}$ , and  $c_{66}$  can be obtained by:<sup>9</sup>

$$c_{66} = \left(\frac{\pi}{6}\right)^{1/2} \frac{\varepsilon_0}{\lambda^2} \left(\frac{\lambda}{a_0}\right)^{1/2} e^{-a_0/\lambda} \quad (2.4)$$

where  $\varepsilon_0 = \left(\frac{\Phi_0^2}{4\pi\mu_0\lambda^2}\right)$  is an energy scale that determines the self-energy of the vortex lines as well as their mutual interaction.<sup>9</sup>

In the high field range ( $b > 0.5$ ), for the calculation of the elastic moduli the renormalization of the length scales due to the suppression of the order parameter should be taken into account as described by the GL theory. Therefore,  $\lambda' = \lambda/(1-b)^{1/2}$  should be substituted for  $\lambda$  in eqs. (2.1) and (2.2).<sup>2, 6, 9</sup> On the other hand, in this field range the shear modulus is found to vanish as  $(1-b)^2$  and is given by:<sup>5, 9</sup>

$$c_{66} \approx \frac{B\Phi_0}{16\pi\mu_0\lambda^2} (1-b)^2 \quad (2.5)$$

Notice that at low inductions the London and GL results practically coincide.

The dependence of the elastic moduli on  $k$  as well as on the magnetic induction for a given finite  $k$  is illustrated in Figs. 2.1 and 2.2. It is stressed that only when nonlocality is considered do all moduli vanish at  $B_{c2}$ , as is expected from continuity arguments.<sup>5</sup> Also note the removal of the unphysical discontinuity of  $c_{11}$  and  $c_{44}$  at  $B_{c2}$  for the case of local elasticity or uniform distortions ( $k = 0$ ), when more realistic nonuniform deformations ( $k \neq 0$ ) are considered.<sup>5</sup>

The above results can be easily extended to the case of uniaxially anisotropic superconductors. Indeed, within the London limit ( $b < 0.25$ ),  $\kappa > 2$ , and for a field applied along the  $c$ -axis ( $z$  direction), the elastic moduli become:<sup>6</sup>

$$c_{11}(k) = \frac{B^2}{\mu_0} \frac{1 + k^2\lambda_c^2}{(1 + k^2\lambda_{ab}^2)(1 + k_x^2\lambda_c^2 + k_z^2\lambda_{ab}^2)}, \quad (2.6)$$

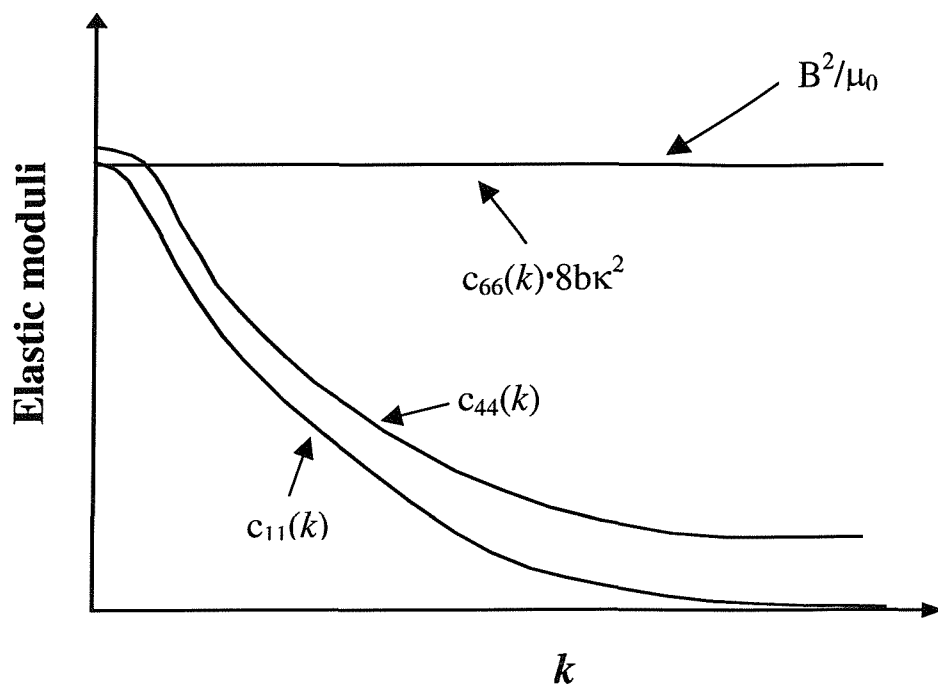


Fig. 2.1. The elastic moduli as calculated from the isotropic GL theory in Ref. 6, are plotted as a function of  $k$ .

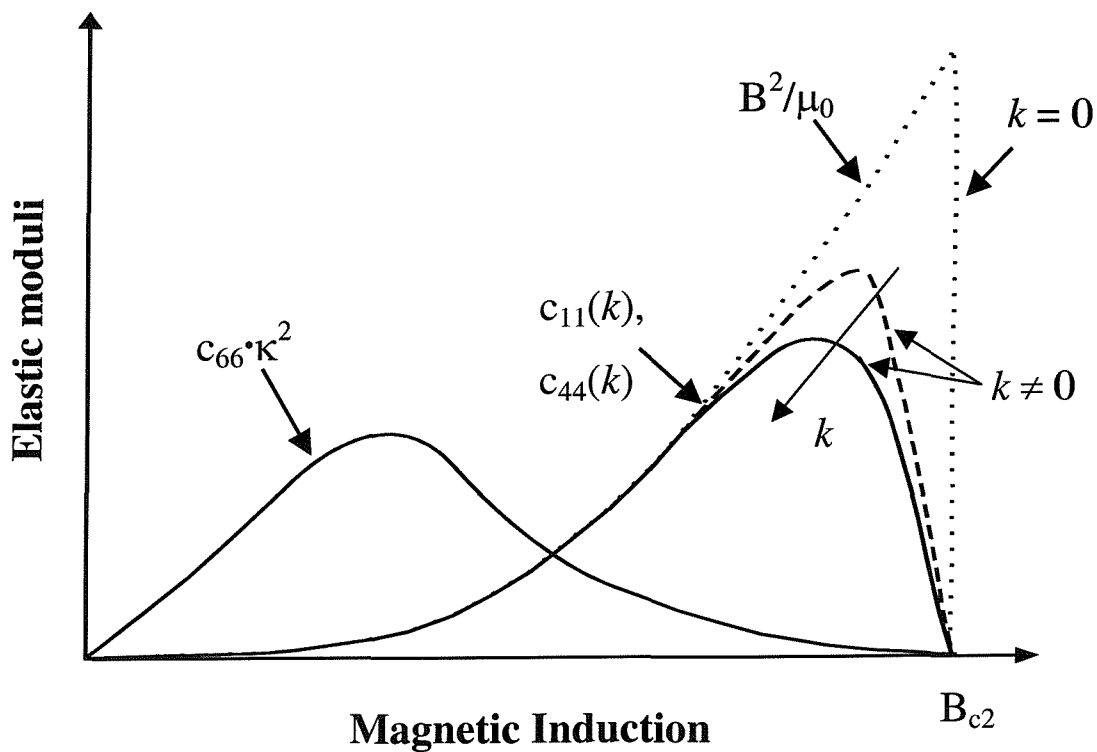


Fig. 2.2. The dependence of the elastic moduli on the induction for  $k = 0$  and  $k \neq 0$ , reprinted from *Physica C195*, E. H. Brandt, *Flux line lattices in high- $T_c$  superconductors: anisotropy, elasticity, fluctuations, thermal depinning, AC penetration and susceptibility*, 1-27, Copyright (1992), with permission from Elsevier Science.

$$c_{44}(k) = \frac{B^2}{\mu_0} \left[ \frac{1}{1 + k_{\perp}^2 \lambda_c^2 + k_z^2 \lambda_{ab}^2} + \frac{f(k_z)}{k_{BZ}^2 \lambda_{ab}^2} \right] \quad (2.7)$$

$$\text{with } f(k_z) = \frac{1}{2\gamma^2} \ln \frac{\xi_c^{-2}}{\lambda_{ab}^{-2} + k_z^2 + \gamma^2 k_0^2} + \frac{\ln[1 + \frac{k_z^2}{\lambda_{ab}^{-2} + k_0^2}]}{2k_z^2 \lambda_{ab}^2},$$

$$\text{and } c_{66}(k) \approx \frac{B\Phi_0}{16\pi \mu_0 \lambda_{ab}^2} \quad (2.8)$$

where  $\lambda_{ab}$  and  $\lambda_c$  are the penetration depths for currents flowing along the ab-plane and c-axis respectively,  $\gamma = (\lambda_c/\lambda_{ab})$  is the out-of-plane anisotropy, and  $k_0 \approx k_{BZ}$  is a cutoff.<sup>6</sup> These results can be extended to  $b > 0.5$  by simply dividing the terms  $\lambda_{ab}^2$  and  $\lambda_c^2$  in eqs. (2.6) and (2.7) by (1-b), and replacing the second term in brackets in eq. (2.7) by  $[(1-b)\Phi_0/(4\pi B \lambda_c^2)]$ .<sup>6</sup> For the shear modulus one has to use eq. (2.5) with  $\lambda$  replaced by  $\lambda_{ab}$ . Note again that  $c_{11}$  and the first term in (2.7) originate from the vortex-vortex interactions, whereas the second term in eq. (2.7) is the isolated-vortex contribution, similarly to the case of the isotropic superconductors.<sup>6</sup>

For fields applied at an arbitrary angle  $\theta$  away from the c-axis, the elastic moduli are separated to in- and out-of-plane components, whereas there also appears a “rotation modulus”.<sup>10</sup> In the last investigation Kogan and Campbell, based on the London model determined the in-plane ( $c_{66}^{\parallel}$ ) and the out-of-plane ( $c_{66}^{\perp}$ ) shear modulus for all angles  $\theta$  as:

$$c_{66}^{\parallel}(\theta) = c_{66} \varepsilon_{\theta}^3 \quad (2.9)$$

$$\text{and } c_{66}^{\perp}(\theta) = \frac{c_{66}}{\varepsilon_{\theta}}, \quad (2.10)$$

with  $\varepsilon_{\theta} = (\cos^2\theta + \gamma^{-2} \sin^2\theta)^{1/2}$ . For the special case of fields applied along the ab plane, eqs.

(2.9) and (2.10) give:  $c_{66}^{\parallel} = c_{66} \gamma^{-3}$  and  $c_{66}^{\perp} = c_{66} \gamma$ . This means that  $\frac{c_{66}^{\perp}}{c_{66}^{\parallel}} = \gamma^4$ , illustrating

that in anisotropic superconductors the shear modulus is strongly anisotropic (considering

that for  $\text{YBa}_2\text{Cu}_3\text{O}_{7-\delta}$   $\gamma \approx 6$ ,<sup>11</sup> this ratio amounts to a factor exceeding 1000). Therefore, the vortex lattice is much softer when sheared in such a way that vortices are forced to move along the  $\text{CuO}_2$  planes than for movement across them.

In a similar manner, the tilt and compression moduli can be split up to two components whose values can be calculated analytically within the London approximation for the whole angular range.<sup>12</sup> Although the full presentation of these results is beyond the scope of this thesis, it is, nevertheless, interesting to mention a special and interesting case for  $c_{44}$ . The components of the main term giving the tilt modulus (there is again a correction term that accounts for the single vortex contribution) have a ratio equal to:<sup>9</sup>

$$\frac{c_{44}^{0,\perp}(k)}{c_{44}^{0,\parallel}(k)} = \frac{1 + (\varepsilon_\theta \lambda_c k)^2}{1 + \lambda_{ab}^2 k^2} \quad (2.11)$$

and therefore in-plane tilts are usually easier than the out-of-plane ones (except for  $\theta = \pi/2$ ).

## 2.2 Pinning of the vortex lattice

If an external current density  $\mathbf{J}$  is applied to a superconductor in the presence of a penetrating field, then in the absence of static disorder (pinning) vortices will start to move coherently under the action of the Lorentz force, whose value per unit volume is given by:

$$\mathbf{F}_L = \mathbf{J} \times \mathbf{B}. \quad (2.12)$$

As can be clearly seen from this equation the direction of vortex motion is perpendicular to both the current and the magnetic induction. The movement of vortices with velocity  $\mathbf{v}$ , however, generates an electric field  $\mathbf{E} = \mathbf{B} \times \mathbf{v}$  and since  $\mathbf{J}$  and  $\mathbf{E}$  run parallel, power is dissipated in the system, or equivalently a finite resistivity appears. The latter is conventionally called the flux flow resistivity,  $\rho_{ff}$ , and as predicted theoretically<sup>13</sup> and observed in several experiments<sup>14</sup> it follows the relation:

$$\rho_{ff} = \rho_n \frac{B}{B_{c2}}, \quad (2.13)$$

with  $\rho_n$  the normal state resistivity. Therefore, it is clear that the basic superconducting property of dissipation-free current flow is lost, and as can be seen from eq. (2.13) the dissipation is just reduced by a factor  $B/B_{c2}$  as compared with a normal metal. In order to recover this property,  $F_L$  must be counteracted by another force,  $F_p$ , which should pin the vortex lattice so as to stay still even for finite Lorentz forces. If such a force does exist, then the current density  $J_c$  that results in  $F_L = F_p$  is called the critical current density. For current densities above  $J_c$  the vortex lattice is depinned and can move freely, whereas for  $J < J_c$  the vortices remain immobile, if one disregards for the moment the effect of thermal activation (see section 2.2.3 below). Also note that  $J_c$  is always bounded by the depairing current density  $J_0$  that is determined by the critical field  $B_c$ . Thus the ratio  $J/J_0$  can be regarded as a measure of the strength of the pinning force.<sup>9</sup>

Pinning of vortices can be provided by any material spatial inhomogeneity that affects the superconducting order parameter. Such inhomogeneities can be localized defects of small dimensions, such as departures from stoichiometry at the atomic scale and non-superconducting impurities, or even extended defects such as grain boundaries, second phase inclusions, screw dislocations, twin boundaries and stacking faults. In the position of these defects, the condensation energy is reduced and consequently in order to decrease the energy of the system, vortices prefer to locate themselves in these regions of reduced superconductivity. Hence, unless an amount of energy equal to this energy gain is provided, flux lines will remain pinned.

### 2.2.1 The critical state model

If a field greater than  $B_{c1}$  is applied to a type-II superconductor with pinning centres, then due to the existence of a critical current, a gradient in the flux line density will set up according to Maxwell's equation  $\text{rot } \mathbf{B} = \mu_0 \mathbf{J}_c$ . In such a case, the magnetic response of the superconductor can be conveniently described using a phenomenological model called the critical state model.<sup>15</sup> In this description it is assumed that  $B_{c1} = 0$  and that  $J_c$  is independent or varies very slowly with the field, leading to constant  $J_c$  values or

equivalently a constant slope of the field gradient along the penetrated regions of the sample. According to this model the induction profiles in, for example an infinite slab of thickness  $D$ , for several increasing or decreasing fields can be represented schematically as shown in Fig. 2.3. From this figure it also becomes clear that pinning will always result in a hysteresis in the magnetization versus field curves.

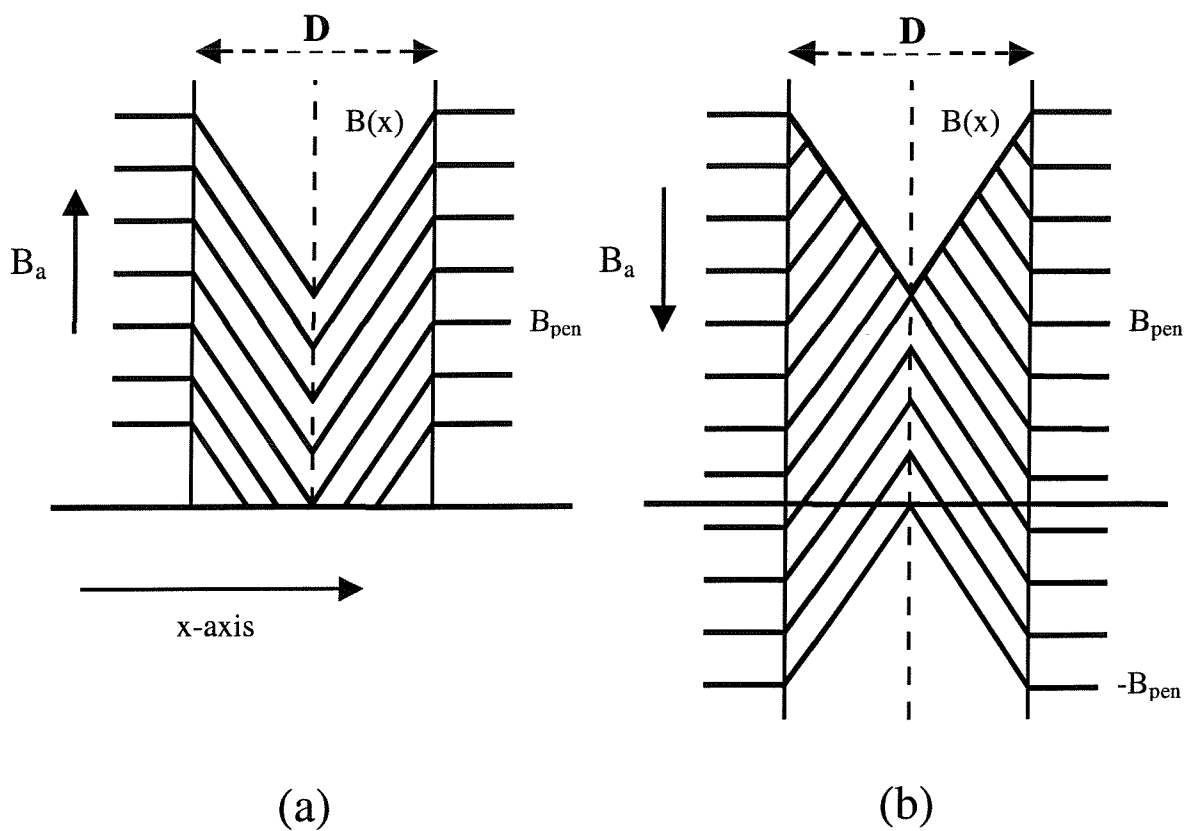


Fig. 2.3. Field profiles in an infinite slab of thickness  $D$ , as described by the critical state model at various (a) increasing and (b) decreasing applied fields  $B_a$ . At a characteristic value  $B_{pen}$ , that is called the penetration field, vortices firstly reach the centre of the sample.

### 2.2.2 Collective pinning theory

The collective pinning theory (CPT) was developed long ago by Larkin and Ovchinnikov,<sup>16-18</sup> in an attempt to describe analytically basic properties of the superconductor such as the pinning force, critical current density and the structure of the vortex lattice, in the presence of a random collection of a large number of weak point pinning sites<sup>19</sup> at zero temperature. The basic idea in this pioneering work is that the vortices, that are considered as elastic objects, can deviate from their ideal positions in the triangular Abrikosov lattice in order to take advantage of the presence of the pinning centers and thus lower the energy of the system by passing through or close to them. As a consequence the flux line lattice is subdivided into correlation volumes,  $V_c = R_c^2 L_c$ , with transverse and longitudinal (with respect to the magnetic field direction) dimensions  $R_c$  and  $L_c$  respectively as illustrated in Fig 2.4 below. Within a certain volume  $V_c$ , short range order exists and vortices are arranged almost periodically.<sup>20</sup> Nevertheless, between different correlation volumes this periodicity is disturbed as a result of shear and tilt distortions of the lattice due to the presence of the random pinning landscape. The distortion of the lattice occurs at the expense of increasing the elastic energy and therefore the values of  $R_c$  and  $L_c$  will be determined by minimization of the sum of the elastic and pinning energies.

Before going on to describe quantitatively the main features of CPT, it is interesting to note that the condition of an elastic lattice is necessary for the existence of a finite pinning force.<sup>16</sup> In the opposite case of a perfectly periodic and rigid lattice pinning would be impossible. Indeed, for a system of volume  $V$ , the Lorentz force is proportional to  $JV$ , where  $J$  is the current density. On the other hand, the net total pinning force will grow as  $\sqrt{N}$  (Note that the individual pinning forces add as in a random walk, i.e., pinning of the vortex lines is due to fluctuations in the density and force of pinning centres, which is a fundamental concept in the CPT.) or equivalently as  $\sqrt{V}$ , where  $N = nV$  is the total number of pinning centres contained in this volume and  $n$  their density. Therefore the critical current density (defined by the condition  $F_L = F_p$ ) will scale with  $V^{-1/2}$  vanishing for systems with large volumes.<sup>21</sup>

When a current below the critical value flows in the superconductor, then under the action of the Lorentz force each correlation volume will be displaced. Such

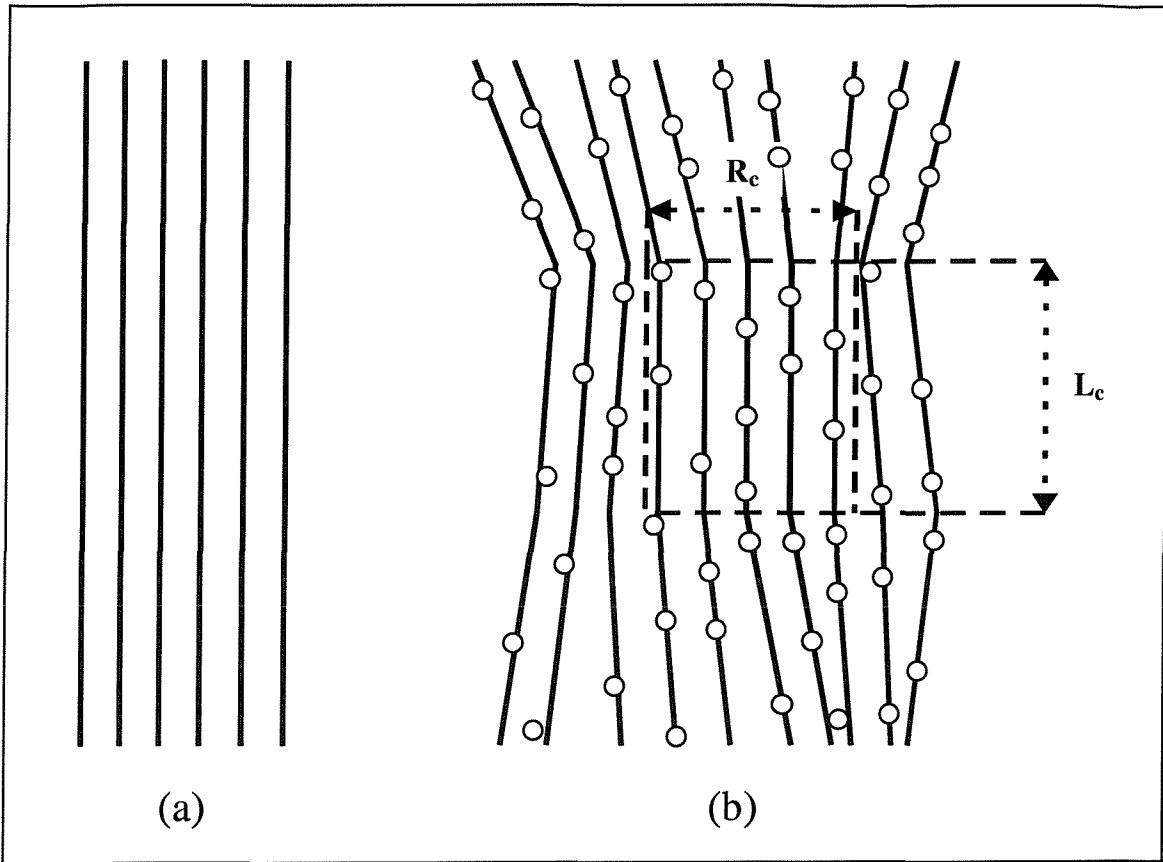


Fig. 2.4. In the absence of pinning the flux line lattice is periodic and parallel to the magnetic field (a). For randomly distributed weak pinning centres, however, the vortex lattice deforms in order to lower its energy by passing through the pinning sites. In this case, periodicity in the lattice is maintained only within a volume  $V_c$  with dimensions  $R_c$  and  $L_c$  transverse and along the field direction respectively (b).

displacements, however, will be constrained to distances smaller than the coherence length  $\xi$  since the pinning force is higher than the Lorentz force.<sup>19</sup> If  $N = nV_c$  is the number of pinning centres in the volume  $V_c$  and  $f_p$  the force exerted on the lattice by each of them, then considering that these forces add randomly the maximum pinning force acting upon  $V_c$  will be of the order of  $N^{1/2}f_p$ .<sup>16, 17</sup> The critical current density then can be found from the condition:

$$BJ_c = f_p N^{1/2} V_c^{-1} = f_p (n/V_c)^{1/2} \quad (2.14)$$

demonstrating that at a certain field value the critical current is higher for stronger and/or denser pinning centres as well as for a more distorted vortex lattice (i.e., smaller  $V_c$ ).

Since the pinning force acts through a distance  $\sim \xi$ , the corresponding pinning energy for the volume  $V_c$  will be  $\sim \xi f_p N^{1/2} = \xi f_p (nV_c)^{1/2}$ . On the other hand, if  $s_s = \xi/R_c$  and  $s_t = \xi/L_c$  are the resulting shear and tilt strains respectively due to the distortion of the vortex lattice by the presence of the pins, that is accommodated over distances  $R_c$  or  $L_c$ , the resulting increase in the elastic free energy per unit volume will be equal to  $\frac{1}{2}[c_{66}s_s^2 + c_{44}s_t^2]$ .<sup>21</sup> As a consequence, the free energy change,  $\delta F$ , per unit volume caused by pinning will be equal to:

$$\delta F = \frac{1}{2}c_{66}\left(\frac{\xi}{R_c}\right)^2 + \frac{1}{2}c_{44}\left(\frac{\xi}{L_c}\right)^2 - f_p\xi\left(\frac{n}{V_c}\right)^{1/2} \quad (2.15)$$

Note that the compression modulus  $c_{11}$  has been omitted since due to its large values the shear deformations of the lattice significantly exceed the compression displacements.<sup>18</sup> Substituting  $R_c^2 L_c$  for  $V_c$  and minimizing eq. (2.15) with respect to  $R_c$  and  $L_c$  gives:<sup>21</sup>

$$L_c = \frac{2c_{44}c_{66}\xi^2}{nf_p^2}, \quad R_c = \frac{\sqrt{2}c_{44}^{1/2}c_{66}^{3/2}\xi^2}{nf_p^2}, \quad V_c = \frac{4c_{44}^2c_{66}^4\xi^6}{n^3f_p^6}. \quad (2.16)$$

From the expressions (2.16) it becomes clear that with decreasing the elastic moduli or increasing the density and/or the strength of the pinning centres the lattice becomes more distorted as one would intuitively expect. Moreover, considering that  $L_c \gg R_c$ , it turns out that  $V_c$  is a volume elongated along the field direction.<sup>6</sup> Combining eqs. (2.15) and (2.16) one can obtain the energy gain from the presence of the pins, namely :

$$\delta F = -\frac{n^2 f_p^4}{8c_{44}c_{66}^2\xi^2} \quad (2.17)$$

Finally substitution of the value of  $V_c$  from eq. (2.16) into eq. (2.14) gives for the critical current density:

$$J_c = \frac{n^2 f_p^4}{2Bc_{44}c_{66}^2\xi^3}. \quad (2.18)$$

One of the most significant successes of CPT was to provide with a possible explanation of the peak effect in the critical current seen close to  $B_{c2}$  in the low temperature superconductors (see for instance Ref. 22). In the limit of a large number of pinning centres ( $nV_c \gg 1$ ), due to the strong dispersion of  $c_{44}$  close to  $B_{c2}$  there arises an effective softening of the lattice.<sup>2</sup> As a consequence  $V_c$  decreases and the current density increases [see eq. (2.14)]. This enhancement, however, will stop when  $R_c$  becomes of the order of  $a_0$ , where the current will eventually start decreasing due to the field dependence of intrinsic parameters on approaching  $B_{c2}$ , thus resulting in a peak.<sup>18</sup> On the other hand, when individual pinning sites are strong enough so as to define individual coherence volumes ( $nV_c \approx 1$ ), that as can be seen from eq. (2.16) can occur for sufficiently large  $f_p$  or small elastic moduli (as for example near  $B_{c2}$ ), each pinning site deforms the lattice plastically, and holds it with a maximum force  $f_p$ . In such a case a direct summation of the pinning forces becomes valid, and the critical current will be equal to  $J_c = nf_p/B$ .<sup>18, 21</sup> This value greatly exceeds the one determined by eq. (2.14) obtained with a random walk, thus leading to a sharp increase in the current that subsequently falls to zero at  $B_{c2}$ .

### 2.2.3 Flux creep

Strictly speaking, the ideal pinning picture given by Larkin and Ovchinnikov is appropriate only in the limit of zero temperature. This is because in their approach the effect of thermal activation in assisting flux motion is ignored, and therefore no movement of vortices should be expected as long as the current flowing in the superconductor satisfies  $J < J_c$ . Nevertheless, in practice due to thermal fluctuations vortices can move even for  $J < J_c$ , leading to the so-called flux creep,<sup>23</sup> which results in a non-vanishing resistivity for currents below  $J_c$  (At very low temperatures quantum creep can also become important.<sup>24</sup> However, this effect is beyond the scope of this thesis and will not be discussed).

The theoretical description of flux creep was developed for the first time by Anderson and Kim,<sup>23, 25</sup> and subsequently was extended further in Ref. 26, in order to

account for experimental observations in conventional superconductors.<sup>27</sup> An assumption made by the Anderson-Kim model is that vortices can move between different pinning states not individually but as “flux bundles” i.e., as clusters of neighboring vortex lines that act collectively in each thermally activated jump and are elastically independent from each other.<sup>23, 25</sup> This is a consequence of the long range interaction between vortices, which for the usual case of  $a_0 < \lambda$  makes the activation of single flux lines over the pinning barrier energetically unfavourable.<sup>23</sup> Another simplification in this model is the assumption that the volume and hop distance of the bundle as well as the depth of the pinning well are current independent.

If  $U_0$  is the pinning potential height, or equivalently the difference in the Gibbs energy of the system between when the flux bundle is in the pinning well and when it is moved away from it, then in the absence of any driving forces, due to thermal activation bundles hop out of the pinning well at a rate:<sup>23, 25</sup>

$$R = v_0 \exp(-U_0/k_B T) \quad (2.19)$$

where  $v_0$  is an attempt frequency and  $k_B$  the Boltzmann constant. This rate is the same for both forward and backward hopping and therefore no net motion of vortices will be observed.  $U_0$  can be related to the critical current density via the equation:

$$U_0 = J_c B V_c r_p \quad (2.20)$$

with  $V_c$  the volume of the bundle and  $r_p$  the range of the pinning potential. If now a current  $J < J_c$  flows in the superconductor, the driving force favours hopping at a certain direction, to which we refer hereafter as the forward direction, due to a reduction in the corresponding energy barrier by an amount  $\Delta W$ , namely:

$$U = U_0 - \Delta W. \quad (2.21)$$

At the same time the barrier for backward hopping is increased by the same amount and as a consequence hopping in this direction becomes less favorable.  $\Delta W$  is the work done by the Lorentz force when the volume  $V_c$  moves a distance  $w$  in a thermally activated jump and is given by:

$$\Delta W = U_0 \left( \frac{J}{J_c} \right) \left( \frac{w}{r_p} \right). \quad (2.22)$$

It is stressed that although for  $b > 0.2$ ,  $w$  can be taken equal to  $r_p$ , at lower fields these quantities might deviate significantly from each other.<sup>28</sup> Also note that both  $U_0$  and  $\Delta W$  are functions of the magnetic induction and temperature whose exact forms depend on the model used to describe vortex interactions.

Following these arguments, the forward,  $R_f$ , and backward,  $R_b$ , hopping rates become:

$$R_f = v_0 \exp[-(U_0 - \Delta W) / k_B T] \quad (2.23)$$

and

$$R_b = v_0 \exp[-(U_0 + \Delta W) / k_B T] \quad (2.24)$$

resulting in a net rate  $R_{\text{net}} = R_f - R_b$  for forward hopping:

$$R_{\text{net}} = 2v_0 \exp(-U_0 / k_B T) \sinh(\Delta W / k_B T). \quad (2.25)$$

In the special case that the entire lattice moves through one lattice spacing at the rate  $R_{\text{net}}$ ,<sup>29</sup> the average velocity will be  $v = R_{\text{net}} a_0$ , resulting in an electric field  $E$ :

$$E = B R_{\text{net}} a_0 = 2B a_0 v_0 \exp(-U_0 / k_B T) \sinh(\Delta W / k_B T). \quad (2.26)$$

Two interesting limits can be further considered. The first one is when  $\Delta W \gg k_B T$  (and therefore  $U_0 \gg k_B T$ ) that holds for currents close to the critical value and low temperatures, which is the case seen in the low- $T_c$  compounds close to the critical temperature.<sup>26, 27</sup> Under this condition eq. (2.26) becomes  $E \approx B a_0 v_0 \exp[(\Delta W - U_0) / k_B T]$ , which with the help of eq. (2.22) gives for the current density:

$$J = J_c \left( \frac{r_p}{a_0} \right) \left( 1 + \frac{k_B T}{U_0} \ln \frac{E}{B a_0 v_0} \right). \quad (2.27)$$

On the other hand, in the opposite limit of  $\Delta W \ll k_B T$ , that is realized for high temperatures and  $J \ll J_c$ , the electric field (2.26) reads  $E \approx 2B a_0 v_0 (\Delta W / k_B T) \exp(-U_0 / k_B T) = 2B a_0 v_0 (U_0 / k_B T) (J / J_c) (a_0 / r_p) \exp(-U_0 / k_B T)$ . With the help of eq. (2.20) and considering that  $a_0 = 1.07 (\Phi_0 / B)^{1/2}$ ,<sup>29</sup> one obtains for the resistivity  $\rho$ :

$$\rho = \frac{E}{J} = 2.3 \Phi_0 B v_0 \frac{V_c}{k_B T} \exp\left(-\frac{U_0}{k_B T}\right). \quad (2.28)$$

which can be exponentially small but not zero, and increases linearly with field. This case ( $\Delta W \ll k_B T$ ) is known as *thermally assisted flux flow* (TAFF),<sup>28</sup> and was first examined in Refs. 28 and 29.

Finally, based on the Anderson-Kim model one can estimate the temporal dependence of the current density. Combining eqs. (2.21) and (2.22), the activation energy for creep can be written as:

$$U(J) = U_0 \left[ 1 - \left( \frac{J}{J_c} \right) \left( \frac{w}{r_p} \right) \right] \quad (2.29)$$

As shown by Geshkenbein and Larkin the energy  $U$  can be generally given by:<sup>30</sup>

$$U(J) = k_B T \ln(t/t_0) \quad (2.30)$$

where  $t_0$  is a macroscopic time scale that depends on the sample size.<sup>9, 30, 31</sup> From the last two equations one can find that within the Anderson-Kim approach the current decays logarithmically with time, namely:

$$J = \left( \frac{r_p}{w} \right) J_c \left[ 1 - \frac{k_B T}{U_0} \ln\left(\frac{t}{t_0}\right) \right]. \quad (2.31)$$

## 2.2.4 Theory of collective flux creep

Soon after the discovery of the HTSC, it became clear that the Anderson-Kim model expression (2.31) could not account for the experimental observation of a strong, non-logarithmic, time decay of the current density.<sup>32, 33</sup> This led Feigel'man et al.<sup>31</sup> to develop a more realistic model, known as the theory of collective flux creep (TCFC). This theory goes beyond the conventional flux creep model and for the case of elastic deformations of the vortex lattice predicts that both the hopping distance and volume of the flux bundles are dependent on the values of the current. In specific, the activation volume was found to diverge as  $J \rightarrow 0$ .

The first improvement made by TCFC was the precise estimation of the size of the hopping bundle. It was demonstrated that for fields well above  $B_{c1}$  and  $J \sim J_c$ , each bundle is made up of a large number  $[\sim (c_{11}/c_{66})^{1/2}]$  of subbundles of volume  $V_c = R_c^2 L_c$ . These subbundles are formed independently from each other by the competition between the elastic and pinning energies and hop all together. Independent hopping of subbundles is prohibited due to the considerable compression deformation that is induced when a large region of the lattice is shifted by a distance of the order of  $\xi$ . Since  $c_{11} \gg c_{66}$ , the requirement that the energies of shear and compression deformations should be of the same order of magnitude results in a large bundle, whose size  $R_{||}$  in the direction of hopping is much larger than the size  $R_{\perp}$  corresponding to the transverse direction.<sup>31</sup> In addition the bundle size was proven to be even larger in the region  $J \ll J_c$ .<sup>31</sup>

TCFC proposes an inverse power-law activation barrier,  $U(J) = U_{\alpha}[(J_c/J)^{\alpha}-1]$ , between different pinning states of the lattice, which for  $J \ll J_c$  grows with decreasing current density as:

$$U(J) \approx U_{\alpha} \left( \frac{J_c}{J} \right)^{\alpha} \quad (2.32)$$

where  $U_{\alpha}$  is a characteristic energy scale and  $\alpha$  an exponent that depends on the dimensionality of the problem and the particular regime of flux creep.<sup>9, 31</sup> More specifically, in three dimensions  $\alpha = 1/7$  in the region where creep is dominated by the motion of individual vortices ( $L_c < a_0$ ),  $\alpha = 5/2$  for small bundles ( $a_0 < R_{\perp}$ ,  $R_{||} < \lambda$ ),  $\alpha = 1$

for intermediate bundles ( $a_0 < R_{\perp} < \lambda < R_{\parallel}$ ) and  $\alpha = 7/9$  for large bundles ( $\lambda < R_{\perp}, R_{\parallel}$ ). Note that these results are valid for the case of weak randomly distributed defects and  $w < a_0$ .<sup>9, 31, 34</sup>

The form for  $U(J)$  given by eq. (2.32) results in nonlinear current-voltage characteristics,  $E \propto \exp[-(U_{\alpha}/k_B T)(J_c/J)^{\alpha}]$ , whereas the thermally activated resistivity,  $\rho(J, T) \propto \exp[-U(J)/k_B T]$ , becomes truly zero as  $J \rightarrow 0$ . Hence, the dissipation-free current flow property of the superconductor is “recovered”. Note also that in this model there is no metastable configuration with a simple energy barrier for backward jumps and therefore there is no correction term for hopping in this direction. Indeed simple arguments show that such configurations are unstable and the lattice must return to its initial state.<sup>21</sup>

From eqs. (2.30) and (2.32), one can obtain the time dependence of the current density, namely:

$$J(t) \approx J_c \left[ \frac{k_B T}{U_{\alpha}} \ln \left( \frac{t}{t_0} \right) \right]^{-1/\alpha}. \quad (2.33)$$

Eq. (2.33) can be generalized in order to include the Anderson result (2.31) in the so-called interpolation formula:<sup>35, 36</sup>

$$J(t) = J_c \left[ 1 + \frac{\alpha k_B T}{U_0} \ln \left( \frac{t}{t_0} \right) \right]^{-1/\alpha}. \quad (2.34)$$

It is stressed that the condition of an elastically distorted lattice, upon which TCFC is based, can be violated in cases where the current decreases rapidly during the experiment, for instance at high temperatures. In this case the activation energy given by eq. (2.32) becomes extremely large and creep occurs via plastic deformations of the lattice, rendering the TCFC invalid.<sup>31, 35, 37</sup> The activation energy for the latter process is independent or very weakly dependent on the current, and at low temperatures and high currents is usually much higher than the energy barriers for collective creep.<sup>31, 35, 37</sup> The significance of such plastic creep in the high temperature superconductors has been demonstrated experimentally in Refs. 37 and 38.

Finally, it is mentioned that a vanishing linear resistivity in the limit  $J \rightarrow 0$  as well as the interpolation formula (see eq. (2.34)) have also been obtained within the vortex glass picture,<sup>39</sup> which is discussed in more detail in Chapter 5.

## References

- <sup>1</sup> A. M. Campbell and J. E. Evetts, *Adv. Phys.* 21, 129 (1972)
- <sup>2</sup> E. H. Brandt, *J. Low Temp. Phys.* 26, 709 (1977); 26, 735 (1977)
- <sup>3</sup> E. H. Brandt, *J. Low Temp. Phys.* 28, 263 (1977); 28, 291 (1977)
- <sup>4</sup> E. H. Brandt, *Phys. Rev. B* 34, 6514 (1986)
- <sup>5</sup> E. H. Brandt, *Physica C* 195, 1 (1992)
- <sup>6</sup> E. H. Brandt, *The Flux-Line Lattice in Superconductors*, *Rep. Prog. Phys.* 58, 1465 (1995), published by the *Institute of Physics*
- <sup>7</sup> E. H. Brandt, *Physica C* 180, 426 (1991)
- <sup>8</sup> A. Sudbø and E. H. Brandt, *Phys. Rev. Lett.* 66, 1781 (1991)
- <sup>9</sup> G. Blatter, M. V. Feigel'man, V. B. Geshkenbein, A. I. Larkin and V. M. Vinokur, *Rev. Mod. Phys.* 66, 1125 (1994)
- <sup>10</sup> V. G. Kogan and L. J. Campbell, *Phys. Rev. Lett.* 62, 1552 (1989)
- <sup>11</sup> S. Kokkaliaris, K. Deligiannis, M. Oussena, A. A. Zhukov, P. A. J. de Groot, R. Gagnon, and L. Taillefer, *Supercond. Sci. Technol.* 12, 690 (1999)
- <sup>12</sup> E. Sardella, *Phys. Rev. B* 45, 3141 (1992)
- <sup>13</sup> J. Bardeen and M. J. Stephen, *Phys. Rev. B* 140, 1197 (1965)
- <sup>14</sup> C. F. Hempstead and Y. B. Kim, *Phys. Rev. Lett.* 12, 145 (1964); Y. B. Kim, C. F. Hempstead, and A. R. Strnad, *Phys. Rev. B* 139, A1163 (1965)
- <sup>15</sup> C. P. Bean, *Phys. Rev. Lett.* 8, 250 (1962); *Rev. Mod. Phys.* 36, 31 (1964)
- <sup>16</sup> A. I. Larkin, *Zh. Eksp. Teor. Fiz.* 58, 1466 (1970)
- <sup>17</sup> A. I. Larkin and Yu. N. Ovchinnikov, *Zh. Eksp. Teor. Fiz.* 65, 1704 (1973)
- <sup>18</sup> A. I. Larkin and Yu. N. Ovchinnikov, *J. Low Temp. Phys.* 34, 409 (1979)
- <sup>19</sup> The assumption that pinning is due to point defects, implies that the disorder correlation length  $r_p$  i.e., the range of the pinning potential, is zero along the vortex and of the order of  $\xi$  in the transverse direction.
- <sup>20</sup> By definition, within  $V_c$  the pinning-caused mean square vortex displacement is of the order of the pinning force range squared ( $\sim \xi^2$ ).
- <sup>21</sup> M. Tinkham, *Introduction to Superconductivity*, (McGraw-Hill, Singapore, 1996)
- <sup>22</sup> M. Steingart, A. G. Purz, and E. J. Kramer, *J. Appl. Phys.* 44, 5580 (1973)
- <sup>23</sup> P. W. Anderson, *Phys. Rev. Lett.* 9, 309 (1962)

- <sup>24</sup> R. Griessen, Phys. Rev. Lett. 64, 1674 (1990); L. Radzihovsky, *ibid.* 74, 4919 (1995)
- <sup>25</sup> P. W. Anderson and Y. B. Kim, Rev. Mod. Phys. 36, 39 (1964)
- <sup>26</sup> M. R. Beasley, R. Labusch, and W. W. Webb, Phys. Rev. 181, 682 (1969)
- <sup>27</sup> Y. B. Kim, C. F. Hempstead, and A. Strnad, Phys. Rev. Lett. 9, 306 (1962)
- <sup>28</sup> P. H. Kes, J. Aarts, J. van den Berg, C. J. van der Beek, and J. A. Mydosh, Supercond. Sci. Technol. 1, 242 (1989)
- <sup>29</sup> D. Dew-Hughes, Cryogenics 23, 674 (1988)
- <sup>30</sup> V. B. Geshkenbein and A. I. Larkin, Zh. Eksp. Teor. Fiz. 95, 1108 (1989) [Sov. Phys. (JETP) 68, 639 (1989)]
- <sup>31</sup> M. V. Feigel'man, V. B. Geshkenbein, A. I. Larkin, and V. M. Vinokur, Phys. Rev. Lett. 63, 2303 (1989)
- <sup>32</sup> Y. Yeshurun and A. P. Malozemoff, Phys. Rev. Lett. 60, 2202 (1988)
- <sup>33</sup> J. R. Thompson, Y. R. Sun, and F. Holtzberg, Phys. Rev. B 44, 458 (1991)
- <sup>34</sup> M. V. Feigel'man, V. B. Geshkenbein, and V. M. Vinokur, Phys. Rev. B 43, R6263 (1991)
- <sup>35</sup> V. B. Geshkenbein, A. I. Larkin, M. V. Feigel'man, and V. M. Vinokur, Physica C 162-164, 239 (1989)
- <sup>36</sup> A. P. Malozemoff and M. P. A. Fisher, Phys. Rev. B 42, R6784 (1990)
- <sup>37</sup> C. J. van der Beek and P. H. Kes, Phys. Rev. B 43, 13032 (1991)
- <sup>38</sup> Y. Abulafia, A. Shaulov, Y. Wolfus, R. Prozorov, L. Burlachkov, Y. Yeshurun, D. Majer, E. Zeldov, H. Wühl, V. B. Geshkenbein, and V. M. Vinokur, Phys. Rev. Lett. 77, 1596 (1996)
- <sup>39</sup> D. S. Fisher, M. P. A. Fisher, and D. A. Huse, Phys. Rev. B 43, 130 (1991)

---

# Chapter 3

---

## The high temperature superconductor $\text{YBa}_2\text{Cu}_3\text{O}_{7-\delta}$

Following the discovery of high temperature superconductivity in the La-(Ba, Sr)-Cu-O systems at 30-50 K,<sup>1, 2</sup> several groups almost simultaneously reported the observation of transition temperatures near 90 K in an Yttrium, Barium, Copper ternary oxide.<sup>3, 4</sup> This compound is described by the formula  $\text{YBa}_2\text{Cu}_3\text{O}_{7-\delta}$  (the abbreviated form Y-123 is also used), with  $\delta$  varying in the range  $0 \leq \delta \leq 1$ . The possibility of changing the oxygen content, that can be succeeded rather trivially by simply varying the annealing conditions, makes this compound of great interest, as it allows for a systematic study of the effect of doping on its structural and superconducting properties. Indeed, as the oxygen concentration varies from 7 to 6,  $\text{YBa}_2\text{Cu}_3\text{O}_{7-\delta}$  exhibits structural transitions, a bizarre variation of  $T_c$  with  $\delta$ , the disappearance of superconductivity and the onset of antiferromagnetism.

### 3.1 Structural properties

The initial discovery of  $\text{YBa}_2\text{Cu}_3\text{O}_{7-\delta}$  was accompanied by confusion concerning the exact crystal structure of this compound. Single crystal x-ray studies yielded a tetragonal structure composed of three perovskite cells stacked in the c-direction with ordered Y and Ba cations.<sup>5, 6</sup> On the other hand, x-ray diffraction from powdered samples indicated an orthorhombic structure.<sup>7</sup> The obvious discrepancy among these x-ray investigations was either due to the intrinsically poor sensitivity of this technique for determining oxygen-atom displacements and vacancy ordering or due to true differences in the studied

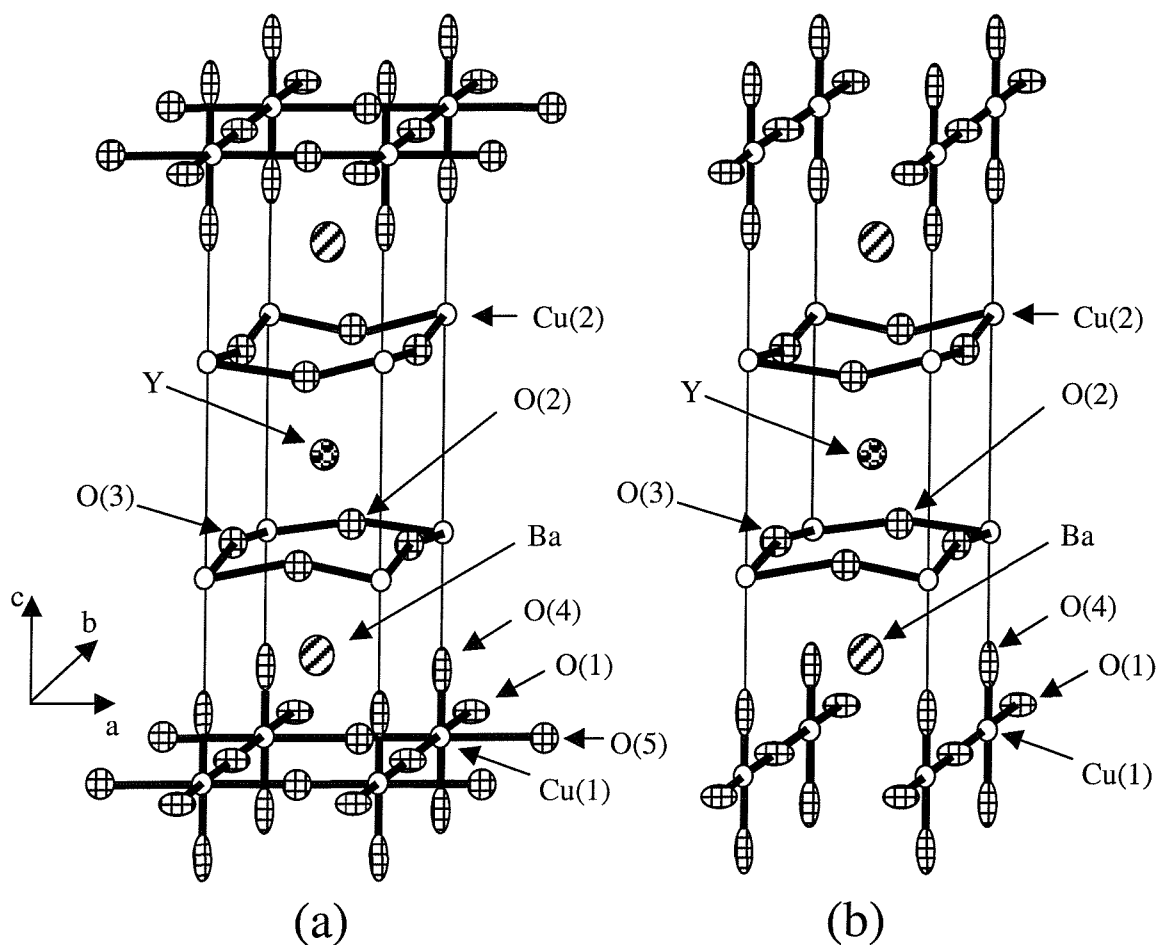


Fig. 3.1 (a) Tetragonal and (b) orthorhombic structures of  $YBa_2Cu_3O_{7-\delta}$ . The various oxygen and copper sites as well as the yttrium and barium cations are indicated on the graph. Note that the O(1) and O(5) sites in the tetragonal structure are drawn to be fully occupied in order to stress that they are equivalent. The different atom symbols for these sites indicate the fact that in practice they are not fully occupied (see text).<sup>11</sup> The Cu-O chains in the  $b$ -direction are obvious in the orthorhombic phase. In both structures a puckering of the  $CuO_2$  sheets is seen that is attributed to the large ionic attraction between  $O^{2-}$  and  $Y^{3+}$  due to the small ionic radius and high charge of the latter.<sup>13</sup>

samples that were prepared under different conditions. Hence these results could not be conclusive. Nevertheless, subsequent more accurate neutron diffraction studies succeeded in shedding light into the structure of Y-123. They demonstrated clearly that this compound can exist in two stable phases: One with a tetragonal unit cell ( $a = b \neq c$ ,  $\alpha = \beta$

$= \gamma = 90^\circ$ ) and one with an orthorhombic unit cell ( $a \neq b \neq c \neq a$ ,  $\alpha = \beta = \gamma = 90^\circ$ ).<sup>8-12</sup> These two structures are shown schematically in Figures 3.1 (a) and 3.1 (b) respectively.

As can be clearly seen, the unit cell of this compound is made up of stacks of  $CuO_2$  layers that lie in the  $ab$ -plane of the superconductor. These sheets are believed to be the “seat” of superconductivity, and are separated from one another by insulating block layers. The latter except acting as spacers for the  $CuO_2$  planes, also play the significant role of the charge reservoir for them.<sup>13</sup> Consequently, their nature controls the carrier concentration and the ease of charge transfer from and to the  $CuO_2$  layers thus determining the superconducting transition temperature.<sup>13</sup>

The main difference between the two structures depicted in Fig. 3.1 is that although in the tetragonal structure the  $(0,1/2,0)$  and  $(1/2,0,0)$  sites [denoted as O(1) and O(5) respectively in Fig. 3.1 (a)] are symmetry equivalent and thus equally occupied, this is not the case in the orthorhombic phase. Indeed, in the latter these sites are crystallographically inequivalent and the oxygen atoms are mainly ordered onto the  $(0,1/2,0)$  [O(1)] site. This results in the presence of one-dimensional Cu-O chains along the  $b$ -axis,<sup>10, 14</sup> which are characteristic of Y-123 as well as of its homologs Y-247 and Y-124. Fragments of chains begin to form when  $7-\delta$  is raised above 6 and their density increases with the oxygen concentration thus destroying the tetragonal structure on a local basis.<sup>15</sup> Nevertheless, the average symmetry of many unit cells as seen in diffraction experiments remains tetragonal, until the chains become sufficiently organized to all align in the same direction, leading to the tetragonal-to-orthorhombic structural transition discussed below.<sup>15</sup>

Concerning the nature of the chains, it is believed that they have a metallic character and become superconducting by proximity to the intrinsically superconducting  $CuO_2$  planes.<sup>16</sup> As a consequence, due to their relatively high carrier density, chains can act as charge reservoirs, enhancing significantly the superconducting condensate density in the  $CuO_2$  layers.<sup>17</sup> This, however, occurs only for very low densities of oxygen vacancies since otherwise some of the chain Cu atoms develop magnetic moments and act as *Cooper* pair breakers.<sup>16, 17</sup>

The orthorhombic and tetragonal phases are related by an order-disorder phase transition involving disordering of the oxygen atoms that destroys the one-dimensional chains and results in a two-dimensional structure [compare Figs. 3.1 (a) and (b)].<sup>10</sup> As shown by Jorgensen et al.<sup>11</sup> with increasing oxygen deficiency from  $\delta = 0$ , the

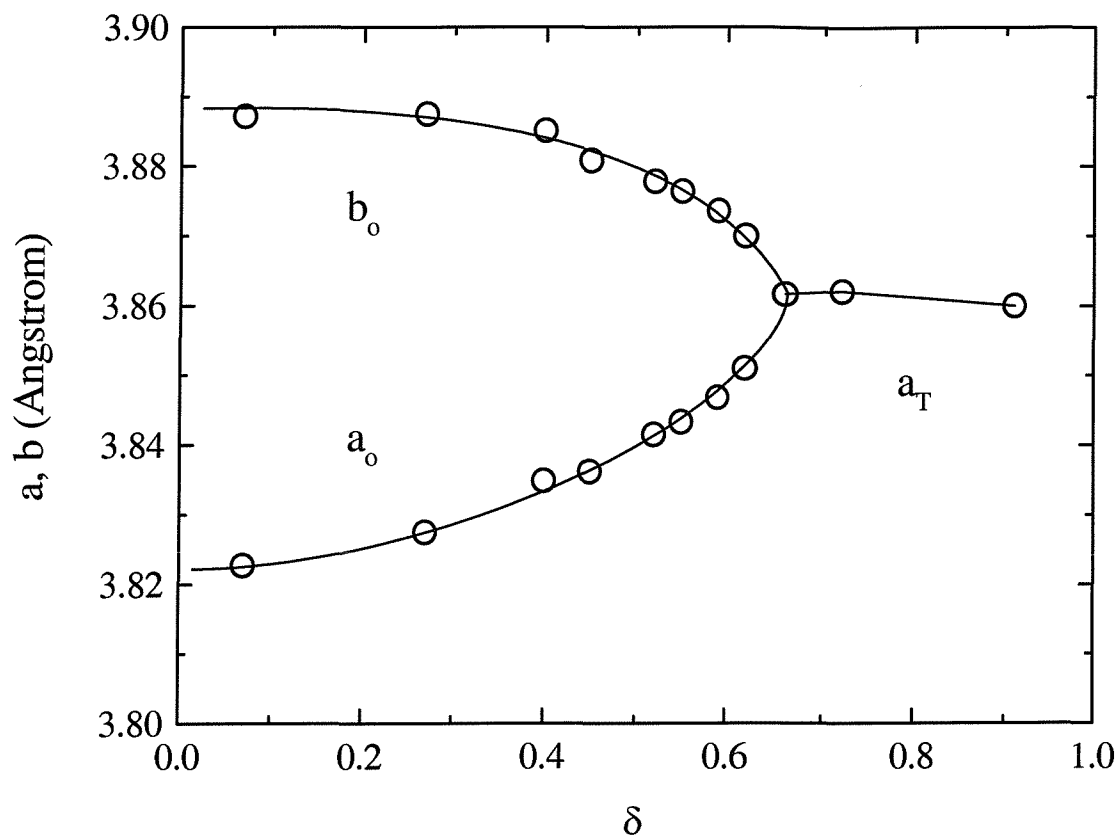


Fig. 3.2. Variation of the lattice parameters  $a_0$  and  $b_0$  in the orthorhombic phase and  $a_T$  in the tetragonal phase of  $YBa_2Cu_3O_{7-\delta}$  with the oxygen deficiency  $\delta$ , as obtained using Rietveld refinement of neutron powder diffraction by Jorgensen et al.<sup>11</sup> As can be seen at  $\delta \approx 0.65$ ,  $a_0$  and  $b_0$  collapse onto a single value  $a_T$  demonstrating the tetragonal-to-orthorhombic structural transition. The lines are guides to the eye.

orthorhombic-to-tetragonal phase transition occurs for  $\delta \approx 0.65$ , which is near the composition where superconductivity disappears. This is illustrated clearly in Fig. 3.2 where the lattice parameters along the a- and b-directions are plotted versus  $\delta$ . As can be seen, at an oxygen content of almost 6.35 the lattice parameters  $a_0$  and  $b_0$  in the orthorhombic phase collapse onto a single value  $a_T$  and the structure becomes tetragonal. The variations of the c-axis lattice parameter and the unit-cell volume with  $\delta$ , as obtained in Ref. 11, are shown in Fig. 3.3. Both parameters increase smoothly with oxygen deficiency and no measurable discontinuity at the orthorhombic-to-tetragonal transition is

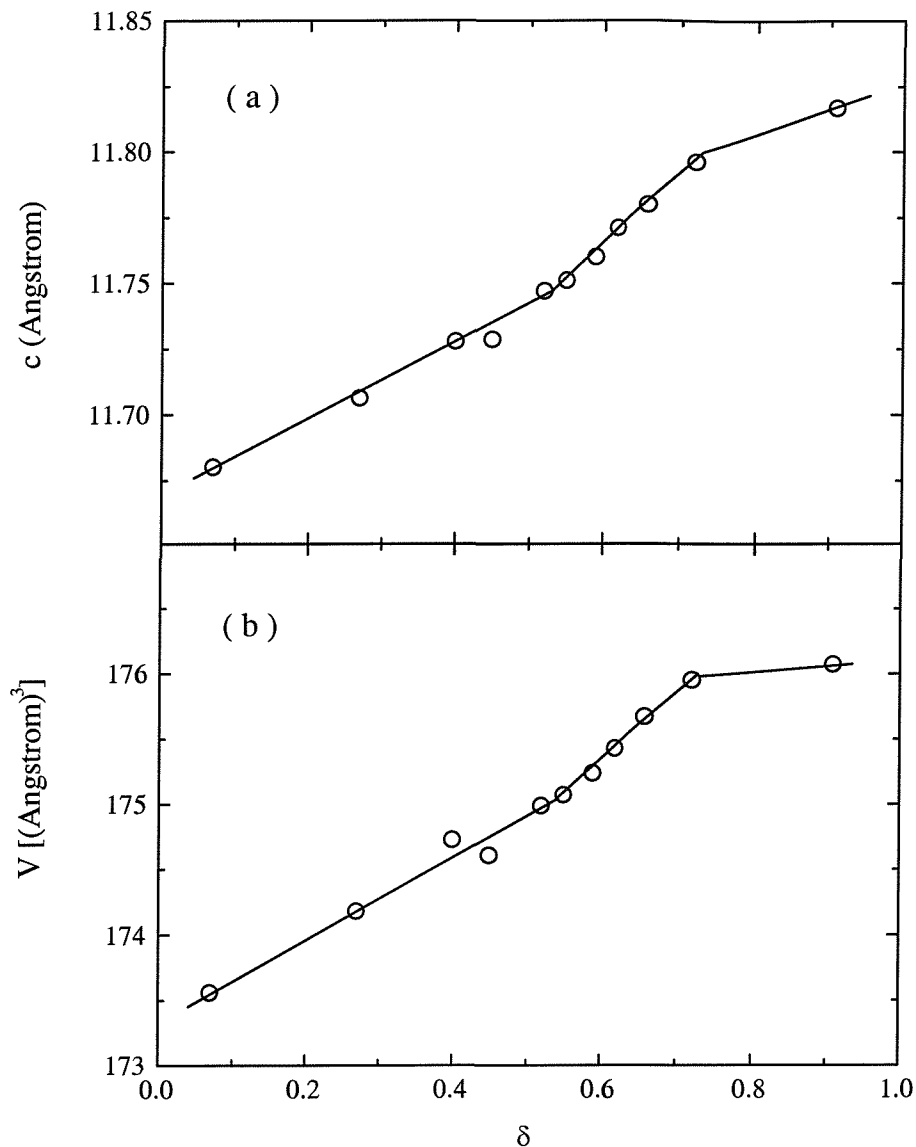


Fig. 3.3. (a) The  $c$ -axis lattice parameter and (b) the unit-cell volume of Y-123 are plotted as a function of the oxygen deficiency  $\delta$ , after Jorgensen et al.<sup>11</sup> The lines are guides to the eye.

observed.<sup>10, 11</sup>

Using Rietveld refinement of neutron powder diffraction data, Jorgensen et al.<sup>11</sup> also estimated the occupancy of all the oxygen sites. The O(2) and O(3) sites (see Fig. 3.1) were found to be fully occupied at all oxygen stoichiometries. The occupancies of the

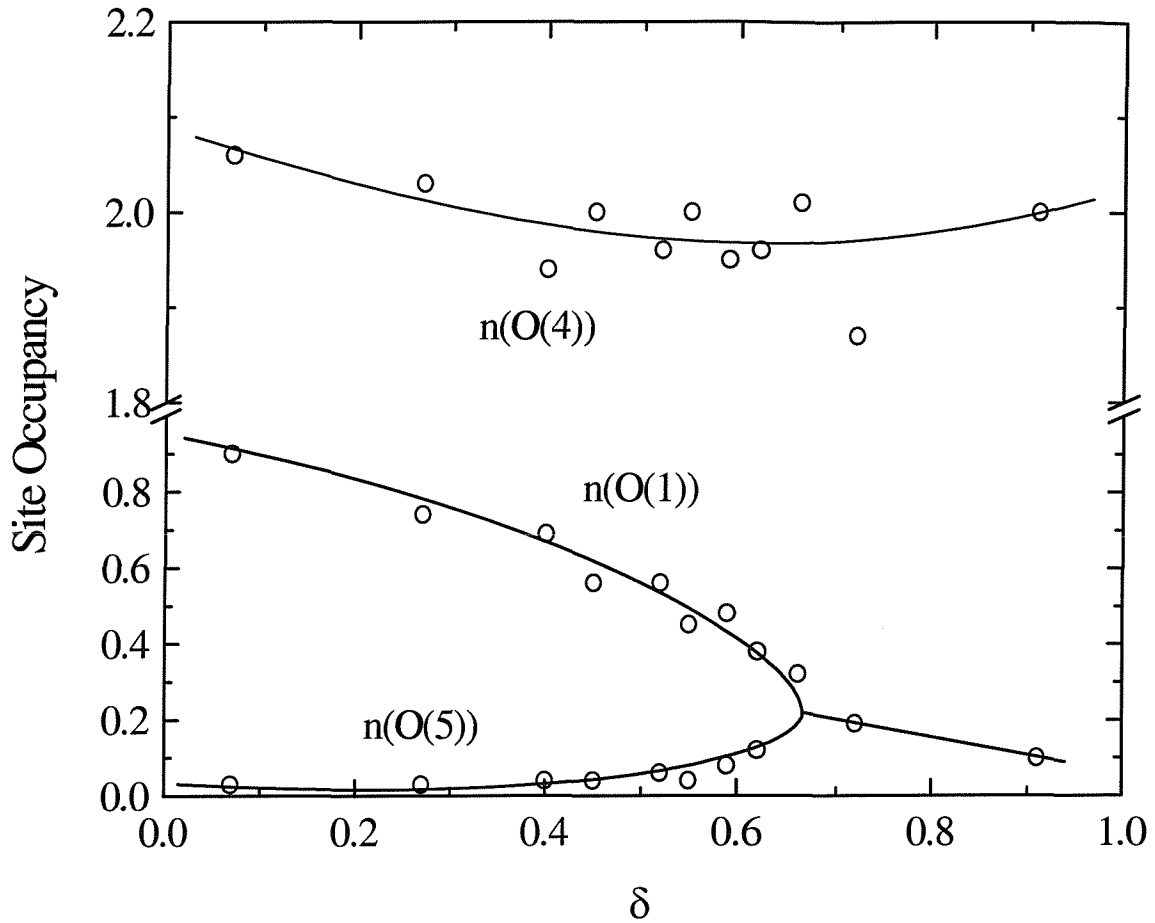


Fig. 3.4. The dependence of the site occupancy for the O(1), O(4) and O(5) oxygen sites of  $YBa_2Cu_3O_{7-\delta}$  on the oxygen deficiency  $\delta$ , as taken from Ref. 11. The lines are guides to the eye.

O(1), O(4) and O(5) sites are depicted in Fig. 3.4. As one can see, with decreasing oxygen content a continuous removal of oxygen atoms from the O(1) site and therefore from the Cu-O chains takes place.<sup>18</sup> On the other hand, the O(5) occupancy remains close to zero for a broad range of oxygen concentrations ( $7-\delta > 6.5$ ), increases rapidly close to the transition and meets with the O(1) occupancy at  $\delta \approx 0.65$ . Finally, these results also point out the presence of a small number of O(4) vacancies that reaches a smooth maximum for  $\delta$  near 0.7 (see Fig. 3.4).<sup>11</sup>

### 3.2 Effect of variations in the oxygen stoichiometry on the physical parameters of $\text{YBa}_2\text{Cu}_3\text{O}_{7-\delta}$

As mentioned in the last section, superconductivity is present in  $\text{YBa}_2\text{Cu}_3\text{O}_{7-\delta}$  for a broad range of oxygen stoichiometries ( $\delta < 0.66$ ).<sup>11</sup> The oxygen concentration is directly related to the fraction  $p$  of holes per Cu atom in the  $\text{CuO}_2$  layers and thus to the density of itinerant charge carriers. As demonstrated by Tallon et al.,<sup>19</sup> for  $\delta \leq 0.55$   $p$  can be obtained via the relation:

$$p = 0.187 - 0.21 \cdot \delta \quad (3.1)$$

Hence, one would expect the physical parameters of this compound to be directly dependent on the oxygen stoichiometry.

The most important physical parameter is the superconducting transition temperature  $T_c$ . Jorgensen et al.<sup>11</sup> have studied  $T_c$  as a function of the oxygen deficiency  $\delta$  by means of both resistivity and Meissner effect measurements. Their results are reproduced in Fig. 3.5. As can be seen, in the range  $0 < \delta < 0.2$ ,  $T_c$  decreases with increasing  $\delta$ , but the reduction is rather weak and its values remain close to  $\sim 90$  K. With further increasing  $\delta$ ,  $T_c$  drops fast until it reaches a value of  $\sim 56$  K at  $\delta \approx 0.35$ . From this point and in the region  $0.35 < \delta < 0.45$ ,  $T_c$  exhibits a plateau, which is commonly referred to as the “60 K plateau”.<sup>11, 12</sup> Finally the transition temperature starts to drop rapidly again for  $\delta > 0.45$  and reaches zero near  $\delta = 0.65$ .

However, more detailed studies of the  $T_c(\delta)$  dependence have revealed that in the region  $0 < \delta < 0.2$ ,  $T_c$  actually shows a paraboliclike dependence on  $\delta$ ,<sup>20,21</sup> as illustrated in Fig. 3.6.  $T_c$  exhibits a maximum for  $7-\delta \approx 6.94$ , which is commonly referred to as the optimal doping level.<sup>21</sup>

In a recent study by Tallon et al.,<sup>19</sup>  $T_c$  was also found to show a parabolic dependence on the hole concentration  $p$ . In this investigation it was demonstrated that  $T_c$  is maximized at  $p \approx 0.16$  and can be conveniently represented by the curve:<sup>19</sup>

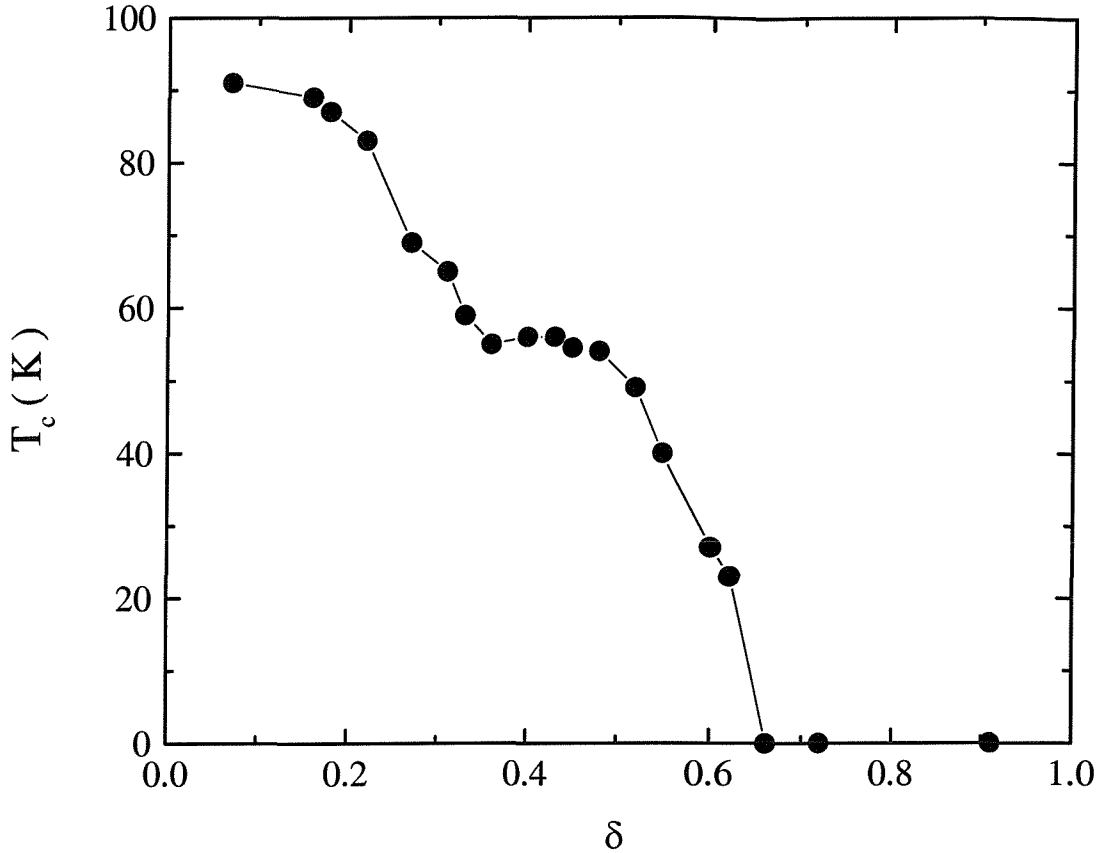


Fig. 3.5. The superconducting transition temperature of  $YBa_2Cu_3O_{7-\delta}$  is plotted as a function of oxygen deficiency, as measured by Jorgensen et al.<sup>11</sup> For  $0 < \delta < 0.2$ ,  $T_c$  decreases but only smoothly with  $\delta$ , whereas for  $0.35 < \delta < 0.45$  it shows a plateau at  $\sim 56$  K. In all other regions  $T_c$  decreases fast with increasing  $\delta$  and drops to zero at  $\delta \approx 0.65$ .

$$\frac{T_c}{T_{c,\max}} = 1 - 82.6 \cdot (p - 0.16)^2. \quad (3.2)$$

Note that the same generic parabolic dependence upon  $p$  has also been observed for  $La_{2-x}Sr_xCuO_4$ ,  $Tl_{0.5+x}Pb_{0.5-x}Sr_2Ca_{1-y}Y_yCu_2O_7$  and  $Bi_2Sr_{1-x}La_xCuO_{6+\delta}$  samples,<sup>22, 23</sup> implying a universal behaviour of the high- $T_c$  cuprates.

The high- $T_c$  superconducting oxides are layered compounds and exhibit strong electronic anisotropy. As a consequence their superconducting parameters attain different

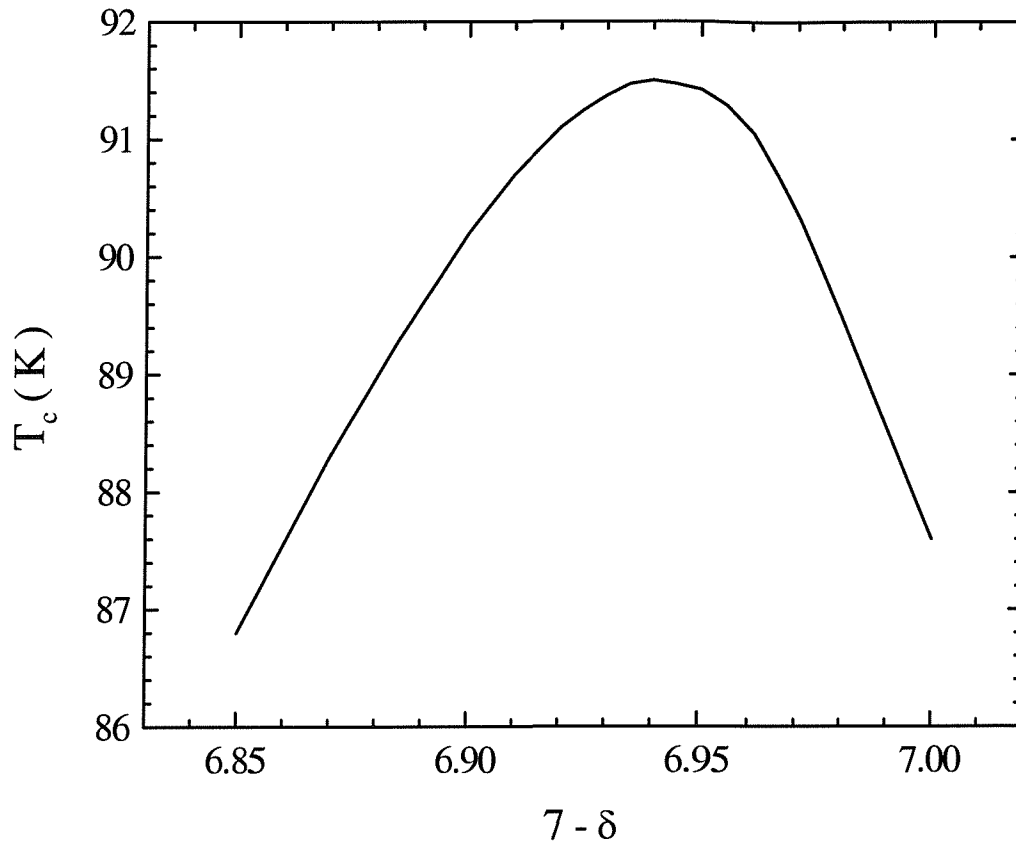


Fig. 3.6. Variation of the critical temperature with oxygen concentration in the region close to the stoichiometric state ( $6.85 < 7 - \delta < 7$ ), taken from Ref. 21. As can be seen,  $T_c$  shows an almost parabolic dependence on the oxygen content and attains a maximum for  $7 - \delta \approx 6.94$  (optimal doping).

values for different crystallographic directions.<sup>24</sup> The large out-of-plane anisotropy is attributed to the fact that the  $CuO_2$  planes, where superconductivity mainly resides, are weakly coupled with each other. It is usually expressed by a dimensionless parameter  $\gamma_{ck}$  defined as  $\gamma_{ck} \equiv (m_c/m_k)^{1/2}$  ( $k$  denotes either  $a$  or  $b$ ), where  $m_c$  and  $m_k$  are the effective masses for carrier motion in the directions transverse and parallel to the  $CuO_2$  planes respectively. It is mentioned that the anisotropy can also be determined by the ratio of the coherence lengths or the penetration depths along the  $k$  and  $c$  directions or the  $c$  and  $k$  directions respectively, i.e.,  $\gamma_{ck} = (\xi_k/\xi_c) = (\lambda_c/\lambda_k)$ .<sup>24</sup>

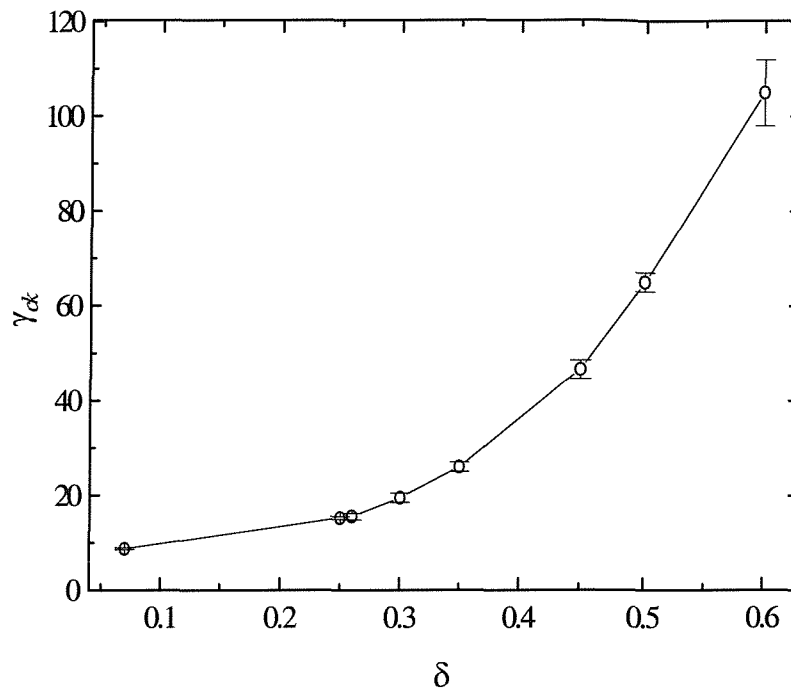


Fig. 3.7. The out-of-plane anisotropy  $\gamma_{ck}$  of  $YBa_2Cu_3O_{7-\delta}$  single crystals, as estimated using the equilibrium torque magnetometry method,<sup>1</sup> is plotted as a function of the oxygen deficiency  $\delta$ .

Experiments show that similar to the transition temperature, the anisotropy in  $YBa_2Cu_3O_{7-\delta}$  depends on the oxygen content and thus on the doping state of the superconductor. In this case, however, it has been found that  $\gamma_{ck}$  increases monotonically with increasing oxygen deficiency.<sup>25-27</sup> This behaviour is attributed to the decrease of the interlayer coupling with decreasing oxygen concentration that reduces the three-dimensional character of the superconductor. The variation of  $\gamma_{ck}$  with  $\delta$  in a broad range of oxygen contents of  $YBa_2Cu_3O_{7-\delta}$  single crystals has been studied by Chien et al.<sup>26</sup> using equilibrium torque magnetometry. Their results are illustrated in Fig. 3.7.

Changes in the oxygen stoichiometry of  $YBa_2Cu_3O_{7-\delta}$  also affect the values of the penetration depth  $\lambda$  and coherence length  $\xi$  and accordingly the lower and upper critical

<sup>1</sup> Reprinted from Physica C229, T. R. Chien, W. R. Datar, B. W. Veal, A. P. Paulikas, P. Kostic, C. Gu, and Y. Jiang, Dimensional crossover and oxygen deficiency in  $YBa_2Cu_3O_x$  single crystals, 273-279, Copyright (1994), with permission from Elsevier Science.

fields respectively. Torque magnetometry results by Janossy et al.<sup>25</sup> have shown that the in-plane London penetration depth  $\lambda_{ab}$  at  $T = 0$  K, increases from 130 nm for  $\delta = 0$  to 340 nm for  $\delta = 0.5$ . Similar is the behaviour and for the out-of-plane penetration depth  $\lambda_c$  that increases from 800 nm for  $\delta = 0$  to  $10.7 \mu\text{m}$  for  $\delta = 0.5$ . The dependence of  $\xi$  on  $\delta$  is more difficult to study. By analyzing the temperature dependence of the reversible magnetization, Ossandon et al.<sup>28</sup> were able to demonstrate that for  $\delta \leq 0.2$ , the in-plane coherence length  $\xi_{ab}$  at  $T = 0$  K, decreases with increasing oxygen content from 2.45 nm for  $7-\delta = 6.80$  to 1.64 nm for  $7-\delta = 7$ . However,  $\xi_{ab}$  was found to be nearly constant for  $\delta \leq 0.11$  in agreement with recent reports by our group.<sup>29</sup> Although the sensitivity of the technique used in Ref. 28 was not high enough to determine accurately the values of the out-of-plane coherence length  $\xi_c$ , nevertheless, an unambiguously increasing  $\xi_c$  with  $\delta$  was also observed.<sup>28</sup>

Finally, another important role of the oxygen concentration is in controlling the pinning properties of Y-123. This role is dual. As discussed in the last paragraphs, variations in the oxygen content alter the values of intrinsic parameters of the superconductor such as the anisotropy, penetration depth and coherence length. On the other hand, they also change the density of oxygen vacancies, that are created by removal of oxygen from the Cu-O chains, and thus the density of effective pinning centres.<sup>18</sup> The variations of all these parameters affect directly the pinning energy<sup>24</sup> (see also Chapter 2). It is mentioned that the influence of changes in the density of oxygen vacancies on pinning is realized only for pure enough samples, where pinning by defects other than oxygen vacancies is not important. Such defects can be copper vacancies, interstitials, voids, precipitates of other phases, screw dislocations, non-superconducting impurities introduced during the crystal growth (such as Zn, Al, Mg, Fe, La, Au, Ti, Zr, Th), correlated defects, such as twin planes and columns, as well as point defects introduced by ion irradiation.

### 3.3 Single crystals

In order to investigate reliably the physical properties of a superconductor, it is very important for the experimentalist to use high quality materials. The composition of such specimens should be precisely defined and artefacts due to the presence of multiple

phases or large scale inhomogeneities must be eliminated. Therefore, single crystalline samples are considered as ideal for such studies since they are characterized by long range structural order over macroscopic dimensions. In the case of the cuprate superconductors, however, the growth of homogeneous, pure single crystals is a rather tedious task due to the complexity of the growing procedure and the easiness of introducing impurities.<sup>30</sup> In the University of Southampton we have obtained very pure  $YBa_2Cu_3O_{7-\delta}$  single crystals from two sources: The McGill University where the crystals were grown by R. Gagnon and L. Taillefer<sup>31</sup> and the Forschungszentrum at Karlsruhe by T. Wolf.<sup>32</sup>

### 3.3.1 Single crystal growth

Due to the incongruent melting of  $YBa_2Cu_3O_{7-\delta}$ , many melt growth techniques cannot be used and bulk single crystals can be obtained only by flux methods.<sup>33</sup> In this way, in order to obtain high quality single crystals several problems have to be addressed. First, one has to avoid contamination from the crucible. This is because most crucibles are soluble in the high temperature CuO or CuO-BaO fluxes that are commonly used. Impurities from the crucible material can deteriorate significantly the quality of the single crystal, resulting in low critical temperatures and broad superconducting transitions. In addition, they impede proper oxygenation of the sample. Ytria-stabilised zirconia crucibles have been found to introduce very low levels of impurities. There are two reasons for this. First, the  $Zr^{4+}$  ion has a much higher charge compared to Cu ions in  $YBa_2Cu_3O_{7-\delta}$ , and therefore the solubility of  $Zr^{4+}$  in Cu sites should be very small. Second,  $Zr^{4+}$  is unlikely to substitute for Y since its ionic radius (0.84 Å) is much smaller than the one of  $Y^{3+}$  (1.02 Å).<sup>33</sup>

Whilst growing samples, one also has to take into account the desired size of the produced single crystals. The latter depends on the cooling rate, the temperature gradient maintained in the crucible<sup>34</sup> and the soaking time.<sup>33</sup> Low cooling rates, large temperature gradient and long soaking times result in thick crystals. Nevertheless, in this way one increases the impurity level from the crucible material.<sup>33, 35</sup> In addition, large crystals are difficult to oxygenate uniformly, and they may have broad superconducting transitions.<sup>33</sup> On the other hand, reasonably big crystals are advantageous since due to their size the sensitivity of the measurements can be significantly increased, thus extending the range of

experiments that can be subjected to. Moreover they can be handled more easily. Thus in practice, depending on the necessities of each experiment a compromise between the “cooking” variables has to be achieved.

The  $YBa_2Cu_3O_{7-\delta}$  single crystals investigated in this thesis were grown in yttria-stabilised zirconia crucibles. The crystals from McGill University were grown by a conventional self-flux method,<sup>33</sup> starting with powders of  $Y_2O_3$  (99.9999%),  $BaCO_3$  (99.999%) and  $CuO$  (99.9999%), mixed in a molar ratio Y:Ba:Cu of 1:18:45. The crystal growth is a complicated, multiple-stage process.<sup>33</sup> Initially the crucible is heated up to  $\sim 870$  °C and kept at this temperature for 4 hours in order to evaporate carbonates. Subsequently the temperature is increased to  $\sim 1010$  °C where it is held for another 4 hours before the crucible is cooled down to 990 °C. Then soaking takes place for 8-16 hours and afterwards the crucible is cooled to 950-970 °C at a rate of 0.3-0.8 °C/hour. Finally the flux is poured out and the crucible is cooled to room temperature at a rate of 150 °C/hour. The single crystals produced in this way have a very low oxygen content and are not superconducting. For this reason, they are subsequently annealed at 500 °C (a temperature far below the tetragonal-to-orthorhombic phase transition) for 6 days in an oxygen atmosphere and finally quenched to room temperature. This treatment results in a high oxygen content ( $7-\delta = 6.934$ ),  $T_c$  above 92.8 K and a sharp superconducting transition with a width of less than 0.3 K. The crystals from the Forschungszentrum at Karlsruhe were grown by the slow cooling method.<sup>32</sup> Initially powders of  $Y_2O_3$ ,  $BaCO_3$  and  $CuO$  with a purity better than 99.99% were mixed and calcined several times in air between 850 and 880 °C. Single crystals were grown in the temperature range between 1020 and 935.7 °C using cooling rates of 0.8-1 °C/hour. At 935.7 °C the remaining flux was separated from the crystals by pouring off the flux into a porcelain capsule located inside the furnace. The crystals were afterwards cooled to room temperature and further annealed in a tubular furnace under flowing oxygen. The growing procedure was completed by a second annealing at 175 bar of flowing oxygen for about 300 hours that gives an oxygen content of  $7-\delta \geq 6.993$ .

### 3.3.2 Twin boundaries

A very common type of defects present in  $YBa_2Cu_3O_{7-\delta}$  are the so-called twin planes or twin boundaries (see Fig. 3.8). They are planar defects and are produced



Fig. 3.8. The surface of a twinned  $\text{YBa}_2\text{Cu}_3\text{O}_{7-\delta}$  single crystal as seen using a polarized light microscope. The straight black lines represent the two sets of twin planes formed in the directions  $[110]$  and  $[1-10]$ .

spontaneously during the structural transition from the tetragonal high temperature phase to the orthorhombic low temperature phase, in order to accommodate the crystal mismatch accompanying the reduction of the symmetry of the Bravais lattice.<sup>36</sup> This occurs when for example during annealing the single crystal is cooled through the temperature that corresponds to the tetragonal-to-orthorhombic phase transition. The resulting twin planes are formed in the  $[110]$  and  $[1-10]$  crystallographic directions, and separate regions where the Cu-O chains run alternately along directions perpendicular to each other. Note that the appearance of the Cu-O chains is responsible for the elongation and contraction of the b- and a-axis respectively as compared to the tetragonal phase, leading to internal stresses. A diagrammatic representation of a twin plane is shown in Fig. 3.9. The structural nature of the twin boundaries has been investigated using electron microscopy techniques (see e.g. Ref. 37) as well as high-resolution x-ray diffractometry (see e.g. Ref. 38). In the last investigation it was shown that the effective wall thickness of a twin boundary is of the order of 7 Å. The average distance between twin planes varies from sample to sample and for our single crystals it ranges from  $\sim 5 \mu\text{m}$  to  $\sim 100 \text{ nm}$ .

Twin planes influence both the superconducting and pinning properties of  $\text{YBa}_2\text{Cu}_3\text{O}_{7-\delta}$ . They are likely to affect the critical temperature,<sup>39, 40</sup> as well as the vortex

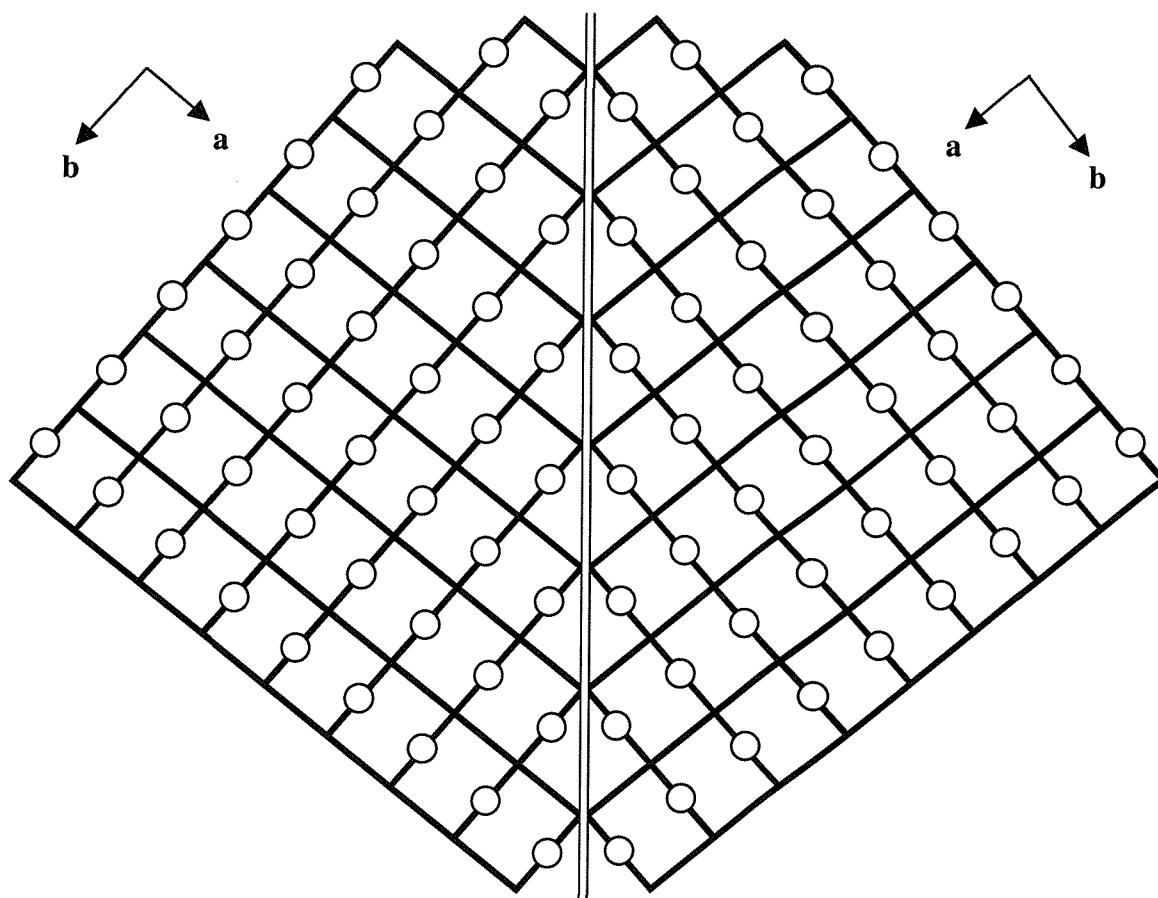


Fig. 3.9. Schematic representation of the formation of a twin boundary in Y-123. For simplicity we consider the case corresponding to  $\delta = 0$ . The rectangular lattice represents the Cu-O sublattice in the basal plane, with the open circles showing chain-oxygen atoms. The copper atoms are located at the corners. The twin plane (shown by the two parallel lines) is the interface between the two illustrated domains where the a- and b-axis exchange directions. Note that for better presentation the difference between the lengths of the unit vectors along the a- and b-axis has been exaggerated.

dynamics since due to their planar nature can act as correlated pinning centres for vortices.<sup>24</sup> The latter effect, however, is complicated and still not very well understood. Although at high temperatures twins can lead to increased pinning by either reducing the effect of thermal fluctuations,<sup>41</sup> or impeding vortex motion across them,<sup>42</sup> at lower temperatures they can become channels for easy flux penetration thus reducing pinning.<sup>42, 43</sup> In addition, the strain fields associated with the twins result in accumulation

of atomic defects and impurities, leading to attraction of vortices in these regions.<sup>44</sup> Therefore, in order to avoid the complicated consequences from their presence, twins have to be removed. This can be succeeded by applying a uniaxial compressive stress along the a- or b-directions of the perovskite lattice in a properly controlled oxygen atmosphere, which is required in order to maintain the composition.<sup>45</sup> The compressive stress induces jumps of oxygen atoms that transform a Cu-O-Cu arrangement oriented along the compression axis into a Cu-Cu arrangement. This transforms a b-axis into an a-axis thus leading to the disappearance of the twins.<sup>46</sup> Such jumps are energetically favourable since they relieve the applied stress by shortening the specimen.<sup>46</sup> In order to achieve a high oxygen mobility, detwinning usually occurs at elevated temperatures (400 °C – 550 °C). In this way one can succeed in a high rate of twin boundary displacement and avoid the use of rather high pressures.

### 3.3.3 Investigated samples

The details of the  $YBa_2Cu_3O_{7-\delta}$  single crystals investigated in the present thesis are shown in table 3.1. In this table one can find the oxygen content, the conditions (temperature and pressure) of the annealing treatment to which each crystal was subjected after growth, the dimensions, the superconducting transition temperature  $T_c$ , as well as the defect status and origin of each sample. In all cases the oxygen content was determined from eq. (6) of Ref. 47 that relates the oxygen concentration with the annealing pressure and temperature. Crystal thicknesses were estimated using the mass and the theoretical density of 6.8 g/cm<sup>3</sup>. For samples DT2, DT1B, DT1C, T1A, T1B and T1C,  $T_c$  was determined from the onset of diamagnetic signal in a field of 1 mT after zero field cooling the superconductor. For all other samples,  $T_c$  was defined as the mid point of the temperature range over which the in-phase component of the ac susceptibility in a field of 0.03 mT varied from 10 % to 90 % of its saturation value.

Detwinning of our crystals was achieved by applying a uniaxial pressure of ~ 50 MPa at a temperature of 550 °C in air for 15 min. The detwinned samples were then reoxygenated for 1 day at 500 °C in flowing oxygen and then quenched to room temperature. After detwinning polarised light microscopy did not show any evidence for the presence of twins planes. The quality of the detwinning process is also demonstrated by the absence in the detwinned samples of vortex channelling and the sharp dip in the

angular dependence of the resistivity for fields along the c-axis, effects that are both present in even sparsely twinned samples.<sup>29, 43, 48</sup> Columnar defects were created by 2.2 GeV Au ion irradiation at the Gesellschaft für Schwerionenforschung mbH, Darmstadt (more details concerning the irradiation procedure can be found in Ref. 49). The beam was purposely directed slightly away ( $\sim 1^\circ$ ) from the c-axis in order to avoid channelling.

Sample	$7-\delta$	$T_{\text{anneal}}$ ( $^{\circ}\text{C}$ )	$P(\text{O}_2)$ (bar)	$l \times w \times t$ ( $\text{mm}^3$ )	$T_c$ (K)	Defect status	Origin
U1	6.550	750	1	$0.98 \times 0.72 \times 0.07$	62.8	untwinned	McGill University
ZX	6.760	495	0.026	$2.43 \times 1.59 \times 0.24$	71.7	untwinned	Forschungszentrum Karlsruhe
D1	6.908	525	1	$1.07 \times 0.86 \times 0.08$	92.7	detwinned	McGill University
DT2	6.934	500	1	$1.04 \times 0.80 \times 0.05$	92.5	detwinned	McGill University
D2	6.934	500	1	$1.69 \times 1.08 \times 0.09$	92.8	detwinned	McGill University
DT1B	6.946	485	1	$1.04 \times 0.80 \times 0.52$	92.7	detwinned	McGill University
DT1C	6.970	450	1	$1.04 \times 0.80 \times 0.52$	92.3	detwinned	McGill University
D3	6.970	450	1	$1.29 \times 1.25 \times 0.08$	91.7	detwinned	McGill University
ZY	6.999	400	370	$2.16 \times 0.67 \times 0.24$	88.8	untwinned	Forschungszentrum Karlsruhe
TW1	6.934	500	1	$0.78 \times 0.59 \times 0.09$	92.6	sparsely twinned	McGill University
T1A	6.960	625	100	$0.77 \times 0.66 \times 0.09$	92.9	sparsely twinned	McGill University
T1B	6.948	650	100	$1.03 \times 0.77 \times 0.09$	92.7	sparsely twinned	McGill University
T1C	6.918	700	100	$0.74 \times 0.66 \times 0.09$	92.5	sparsely twinned	McGill University
DN	6.970	450	1	$1.37 \times 0.85 \times 0.03$	89.6	densely twinned	Forschungszentrum Karlsruhe
AW	6.970	450	1	$1.40 \times 0.75 \times 0.02$	90.4	columns ( $B_{\phi}=0.1\text{T}$ )	Forschungszentrum Karlsruhe
AH	6.970	450	1	$1.26 \times 0.57 \times 0.02$	90.4	columns ( $B_{\phi}=3\text{T}$ )	Forschungszentrum Karlsruhe

Table 3.1. Details of the single crystals studied in this thesis.

## References

- <sup>1</sup> J. G. Bednorz and K. A. Müller, Z. Phys. B64, 189 (1986); J. G. Bednorz, K. A. Müller and M. Takashige, Science 236, 73 (1987)
- <sup>2</sup> S. Uchida, H. Takagi, K. Kitazawa, and S. Tanaka, Jpn. J. Appl. Phys. 26, L1 (1987)
- <sup>3</sup> M. K. Wu, J. R. Ashburn, C. J. Torng, P. H. Hor, R. L. Meng, L. Gao, Z. J. Huang, Y. Q. Wang, and C. W. Chu, Phys. Rev. Lett. 58, 908 (1987)
- <sup>4</sup> S. Hikami, T. Hirai, and S. Kagohima, Jpn. J. Appl. Phys. 26, L314 (1987)
- <sup>5</sup> R. M. Hazen, L. W. Finger, R. J. Angle, C. T. Prewitt, W. L. Ross, H. K. Mao, C. S. Hadjidiacos, P. H. Hor, R. L. Meng, and C. W. Chu, Phys. Rev. B 35, 7238 (1987)
- <sup>6</sup> Y. Lepage, W. R. McKinnon, J. M. Tarascon, L. H. Greene, G. W. Hull, and D. M. Hwang, Phys. Rev. B 35, 7245 (1987)
- <sup>7</sup> R. Beyers, G. Lim, E. M. Engler, V. Y. Lee, M. L. Ramirez, R. J. Savoy, R. D. Jacowitz, T. M. Shaw, S. La Placa, R. Boehme, C. C. Tsuei, S. I. Park, M. W. Shafer, and W. J. Gallagher, Appl. Phys. Lett. 51, 614 (1987)
- <sup>8</sup> J. J. Capponi, C. Chaillout, A. W. Hewat, P. Lejay, M. Marezio, N. Nguyen, B. Raveau, J. L. Soubeyroux, J. L. Tholence, and R. Tournier, Europhys. Lett. 3, 1301 (1987)
- <sup>9</sup> F. Beech, S. Miraglia, A. Santoro, and R. S. Roth, Phys. Rev. B 35, R8778 (1987)
- <sup>10</sup> J. D. Jorgensen, M. A. Beno, D. G. Hinks, L. Soderholm, K. J. Volin, R. L. Hitterman, J. D. Grace, I. K. Schuller, C. U. Segre, K. Zhang, and M. S. Kleefisch, Phys. Rev. B 36, 3608 (1987)
- <sup>11</sup> J. D. Jorgensen, B. W. Veal, A. P. Paulikas, L. J. Nowicki, G. W. Crabtree, H. Claus, and W. K. Kwok, Phys. Rev. B 41, 1863 (1990)
- <sup>12</sup> R. J. Cava, A. W. Hewat, E. A. Hewat, B. Batlogg, M. Marezio, K. M. Rabe, J. J. Krajewski, W. F. Peck Jr., and L. W. Rupp Jr., Physica C165, 419 (1990)
- <sup>13</sup> P. P. Edwards and C. N. R. Rao, Chemistry in Britain 30, 722 (1994); A. R. Armstrong and W. I. F. David, *ibid.* 30, 727 (1994)
- <sup>14</sup> M. A. Beno, L. Soderholm, D. W. Capone II, D. G. Hinks, J. D. Jorgensen, J. D. Grace, I. K. Schuller, C. U. Segre, and K. Zhang, Appl. Phys. Lett. 51, 57 (1987)
- <sup>15</sup> A. W. Sleight, Science 242, 1519 (1987)
- <sup>16</sup> V. Z. Kresin and S. A. Wolf, Phys. Rev. B 46, 6458 (1992)

- <sup>17</sup> J. L. Tallon, C. Bernhard, U. Binniger, A. Hofer, G. V. M. Williams, E. J. Ansaldo, J. I. Budnick, and Ch. Niedermayer, *Phys. Rev. Lett.* 74, 1008 (1995) and references therein.
- <sup>18</sup> Note that in this way one also creates oxygen vacancies that can consist effective pinning centres for the flux line lattice (see e.g. C. J. van der Beek and P. H. Kes, *Phys. Rev. B* 43, 13032 (1991)).
- <sup>19</sup> J. L. Tallon, C. Bernhard, H. Shaked, R. L. Hitterman, and J. D. Jorgensen, *Phys. Rev. B* 51, R12911 (1995)
- <sup>20</sup> H. Claus, M. Braun, A. Erb, K. Röhberg, B. Runtsch, H. Wühl, G. Bräuchle, P. Schweib, G. Müller-Vogt, and H. v. Löhneysen, *Physica C* 198, 42 (1992)
- <sup>21</sup> R. Hauff, V. Breit, H. Claus, D. Herrann, A. Knierim, P. Schweiss, H. Wühl, A. Erb, and G. Müller-Vogt, *Physica C* 235-240, 1953 (1994); V. Breit, P. Schweiss, R. Hauff, H. Wühl, H. Claus, H. Rietschel, A. Erb, and G. Müller-Vogt, *Phys. Rev. B* 52, R15727 (1995)
- <sup>22</sup> M. R. Presland, J. L. Tallon, R. G. Buckley, R. S. Liu, and N. E. Flower, *Physica C* 176, 95 (1991)
- <sup>23</sup> B. C. Sales and B. C. Chakoumakos, *Phys. Rev. B* 43, 12994 (1991)
- <sup>24</sup> G. Blatter, M. V. Feigel'man, V. B. Geshkenbein, A. I. Larkin and V. M. Vinokur, *Rev. Mod. Phys.* 66, 1125 (1994); H. E. Brandt, *Rep. Prog. Phys.* 58, 1465 (1995)
- <sup>25</sup> B. Janossy, D. Prost, S. Pekker, and L. Fruchter, *Physica C* 181, 51 (1991)
- <sup>26</sup> T. R. Chien, W. R. Datar, B. W. Veal, A. P. Paulikas, P. Kostic, C. Gu, and Y. Jiang, *Physica C* 229, 273 (1994)
- <sup>27</sup> S. Kokkaliaris, K. Deligiannis, M. Oussena, A. A. Zhukov, P. A. J. de Groot, R. Gagnon, and L. Taillefer, *Supercond. Sci. Technol.* 12, 690 (1999)
- <sup>28</sup> J. G. Ossandon, J. R. Thompson, D. K. Christen, B. C. Sales, H. R. Kercher, J. O. Thomson, Y. R. Sun, K. W. Lay, and J. E. Tkaczyk, *Phys. Rev. B* 45, 12534 (1992)
- <sup>29</sup> R. M. Langan, S. N. Gordeev, P. A. J. de Groot, A. G. M. Jansen, R. Gagnon, and L. Taillefer, *Phys. Rev. B* 58, 14548 (1998)
- <sup>30</sup> C. N. Rao, R. Nagarajan, and R. Vijayaraghavan, *Supercond. Sci. Technol.* 6, 1 (1993)
- <sup>31</sup> R. Gagnon, M. Oussena, and M. Aubin, *J. Cryst. Growth* 114, 186 (1991); R. Gagnon, C. Lupien, and L. Taillefer, *Phys. Rev. B* 50, 3458 (1994)

- <sup>32</sup> Th. Wolf, W. Goldacker, B. Obst, G. Roth, and R. Flükinger, *J. Cryst. Growth* 96, 1010 (1989); H. Küpfer, Th. Wolf, C. Lessing, A. A. Zhukov, X. Lançon, R. Meier-Hirmer, W. Schauer, and H. Wühl, *Phys. Rev. B* 58, 2886 (1998)
- <sup>33</sup> R. Liang, P. Dosanjh, D. A. Bonn, D. J. Baar, J. F. Carolan, and W. N. Hardy, *Physica C* 195, 51 (1992)
- <sup>34</sup> During crystal growth it is worth maintaining a temperature gradient, i.e., keeping one side of the crucible warmer than the other. In this way and for appropriate temperature gradient values, the crystals, that usually tend to grow in large cavities in the flux, can be more easily removed from the solidified flux.
- <sup>35</sup> W. Sadowski and H. J. Scheel, *J. Less-Common Met.* 150, 219 (1989)
- <sup>36</sup> G. Roth, D. Ewert, G. Heger, M. Hervieu, C. Michel, B. Raveau, F. D'Yvoire, and A. Revcolevschi, *Z. Phys. B* 69, 21 (1987); G. Van Tendeloo, H. W. Zandbergen, and S. Amelinckx, *Solid State Commun.* 63, 389 (1987); Y. Zhu, M. Suenaga, and J. Taftø, *Philos. Mag. A* 67, 1057 (1993)
- <sup>37</sup> A. Rosova, C. Boulesteix, and I. Vavra, *Physica C* 214, 247 (1993) and references therein
- <sup>38</sup> J. Chrosch and E. K. H. Salje, *Physica C* 225, 111 (1994)
- <sup>39</sup> I. N. Khlyustikov and A. I. Buzdin, *Adv. Phys.* 36, 271 (1987); A. A. Abrikosov, A. I. Buzdin, M. L. Kubic, and D. A. Kuptsov, *Int. J. Mod. Phys. B* 1, 1045 (1988); M. M. Fang, V. G. Kogan, D. K. Finnemore, J. R. Clem, L. S. Chumbley, and D. E. Farrell, *Phys. Rev. B* 37, 2334 (1988)
- <sup>40</sup> Yu. A. Krotov and I. M. Suslov, *Physica C* 213, 421 (1993)
- <sup>41</sup> G. W. Crabtree, J. Z. Liu, A. Umezawa, W. K. Kwok, C. H. Sowers, S. K. Malik, B. W. Veal, D. J. Lam, M. B. Brodsky, and J. W. Downey, *Phys. Rev. B* 36, 4021 (1987); W. K. Kwok, U. Welp, G. W. Crabtree, K. G. Vandervoort, R. Hulscher, and J. Z. Liu, *Phys. Rev. Lett.* 64, 966 (1990); J. N. Li, A. A. Menovsky, and J. J. M. Franse, *Phys. Rev. B* 48, 6612 (1993); A. A. Zhukov, H. Küpfer, G. Perkins, L. F. Cohen, A. D. Caplin, S. A. Klestov, H. Claus, V. I. Voronkova, T. Wolf, and H. Wühl, *ibid.* 51, 12704 (1995)
- <sup>42</sup> C. A. Durán, P. L. Gammel, R. Wolfe, V. J. Fratello, D. J. Bishop, J. P. Rice, and D. M. Ginsberg, *Nature (London)* 357, 474 (1992)

- <sup>43</sup> M. Oussena, P. A. J. de Groot, S. J. Porter, R. Gagnon, and L. Taillefer, *Phys. Rev. B* 51, 1389 (1995); A. A. Zhukov, H. Küpfer, H. Claus, H. Wühl, M. Kläser, and G. Müller-Vogt, *Phys. Rev. B* 52, R9871 (1995)
- <sup>44</sup> M. Sarikaya, R. Kikuchi, and I. A. Aksay, *Physica C* 152, 161 (1988); G. Blatter, J. Rhyner, and V. M. Vinokur, *Phys. Rev. B* 43, 7826 (1991);
- <sup>45</sup> H. Schmid, E. Burkhardt, B. N. Sun, and J. P. Rivera, *Physica C* 157, 555 (1989); U. Welp, M. Grimsditch, H. You, W. K. Kwok, M. M. Fang, and G. W. Crabtree, *ibid.* 161, 1 (1989)
- <sup>46</sup> G. Van Tendeloo, D. Broddin, H. W. Zandbergen, and S. Amelinckx, *Physica C* 167, 627 (1990)
- <sup>47</sup> D. J. L. Hong and D. M. Smyth, *J. Am. Ceram. Soc.* 74, 1751 (1991)
- <sup>48</sup> R. Langan, S. N. Gordeev, M. Oussena, P. A. J. de Groot, A. G. M. Jansen, R. Gagnon, and L. Taillefer, *Physica C* 313, 294 (1999)
- <sup>49</sup> A. A. Zhukov, G. Perkins, L. F. Cohen, A. D. Caplin, H. Küpfer, T. Wolf, and G. Wirth, *Phys. Rev. B* 58, 8820 (1998)

---

# Chapter 4

---

## Experimental techniques

The work presented in this thesis has been performed using two different experimental arrangements. These are a vibrating sample and a torque magnetometer. This chapter contains a description of the physical principles upon which these techniques are based and provides with the specific technical details of the set-ups used in our experiments.

### 4.1 Vibrating sample magnetometer

#### 4.1.1 Physical principles

The vibrating sample magnetometer (VSM) has been used for magnetic measurements for over forty years.<sup>1</sup> The operation of the VSM is based on an induction technique, which, with the help of a set of pick-up coils, detects the ac field produced by the magnetic moment of a test sample that is vibrated in a controlled manner in an applied magnetic field. In this way the total magnetic moment of the sample can be determined, as described in more detail in the following paragraphs.

The VSM coil system usually consists of a pair of pick-up coils that are connected series-opposing. If the coils are properly matched, then this configuration eliminates the influence of the background noise due to magnetic field instability or mechanical vibrations of the magnet, or variations in any stray magnetic fields. In general, the electromotive force (emf),  $\varepsilon$ , induced in a pick-up coil assembly (see Fig. 4.1) due to an oscillating sample moment is given by:

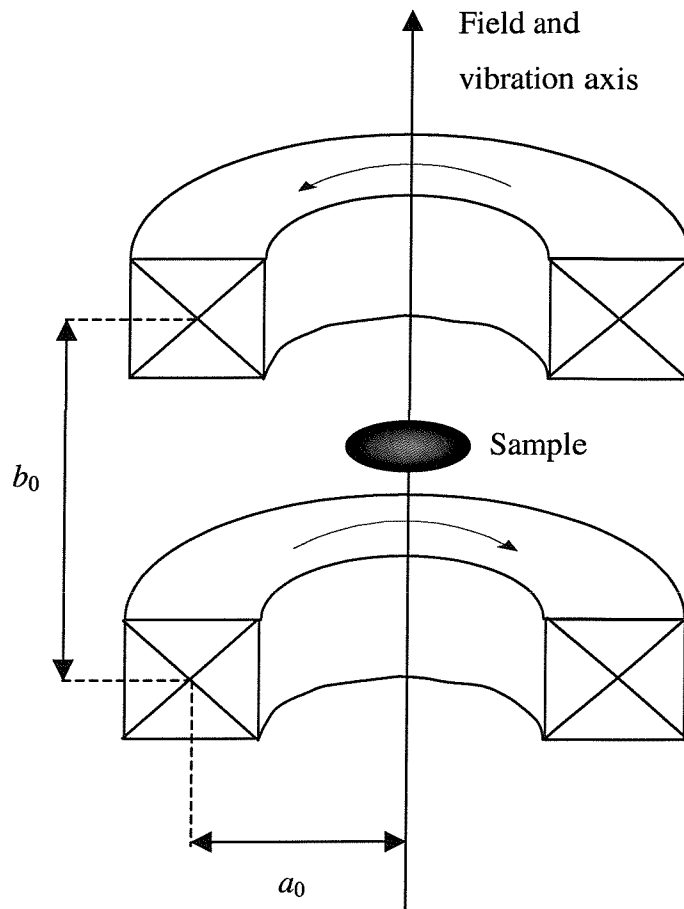


Fig. 4.1. Schematic illustration of the system sample – pick-up coil set in the VSM.

$$\varepsilon = -\frac{d\Phi}{dt} \quad (4.1)$$

where  $\Phi$  is the magnetic flux induced by the sample in the detection coil array. If the sample is homogeneously magnetized and small enough to be considered as a dipole, then application of the reciprocity theorem gives for the net flux of the dipole:<sup>2,3</sup>

$$I\Phi = \int \mathbf{M} \cdot \mathbf{B} dV \quad (4.2)$$

with the integral extending over the sample volume. In this equation  $\mathbf{M}$  is the sample magnetization vector and  $\mathbf{B}$  the field vector produced by the pick-up coil carrying a current  $I$ , at the position of the sample. Combination of eqs. (4.1) and (4.2) gives for the induced emf:

$$\varepsilon = -\frac{d}{dt} \left[ \int \frac{\mathbf{M} \cdot \mathbf{B}}{I} dV \right] \quad (4.3)$$

The position of the sample along the vibration axis ( $z$ -axis) can be written as:

$$z(t) = z_0 + z_a \cos(\omega t) \quad (4.4)$$

where  $z_0$  and  $z_a$  are the mean point and amplitude of sample oscillation respectively,  $\omega = 2\pi f$ , and  $f$  the frequency of oscillation. Thus for vibrations along the  $z$ -axis, eq. (4.3) becomes:

$$\varepsilon = z_a \omega \sin(\omega t) \int M_z \frac{\partial}{\partial z} \left( \frac{B_z}{I} \right) dV = z_a \omega \sin(\omega t) \int M_z G(z) dV \quad (4.5)$$

with  $G(z) = \frac{\partial}{\partial z} \left( \frac{B_z}{I} \right)$  the so-called sensitivity function,<sup>4, 5</sup> that represents the dependence of the VSM output on the position of the specimen along the  $z$ -axis. If the sample is uniformly magnetized and oscillates with a small amplitude along the  $z$ -axis in a homogeneous field, then within the dipole approximation, expansion of  $G(z)$  to a power series about the equilibrium position  $z_0$  gives for  $\varepsilon$ :<sup>4, 5</sup>

$$\varepsilon \approx z_a \omega m G(z_0) \sin(\omega t) \quad (4.6)$$

with  $G(z_0)$  being the zero order term. Thus the induced emf is proportional to the vibration amplitude and frequency, the magnetic moment  $m$  and the sensitivity function. Consequently, in order to increase the sensitivity of the measurement an optimum detection coil configuration should be designed so as to attain as high and  $z$  independent  $G(z)$  values as possible.

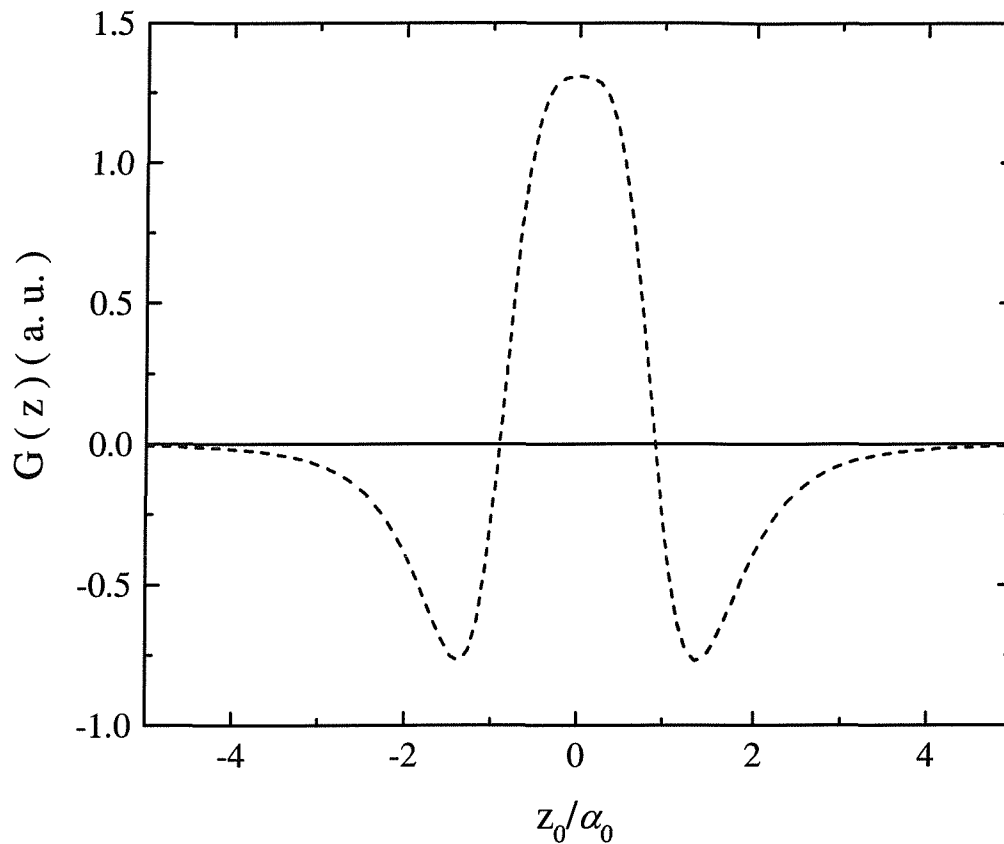


Fig. 4.2. The sensitivity function normalized by its value at  $z_0 = 0$  is plotted versus  $z_0$  for the coil geometry of Fig. 4.1.  $G(z)$  was calculated for the case of a dipole parallel to the  $z$ -axis and  $b_0 = 1.7a_0$ . The point  $z_0 = 0$  was taken mid-way between the coils.

The typical form of the sensitivity function for a pick-up coil system such as the one shown in Fig. 4.1 is illustrated in Fig. 4.2. As can be seen,  $G(z)$  attains a maximum at  $z_0 = 0$ . Hence, for best performance the specimen should be fixed to oscillate around this point.

From eq. (4.6) it is obvious that in order to obtain absolute values for the magnetic moment, one should be able to estimate the exact values of  $G(z_0)$ . Although this quantity can be calculated in closed form for several coil arrangements, it is usually more accurate to use a comparison method, i.e., to calibrate the signal from the pick-up coils against a sample of known magnetic properties. One of the most commonly used calibration materials is Nickel, mainly because it can be obtained in high purity and has a small

saturation field. One could also use a superconductor, such as Niobium, in the Meissner state where the susceptibility is equal to minus one.

On calibrating the system, considerable care should be taken of parameters that can introduce errors.<sup>6</sup> One of them is limitations of the point dipole approximation. To minimize this error both the calibration and test samples should remain sufficiently small in comparison to the pick-up coils. The stability of the applied magnetic field can also affect the calibration. For this reason it is suggested the use of ferromagnetic materials in saturation. In this case, however, a significant problem that may arise is the difficulty in determining the exact value of the saturation field that might further depend on the mechanical history of the sample. Therefore, one should take considerable care that the calibrants are not subjected to any mechanical stresses, whereas frequent cleaning of the material and checking of the saturation field are strongly recommended. Another important parameter that one has to take into account is the magnitude of the signal. If the measured moment is much larger than that of the calibrant, nonlinearity of components within the audio amplification can result in errors. Finally, the position of the sample within the coil system also affects the calibration via its effect on the sensitivity function.

### 4.1.2 Technical details

Our laboratory at the University of Southampton is equipped with a commercial Oxford Instrument VSM (model 3001).<sup>7</sup> It allows us to measure the magnetic moment of a sample as a function of time, field and temperature, for fields up to 12 T in a broad temperature range (1.5 K – 300 K). A schematic diagram of this VSM is shown in Fig. 4.3. The most important components of the system and their functions can be briefly outlined as follows.<sup>7</sup>

**Cryostat:** The VSM cryostat is of a vacuum insulated (vacuums of better than  $10^{-4}$  torr can be succeeded), all metal construction with intermediate temperature radiation shielding that is kept cold by a liquid nitrogen reservoir. The cryostat contains two vessels that are filled with liquid helium and nitrogen as can be seen from Fig. 4.3. The outer surfaces of both vessels as well as the inside surface of the cryostat are covered with multilayer superinsulation to reduce emissivity. To avoid pressure build up in the event of a cryogenic leak to the vacuum space, the outer vacuum case of the dewar is fitted with an evacuation valve incorporating a pressure relief safety feature. For the construction of the

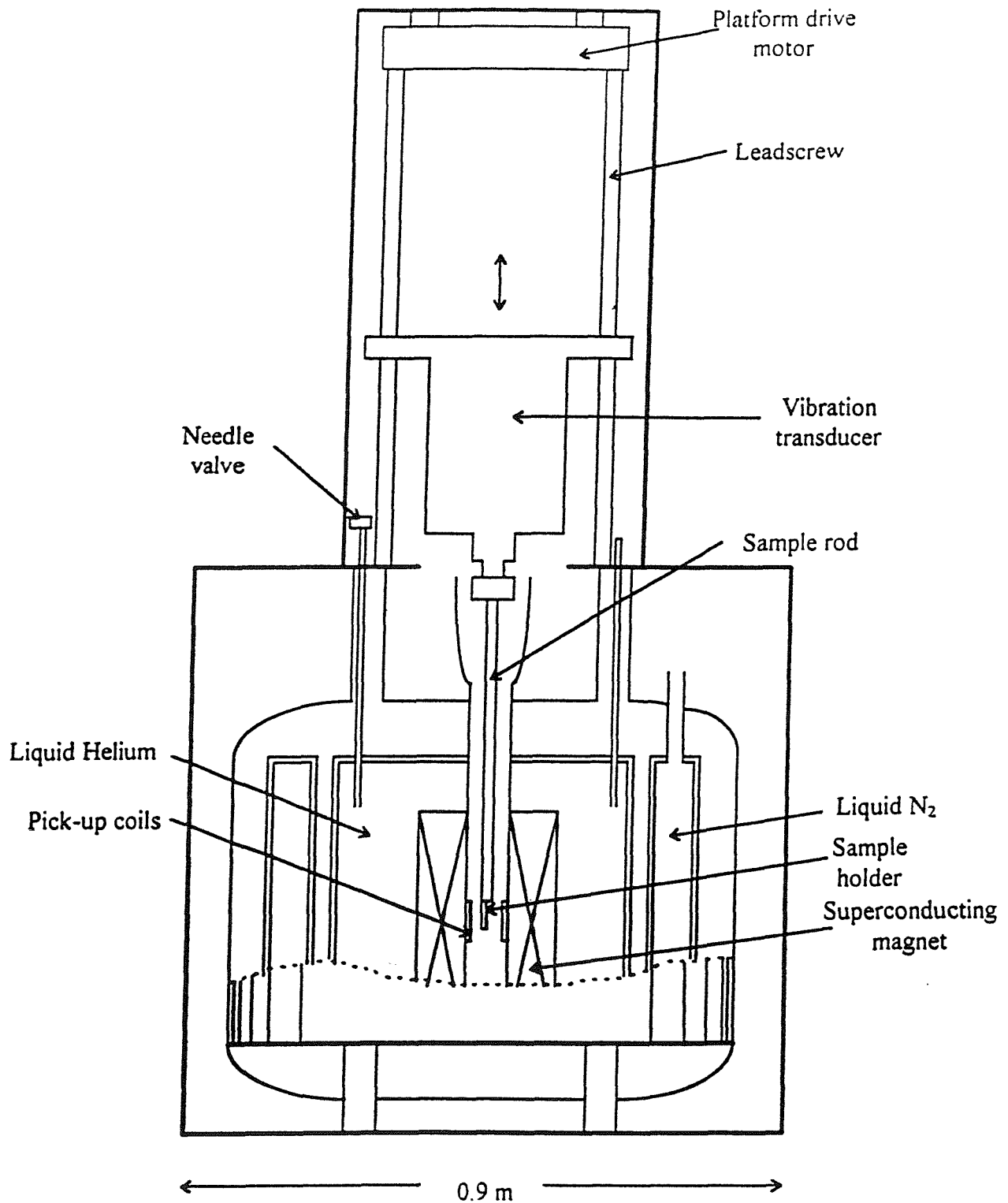


Fig. 4.3. Schematic diagram of the Oxford Instruments 3001 Vibrating Sample Magnetometer.

cryostat great care is also taken to use materials of low thermal conductivity and strong mechanical strength so as to avoid metallic conduction and support efficiently the cryogenics in their vacuum.

**Superconducting magnet:** The superconducting magnet is placed into the helium vessel. It consists of two concentric solenoids together with compensating coils, which are used in order to achieve high levels of homogeneity. The outer coil is wound from multifilamentary superconducting wire formed from Niobium Titanium (NbTi) filaments surrounded by a stabilizing matrix of copper. The matrix is used due to its very high thermal conductivity in order to prevent thermal instabilities caused by energy dissipation due to flux creep. The inner coil is used to obtain fields up to 12 T and is fashioned from Niobium Tin (Nb<sub>3</sub>Sn). For the construction of the magnet considerable care is taken so as the structure to be physically stable under the strong Lorentz forces that are produced during operation. The solenoid is driven by an Oxford Instruments PS120 power supply that is capable of providing a maximum d.c. current of 120 A within the voltage range of  $\pm 10$  V. This allows the field to be swept between  $-12$  T and 12 T with sweep rates of up to 20 mT/s. The produced field has a homogeneity of 0.1% over a 10 mm diameter sphere and the remanent field can be as low as 2 mT. Due to the lack of a persistent mode switch, in order to maintain a constant field the power supply has to remain “on”.

**Variable temperature insert (VTI):** The VTI plays the dual role of isolating the sample from the ambient environment and at the same time providing the necessary means that enable control of the sample temperature. In our VSM the VTI is loaded from the top of the cryostat and is indium sealed onto the top of the magnet, having a common vacuum with the main cryostat. It has an inner diameter of 10 mm. The sample is properly supported inside the insert and its temperature can be varied over the range 1.5 K – 300 K using liquid helium as a coolant. The last is drawn from the helium reservoir and its flow is controlled using a needle valve that can be adjusted from the top of the cryostat. The valve operates in the “dynamic” mode which means that during the measurement it remains always open. In this way, by pumping the sample space helium is drawn into the VTI and then exits to the recovery line through an exhaust at the top. As helium passes the needle, flash evaporation occurs producing cold superfluid helium. The cooling power of the flowing helium is balanced using an Oxford Instruments Intelligent Temperature Controller (ITC4) that gives the appropriate power with the help of an electrical heater fitted close to the sample. The amount of heat provided by the ITC4 is regulated with the

help of a temperature sensor, so as the temperature of the sample to remain either constant or vary with a desired rate. The temperature sensor for our VSM is a carbon glass resistor, which has been chosen due to its small response to magnetic fields.

**Pick-up coils:** The sense coil arrangement mounted in the magnet system consists of two coils separated by a distance of 5 mm. The coils have the same axis of symmetry with the magnet coil and are wound in opposition forming a first order gradiometer (see Fig. 4.1). The vibrating sample induces an emf that, as discussed in section 4.1.1, for small enough samples is proportional to the magnetic moment of the specimen. The output from the pick-up coils is amplified, summed in a low noise amplifier, rectified and integrated over a period synchronized to the period of the vibrator. The integration time can be adjusted depending on the demands of the experiment, minding that the shorter the integration time the lower the signal to noise ratio and the faster the response to slight changes in the measuring quantity. The sense coil arrangement has been calibrated using a nickel sample. The resolution of the system is of the order of  $10^{-6}$  emu.

**Sample support unit:** The sample is mounted on a sampleholder using high vacuum grease. The sampleholders are made up of either *tufnol* or *peek*, both materials characterized by very weak magnetic response in the whole temperature range. After being fixed, the sample is wrapped with P. T. F. E. thread seal tape in order to prevent it from dropping into the VTI. Then the sampleholder is attached to a carbon fiber rod. The latter is extremely rigid and yet light that together with the precision of the rod alleviate the chance of sample lateral vibration. The rod is finally connected to the vibration transducer and is lowered when the measurement is performed.

**Vibration unit:** During the measurement the sample vibrates with the help of a vibration transducer that allows for a sinusoidal motion of the sample along the magnet symmetry axis (z-axis) at a frequency of 66.66 Hz (so as to avoid mains interference) and amplitude of 1.5 mm. In order to minimize transmission of vibrations to the magnet and pick-up coil arrangement, around the vibration transducer there are two weights on spring sections that are tuned to resonate at the vibration frequency thus providing with the necessary damping. The vibration transducer is housed in a bell arrangement and the whole unit is mounted on a table suspended between two high precision lead screws. The screws are locked together with a belt drive and are motorized using a “micro-step” stepping motor. The whole vibration unit and consequently the sample itself can move

along the z-axis with a resolution of 5 micron. In this way, by performing a z-axis scan the position of the sample in the sense coils can be optimized for maximum signal.

**System control:** The operation of the VSM is fully automated and control is achieved by the use of a PC via RS232 serial interfaces. A commercial software package written by AEROSONIC is utilized, and allows the performance of complete sets of measurements through a large range of commands. Data are saved in the computer in the form of ASCII files and can be accessed easily after the end of the experiment.

## 4.2 Torque magnetometer

### 4.2.1 Physical principles

As already discussed in the previous chapters, the high- $T_c$  cuprates are highly anisotropic superconductors. Hence, for a general orientation of the applied field with respect to the c-axis, the equilibrium orientation of the vortices is not parallel to the field, i.e., the magnetization has a component normal to the applied magnetic field.<sup>8</sup> In such a case a finite torque  $\tau$  is exerted on the specimen that is given by:

$$\frac{\tau}{V} = \mathbf{M} \times \mathbf{B}_a \quad (4.7)$$

where  $V$  is the volume of the sample,  $\mathbf{M}$  the magnetization and  $\mathbf{B}_a$  the applied magnetic field vectors respectively.

Torque measurements are usually performed using the so-called “deflection method”. This technique is based on the detection of the capacitance changes,  $\delta C$ , induced on a metallic two-arm capacitor by the elastic deflection of its mobile arm due to the exertion of a finite torque on a sample fixed on it (see Fig. 4.4 below). If the deflection angles are small, then a linear relation between  $\tau$  and  $\delta C$  holds.

Indeed, in the presence of a finite torque, the initial capacitance  $C_0$  of the system is changed to  $C_{\text{total}}$  that can be written as:<sup>9</sup>

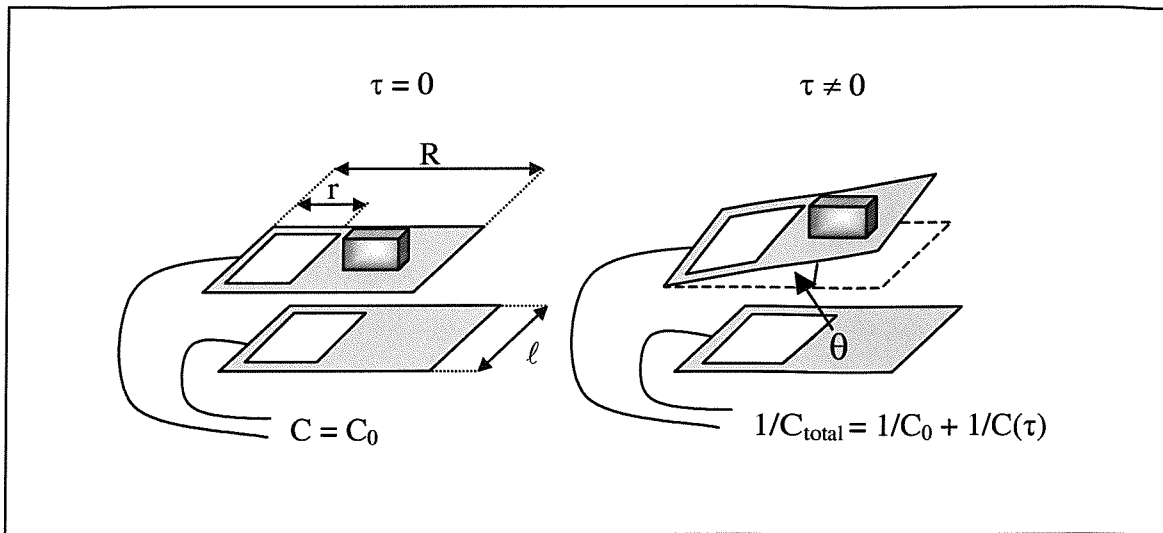


Fig. 4.4. A two-arm capacitor system without and with a small deflection of its mobile arm. The values of the capacitance for each case are indicated on the figure.

$$\frac{1}{C_{\text{total}}(\tau)} = \frac{1}{C_0} + \frac{1}{C(\tau)} \quad (4.8)$$

where  $C(\tau)$  is the extra capacitance due to the deflection of the capacitor plate. The change in the capacitance will be:

$$\delta C(\tau) = C_{\text{total}}(\tau) - C_0 = \frac{C_0 C(\tau)}{C_0 + C(\tau)} - C_0 \quad (4.9)$$

If  $C(\tau) \gg C_0$ , then eq. (4.9) becomes:

$$\delta C(\tau) = -\frac{C_0^2}{C(\tau)}. \quad (4.10)$$

For the configuration shown in Fig. 4.4 and small deflection angles  $\theta$ ,  $C(\tau)$  is given by the relation:<sup>9</sup>

$$C(\tau) = C(\theta(\tau)) = \frac{\varepsilon_0 \ell}{\theta} \ln \frac{R}{r} \quad (4.11)$$

where  $\varepsilon_0$  is the permittivity of vacuum and the lengths  $\ell$ ,  $R$  and  $r$  are defined in Fig. 4.4. Thus eq. (4.10) becomes:

$$\delta C(\tau) = -\theta \frac{C_0^2}{\varepsilon_0 \ell \ln(R/r)} \quad (4.12)$$

Since  $\theta$  is proportional to  $\tau$ , from eq. (4.12) it becomes clear that for small deflection angles  $\delta C(\tau)$  is also linearly related to  $\tau$  (provided that the condition  $C(\tau) \gg C_0$  is fulfilled). Therefore, if the torque magnetometer is calibrated, by measuring  $\delta C(\tau)$  one can obtain absolute values for the torque. The calibration of the torque magnetometer can be performed by e.g. replacing the sample with a small coil of known dimensions and number of turns and measuring the resulting torque when a small current is allowed to flow in the coil.<sup>10</sup>

## 4.2.2 Technical details

Torque measurements were performed using a home-built deflection torque magnetometer at the Université Paris-Sud at Orsay in collaboration with Dr. L. Früchter and Dr. K. Deligiannis. A diagrammatic representation of this experimental arrangement is illustrated in Figs. 4.5 and 4.6.

The *cryostat* contains two vessels separated from each other by a vacuum shield. The inner vessel is used as a liquid helium container whereas the outer one contains liquid nitrogen and is vacuum insulated from the laboratory environment. Located into the helium dewar is the main *superconducting magnet* that can produce a transverse field with a maximum value of 4 T. It is driven by an *Oxford Instruments MK3* power supply that can provide with a maximum current of 120 A at 4 V. The magnet can be rotated around a vertical axis with the help of a stepper motor with an angular resolution of 0.037°. In order to further increase the latter, in addition to this magnet there are also two smaller transverse solenoids that can provide with fields of up to 0.3 T (see Fig. 4.5). The

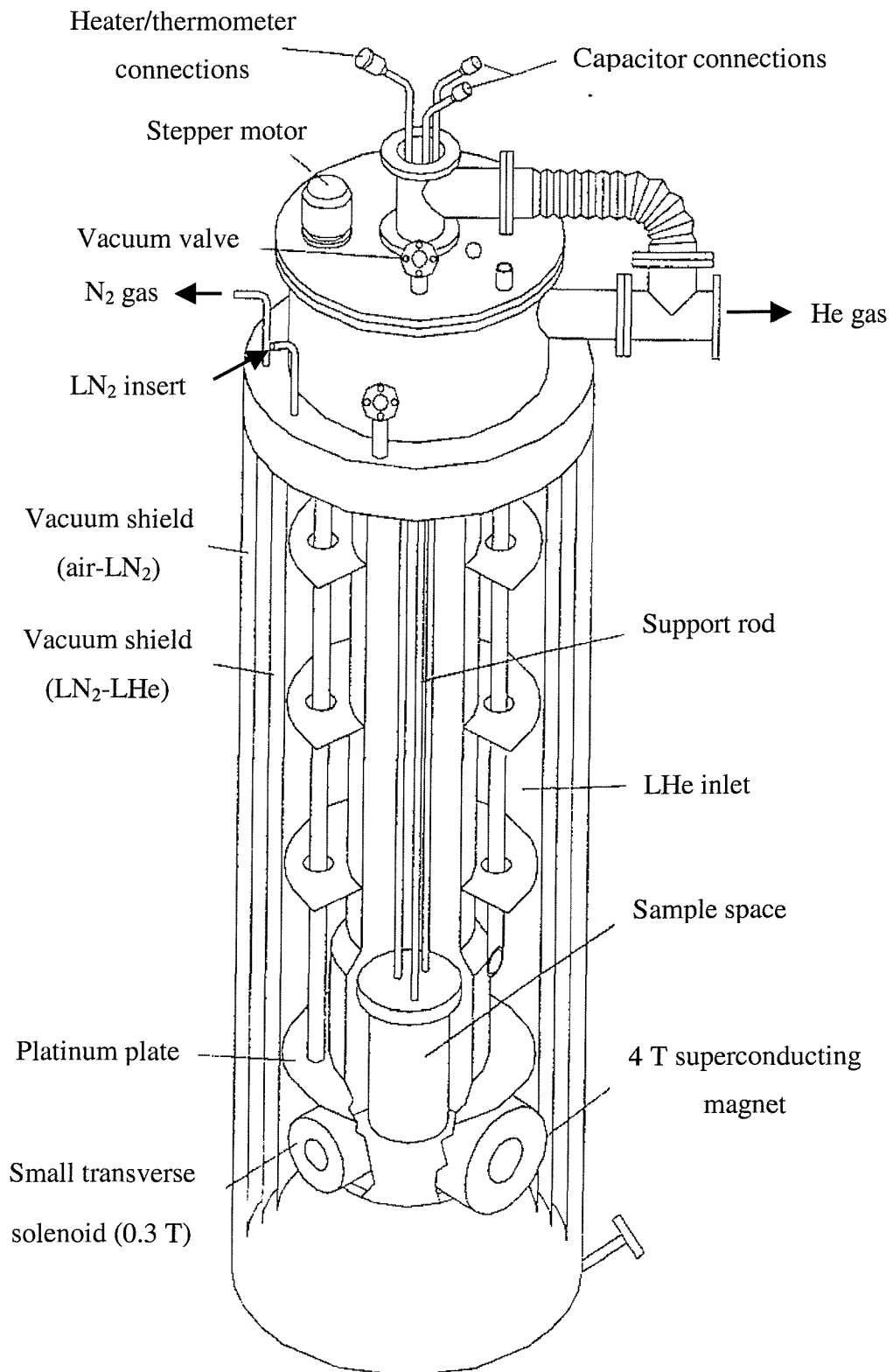


Fig. 4.5. Diagram showing the main units of the torque magnetometer utilized in the present study.

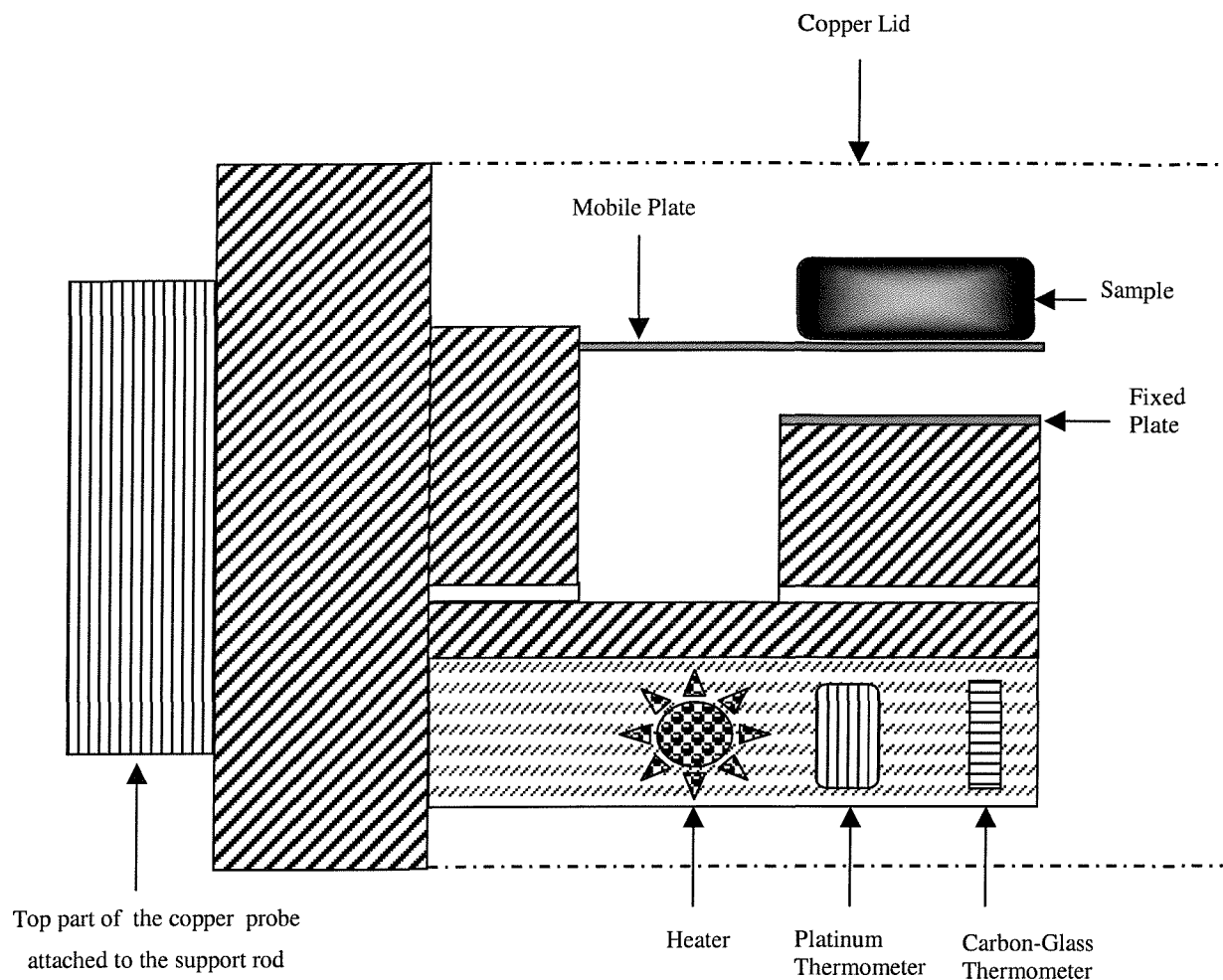


Fig. 4.6. Side view of the capacitor – copper probe system used for the torque measurements.

capacitor has been machined from a beryllium-copper alloy, due to its good elastic properties and poor magnetic response, and is fitted on a copper probe (see Fig. 4.6). The sample is mounted on the mobile plate of the capacitor using high vacuum grease. The bottom part of the copper probe, that contains the system capacitor – sample, is then covered with a copper lid and its top part is screwed onto a support rod. The whole unit is then immersed in the liquid helium bath.

The temperature of the sample is controlled using a Lakeshore temperature controller, which regulates an electrical heater that is fixed on a copper plate close to the sample (see Fig 4.6). The amount of heat provided is controlled by measuring the temperature with the help of two thermometers: A carbon glass resistor for the

temperature region from 4 K to 40 K, with the resistance varying in the range  $700 \Omega - 20 \Omega$ , and a Platinum resistance thermometer in the range 40 K – 300 K, with the resistance varying from  $20 \Omega$  to  $120 \Omega$ . The attained temperature resolution is better than 0.05 K.

The capacitor plates have rectangular shape with an effective surface of  $16 \text{ mm}^2$  and at equilibrium are separated by a distance of  $\sim 0.1 \text{ mm}$ . In order to avoid problems arising from non-linearity, considerable care has been taken to keep the deflection of the mobile arm as small as possible. Hence, depending on the mass of the sample under study, plates with thicknesses in the range 0.05 mm to 0.2 mm can be used. The equilibrium capacitance is of the order of  $0.8 - 1.5 \text{ pF}$ , whereas variations of less than  $10^{-4} \text{ pF}$  can be detected, which means changes in the angle of less than  $10^{-3} \text{ deg.}$ <sup>9</sup> The capacitance is measured with the help of a *General Radio 1615A* capacitance bridge that is equilibrated using an *EG&G 5206* lock-in amplifier.

The torque magnetometer is fully automated and is controlled using a PC that utilizes a home-written software package. The latter allows the composition of sequences based on simple commands and the performance of unattended measurements.

---

## References

---

- <sup>1</sup> S. Foner, Rev. Sci. Instrum. 30, 548 (1959)
- <sup>2</sup> J. Mallinson, J. Appl. Phys. 37, 2514 (1966)
- <sup>3</sup> H. Zijlstra, *Experimental Methods in Magnetism*, (North-Holland Publishing Company, Amsterdam, 1967)
- <sup>4</sup> C. N. Guy and W. Howarth, J. Phys. C 11, 1635 (1978)
- <sup>5</sup> A. Zieba and S. Foner, Rev. Sci. Instrum. 53, 1344 (1982)
- <sup>6</sup> VSM Technical Bulletin, Oxford Instruments Limited
- <sup>7</sup> Vibrating Sample Magnetometer with Superconducting Magnet, System Manual, Oxford Instruments Limited.
- <sup>8</sup> L. Bulaevskii, Zh. Eksp. Teor. Fiz. 64, 2241 (1973) [Sov. Phys. JETP 37, 1133 (1973)];  
R. A. Klemm and J. R. Clem, Phys. Rev. B 21, 1868 (1980)
- <sup>9</sup> V. Vulcanescu, Ph. D. thesis (Université Paris-Sud, 1997)
- <sup>10</sup> R. Griessen, Cryogenics 13, 375 (1973)

---

# Chapter 5

---

## The vortex phase diagram of $\text{YBa}_2\text{Cu}_3\text{O}_{7-\delta}$

### 5.1 Flux line lattice melting in high- $T_c$ superconductors

As already mentioned in Chapter 1, in the traditional mean-field limit the field-temperature phase diagram of a type-II superconductor comprises a Meissner phase below the lower critical field  $B_{c1}$ , above which vortices penetrate the specimen forming a homogeneous triangular lattice. This constitutes the so-called Shubnikov phase or mixed state that persists up to the upper critical field  $B_{c2}$  where superconductivity is destroyed. Such a conventional (or mean-field) phase diagram is shown schematically in Fig. 5.1. In the case of the high temperature superconductors (HTSC), however, this simplified picture has to be re-examined.<sup>1,2</sup> This is because in these compounds thermal fluctuations are significantly enhanced due to the high operating temperatures and small coherence lengths as well as the softness of the vortex lattice caused by the large anisotropies and penetration depths.<sup>1,2</sup> Thus in contrast to the conventional superconductors, where these fluctuations become important indistinguishably close to  $B_{c2}$ ,<sup>1,3</sup> in the HTSC they take place in the London regime and consequently affect the behaviour of the vortex system (VS) in a large part of the  $B - T$  phase diagram. Accordingly, on the basis of Lindemann-type calculations, it has been predicted that in these systems thermal fluctuations can melt the vortex lattice well below  $B_{c2}$ , thus defining a transition between a solid and a liquid vortex phases.<sup>4,5</sup> The existence of such a transition has also been confirmed by simulations of the VS.<sup>6-9</sup>

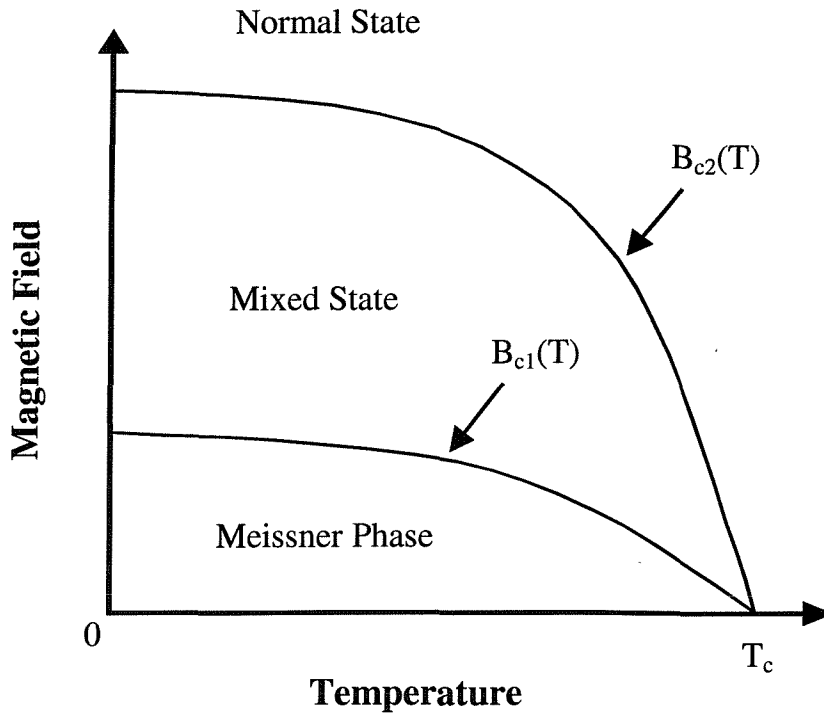


Fig. 5.1. Mean-field  $B - T$  phase diagram for a type-II superconductor.

### 5.1.1 Theoretical approach

Up to now, no consistent quantitative theory of melting has been developed. Therefore, much of the analytical work on the problem of vortex lattice melting relies on the Lindemann criterion.<sup>10</sup> Although this approach is unable to explain the exact mechanism of melting, it is nevertheless particularly fruitful, as it allows to determine the shape and position of the melting line over a broad range of fields. The Lindemann condition states that the vortex lattice becomes unstable and melts at a temperature  $T_m$ , where the mean-squared amplitude of fluctuations,  $\langle u^2 \rangle_{th}$ , of vortices around their equilibrium positions has reached a certain fraction  $c_L$  of the lattice constant  $a_0$ , namely:

$$\langle u^2(T_m) \rangle_{th} \approx c_L^2 a_0^2. \quad (5.1)$$

$c_L$  is called the Lindemann number and usually takes values between 0.1 and 0.2.<sup>1</sup> Therefore, in order to determine the transition line one has to evaluate  $\langle u^2 \rangle_{th}$ . This

quantity, however, depends strongly on the values of the magnetic field. This is because the elastic properties of the flux line lattice and therefore its stability with respect to thermal fluctuations are different for different field regions.<sup>11</sup> Neglecting the influence of quenched disorder on the thermodynamic properties of the vortex system,<sup>12</sup> for the estimation of the melting transition the following regimes are discussed:<sup>1</sup>

### A. Intermediate magnetic fields: $B_{c1} \ll B_a < 0.2B_{c2}$

In this region the interaction between vortices is large and strongly nonlocal since  $a_0$  is small as compared to the in-plane penetration depth  $\lambda_{ab}$ . Nevertheless, the vortex density is still not high enough for the vortex cores to overlap and one can use the London approximation to determine  $\langle u^2 \rangle_{\text{th}}$ . This problem has been addressed analytically in Ref. 5 by taking into account the nonlocality of the elastic moduli (see Chapter 2). It was found that for an uniaxially anisotropic superconductor and for fields along the c-axis, the melting line,  $B_m(T)$ , can be obtained by solving the equation:<sup>1,5</sup>

$$\frac{\sqrt{b_m(t)}}{1-b_m(t)} \frac{t}{\sqrt{1-t}} \left[ \frac{4(\sqrt{2}-1)}{\sqrt{1-b_m(t)}} + 1 \right] = \frac{2\pi c_L^2}{\sqrt{Gi}} \quad (5.2)$$

with  $b_m(t) = B_m(T)/B_{c2}(T)$ ,  $t = T/T_c$  and  $Gi$  the Ginzburg number,<sup>13</sup> which determines the width of the fluctuation region near  $B_{c2}$ . For temperatures close to  $T_c$  and  $b_m \ll 1$ , eq. (5.2) can be simplified considerably reading:

$$B_m(T) \approx \beta_m \frac{c_L^4}{Gi} B_{c2}(0) \left( 1 - \frac{T}{T_c} \right)^2 \quad (5.3)$$

with  $\beta_m \approx 5.6$  and  $B_{c2}(0)$  the upper critical field at zero temperature.<sup>1</sup> This relation is valid for as long as  $(1-T/T_c) \geq Gi$ , i.e., outside the fluctuation regime. On the other hand, with the help of eq. (5.3) the condition  $B_m \ll 0.2B_{c2}(T)$  leads to  $\left( 1 - \frac{T}{T_c} \right) \ll 0.2 \frac{Gi}{\beta_m c_L^4}$ . For parameters pertinent to  $\text{YBa}_2\text{Cu}_3\text{O}_{7-\delta}$  ( $Gi \sim 10^{-2}$ ) and  $c_L \approx 0.2$ , this gives  $(1-T/T_c) \ll 0.2$  and therefore the regime of applicability of eq. (5.3) should be restricted near the critical temperature.<sup>14</sup> For temperatures far below  $T_c$ ,  $B_m$  moves closer to  $B_{c2}$  and the full result

given by eq. (5.2) should be used. An improvement of the simple power-law relation (5.3) that accounts for the suppression of the order parameter and describes the melting line at lower temperatures can be written as:<sup>1</sup>

$$B_m(T) \approx B_{c2}(0) \frac{4\zeta^2}{(1 + \sqrt{1 + 4\zeta \frac{T_s}{T}})^2} \quad (5.4)$$

with  $\zeta = c_L^2 \sqrt{\frac{\beta_m}{Gi}} (\frac{T_c}{T} - 1)$  and  $T_s = T_c c_L^2 \sqrt{\frac{\beta_m}{Gi}}$ . From eq. (5.4) then it becomes clear that the melting line cannot anymore be expressed in terms of a simple power-law.

Finally, for the general situation that the magnetic field makes an angle  $\theta$  with the  $c$ -axis and as long as the condition  $a_0 < \lambda_{ab}$  holds, the melting field can be obtained using the scaling relation:<sup>15</sup>

$$B_m(T, \theta) = \varepsilon_\theta^{-1} B_m(T, \theta^\circ) \quad (5.5)$$

where  $\varepsilon_\theta = (\cos^2\theta + \gamma^{-2}\sin^2\theta)^{1/2}$ .

### B. Low magnetic fields: $B_a \sim B_{c1}$

For fields of the order of  $B_{c1}$ ,  $a_0$  increases beyond  $\lambda_{ab}$  and the interaction between the vortex lines decreases exponentially. As a result the applicability of the Lindemann criterion becomes less obvious. Nevertheless, this approach is still useful as it can provide with an order of magnitude estimate for the melting transition. Thus using the appropriate expressions for the elastic moduli in this range of fields and following the previous procedure, one can obtain an implicit equation for the melting line at low inductions, namely:<sup>1</sup>

$$\left(\frac{\lambda_{ab}}{a_0}\right)^{7/2} e^{a_0/\lambda_{ab}} = \beta_m' \frac{c_L'^4 \kappa^2 \ln \kappa}{Gi} \left(\frac{T_c}{T}\right)^2 \left(1 - \frac{T}{T_c}\right) \quad (5.6)$$

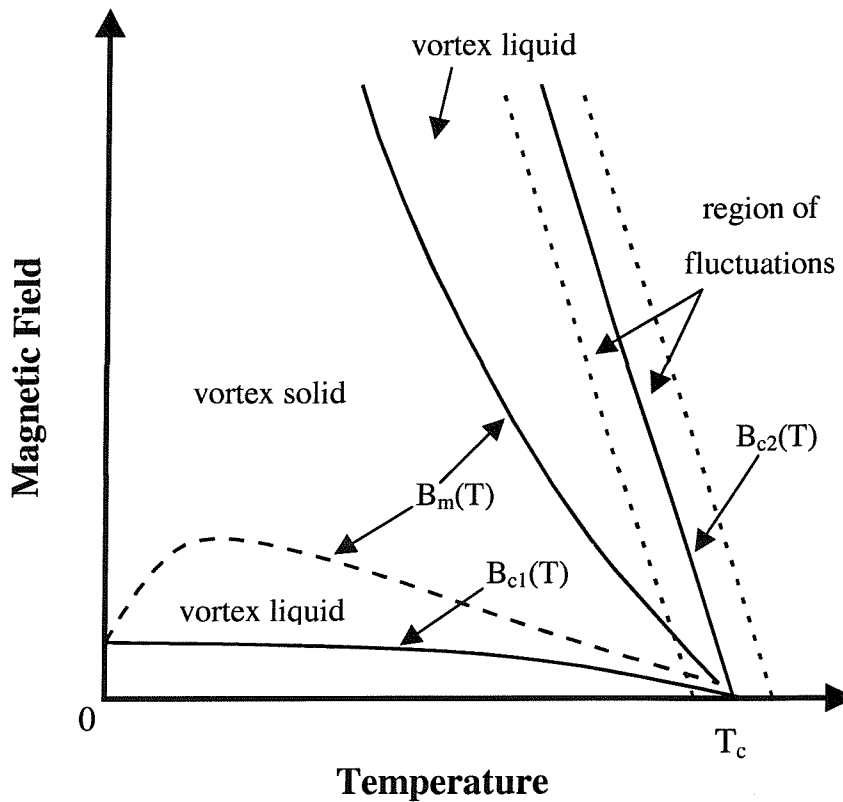


Fig. 5.2. Field-Temperature phase diagram for a high temperature superconductor. Due to thermal fluctuations the Abrikosov lattice melts over a substantial part of the phase diagram. Note that the drawing is not to scale.

with  $\beta'_m \approx 0.5$  and  $c'_L$  the Lindemann number that can be different than the one corresponding to the region  $B_{c1} \ll B_a \ll B_{c2}$ . Note that the approximation  $\ln(B_{c2}/B_a) \approx 2 \ln \kappa$  has been used for the derivation of eq. (5.6).

The melting lines given by eqs. (5.3) and (5.6) are shown with the continuous and long-dashed lines respectively in the phase diagram of Fig. 5.2. As can be seen the vortex liquid phase occupies a large portion of the  $B - T$  plane and moreover shows a reentrant behaviour. Therefore, by varying the field at a fixed temperature a sequence of phases from a normal conductor to a vortex liquid, a vortex lattice and then again a vortex liquid can be observed. Interestingly, in the low temperature part of the low field melting line,  $B_m$  increases with  $T$  whereas the lines (5.3) and (5.6) merge at a point thus giving to the melting line a nose-like shape. Nevertheless, for high- $\kappa$  materials, such as the high- $T_c$  cuprates, this point lies into the fluctuation region and therefore cannot be treated using

the mean-field-type description outlined above.<sup>1</sup> Finally it is stressed that the width of the low field liquid phase is rather narrow (with a maximum value of the order of a few Gauss),<sup>1</sup> making its experimental observation a remarkably tedious task.

### C. High magnetic fields: $B_a \sim B_{c2}$

The estimation of the melting line in this case is based on the lowest Landau-level approximation that is valid for high magnetic fields and has been carried out in Ref. 16. In this case one defines the parameter  $y = [T - T_{c2}(B)]/Gi(B)$ , with  $T_{c2}(B)$  the inverse of the  $B_{c2}(T)$  function and  $Gi(B)$  the field dependent width of the fluctuation region,  $Gi(B) \approx Gi^{1/3}[B/B_{c2}(0)]^{2/3} \gg Gi$ .<sup>1</sup> The melting transition turns out to be first order and occurs when  $y \approx -7$ , which is quite far from the critical fluctuation regime.<sup>16</sup>

## 5.1.2 The melting transition

Although the approach based on the Lindemann criterion is rather convenient, it cannot provide with any fundamental information concerning the nature of the melting transition. Therefore, in order to gain more insight into the mechanism of melting, a large amount of theoretical work has been invested in numerical simulations. In turn, numerous studies, that have used various approaches, such as the London model, the Bose model, the frustrated XY model and the lowest Landau-level approximation, have reported and established the existence of a melting transition that for clean enough systems should be of the first order.<sup>7-9, 17-20</sup> For this case they have also provided with calculations of the latent heat, entropy and magnetization jump at the transition that have been found to be in satisfactory agreement with experimental observations.<sup>7, 18-20</sup> Finally they have estimated the Lindemann number and justified the use of the Lindemann criterion for the determination of the melting line.<sup>19, 20</sup>

At the experimental level, there have been plenty of reports indicating the presence of a melting transition in HTSC. A first hint in this direction was initially given by vibrating reed data that showed a sharp peak in the damping of the oscillatory motion of  $\text{YBa}_2\text{Cu}_3\text{O}_{7-\delta}$  single crystals.<sup>21</sup> However, these data could also be accounted by thermally activated depinning,<sup>22</sup> and enthusiasm soon gave way to skepticism. Then another indication came by a sharp dissipation peak observed in very low frequency torsional

oscillator studies.<sup>23</sup> The position of this peak in the  $B - T$  plane showed the predicted  $(T_c - T)^2$  dependence [see eq. (5.3)] and for this reason it was interpreted as a signature of vortex lattice melting. Nevertheless, these data were not compelling enough either, as this peak could result from the complete penetration of the ac field into the sample cross section. In this sense the observed square-like dependence can also be interpreted as measuring a constant resistivity within the thermally activated flux flow regime.<sup>1</sup>

However, the improvement in the quality of available  $\text{YBa}_2\text{Cu}_3\text{O}_{7-\delta}$  single crystals together with more intensive investigations, brought along stronger and more reliable experimental evidence about the existence of melting. In addition, now data were suggesting that the melting transition might be of the first order. Indeed, several transport studies revealed a sharp drop in the resistivity versus temperature curves at low currents, which was additionally accompanied by hysteresis in the resistivity temperature

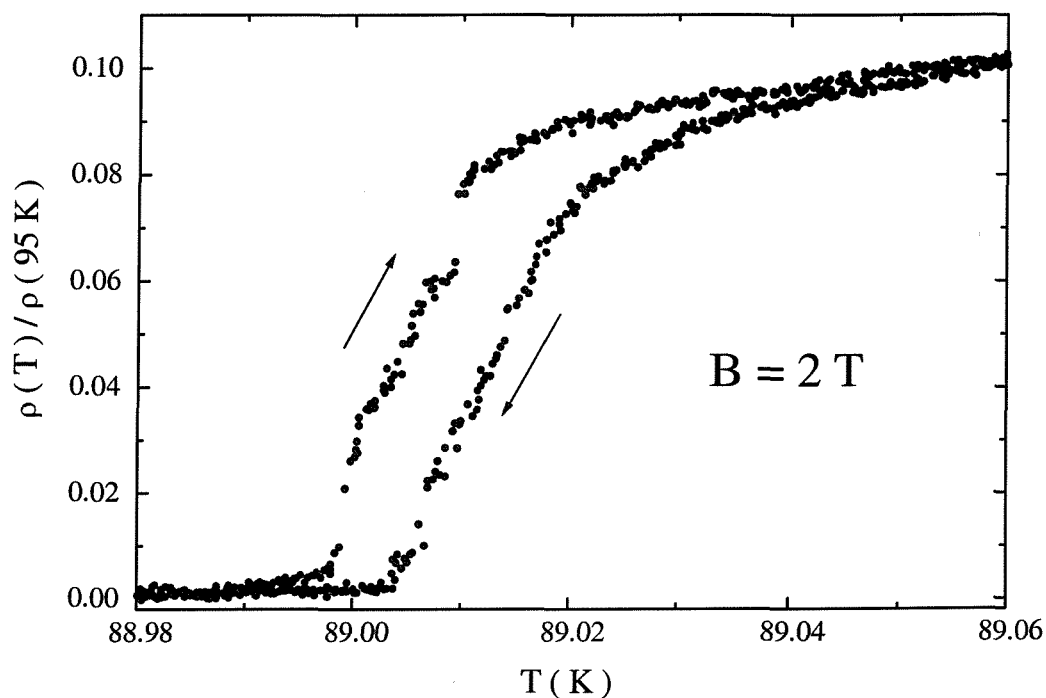


Fig. 5.3. Normalized resistivity of a detwinned  $\text{YBa}_2\text{Cu}_3\text{O}_{7-\delta}$  single crystal plotted as a function of temperature at a field of 2 T taken from Ref. 28. Arrows indicate the direction of temperature sweep. As can be seen the resistivity shows a hysteretic sharp drop that takes place in a temperature range of less than 30 mK.

dependence (see Fig. 5.3). This was regarded as a signature of a first order melting transition.<sup>24-28</sup> The jumplike decrease in the resistivity points indeed to a sharp transition from a highly dissipative VS at high temperatures, to a strongly pinned one at lower ones with significantly increased vortex correlations, i.e., from a vortex liquid to a vortex solid. However, resistivity is not a thermodynamic quantity and as pointed out by Jiang et al.,<sup>29</sup> the observed hysteresis is neither a sufficient nor a necessary condition for a first order melting transition. Indeed, in this study it was demonstrated that the resistive hysteresis can be the result of current-induced non-equilibrium effects near the onset of dissipation rather than of a first order phase transition.

These difficulties in determining unambiguously the nature of the melting transition obliged experimentalists to investigate the behaviour of thermodynamic quantities, such as the equilibrium magnetization, entropy and specific heat in the region of the alleged melting. But what would one expect to observe? In the Landau classification a transition is of the  $n$ th order, if the  $n$ th derivatives of the free energy are the lowest ones to show a discontinuity.<sup>30</sup> Therefore, in a first order melting transition one would observe a discontinuity (jump) in both the magnetization and entropy. This means that the specific heat would show a delta function peak. On the other hand, in a second order transition only a change in the slope of the magnetization and entropy curves would be present, i.e., a discontinuity in the specific heat.

The first result in this direction was obtained by Liang et al.<sup>31</sup> from magnetization measurements. Using a SQUID magnetometer and high quality untwinned  $\text{YBa}_2\text{Cu}_3\text{O}_{7-\delta}$  single crystals, they were able to observe a jump in the reversible magnetization thus illustrating the first order character of the melting transition. Moreover, from the Clausius-Clapeyron equation:

$$\Delta S = -\Delta M \frac{dB_m}{dT} \quad (5.7)$$

and the magnetization jump  $\Delta M$ , they estimated the corresponding entropy jump per vortex per  $\text{CuO}_2$  layer and found it to be in good agreement with the calculations of Hetzel et al.<sup>17</sup> Subsequently Welp et al.,<sup>32</sup> after proving that the magnetization jump was not due to experimental artefacts, compared it with the resistivity kink for the same sample and demonstrated that the positions of these features coincide, thus confirming

that the resistivity kink is a signature of first order melting. The same behaviour was also found by Fendrich et al.<sup>33</sup> who performed simultaneous transport and magnetization measurements on an untwinned  $\text{YBa}_2\text{Cu}_3\text{O}_{7-\delta}$  single crystal. However, the most definite proof of the occurrence of a first order transition was provided by calorimetric measurements of the latent heat in an untwinned  $\text{YBa}_2\text{Cu}_3\text{O}_{7-\delta}$  single crystal.<sup>34</sup> The observed entropy jump was found to be almost temperature independent and consistent with that inferred from magnetization data. These results were subsequently further strengthened by adiabatic specific heat measurements.<sup>35</sup> Finally, note that similar data indicating first order melting have also been obtained for other high- $T_c$  compounds as well, such as  $\text{Bi}_2\text{Sr}_2\text{CaCu}_2\text{O}_x$  (BSCCO),<sup>36, 37</sup>  $\text{NdBa}_2\text{Cu}_3\text{O}_{7-\delta}$ ,<sup>38</sup>  $\text{DyBa}_2\text{Cu}_3\text{O}_7$ ,<sup>39</sup> and  $(\text{La}_{1-x}\text{Sr}_x)_2\text{CuO}_4$ ,<sup>40</sup> pointing out the universal nature of melting.

Although present, the first order melting transition does not extend to the whole  $B - T$  phase diagram. As was firstly shown by Safar et al.<sup>41</sup> by means of transport measurements on untwinned  $\text{YBa}_2\text{Cu}_3\text{O}_{7-\delta}$ , with increasing field above a well defined value  $B_{mc}$ , termed the multicritical field, the sharp resistivity drop broadens significantly. This effect was attributed to the suppression of the first order transition seen at lower fields and its substitution by a continuous, second order one. This behaviour is demonstrated in Fig. 5.4 for one of our detwinned samples. As can be seen, above  $B_{mc} \approx 9$  T, the sharp resistivity drop seen at lower fields is substituted by a long tail, which can be well described by the vortex glass theory outlined below, indicating the formation of a highly disordered vortex state below the melting line.<sup>41, 42</sup> The change in the order of the melting transition with increasing field, was recently demonstrated unambiguously by specific heat measurements.<sup>35</sup> In this investigation it was also shown the existence of a low-field end of the first order transition, which has not received any explanation as yet. Another important result in Ref. 35 was a shift of  $B_{mc}$  to lower fields with increasing quenched disorder, an effect also seen in transport studies.<sup>42</sup> This implies that no first order melting should be expected for samples characterized by strong disorder, as has been indeed observed experimentally.<sup>43, 44</sup> Note that a similar behaviour of the multicritical point has also been seen in BSCCO single crystals.<sup>45</sup>

The physical mechanism underlying the change of the order of the melting transition at  $B_{mc}$  has still not been fully elucidated. The most recent theories attribute it to the presence of a field induced phase transition in the vortex solid. This transition separates a low-field quasi-ordered vortex phase from a high-field disordered phase that

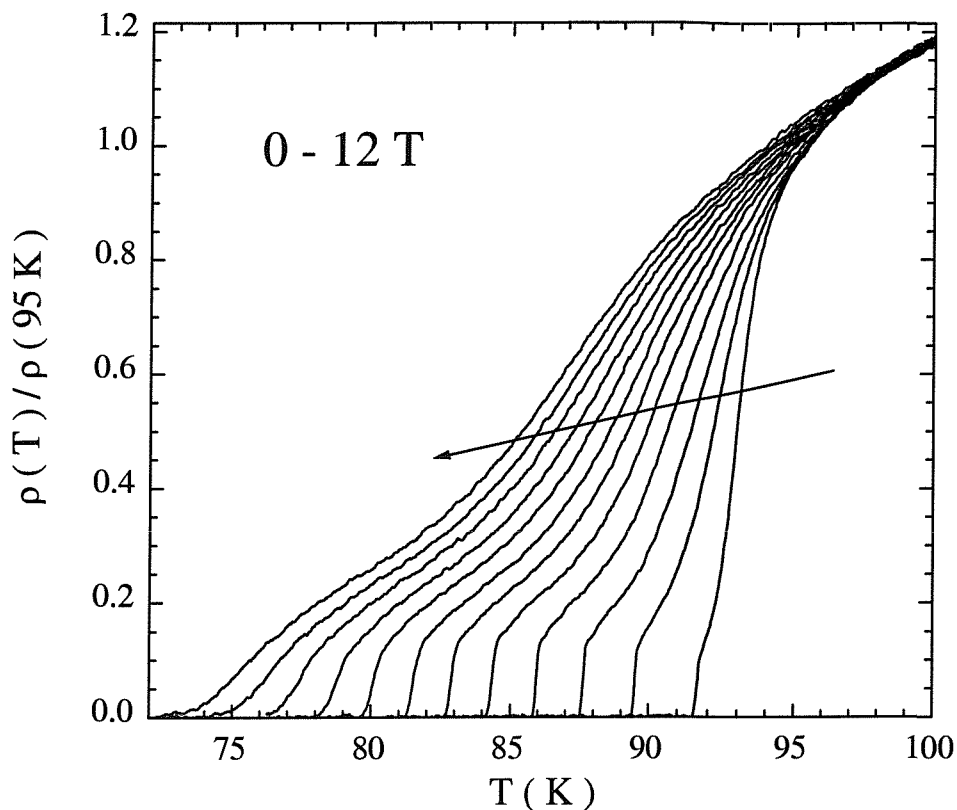


Fig. 5.4. Temperature dependence of the normalized resistivity for a detwinned  $\text{YBa}_2\text{Cu}_3\text{O}_{7-\delta}$  single crystal for fields in the range 0-12 T. Field increases with a step of 1 T in the direction of the arrow. As can be seen for  $B < 9$  T there is a clear sharp resistivity drop indicative of a first order melting transition. At higher fields this feature broadens significantly, which reflects the suppression of the first order transition that now becomes a second order one. The graph is courtesy of Dr. S. N. Gordeev.

lacks long-range order, and which, unlike the former, is expected to melt via a second order transition as discussed in more detail in the following sections.

### 5.1.3 The vortex liquid phase

After having established the existence of a melting transition, that depending on the strength of the effective disorder can be either a first or a second order one, the question

that immediately arises concerns the nature of the vortex liquid phase. As a liquid this phase should be characterized by the absence of translational order in the direction transverse to the field. Moreover, since by definition in this phase the thermal energy dominates over the elastic one, shear rigidity should be diminished and ideally vortices will be able to move freely past each other. In the case that, due to thermal fluctuations, vortex lines can wander to distances of the order of  $a_0$ , neighboring vortices will interweave with each other leading to an entangled vortex configuration.<sup>4</sup>

In the presence of weak disorder and well above the melting line, the vortex liquid is unpinning and exhibits a resistivity that follows the Bardeen-Stephen relation given by eq. (2.13). Nevertheless, this is not true close to the melting line where the liquid can be very viscous. This is due to the presence of energy barriers  $U_{pl}$ , associated with the plastic motion of the vortex structure (due to e.g. vortex entanglement).<sup>1</sup> In such a liquid, relative movement of vortices takes place either by reptation or via cutting and reconnection of the vortex lines.<sup>1, 4, 46</sup> Under such conditions, the barriers impeding motion of vortices remain finite at all current densities, and in the limit  $J \rightarrow 0$  the vortex motion enters the TAFF regime with a resistivity  $\rho_{pl} \ll \rho_{ff}$  given by:<sup>1</sup>

$$\rho_{pl} \approx \rho_0 \exp\left(-\frac{U_{pl}}{k_B T}\right) \quad (5.8)$$

with  $\rho_0 \approx \frac{1}{\pi^2 \sqrt{2Gi}} \left[ \frac{J_0(0)Gi}{J_c(0)} \right]^{3/2} \rho_n$ . With increasing temperature, however, the size of the characteristic plastic barriers decreases and the vortex liquid crosses from a pinned to an unpinning regime characterized by free flux flow.<sup>1</sup>

Concerning the reentrant liquid phase close to the  $B_{c1}(T)$  line (see Fig. 5.2), in the absence of pinning theory predicts that at low temperatures there exists a disentangled liquid that with increasing temperature is transformed into an entangled one.<sup>4</sup> In the presence of pinning, both phases can still be realized. Nevertheless, in this case the entangled liquid survives only near  $T_c$ , since at lower temperatures disorder is expected to transform it into a pinned disentangled liquid or unexpectedly even into a vortex glass.<sup>1</sup>

Another important issue is whether or not the vortex liquid is a new genuine thermodynamic phase with macroscopic properties that differ from those of a normal metal. Blatter et al.<sup>1</sup> have shown that the entangled vortex liquid qualitatively has the

same properties as a normal metal. Therefore, it does not represent a distinct thermodynamic phase and there is no other phase transition in the system except the melting one.<sup>1</sup> On the other hand, the disentangled vortex liquid differs from both the vortex lattice and the normal metal: It is characterized by the absence of long range translational order and superconductivity along the field direction. In the absence of disorder, the disentangled liquid can exist as an intermediate phase just above the melting line.<sup>1, 47</sup> If this is the case, then on decreasing the temperature from above the normal state one firstly crosses the crossover  $B_{c2}(T)$  line and then two transition lines, initially to the disentangled vortex liquid and then to the vortex solid phases.<sup>1</sup> A disentangled liquid was possibly observed in Ref. 48. Nevertheless, more detailed studies are necessary to clarify whether such an equilibrium phase diagram can be realized in practice.

## 5.2 The vortex glass phase

By analogy with the droplet theory of spin glasses, it has been suggested that in disordered, bulk type-II superconductors, at low temperatures the VS can form a thermodynamic glass phase, termed the vortex glass.<sup>49</sup> According to this theory the vortex glass phase is topologically disordered, lacking translational order, whereas the presence of dislocations is expected to be favoured.<sup>49</sup> It is also a true superconducting phase, characterized by diverging activation barriers and therefore zero resistivity at vanishing driving forces.<sup>49</sup> With increasing temperature this phase melts into a liquid at a critical temperature  $T_g$ . For strong enough disorder, the melting transition is expected to be of the second order. If this is the case, one can then use a scaling analysis to describe the static and dynamic behaviour of the system within a critical region around the transition. Note that the width of this regime should depend on the strength of the disorder.<sup>49</sup>

The principal scaling parameter of the vortex glass transition is the vortex glass correlation length  $\xi_g \sim |T-T_g|^{-\nu}$  that describes the diverging size of glassy regions at  $T_g$ , with  $\nu$  the static exponent. The dynamic features of the transition are then determined by a characteristic relaxation time  $\tau_g \sim \xi_g^z$ .<sup>49</sup> In three dimensions the dynamical exponent  $z$  is expected to take values in the range 4-7. According to the predictions of the vortex glass theory, in  $d$  dimensions and near the transition, the current density  $J$  and electric field  $E$  scale in terms of the exponents  $\nu$  and  $z$  as:

$$E\xi_g^{z+1} \propto G_{\pm}(J\xi_g^{d-1}) \quad (5.9)$$

where  $G_{\pm}$  is an appropriate scaling function with (+) and (-) corresponding to temperatures above and below  $T_g$  respectively.<sup>49</sup>

From eq. (5.9) the following general behaviour for the current-voltage characteristics near the glass transition is obtained:<sup>1, 49, 50</sup> Above  $T_g$  the scaling function  $G_+$  goes to a constant value ( $\sim J\xi_g^{d-1}$ ) as  $J\xi_g^{d-1} \rightarrow 0$ , implying a linear resistivity  $\rho \sim |T-T_g|^{\nu(z+2-d)}$  at small current values. Nevertheless, at high current densities [ $J > J_+ \sim (T-T_g)^{\nu(d-1)}$ ] a power-law behaviour is expected. At  $T_g$ , a power-law current-voltage characteristics is obtained according to the relation:  $E(J, T = T_g) \propto J^{(z+1)/(d-1)}$ . Finally, below the transition a glassy response  $E \propto \exp[-(J_g/J)^{\mu}]$  is expected at low currents [ $J < J_- \sim (T_g-T)^{\nu(d-1)}$ ], with  $0 \leq \mu \leq 1$ , and  $J_g = \varepsilon_l^2/k_B T$  ( $\varepsilon_l$  is the single vortex line tension), and a power-law behaviour at higher current densities.

The exponential current-voltage characteristics in the vortex glass phase leads to a time dependence of the current density that can be given by the so-called interpolation formula:<sup>49, 51</sup>

$$J(t) \approx J_c \left[ 1 + \frac{\mu k_B T}{U_0} \ln\left(\frac{t}{t_0}\right) \right]^{-1/\mu} \quad (5.10)$$

with  $J_c$  and  $U_0$  the critical current density and the energy barrier in the absence of flux creep respectively and  $t_0$  an attempt time. Interestingly, this formula is the same with eq. (2.34) obtained from the collective creep theory with  $\alpha$  replaced by  $\mu$ .

There have been several experimental works on disordered superconducting systems providing evidence for a continuous transition into a vortex glass.<sup>44, 52</sup> In transport studies, analysis of the current-voltage characteristics at the vicinity of the transition has been used to extract the exponents  $\nu$  and  $z$  and their values were found to be in good agreement.<sup>44</sup> This represents a nice example of universality since the samples used in these investigations were very different ( $YBa_2Cu_3O_{7-\delta}$  epitaxial films, microtwinning single crystals and polycrystalline samples). On the other hand, reports about both sample and field dependent scaling exponents are not missing.<sup>53, 54</sup> Nevertheless, in the absence of a firm description of the glassy state and an analytical

determination of both the scaling exponents and functions, the issue of the existence or not of critical universality, even after recent supporting studies,<sup>55</sup> remains unresolved (for an interesting discussion on this topic see Ref. 1).

Finally, it is stressed that the existence of a disordered vortex phase with diverging activation barriers at low currents has also been predicted by the collective creep theory presented in detail in Chapter 2, which treats the vortex lattice as an elastic medium interacting with a weak random pinning landscape.<sup>56</sup> In the theory of collective creep there is no explicit glass temperature. Nevertheless, the picture is similar, since collective creep is realized only below the melting temperature where the lattice has some elastic rigidity.<sup>2</sup> There are several experimental works supporting the applicability of the collective creep theory in HTSC.<sup>57</sup> However, as the manifestations of the glassy phase in both descriptions should be very similar, at the moment it is not clear which of these theories is more appropriate for the description of real-life systems. Further experimental and theoretical work is necessary to clarify this point.

### 5.3 The Bose glass phase

The vortex glass phase outlined above is relevant for the case of uncorrelated disorder. On the other hand, in the presence of correlated defects such as twin planes, columns, grain boundaries etc., it has been shown that again a glassy phase can be formed at low temperatures. This phase was termed Bose glass due to the analogy of this system with the physics of 2D bosons subject to a static disorder potential.<sup>58, 59</sup> The main difference in this case is that due to the extended character of correlated defects, the pinning energy grows linearly with the length of a vortex line localized into the defect. This leads to strong and anisotropic pinning as compared with the weak isotropic pinning produced by pointlike defects, changing significantly the behaviour of the VS.<sup>1</sup>

Similarly to the vortex glass, in the Bose glass phase the resistivity vanishes in the limit  $J \rightarrow 0$ , whereas the most important mechanism for vortex transport is “tunneling” between different defect sites via the formation of kinks. Nonlinear current-voltage characteristics is expected, namely:<sup>59</sup>

$$E \propto \exp\left[-\left(\frac{E_K}{k_B T}\right)\left(\frac{J_0}{J}\right)^\mu\right] \quad (5.11)$$

with  $E_K$  a typical kink energy and  $J_0$  a current scale that depends on the distance between the defects.  $\mu$  is an exponent that equals 1/3 at low current values and 1 at higher ones.<sup>59</sup> There is again a characteristic temperature  $T_{BG}$ , above which melting to an entangled vortex liquid is expected to take place.<sup>1</sup> At low enough fields, where the disorder is relevant, this transition is a continuous, second order one. In the Bose-glass formalism there are two diverging scaling lengths  $l_{||} \sim (T_{BG} - T)^{-\nu_{||}}$  and  $l_{\perp} \sim (T_{BG} - T)^{-\nu_{\perp}}$  that describe the distance within which a localized vortex fluctuates parallel and perpendicular to the field direction respectively, with  $\nu_{\perp} \geq 1$  and in the simplest approach  $\nu_{||} = 2\nu_{\perp}$ .<sup>58, 59</sup> Finally using scaling arguments one can show that as in the case of the vortex glass, at  $T_{BG}$  the current-voltage characteristics is described by a power-law relation.<sup>1</sup>

## 5.4 The Bragg glass phase

Although the vortex glass and collective creep theories are different in nature, they both agree that the disorder necessary to produce the glasslike low temperature vortex phase, that is characterized by a vanishing linear resistivity, also destroys at large scales the ideal Abrikosov lattice. As a consequence the VS is expected to form a topologically disordered phase, without long range translational order. Moreover general arguments have supported the idea that in such a case disorder will always favour the proliferation of dislocations.<sup>49</sup> However, this picture is in contradiction with several experimental observations. First, as discussed in detail in section 5.1.2, there is unambiguous evidence about the existence of a first order melting transition at low fields as opposed to the continuous one expected for the case of a highly disordered vortex glass. Second, decoration,<sup>60</sup> neutron diffraction,<sup>61</sup> and Lorentz microscopy<sup>62</sup> studies have revealed the presence of a quasi-ordered lattice at low fields, with large regions free of dislocations, which is inconsistent with the above descriptions. At high magnetic fields, however, both the ideal lattice and the first order melting transition are found to disappear, indicating that at these elevated fields the influence of disorder becomes essential.

Hence, the notion that pinning would always destroy long range order had to be

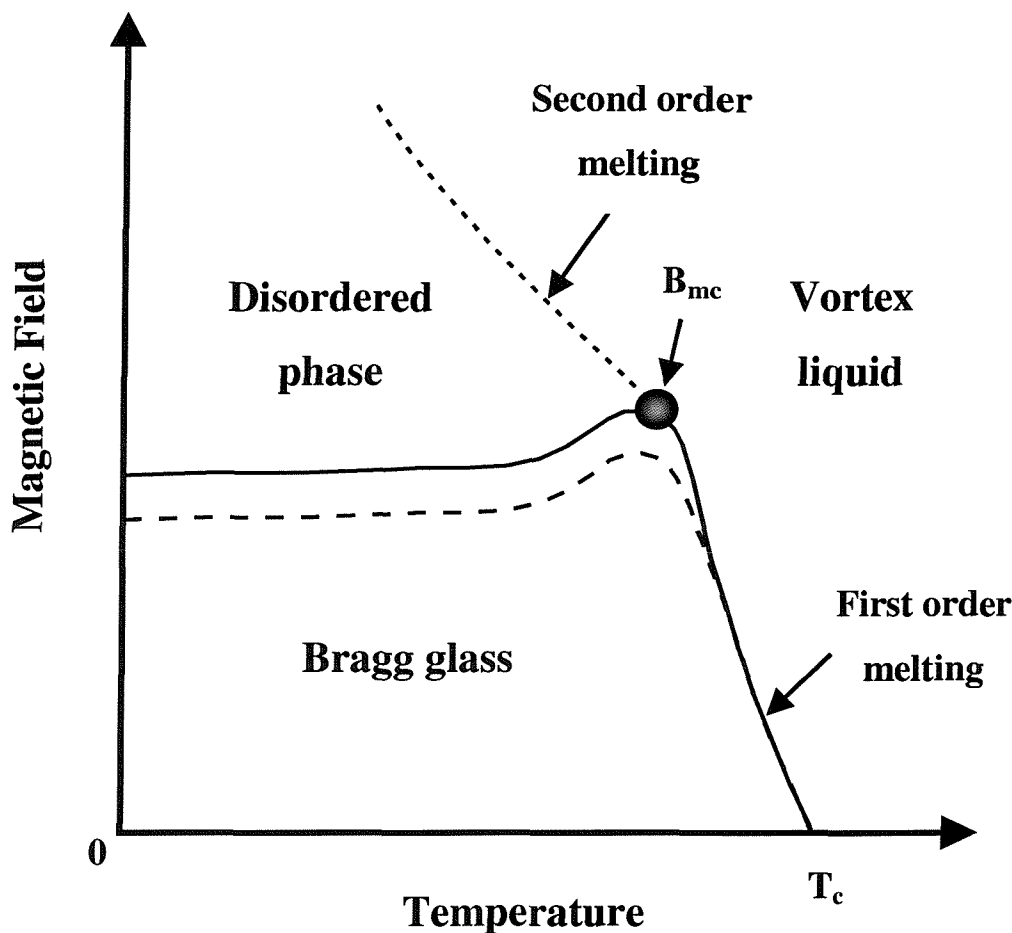


Fig. 5.5. Schematic phase diagram of a type-II superconductor in the presence of thermal fluctuations and weak random uncorrelated disorder, showing the various phases and transition lines (see text). The stability region of the Bragg glass shrinks with increasing disorder as shown by the dashed line. For simplicity here the most widely accepted picture of all lines meeting at a multicritical point  $B_{mc}$  has been adapted. For other possible topologies of the phase diagram we refer the reader to Ref. 41. Also note that for simplicity the reentrant low field disordered phase has not been included.

questioned. After some early results in this direction by Nattermann<sup>63</sup> and Korshunov,<sup>64</sup> Giamarchi and Le Doussal developed a theory of the elastic lattice in the presence of weak point disorder, which, by taking into account the fact that at large scales the periodic structure of the lattice becomes essential, predicted the existence at low fields of a thermodynamic glass phase that retains long range translational order and perfect

topological order and where dislocations are energetically unfavourable.<sup>65</sup> As a glass this phase is characterized by diverging energy barriers for creep and a vanishing resistivity in the limit  $J \rightarrow 0$ .<sup>65</sup> Since it exhibits Bragg diffraction peaks they proposed to call this phase the “Bragg glass”. This result was later further supported by several analytical studies and numerical simulations.<sup>66-71</sup> Since the Bragg glass is almost as good as a perfect lattice as far as translational order is concerned it would be expected to melt through a first order transition. Therefore, such a phase can account for both the thermodynamic and structural results.

Following Refs. 65-67, the stability region of the Bragg glass in the  $B - T$  phase is shown schematically in Fig. 5.5. As can be seen, this phase can be destroyed in two ways: With increasing temperature it melts into a liquid via a first order phase transition,<sup>65-67</sup> whereas with raising the field the effective disorder is enhanced, leading to vortex entanglement and the proliferation of topological defects in the vortex lattice.<sup>65-67, 69, 70</sup> In this way the VS transforms into a highly disordered phase with no translational order. Provided that flux line cutting barriers<sup>72</sup> are large, vortex entanglement and dislocations would increase the effectiveness of pinning and accordingly the critical current.<sup>65, 66</sup> Therefore, on approaching the field-induced transition one would expect to observe an increase in the critical current.<sup>65, 66</sup>

The nature of the high field entangled phase is still poorly understood. It has been proposed that it can be either a vortex glass or a very viscous form of the liquid phase.<sup>65-67</sup> In any case, however, this phase is much more continuously related to the liquid, and therefore one would expect it to melt through a second order transition.<sup>65</sup> If this is the situation, then the Bragg glass provides with a very plausible explanation regarding the change of the order of the melting transition with increasing field, seen in several experimental studies.<sup>35, 41</sup> In addition, the fact that similarly to the multicritical point, the Bragg glass – disordered phase transition line is predicted to shift to lower fields with increasing disorder, it has been suggested that the former could be considered as just the end point of this line.<sup>65-67</sup> Nevertheless, more work is required to clarify this point and establish the exact topology of the phase diagram.

Finally, a distinct feature of the field-induced transition line depicted in Fig. 5.5 is that although at low temperatures it is fairly temperature independent, at elevated temperatures this line shows an upward curvature.<sup>65-67</sup> This is attributed to the weakening of the pinning disorder by thermal fluctuations. Note also that at very low fields ( $B \sim B_{c1}$ )

the Bragg glass becomes unstable and with decreasing field a similar transition should take place, leading to either a pinned liquid or a glassy phase.<sup>65,71</sup>

The order of the Bragg glass – disordered phase transition is still contentious. The numerical simulations of Ryu et al.<sup>71</sup> have proposed a first order transition, whereas Vinokur et al.<sup>67</sup> have speculated a second order one. Analytical calculations in a layered geometry have also suggested a first order transition; however, peculiarities of this configuration make generalization of this result to other geometries rather difficult.<sup>73</sup> It has also been argued that the field-induced transition does not coincide with a decoupling between the layers but it rather takes place in the three-dimensional regime and therefore is expected to be present even in purely isotropic systems.<sup>65,67</sup>

Finally, note that the phase diagram shown in Fig. 5.5 has been constructed for the case of a static vortex lattice. In the presence of a large driving force, the behaviour of the VS is far more complicated and has not been studied in its full extent yet. However, it has been argued that in the case of weak uncorrelated disorder in three dimensions, and at large enough velocities, quasi-long range translational and topological order can still persist in the moving lattice, leading to a *moving* Bragg glass phase that is stable even at nonzero temperature.<sup>74</sup>

## 5.5 Evidence for a transition from elastic to plastic vortex phases in $\text{YBa}_2\text{Cu}_3\text{O}_{7-\delta}$ single crystals

### 5.5.1 Introduction

As discussed in the previous section, several recent theoretical investigations have predicted that at low enough magnetic fields and temperatures the VS forms the Bragg glass phase that is characterized by quasi-long range order, elasticity, and the absence of dislocations. However, with increasing field at constant temperature above a certain value, dislocations will eventually proliferate leading to a highly disordered vortex phase. A distinct difference between such a topologically disordered, plastic phase and a dislocation-free elastic lattice should be the observation of prominent thermomagnetic history effects, similarly to other disordered systems like spin glasses.<sup>75</sup> Indeed, as discussed in detail in Ref. 76 topological disorder present in the VS manifests metastable behaviour and consequently in the presence of dislocations the magnetotransport

properties should depend on the past history of the superconductor. Such memory effects have been observed for a long time in the low temperature superconductors in the region of the conventional peak effect close to the  $B_{c2}(T)$  line.<sup>77-81</sup> For the high temperature superconductors, however, although magnetic measurements,<sup>45, 82-85</sup> together with the hysteretic behavior of the driven vortex solid seen in transport studies,<sup>33</sup> have indicated the importance of plasticity in the vortex lattice in these systems, no detailed investigations of history effects have been performed until now.

This gap is bridged in this chapter, where by means of magnetization measurements we present a detailed study of memory effects in the magnetic hysteresis of pure  $\text{YBa}_2\text{Cu}_3\text{O}_{7-\delta}$  single crystals, with various types and densities of pinning sites.<sup>86-88</sup> A partial magnetization loop technique is employed, which introduces specific protocols that permit the detection of the point where dislocations first invade the vortex system.<sup>86</sup> By studying twin-free single crystals with low densities of point defects, we succeed in the observation of a transition in the mixed state of  $\text{YBa}_2\text{Cu}_3\text{O}_{7-\delta}$  that separates an elastic dislocation-free Bragg glass from a disordered vortex phase. The location of this transition is mapped in the  $B - T$  phase diagram and found to be in proximity to the onset of the second magnetization peak. This line is found to depend on the oxygen stoichiometry, shifting to lower fields with increasing oxygen deficiency in the region  $6.908 \leq 7-\delta \leq 6.999$ , and disappearing for the lowest oxygen contents under study ( $7-\delta = 6.550$  and  $6.760$ ). Above the disorder induced transition, due to the proliferation of dislocations that exhibit metastable behaviour, the critical current density displays a strong dependence on the magnetic history of the superconductor, attaining higher values for increasing the maximum field to which the VS is exposed. For low oxygen concentrations near optimal doping, the memory effects are shown to diminish at high fields due to saturation in the density of dislocations. This effect, however, is absent for the highest oxygen contents under investigation. The influence of extended defects, such as twin boundaries and columns is also studied. We find that for a low density of twin planes the transition is almost unaffected. In contrast, a high density of twins as well as even low densities of columnar defects are shown to destroy the Bragg glass and eliminate the memory effects.

## 5.5.2 Experimental details

### A. Samples

In this study we present results acquired on several pure  $\text{YBa}_2\text{Cu}_3\text{O}_{7-\delta}$  single crystals grown at McGill University and Forschungszentrum Karlsruhe as discussed in detail in Chapter 3. From the first source we have investigated three detwinned (D1, D2, D3), one naturally untwinned (U1) and one twinned (T1) single crystals. Initially all samples had an oxygen content of 6.934. D1 and D3 were subsequently annealed for a further 8 days at 525 °C and 450 °C respectively in 1 bar of oxygen, which should give oxygen contents of 6.908 and 6.970 respectively. After growth, U1 was reannealed at 750 °C in 1 bar for 24 hours that results in  $7-\delta = 6.550$ . From the second source we have studied two naturally untwinned (ZY and ZX), one densely twinned (DN) and two columnar irradiated (AH and AW)  $\text{YBa}_2\text{Cu}_3\text{O}_{7-\delta}$  single crystals with matching fields of 0.1 T and 3 T respectively. All samples were from the same batch and initially had an oxygen content of  $7-\delta = 6.970$ . ZY and ZX, that were the two parts of a larger crystal, were subsequently reannealed in 370 bar of oxygen at 400 °C for 143 hours and in 26.2 mbar at 495 °C for 140 hours respectively, obtaining oxygen contents of  $7-\delta = 6.999$  and 6.760 respectively. Oxygen concentrations were determined from eq. (6) of Ref. 89. The oxygen contents, dimensions, the superconducting transition temperature  $T_c$  as well as the defect status of these samples can be found in table 5.1.

For comparison purposes, we also present briefly some results obtained on a single crystalline sample of the low temperature superconductor 2H-NbSe<sub>2</sub>. This crystal was grown by M. J. Higgins and S. Bhattacharya as described in Ref. 90 and contained 200 ppm of Fe impurities. The sample had dimensions  $2.12 \times 1.70 \times 0.10 \text{ mm}^3$  and the diamagnetic onset of the superconducting transition occurred at  $T_c = 6.0 \text{ K}$  with a width of  $\Delta T_c < 0.3 \text{ K}$ .

### B. Measuring procedure

Magnetic hysteresis measurements were performed using the *Oxford Instruments* vibrating sample magnetometer (model 3001) described in detail in Chapter 4, for applied fields up to 12 T. A measuring procedure that involved partial magnetization loops (PLs) was employed and was realized in two different ways. In *method I* the sample was cooled

Sample	7- $\delta$	$l \times w \times t$ (mm <sup>3</sup> )	$T_c$ (K)	Defect Status	History Effects
U1	6.550	$0.98 \times 0.72 \times 0.07$	62.8	untwinned	no
ZX	6.760	$2.43 \times 1.59 \times 0.24$	71.7	untwinned	no
D1	6.908	$1.07 \times 0.86 \times 0.08$	92.7	detwinned	yes
D2	6.934	$1.69 \times 1.08 \times 0.09$	92.8	detwinned	yes
D3	6.970	$1.29 \times 1.25 \times 0.08$	91.7	detwinned	yes
ZY	6.999	$2.16 \times 0.67 \times 0.24$	88.8	untwinned	yes
TW1	6.934	$0.78 \times 0.59 \times 0.09$	92.6	sparsely twinned	yes
DN	6.970	$1.37 \times 0.85 \times 0.03$	89.6	densely twinned	no
AW	6.970	$1.40 \times 0.75 \times 0.02$	90.4	columns ( $B_\Phi = 0.1$ T)	no
AH	6.970	$1.26 \times 0.57 \times 0.02$	90.4	columns ( $B_\Phi = 3$ T)	no

Table 5.1. Oxygen content, dimensions, transition temperature, defect status and the observation or not of history effects for the investigated  $YBa_2Cu_3O_{7-\delta}$  single crystals.

in zero field that was subsequently swept up to a maximum value,  $B_{\max}$ , before it was decreased back to zero. In a series of runs  $B_{\max}$  increased with a fine step (steps as small as 50 mT were used) finally reaching a value either above the irreversibility field,  $B_{\text{irr}}$ , or of 12 T, depending on which one was smaller. In this case we obtained a complete loop (CL). In *method II* the previous procedure was inverted: After cooling the sample in zero field, the field was increased to a maximum value above the irreversibility line (or up to 12 T if  $B_{\text{irr}} > 12$  T) and then after decreasing it down to a certain value  $B_{\min}$  it was swept again to the same maximum field. This procedure was repeated for several values of  $B_{\min}$ . In all cases, after completion of each run the sample was heated up into the normal state and then cooled again to the desired temperature in zero field. The sweep rate of the magnetic field was varied in the range 2 – 20 mT/sec.

### 5.5.3 Results

Figure 5.6 shows hysteretic magnetization loops for D2 at 74 K. The solid line represents the complete magnetization loop whereas with the dashed and dotted lines we show PLs obtained by *methods I* and *II* respectively for  $B_{\max} = B_{\min} = 2$  T. Remarkably the PLs do not follow the CL but the hysteretic magnetization, and therefore the critical current density  $J_c$ , depends on the measuring procedure. In particular, the magnetization (or  $J_c$ ) on the descending branch of the *method I* PL attains lower values than the ones corresponding to the CL. This effect persists until the field is reduced by a value  $\Delta B_{\text{sup}} \approx 1$  T below  $B_{\max}$ , where the PL finally merges with the CL. On the other hand, for the *method II* PL the effect is opposite: Increasing the field above  $B_{\min}$  results in enhanced hysteresis. No merging with the CL is seen and a small increase in the magnetization persists up to the irreversibility field.

It is stressed that  $\Delta B_{\text{sup}}$  is rather large for the deviation of the PLs from the CL to be associated with the influence of an incomplete reversal of the field profile in the superconductor. Indeed, as has been predicted for thin disks in an axial magnetic field, the field of full penetration should be approximately equal to  $\mu_0 \frac{J_c t}{2} \ln\left(\frac{4a}{t}\right)$ , where  $a$  is the radius and  $t$  the thickness of the disk.<sup>91</sup> For a rectangular sample of large aspect ratio (like D2),  $a$  can be replaced by an effective radius given by  $a_{\text{eff}} = \frac{3w}{4}\left(1 - \frac{w}{3l}\right)$ ,<sup>92</sup> with  $l$  and  $w$  being the length and width of the crystal respectively. Accordingly, from the critical current density values, as calculated from the magnetization width using the critical state formula,<sup>92</sup> one can easily find that for D2 at  $T = 74$  K the penetration field is less than 10 mT, a value much too small to account for the results displayed in Fig. 5.6.

The memory effects are shown more quantitatively in Figure 5.7. There the ratio,  $R = (\Delta M_{\text{CL}} - \Delta M_{\text{PL}})/\Delta M_{\text{CL}}$ , of the difference in the hysteresis widths between the CL and several PLs obtained by *methods I* or *II* at 74 K to the hysteresis width of the CL, is plotted as a function of  $B_{\max}$  or  $B_{\min}$  respectively.<sup>93</sup> As can be seen, the magnetization on the decreasing or increasing field branches of PLs obtained by *methods I* or *II* respectively can deviate by as much as 25% from the CL magnetization width, suggesting that the current density on these branches can be varied by as much as 50%.  $R$  is

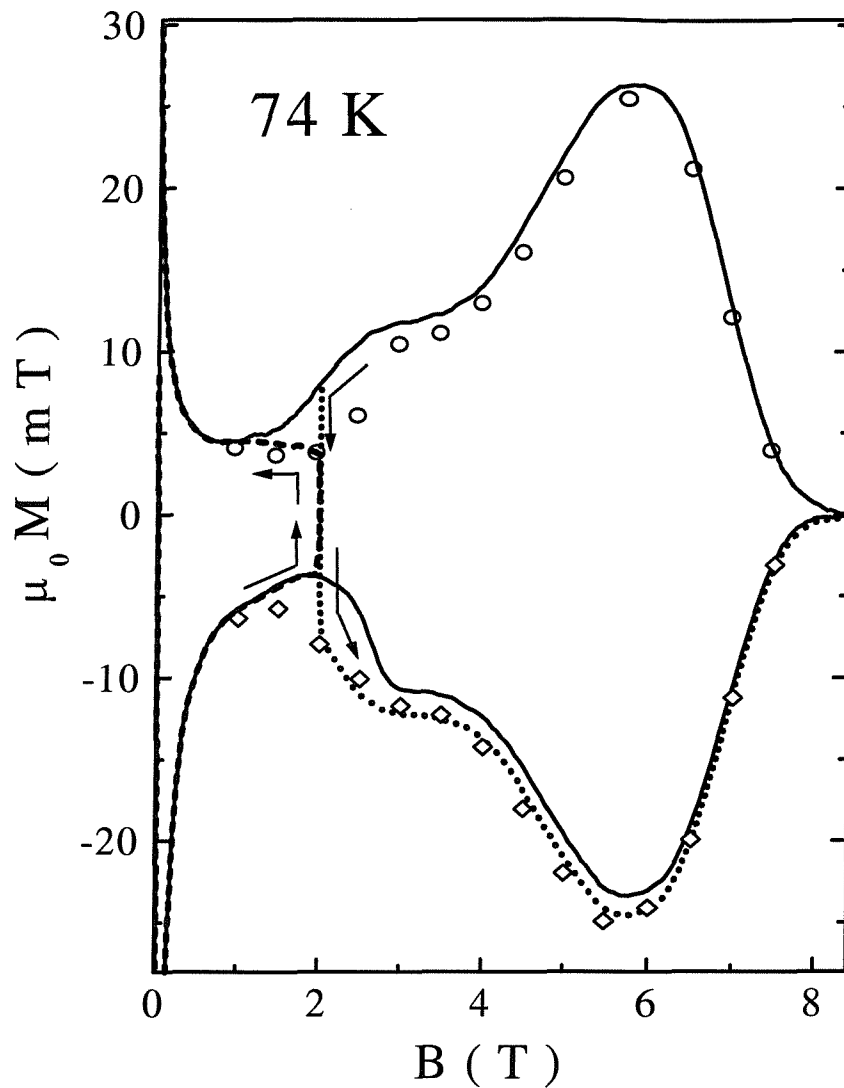


Fig. 5.6. Magnetic hysteresis curves for sample D2 ( $7-\delta = 6.934$ ) at 74 K. The solid line is the CL whereas the dashed and dotted lines show PLs obtained by methods I and II respectively for  $B_{\max} = B_{\min} = 2$  T. The arrows indicate the direction of the field sweep. Note that according to the critical state model (see Chapter 2), in the absence of history effects the PLs must fall onto the CL after a field change equal to twice the penetration field, i.e.,  $\sim 20$  mT for the present case (see text). The open circles or diamonds represent magnetization values in the descending or ascending legs of several method I or II PLs respectively directly after reversal of the field profile in the sample.

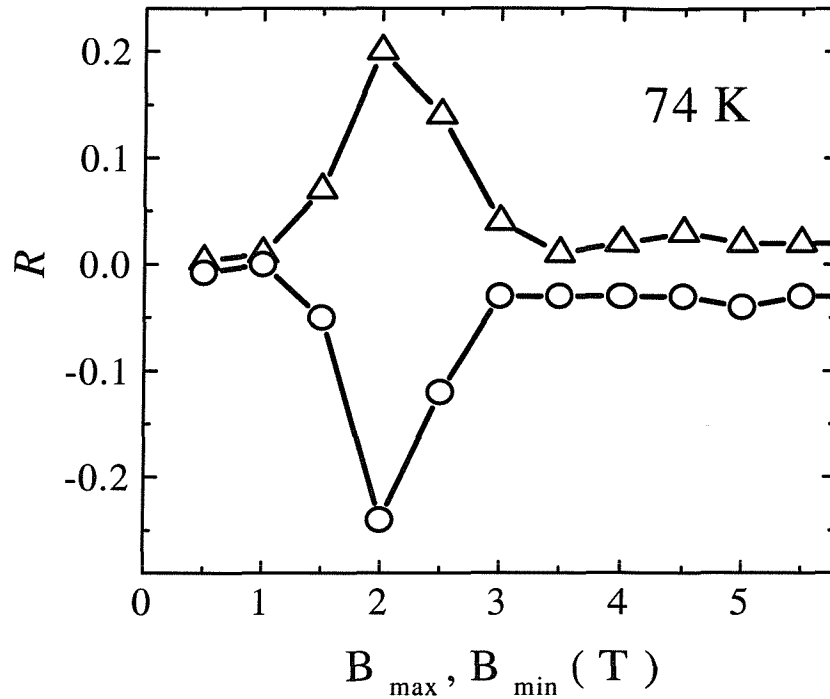


Fig. 5.7.  $R$  (defined in the text), plotted as a function of  $B_{max}$  (triangles) or  $B_{min}$  (circles) for sample D2 at 74 K.

maximum in the intermediate field region ( $1 \text{ T} < B < 3 \text{ T}$ ) whereas for higher or lower fields the effect becomes weak and only small traces of the memory effects are observed.

From these results we conclude that field cycling of the superconductor can lead to increased critical currents i.e., a hardening of the hysteretic response. Since within the elastic description  $J_c$  is a single valued function of the field and temperature, the hardening effect points to the presence of plastic deformations in the VS, which lead to a dependence of the lattice structure on the magnetic history of the sample. The path dependent current further implies that description by a simple critical state model (see Chapter 2), where at a certain temperature,  $J_c$  is determined uniquely by the value of the field, is not applicable.

Another interesting feature depicted in Fig. 5.6 is that for  $1 \text{ T} < B < 3.5 \text{ T}$  the upper and lower branches of the CL are highly asymmetric. This asymmetry is characteristic of pure single crystals and as demonstrated for the first time in Ref. 86, it stems from the history dependence of the irreversible magnetization. Indeed, as shown by the open circles (diamonds) in Fig. 5.6, that represent the magnetization values in the upper (lower)

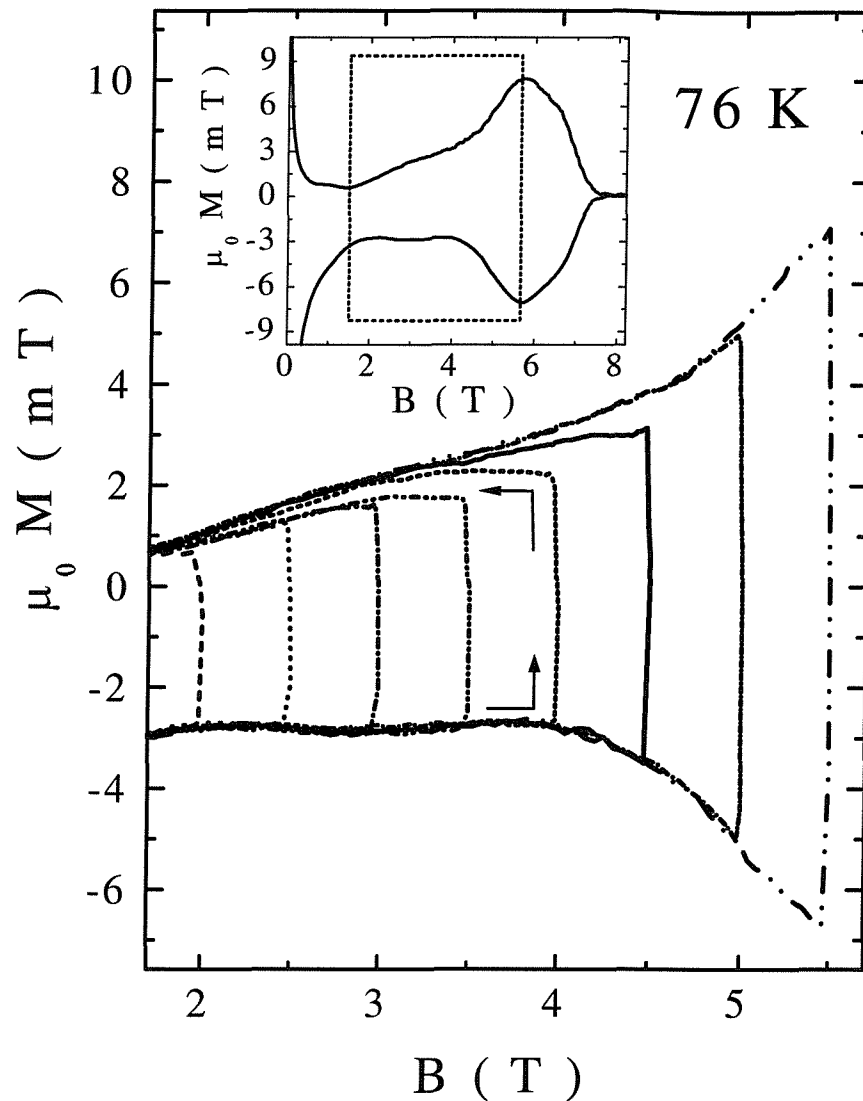


Fig. 5.8. Several PLs for sample D2 obtained by method I at 76 K for  $1.5 \text{ T} < B_{\text{max}} < 6 \text{ T}$ , with  $B_{\text{max}}$  increasing with a step of 0.5 T. Arrows indicate the direction of field sweep. The inset shows the CL for this temperature with the box indicating the field region corresponding to the illustrated PLs.

branches of *method I* (*method II*) PLs directly after reversal of the field profile in the superconductor, the asymmetry disappears and the ascending (descending) branch of the full loop is almost perfectly reproduced.

The most important result of our investigation is illustrated in Fig. 5.8, where we display in detail PLs obtained by *method I* at 76 K for  $1.5 \text{ T} < B_{\text{max}} \leq 5.5 \text{ T}$ . As can be clearly seen, for field excursions up to 3.5 T the PLs follow the same, universal curve and

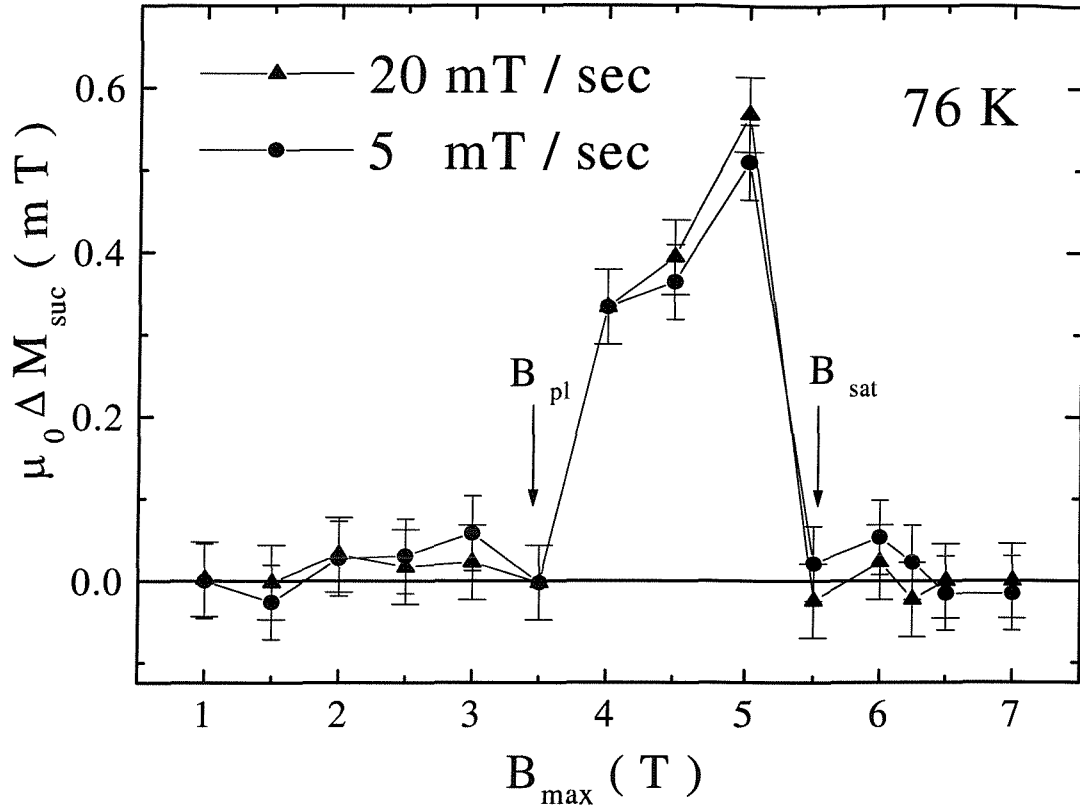


Fig. 5.9. The difference  $\Delta M_{suc}$  in the magnetization widths of successive PLs for D2 at 76 K is plotted versus  $B_{max}$  for two different field sweep rates as indicated on the graph. The arrows mark the positions of  $B_{pl}$  and  $B_{sat}$  (see text).

the current is independent of the magnetic history of the sample. Since the absence of path dependent hysteresis is characteristic of the elastic regime, this observation suggests that in this field range the vortex lattice is only elastically distorted. In contrast, for  $B_{max}$  above 3.5 T the return legs of the PLs start to deviate from the universal curve and the magnetization shows a strong dependence on  $B_{max}$ , gradually attaining higher values and approaching the descending leg of the CL. This behaviour continues up to  $B_{max} = 5$  T above which the PLs fall again onto the same line. These observations become more clear in Fig. 5.9 where we display for two different field sweep rates the difference,  $\Delta M_{suc}$ , in the magnetization widths of successive PLs as a function of  $B_{max}$  of the upper PL.<sup>93</sup> Following a zero plateau, a sharp increase of  $\Delta M_{suc}$  is seen at a sweep rate independent characteristic field  $B_{pl}$  before it drops again below the level of experimental resolution at

a second field  $B_{\text{sat}}$ , above which the PLs coincide independently of the maximum field excursion.

The effect of variations in the oxygen stoichiometry on the memory effects has also been investigated. Figures 5.10 and 5.11 illustrate the CL together with several PLs for crystals D1 and D3 respectively. For brevity only the ones obtained by *method I* are shown. As can be seen, the memory effects are present in both samples. In general, the behaviour of D1 is found to be very similar to D2. On the other hand, D3 shows some distinct features. First, for this low oxygen deficiency ( $\delta = 0.03$ ) the memory effects become more prominent as compared to D1 and D2. Indeed, for D3 the obtained  $R$  values can become as high as 0.5, i.e., field cycling can lead to an increase in the critical current density by up to 100%! In the same manner  $\Delta B_{\text{sup}}$  increases as well attaining values that can be as large as 2 T. Another important observation is that for this high oxygen content no drop of  $\Delta M_{\text{suc}}$  at a characteristic field is seen, i.e., successive PLs do not merge with each other even for the highest accessible fields of our experiment (see Fig. 5.11). The same result was obtained for ZY. Concerning the characteristic field  $B_{\text{pl}}$ , we find that following the behaviour of the magnetization peak, with increasing oxygen stoichiometry shifts to higher fields (see insets of Figs. 5.10 and 5.11).

Nevertheless, for the strongly underdoped samples U1 ( $7-\delta = 6.550$ ) and ZX ( $7-\delta = 6.750$ ) the history effects disappear completely, and the magnetization loop now displays the conventional “fishtail” behaviour, indicating enhanced disorder. This result is illustrated in Fig. 5.12 where we show for U1 the CL together with several PLs as obtained by *method I* at 45 K. In addition, transport studies show that for these low oxygen contents the melting transition becomes of the second order in the whole field range.<sup>94</sup>

Finally, we have also studied the influence on the history effects of extended defects such as twin planes and columns. Figure 5.13 (a) shows PLs for the sparsely twinned T1 for fields applied along the  $c$ -axis. As can be seen, the magnetization history dependence is not significantly affected by the presence of the twin planes and the overall behaviour resembles the detwinned crystals with the same oxygen content (compare this figure with Fig. 5.6).<sup>87, 88</sup> In contrast, as depicted in Fig. 5.13 (b), for the densely twinned DN the history effects are almost completely eliminated (a small remanent effect with  $R \sim 0.02$  can be still seen at fields above 4.5 T). The same result was obtained for the columnar irradiated samples as can be seen in Fig. 5.13 (c) for AW ( $B_{\Phi} = 0.1$  T). From

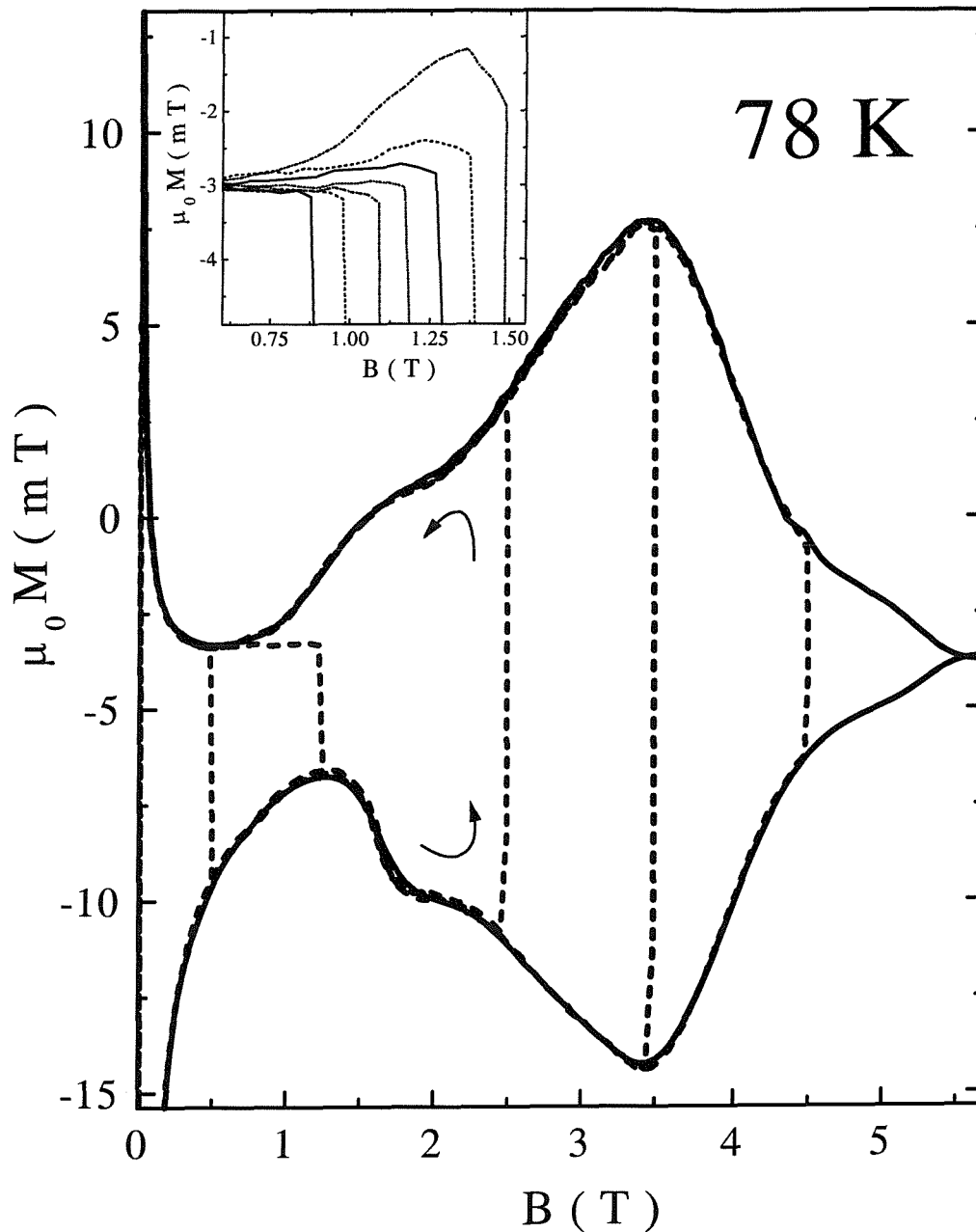


Fig. 5.10. Magnetic hysteresis curves for sample D1 ( $7-\delta = 6.908$ ) at 78 K. The solid line represents the CL whereas the dashed lines indicate PLs obtained by method I for several  $B_{\max}$ . The arrows show the direction of the field sweep. Inset: The descending branches of various PLs (method I) in the region  $0.8 \text{ T} < B_{\max} < 1.6 \text{ T}$ , with  $B_{\max}$  increasing with a fine step of 0.1 T. Note the different behaviour of the PLs for  $B_{\max}$  below and above  $B_{pl} = 1.1 \text{ T}$ .

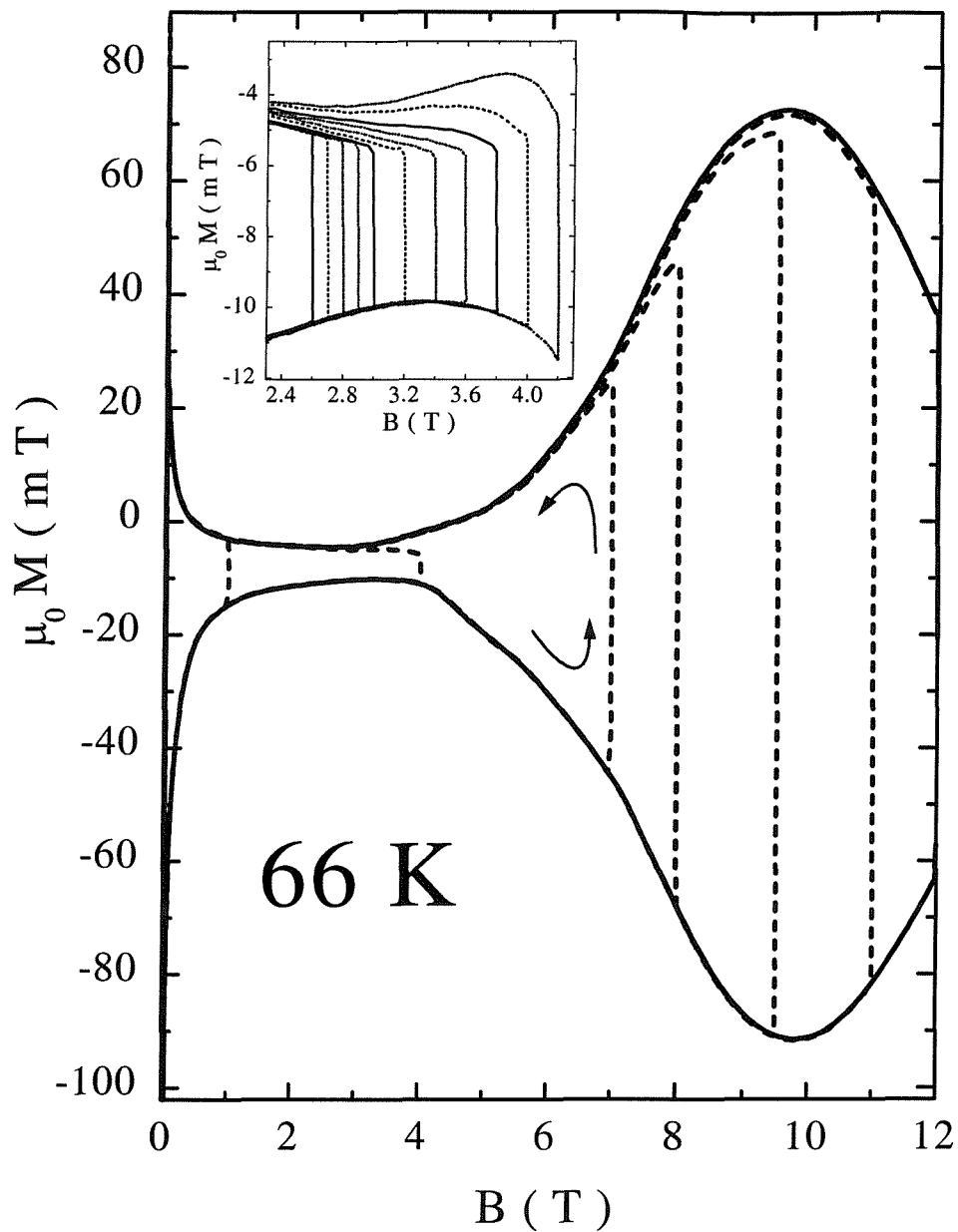


Fig. 5.11. Magnetization loops for sample D3 ( $7-\delta = 6.970$ ) at  $T = 66$  K. The solid line shows the CL whereas the dashed lines represent method I PLs at various  $B_{max}$ . The inset shows in detail several PLs in the range  $2.6 \text{ T} \leq B_{max} \leq 4.2 \text{ T}$  with  $B_{max}$  increasing with a step of 0.1 in the range  $2.6 \text{ T} \leq B_{max} \leq 3 \text{ T}$  and 0.2 T for  $3 \text{ T} \leq B_{max} \leq 4.2$ . Notice again the onset of history effects at  $B_{max} > B_{pl} = 3 \text{ T}$ .

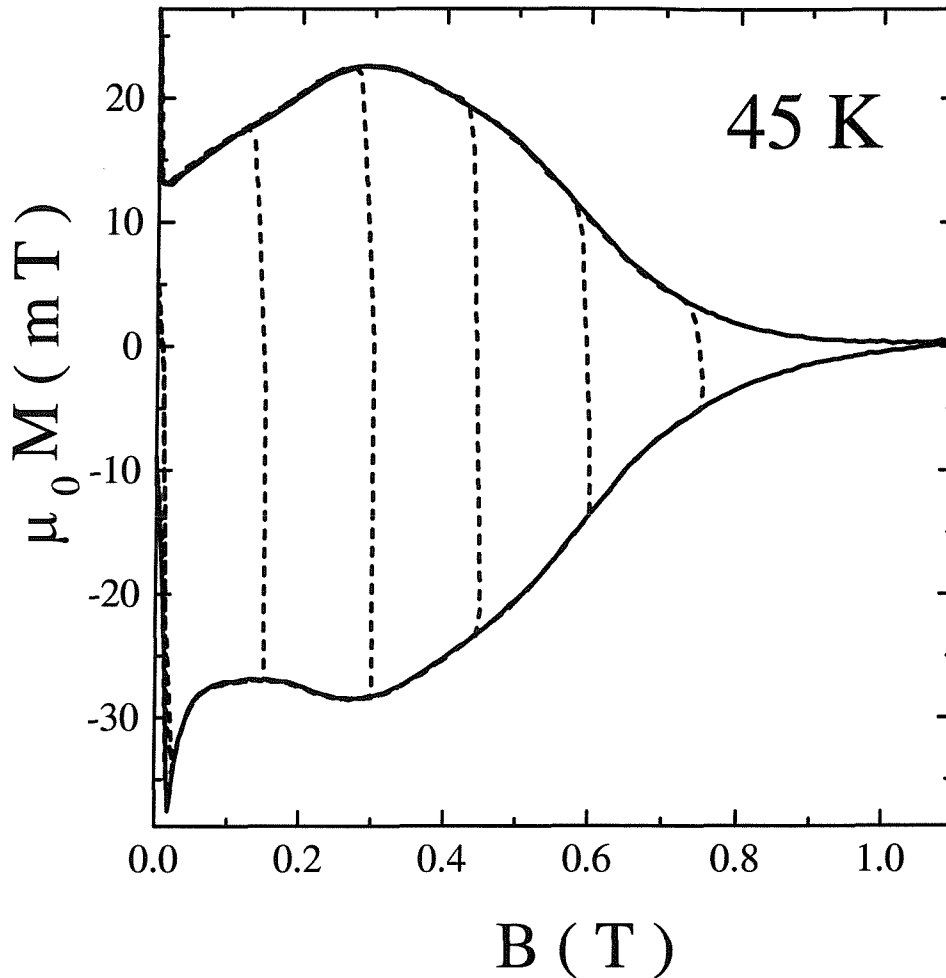


Fig. 5.12. Method I PLs (dashed lines) for U1 ( $7-\delta = 6.550$ ) at 45 K and several values of  $B_{max}$  are illustrated together with the CL (solid line).

Figs. 5.13 (b) and 5.13 (c) one can also discern the significant influence of both a high density of twin planes and the columnar defects on the magnetic hysteresis loop. Indeed, in these samples the characteristic long “neck” observed in the  $M(B)$  curves below the peak for all the detwinned crystals as well as for T1 is significantly suppressed, and the hysteresis width in this field region becomes comparable to the one seen at the peak. The columnar irradiated crystals also show a pronounced increase in pinning in the whole field range. For example, for AW at 70 K, we observe an enhancement in the critical current density by as much as four times as compared to the initial state of the sample.

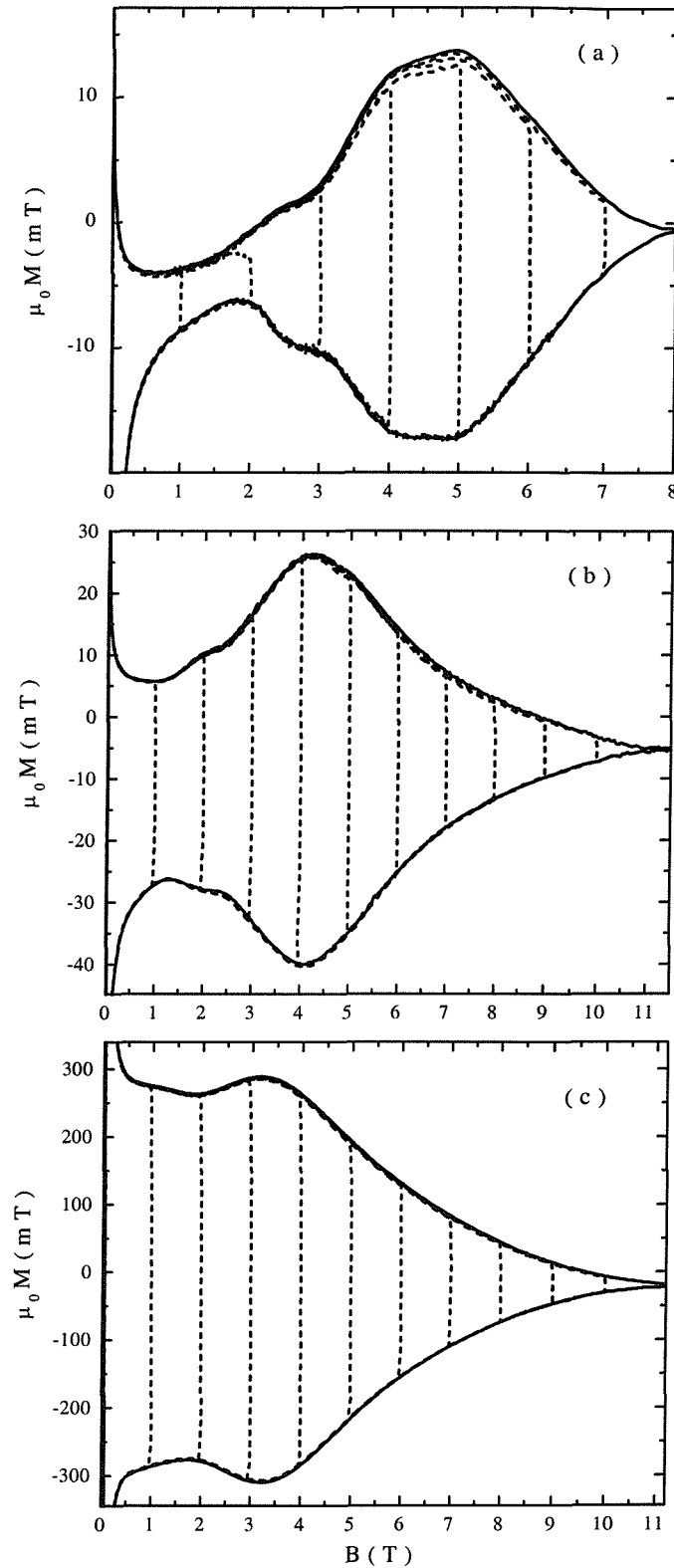


Fig. 5.13. The CL (solid line) together with various method I PLs (dashed lines) are displayed for samples (a) T1, (b) DN, and (c) AW at  $T/T_c = 0.8$ .

## 5.5.4 Discussion

### A. History Effects

As discussed above, several recent analytical studies and numerical simulations have predicted the existence of a disorder-induced phase transition in the mixed state of type-II superconductors. At low fields the Bragg glass phase is realized, where elasticity survives and the vortex lattice maintains quasi-long range translational order. However, upon raising the field above its stability region, topological defects such as dislocations become energetically favorable and invade the vortex lattice. Consequently long range order is either diminished or completely lost and vortices form a highly disordered phase.<sup>65-71</sup>

Dislocations appear due to the influence of both quenched disorder and thermal fluctuations, which induce transverse wandering of vortices from their equilibrium positions, resulting in vortex entanglement. In this sense, the magnetic field plays an important role as it tunes the effective disorder by changing the mean intervortex distance, thus stimulating the injection of dislocations.<sup>65-67</sup> Therefore, with increasing field the elastic structure becomes unstable and a transformation from an elastically to a plastically distorted lattice is expected, a process accompanied by the invasion of topological defects at short length scales.<sup>65</sup> Being of different nature these two phases are characterized by different magnetotransport properties. As discussed in section 5.3 a direct consequence of vortex entanglement and the introduction of topological disorder should be the increase in the critical current density.<sup>65-67</sup>

Our observations can be understood within this framework. When during an isothermal magnetization loop the field increases beyond the elastic regime, dislocations appear and the VS is forced into an increasingly disordered state. By decreasing the field from this state, the amorphous structure of the lattice becomes energetically unfavorable. However, as discussed in detail in Ref. 76, topological disorder exhibits metastable behaviour due to trapping of dislocations in local energy minima. Thus the density of topological defects does not vary reversibly with field and one should expect a path dependent critical current. This is indeed the case shown in Fig. 5.6: With decreasing field the VS in the return leg of the CL tends to retain topological defects from the high field, disordered state, leading to higher currents than the ones corresponding to the ascending

branch. This is clearly demonstrated by the observed reduced or enhanced irreversible magnetization values for the PLs obtained by *methods I* or *II* respectively as compared to the full loop (see Fig 5.6). Only when the field attains low enough values, does the remanent dislocation network completely heal out of the VS. Hence, any memory of the lattice formation history is erased, as illustrated by the coincidence of the PLs with the CL at low fields (see Figs. 5.10 and 5.11).

It is stressed that although for our pure crystals, that demonstrate effects very sensitive to sample homogeneity,<sup>95</sup> it is difficult to suppose the existence of granularity, nevertheless, even if present, the latter could not explain the observed behaviour. In a granular sample the standard relation between hysteresis width and remagnetization field breaks due to the existence of two types of currents: Intergranular and intragranular.<sup>96</sup> As the latter can attain very high values, the self-field of the grains can lead to significant differences between the internal and applied fields.<sup>96</sup> This difference is positive or negative for decreasing or increasing fields respectively. Consequently, when the field-sweep direction is reversed in the region where the current decreases with field (like above the peak), one would expect enhanced or decreased magnetization values for the PLs similarly to the results depicted in Fig. 5.6. Below the peak, however, where the current increases with field, this model requires the opposite behaviour that is not seen in our experiments and it should therefore be rejected.

Finally, we have investigated the influence of time on the metastable disorder in the descending branch of the CL. In the decreasing field leg of a CL, the field was stopped at certain values and after waiting a given time, the field sweep was continued back to zero. Following this procedure, for a waiting time of two hours the magnetization on the decreasing field  $M(B)$  curve was found to be reduced by less than 4% of the CL magnetization width as can be seen in Fig. 5.14. This demonstrates that although annealing of dislocations does occur, the effect is rather weak illustrating that the dislocation network in the VS is stable over long time scales.

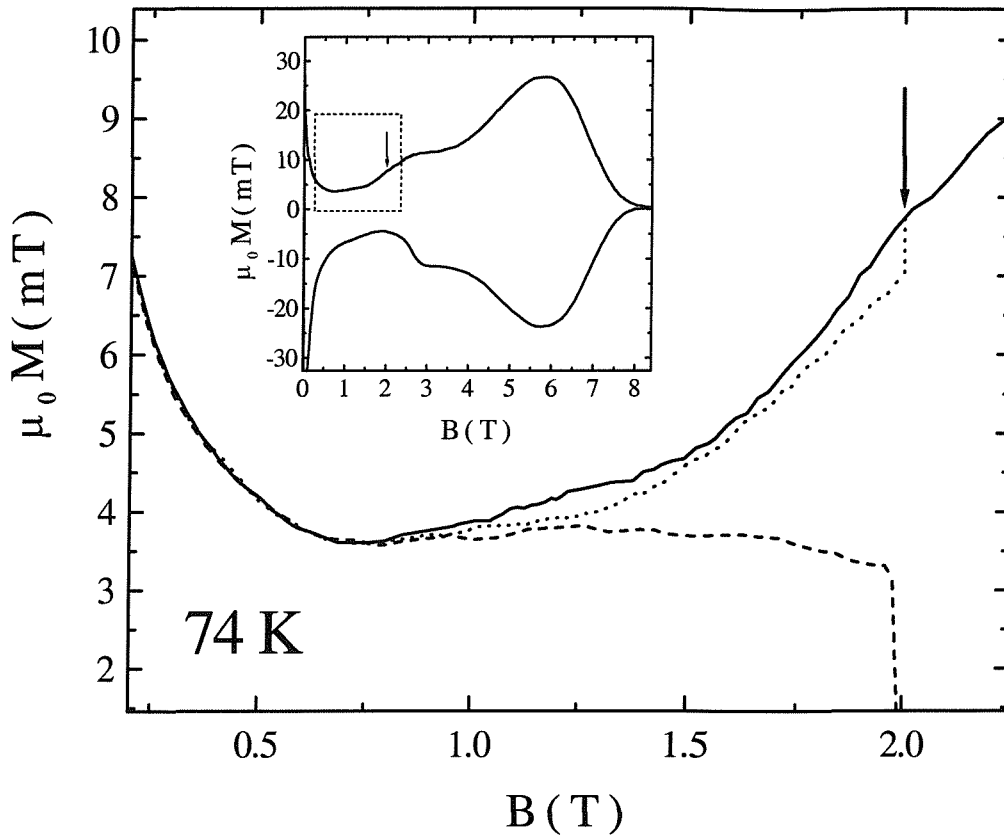


Fig. 5.14. Parts of the CL (solid line) and a method I PL for  $B_{\max} = 2$  T (dashed line) are shown for D2 ( $7-\delta = 6.934$ ) at 74 K. The dotted line represents the magnetization for decreasing field from 2 T, where on the course of a CL the field sweep had been stopped for two hours. The inset shows the CL for this temperature with the rectangle indicating the region illustrated in the main panel.

## B. Phase Diagram

The partial loop technique is very important since it allows the detection of the point where topological disorder invades the vortex system for the first time. Indeed, as long as the maximum field excursion is not high enough to drive the VS out of the region where elasticity dominates, then due to the reversibility characterizing the structural properties of an elastically deformed lattice no history effects should be observed.<sup>1</sup> Consequently, within this range of  $B_{\max}$  the PLs must follow a universal curve. Such behaviour is indeed seen below the characteristic field  $B_{\text{pl}}$ , as depicted in Fig. 5.8, and the

insets of Figs. 5.10 and 5.11. However, when  $B_{\max}$  is raised above this value, the PLs start to deviate significantly from the common line. From this point the critical current displays a strong dependence on the magnetic history of the superconductor (see e.g. Fig. 5.8), which demonstrates the presence of metastable disorder and plasticity in the VS. In this region with increasing field the number of topological defects rises until  $B_{\text{sat}}$  is reached. At this point a saturation in the density of dislocations occurs and the amount of disorder is only negligibly affected by the changing field.<sup>86</sup> For this reason at high fields the PLs closely coincide with each other as well as with the CL. However, as discussed above, such saturation is not seen for the highly oxygenated D3 and ZY up to our maximum field of 12 T (see Fig. 5.11). We attribute this effect to the reduced disorder in these samples due to the much lower density of pinning centres as compared to the crystals with higher oxygen deficiency, which requires fields beyond our maximum accessible values for the saturation in the density of dislocations to occur.<sup>86, 87</sup>

Our results indicate strongly that below  $B_{\text{pl}}$  the VS is elastically deformed and that topological defects are absent. These characteristics are identical to the Bragg glass phase.<sup>65-71</sup> Therefore, as we have proposed in Ref. 86,  $B_{\text{pl}}$  features the transition from the Bragg glass to a disordered vortex phase where plasticity plays a dominant role. The loci of the  $B_{\text{pl}}$  values for the various oxygen contents under study are shown in the  $B - T$  phase diagrams of Fig. 5.15.<sup>97</sup> In these plots we have also included the lines corresponding to the temperature dependence of the saturation field  $B_{\text{sat}}$ , the magnetization peak  $B_{\text{p}}$  and the peak onset  $B_{\text{on}}$ .<sup>98</sup> The first order melting transition lines, that were determined from resistivity measurements similar to the ones shown in Fig. 5.4, on identical crystals from the same batch are also included. Below  $B_{\text{mc}}$  the melting lines for all samples fit well to the equation  $B_{\text{m}} = B_0 (1-T/T_c)^\alpha$  with the same power index  $\alpha = 1.39$ ,<sup>42</sup> in correspondence with other studies.<sup>25, 32</sup> Nevertheless, the values of the prefactor  $B_0$  differed, apparently due to variations in the density of charge carriers and the anisotropy with the oxygen content.<sup>42</sup>

Two interesting features characterize the behaviour of the  $B_{\text{pl}}(T)$  lines. First, although at low temperatures they show a plateau, with increasing temperature an upturn is seen. Second, they shift towards higher fields with decreasing oxygen deficiency. Both trends are in agreement with the theoretically predicted transition line separating the Bragg glass from the high field disordered phase (see Fig. 5.5),<sup>65-67</sup> and can be understood as follows. The structure of the vortex solid is determined in general by the competition

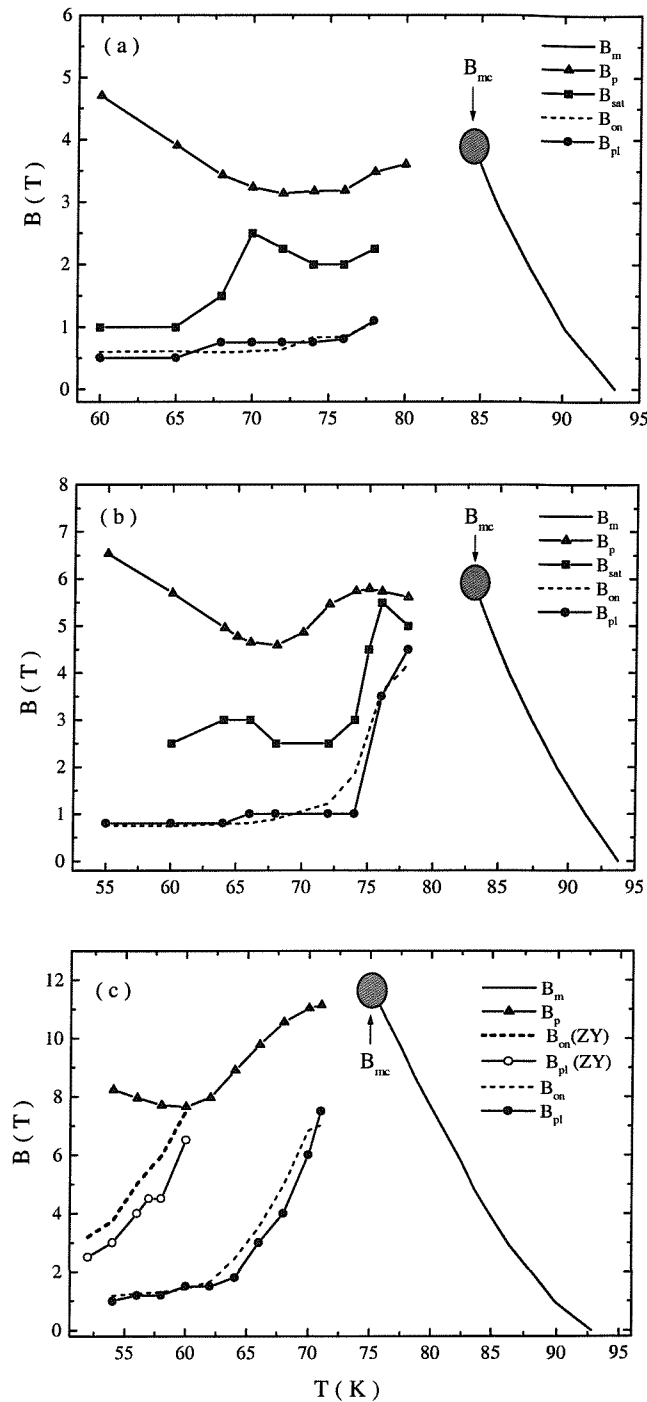


Fig. 5.15. Position of the fields  $B_p$ ,  $B_{pl}$ ,  $B_{on}$  and  $B_{sat}$  in the  $B - T$  phase diagram for D1 ( $7-\delta = 6.908$ ) (a), D2 ( $7-\delta = 6.934$ ) (b) and D3 ( $7-\delta = 6.970$ ) (c). The corresponding melting lines,  $B_m(T)$ , are also displayed. The open circles and thick dashed line in Fig. 5.15(c) show the temperature dependence of  $B_{pl}$  and  $B_{on}$  respectively for ZY ( $7-\delta = 6.999$ ). The position of the peak for this sample is shifted beyond our maximum field of 12 T.

between the pinning and elastic energies. When the pinning energy increases beyond the elastic one, topological defects will proliferate.<sup>67</sup> At elevated temperatures, however, due to thermally activated motion of vortices pinning by point disorder is reduced. Consequently, dislocations will be introduced in the VS only when higher fields (as compared to the lower temperatures) are reached, resulting into the upward curvature of the  $B_{pl}$  line.<sup>65-67</sup> Theory predicts that such an upturn in the temperature dependence of  $B_{pl}$  should occur near the single vortex depinning temperature  $T_{dp}$ ,<sup>66</sup> which is defined by the crossover condition  $\langle u^2(T_{dp}) \rangle_{th} \approx \xi^2$ .<sup>1</sup> In this region  $B_{pl}$  is predicted to vary with temperature according to the relation:<sup>66</sup>

$$B_{pl}(T) \approx B_{pl}(0) \left( \frac{T_{dp}}{T} \right)^{10/3} \exp \left[ \left( \frac{2c}{3} \right) \left( \frac{T}{T_{dp}} \right)^3 \right] \quad (5.12)$$

with  $c$  a constant of order unity. As shown with the solid lines in Fig. 5.16 this relation fits quite well our data using  $T_{dp} \sim 35$  K, a value that is in reasonable agreement with other estimates.<sup>84</sup>

On the other hand, with raising  $\delta$  in the region near optimal doping, due to the increase in the density of oxygen vacancies, disorder is strengthened whereas at the same time the elastic energy remains almost unchanged.<sup>42</sup> Consequently, as predicted in Refs. 65-67, a shift of the location of the  $B_{pl}(T)$  line to lower field values should take place as is indeed the case presented in Fig. 5.15. In addition, for larger  $\delta$  the  $B_{pl}$  plateau is expected to extend to higher temperatures in accordance with our observations. Nevertheless, for the underdoped samples U1 and ZX, due to the high density of oxygen vacancies the role of disorder is substantially enhanced and the pinning energy always dominates over the elastic one. This leads to the destruction of the Bragg glass and the formation of a disordered phase in the whole field range. Accordingly, one would expect the absence of the history effects and the suppression of the first order melting transition in correspondence with our experimental results.

Another important observation from Fig. 5.15 is that the  $B_{pl}(T)$  lines for all the samples showing history effects are located in proximity to the ones corresponding to the onset of the second magnetization peak. This points out that the peak might be related to the destruction of the Bragg glass and the onset of plasticity. Such a possibility has been

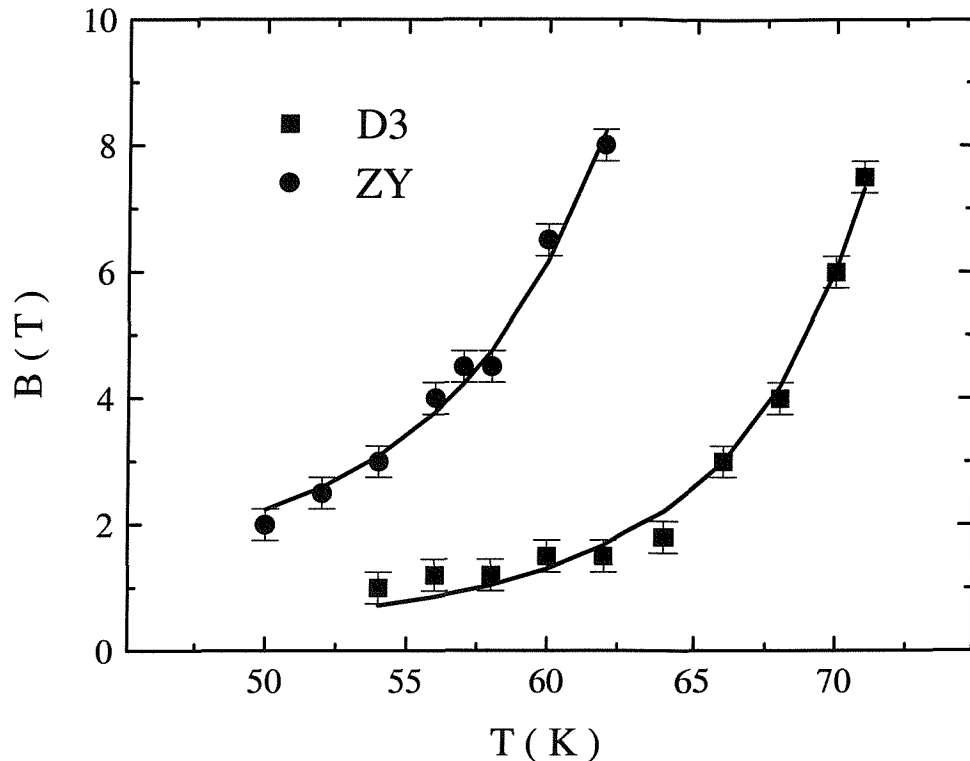


Fig. 5.16. The temperature dependence of  $B_{pl}$  for samples D3 and ZY as indicated in the graph. The solid lines are fits of eq. (5.12) as discussed in the text. The obtained values for the fitting parameters were  $B_{pl}(0) = 0.2 T$ ,  $T_{dp} = 36 K$ ,  $c = 1.2$ , for D3 and  $B_{pl}(0) = 0.8 T$ ,  $T_{dp} = 35 K$ ,  $c = 1.1$ , for ZY. Note that in accordance with the theoretical predictions of Refs. 65-67  $B_{pl}(0)$  decreases with  $\delta$ .

already conjectured in several experimental<sup>45, 82-85</sup> and theoretical works,<sup>65-67, 99</sup> and will be discussed extensively in the following chapter.

It is worth noting that a phase diagram similar to the one shown in Fig. 5.15 has also been constructed from local magnetization measurements for the case of BSCCO single crystals.<sup>45, 82</sup> It was found that in this compound the increase of the current towards the peak at a characteristic field  $B_{sp}$  is extremely sharp (the width of the increasing current region was found to be of the order of only 0.5 mT) suggesting that this feature might mark some phase transition. Hence, it was speculated that  $B_{sp}$  indicates a transition from an ordered to a disordered vortex lattice.<sup>45</sup> This scenario had also been assisted by direct observations of a lattice close to ideal,<sup>60-62</sup> but only at low fields, as well as by indications

for increased vortex wandering above the onset of the peak.<sup>100</sup> The  $B_{\text{sp}}(\text{T})$  lines were found to shift to lower fields with increasing density of point defects and also showed an upward curvature at high temperatures, in correspondence with our results (see Fig. 5.15).<sup>45, 82</sup> Moreover, these lines merged with the first order melting lines at  $B_{\text{mc}}$ , suggesting a phase diagram identical to the one depicted in Fig. 5.5. Although as can be seen from Fig. 5.15, the same trend is rather possible in our case too, unfortunately due to experimental limitations we have not been able to study the high temperature region close to the melting line and confirm such a behaviour for  $\text{YBa}_2\text{Cu}_3\text{O}_{7-\delta}$  as well.

However, it is stressed that the situation in the case of BSCCO is more complicated as compared with  $\text{YBa}_2\text{Cu}_3\text{O}_{7-\delta}$ , mainly due to the much stronger anisotropic properties of the former. Thus, although the suggestion that  $B_{\text{sp}}$  corresponds to the disorder-induced phase transition is very possible, the role of the strong two-dimensional behaviour of this compound, that in the field region under discussion can lead to effects such as a decoupling between the layers,<sup>101</sup> is still unclear and awaits further, more systematic theoretical and experimental investigations.

Finally, several recent experimental studies have supported the presence of the disorder-induced transition in the low temperature superconductors as well.<sup>78-80, 102</sup> Using a PL technique, we have demonstrated that in the weakly anisotropic  $2\text{H-NbSe}_2$  there exists a characteristic field  $B_{\text{pl}}$ , below which  $J_c$  is independent of the magnetic history of the sample (see Fig. 5.16). Similarly to  $\text{YBa}_2\text{Cu}_3\text{O}_{7-\delta}$ , this field is located in proximity to the onset of the second magnetization peak and indicates the existence of a quasi-ordered elastic phase.<sup>102</sup> Nevertheless, the most unambiguous experimental verification for the presence of the disorder-induced transition in these compounds was provided by direct observation of the vortex lattice with neutron scattering experiments.<sup>103</sup> This work revealed the following sequence of vortex phases through the peak effect in Nb single crystals:<sup>103</sup> Below the onset of the peak an ordered phase exists. It is followed by an intermediate phase that is characterized by the disappearance of positional order in the vortex lattice; however, orientational order is still preserved. On the other hand, above the peak a completely disordered phase is realized.

### C. Extended Defects

The effect of twin planes on the vortex dynamics is a complicated and still not fully resolved topic. Twins have been shown to lead to increased pinning at high temperatures

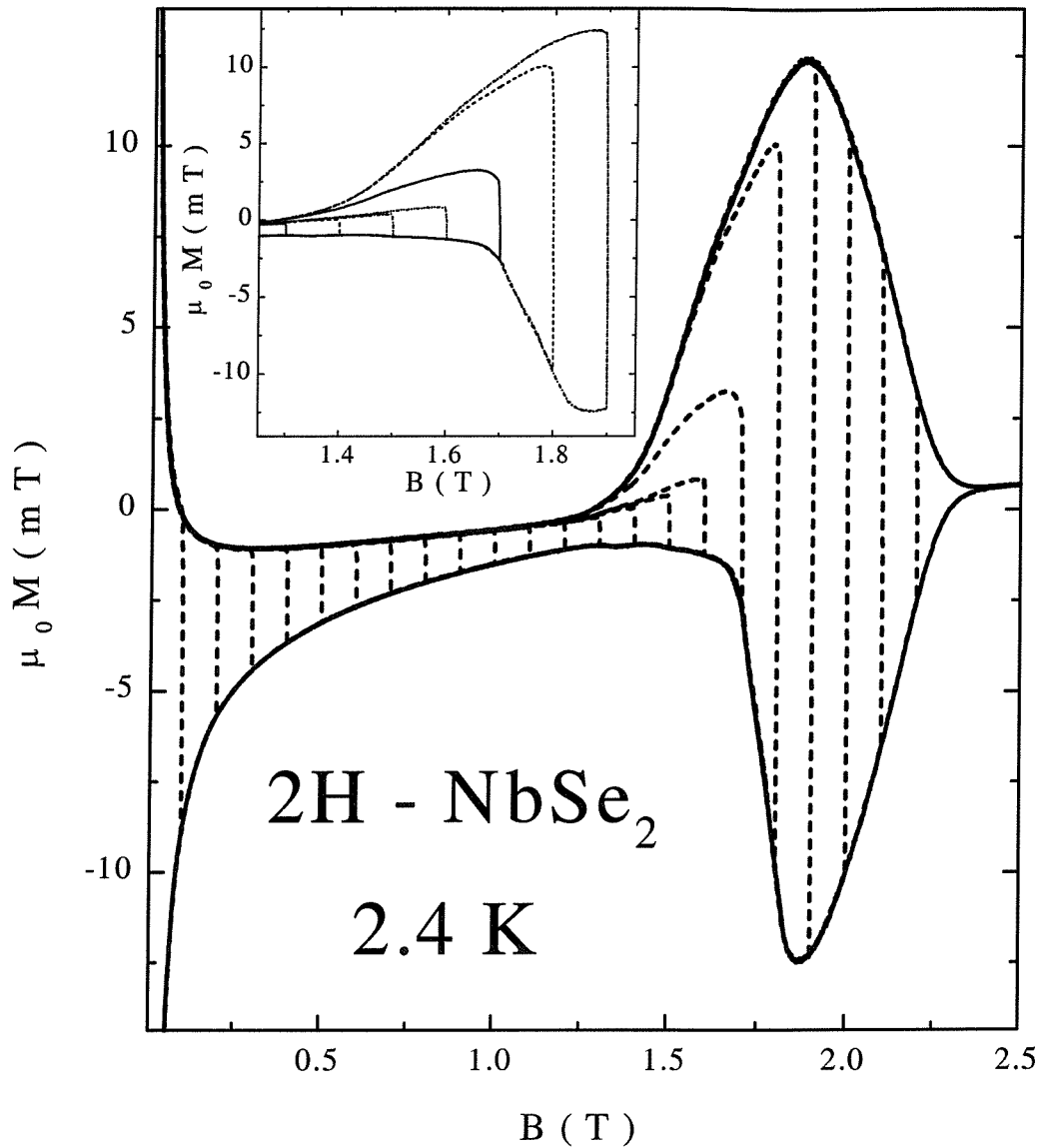


Fig. 5.17. The CL (solid line) together with several method I PLs (dashed lines) are shown for a 2H-NbSe<sub>2</sub> single crystal at 2.4 K.  $B_{\max}$  increases with a step of 0.1 T. Inset: PLs in the region of the onset of the history effects ( $B_{pl} = 1.3$  T). Note the similarity of these results with the ones obtained in  $\text{YBa}_2\text{Cu}_3\text{O}_{7-\delta}$  (see e.g. Fig. 5.10).

due to the reduction of thermal fluctuations,<sup>104</sup> whereas they become channels for easy flux penetration at intermediate temperatures.<sup>105</sup> Our observations on twinned samples demonstrate clearly that the presence or not of the disordered induced transition depends on the density of twin boundaries. Specifically, as can be seen from Fig. 5.13 (a), T1, that

is characterized by a low twin density (mean twin distance of the order of  $\sim 5 \mu\text{m}$ ), shows behaviour almost identical to the detwinned crystals. Nevertheless for the microtwinned DN (average twin separation of  $\sim 100 \text{ nm}$ ) the transition is suppressed (see Fig 5.13 (b)). It is natural to attribute this effect to the much higher density of twin planes in this sample. Indeed, at a typical field of e.g. 1 T, where according to the results for the detwinned crystals the Bragg glass phase should be present, the space between successive twin boundaries for T1 and DN contains on average 110 and 2 lattice parameters respectively. Therefore, for T1 the distortion in the lattice caused by the twins should not be very important and accordingly the Bragg glass is preserved. For DN, however, the role of twin boundaries as pinning centres is expected to be significantly enhanced, deteriorating the periodicity of the vortex lattice and leading to the destruction of the Bragg glass. The weak memory effects seen for DN at higher fields ( $B > 4.5 \text{ T}$ ) can be possibly attributed to the contribution of the regions between twins that becomes important at these fields thus reproducing the behaviour of the highly oxygenated detwinned samples. These observations are also in correspondence with recent calorimetric measurements on high purity twinned  $YBa_2Cu_3O_{7-\delta}$  single crystals.<sup>35</sup> It was found that for as long as the field is high enough for the intervortex distance to be much less than the average twin boundary separation, with increasing temperature the VS melts to a vortex liquid via a first order transition demonstrating the existence of an undistorted vortex lattice.<sup>35</sup> This transition, however, becomes of second order at low enough fields<sup>35</sup> where the vortices are predominantly pinned by twin boundaries probably forming a Bose glass phase.<sup>59</sup>

As shown in section 5.4.3, the history effects are not present in the columnar irradiated samples. Within our interpretation this behaviour can be understood as follows. Columnar defects due to their extended dimensions localize vortices and consequently as has been predicted theoretically,<sup>59</sup> and shown in several experiments,<sup>106-108</sup> they are very efficient pinning centres. Such strong pinning is expected to eliminate long range order in the vortex lattice.<sup>1, 59</sup> As has been predicted by Vinokur et al.,<sup>67</sup> in the case of columns the quenched entanglement transition should disappear for matching fields  $B_\Phi = n\Phi_0 > c_L^2 B_{pl}$ , where  $n$  is the areal density of columns and  $c_L$  the Lindemann number. For  $c_L \approx 0.16$ ,<sup>67</sup> and the  $B_{pl}$  values of  $\sim 1 \text{ T}$  observed in the detwinned samples, the minimum  $B_\Phi$  required for the suppression of the disorder induced transition is found to be of the order of  $10^{-2} \text{ T}$ . Consequently, since the matching fields for both AW and AH are much larger than this value, the memory effects are expected to disappear in these samples in agreement with

our findings. This result is also in correspondence with recent reports for pure BSCCO single crystals, where a low dose of columnar defects was found to suppress the first order melting transition indicating the suppression of the Bragg glass phase.<sup>45</sup>

### 5.5.5 Summary

In summary, in this chapter we have presented a detailed study of history effects in the irreversible magnetization of pure  $YBa_2Cu_3O_{7-\delta}$  single crystals with several types and densities of pinning centres. By using a partial magnetization loop technique it has been possible to detect a transition in the vortex system of the superconductor, between a low field quasi-ordered Bragg glass and a high field disordered phase. The locus of this transition has been identified in the field – temperature phase diagram and found to be in proximity to the onset of the second magnetization peak and in accordance with theoretical predictions. The influence of changes in the density of point-like defects on this transition has also been investigated by varying the concentration of oxygen vacancies in the region  $6.550 \leq 7-\delta \leq 6.999$ . We have found that its location shifts to lower fields with decreasing oxygen content and disappears for the highest oxygen deficiencies under study ( $7-\delta = 6.550, 6.750$ ) in agreement with theory. Above the transition metastable topological disorder invades the VS leading to a pronounced dependence of the critical current density on the maximum field to which the superconductor is exposed and thus on the formation history of the vortex lattice. For low oxygen contents close to optimal doping the history effects diminish for the highest fields of our experiment due to the saturation in the density of topological defects. Such saturation, however, is not observed for the highest oxygen concentrations, which we have attributed to the reduction in pinning by point pinning centres. Finally, studying the influence of extended defects has revealed that a low density of twin boundaries leaves the Bragg glass – disordered phase transition unaffected. However, in densely twinned as well as in columnar irradiated samples the transition is suppressed and the history effects are eliminated.

## References

- <sup>1</sup> G. Blatter, M. V. Feigel'man, V. B. Geshkenbein, A. I. Larkin, and V. M. Vinokur, *Rev. Mod. Phys.* 66, 1125 (1994)
- <sup>2</sup> E. H. Brandt, *Rep. Prog. Phys.* 58, 1465 (1995)
- <sup>3</sup> E. Brézin, D. R. Nelson, and A. Thiaville, *Phys. Rev. B* 31, 7124 (1985)
- <sup>4</sup> D. R. Nelson, *Phys. Rev. Lett.* 69, 1973 (1988); D. R. Nelson and H. S. Seung, *Phys. Rev. B* 39, 9153 (1989)
- <sup>5</sup> A. Houghton, R. A. Pelcovits, and A. Sudbø, *Phys. Rev. B* 40, 6763 (1989)
- <sup>6</sup> T. Chen and S. Teitel, *Phys. Rev. Lett.* 74, 2792 (1995); G. Carneiro, *ibid.* 75, 521 (1995)
- <sup>7</sup> S. Ryu and D. Stroud, *Phys. Rev. Lett.* 78, 4629 (1997); X. Hu, S. Miyashita, and M. Tachiki, *ibid.* 79, 3498 (1997); *Phys. Rev. B* 58, 3438 (1998)
- <sup>8</sup> R. Šášik and D. Stroud, *Phys. Rev. Lett.* 75, 2582 (1995); J. Hu and A. MacDonald, *Phys. Rev. B* 56, 2788 (1997)
- <sup>9</sup> H. Nordborg and G. Blatter, *Phys. Rev. Lett.* 79, 1925 (1997); *Phys. Rev. B* 58, 14556 (1998)
- <sup>10</sup> F. Lindemann, *Phys. Z* 11, 69 (1910)
- <sup>11</sup> E. H. Brandt, *J. Low Temp. Phys.* 26, 709 (1977); 26, 735 (1977)
- <sup>12</sup> The obtained results should not be considerably affected by the presence of weak quenched disorder as discussed in detail in Ref. 1.
- <sup>13</sup> Ginzburg [Sov. Phys. Sol. State 2, 1824 (1960)] showed that in second order phase transitions, the temperature range  $T_f \leq T \leq T_c$  where the relative fluctuations of the order parameter are large, is determined by the Ginzburg number  $Gi = 1 - T_f/T_c$  that for an anisotropic superconductor reads:<sup>2</sup>

$$Gi = \frac{1}{2} \left( \frac{k_B T_c}{\xi^3(0)} \frac{\gamma \mu_0}{4\pi B_c^2(0)} \right)^2 = \frac{1}{2} \left( \frac{2\pi \mu_0 k_B T_c \gamma \lambda^2(0)}{\Phi_0^2 \xi(0)} \right)^2.$$

The values of  $Gi$  indicate the importance of thermal fluctuations in superconductors.<sup>1,2</sup>

<sup>14</sup> Note that for the highly anisotropic Bi- and Tl-based compounds, due to the higher  $Gi$  values the result (5.3) is applicable for a much broader temperature range than for

$YBa_2Cu_3O_{7-\delta}$ . Nevertheless, in this case the validity of eq. (5.3) is limited by the increasing two dimensional behaviour at high fields.

- <sup>15</sup> G. Blatter, V. G. Geshkenbein, and A. I. Larkin, Phys. Rev. Lett. 68, 875 (1992)
- <sup>16</sup> S. Hikami, A. Fujita, and A. I. Larkin, Phys. Rev. B 44, 10400 (1991)
- <sup>17</sup> R. E. Hetzel, A. Sudbø, and D. A. Huse, Phys. Rev. Lett. 69, 518 (1992)
- <sup>18</sup> M. J. W. Dodgson, V. B. Geshkenbein, H. Nordborg, and G. Blatter, Phys. Rev. Lett. 80, 837 (1998); Phys. Rev. B 57, 14498 (1998)
- <sup>19</sup> A. E. Koshelev, Phys. Rev. B 56, 11201 (1997); A. E. Koshelev and H. Nordborg, Phys. Rev. B 59, 4358 (1999)
- <sup>20</sup> Y. Nonomura, X. Hu, and M. Tachiki, Phys. Rev. B 59, R11657 (1999)
- <sup>21</sup> P. L. Gammel, L. F. Schneemeyer, J. V. Waszczak, and D. J. Bishop, Phys. Rev. Lett. 61, 1666 (1988)
- <sup>22</sup> E. H. Brandt, P. Esquinazi, and G. Weiss, Phys. Rev. Lett. 62, C2330 (1989)
- <sup>23</sup> D. E. Farrell, J. P. Rice, and D. M. Ginsberg, Phys. Rev. Lett. 67, 1165 (1991)
- <sup>24</sup> M. Charalambous, J. Chaussy, and P. Lejay, Phys. Rev. B 45, R5091 (1992); M. Charalambous, J. Chaussy, P. Lejay, and V. M. Vinokur, Phys. Rev. Lett. 71, 436 (1993)
- <sup>25</sup> W. K. Kwok, S. Flesher, U. Welp, V. M. Vinokur, J. Downey, G. W. Crabtree, and M. M. Miller, Phys. Rev. Lett. 69, 3370 (1992)
- <sup>26</sup> H. Safar, P. L. Gammel, D. A. Huse, D. J. Bishop, W. C. Lee, and D. M. Ginsberg, Phys. Rev. Lett. 70, 3800 (1993)
- <sup>27</sup> W. K. Kwok, J. Fendrich, S. Flesher, U. Welp, J. Downey, and G. W. Crabtree, Phys. Rev. Lett. 72, 1092 (1994)
- <sup>28</sup> S. N. Gordeev, D. Bracanovic, A. P. Rassau, P. A. J. de Groot, R. Gagnon, and L. Taillefer, Phys. Rev. B 57, 645 (1998)
- <sup>29</sup> W. Jiang, N.-C. Yeh, D. S. Reed, U. Kriplani, and F. Holtzberg, Phys. Rev. Lett. 74, 1438 (1995)
- <sup>30</sup> L. D. Landau and E. M. Lifschitz, *Statistical Physics*, (Pergamon, London, 1958)
- <sup>31</sup> R. Liang, D. A. Bonn, and W. N. Hardy, Phys. Rev. Lett. 76, 835 (1996)
- <sup>32</sup> U. Welp, J. A. Fendrich, W. K. Kwok, G. W. Crabtree, and B. W. Veal, Phys. Rev. Lett. 76, 4809 (1996)
- <sup>33</sup> J. A. Fendrich, U. Welp, W. K. Kwok, A. E. Koshelev, G. W. Crabtree, and B. W. Veal, Phys. Rev. Lett. 77, 2073 (1996)



- <sup>34</sup> A. Schilling, R. A. Fisher, N. E. Philips, U. Welp, D. Dasgupta, W. K. Kwok, and G. W. Crabtree, *Nature* 382, 791(1996)
- <sup>35</sup> M. Roulin, A. Junod, A. Erb, and E. Walker, *Phys. Rev. Lett.* 80, 1722 (1998)
- <sup>36</sup> H. Pastoriza, M. F. Goffman, A. Arribére, and F. de la Cruz, *Phys. Rev. Lett.* 72, 2951 (1994)
- <sup>37</sup> E. Zeldov, D. Majer, M. Konczykowski, V. B. Geshkenbein, V. M. Vinokur, and H. Shtrikman, *Nature* 375, 373 (1995)
- <sup>38</sup> A. K. Pradhan, S. Shibata, K. Nakao, and N. Koshizuka, *Phys. Rev. B* 59, 11563 (1999)
- <sup>39</sup> B. Revaz, A. Junod, and A. Erb, *Phys. Rev. B* 58, 11153 (1998)
- <sup>40</sup> T. Sasagawa, K. Kishio, Y. Togawa, J. Shimoyama, and K. Kitazawa, *Phys. Rev. Lett.* 80, 4297 (1998)
- <sup>41</sup> H. Safar, P. L. Gammel, D. A. Huse, D. J. Bishop, W. C. Lee, G. Giapintzakis, and D. M. Ginsberg, *Phys. Rev. Lett.* 70, 3800 (1993)
- <sup>42</sup> R. M. Langan, S. N. Gordeev, P. A. J. de Groot, A. G. M. Jansen, R. Gagnon, and L. Taillefer, *Phys. Rev. B* 58, 14548 (1998)
- <sup>43</sup> M. Roulin, A. Junod, and E. Walker, *Science* 273, 1210 (1996)
- <sup>44</sup> R. H. Koch, V. Foglietti, W. J. Gallagher, G. Koren, A. Gupta, and M. P. A. Fisher, *Phys. Rev. Lett.* 63, 1511 (1989); P. L. Gammel, L. F. Schneemeyer, and D. J. Bishop, *Phys. Rev. Lett.* 66, 953 (1991); T. K. Worthington, E. Olsson, C. S. Nichols, T. M. Shaw, and D. R. Clarke, *Phys. Rev. B* 43, 10538 (1991)
- <sup>45</sup> B. Khaykovich, M. Konczykowski, E. Zeldov, R. A. Doyle, D. Majer, P. H. Kes, and T. W. Li, *Phys. Rev. B* 56, R517 (1997)
- <sup>46</sup> S. P. Obukhov and M. Rubinstein, *Phys. Rev. Lett.* 65, 1279 (1990)
- <sup>47</sup> Y. -H. Li and S. Teitel, *Phys. Rev. B* 47, 359 (1993)
- <sup>48</sup> H. Safar, P. L. Gammel, D. A. Huse, S. N. Majumdar, L. F. Schneemeyer, D. J. Bishop, D. Lopez, G. Nieva, and F. de la Cruz, *Phys. Rev. Lett.* 72, 1272 (1994)
- <sup>49</sup> M. P. A. Fisher, *Phys. Rev. Lett.* 62, 1415 (1989); D. S. Fisher, M. P. A. Fisher, and D. A. Huse, *Phys. Rev. B* 43, 130 (1991)
- <sup>50</sup> D. A. Huse, M. P. A. Fisher, and D. S. Fisher, *Nature* 358, 553 (1992)
- <sup>51</sup> A. P. Malozemoff and M. P. A. Fisher, *Phys. Rev. B* 42, R6784 (1990)

- <sup>52</sup> J. Kötzler, M. Kaufmann, G. Nakielski, R. Behr, and W. Assmus, Phys. Rev. Lett. 72, 2081 (1994); J. Kötzler, G. Nakielski, M. Baumann, R. Behr, F. Goerke, and E. H. Brandt, Phys. Rev. B 50, 3384 (1994) and references therein.
- <sup>53</sup> J. M. Roberts, B. Brown, B. A. Hermann, and J. Tate, Phys. Rev. B 49, 6890 (1994) and references therein.
- <sup>54</sup> J. A. Fendrich, W. K. Kwok, J. Giapintzakis, C. J. van der Beek, V. M. Vinokur, S. Flesher, U. Welp, H. K. Viswanathan, and G. W. Crabtree, Phys. Rev. Lett. 74, 1210 (1995)
- <sup>55</sup> K. Moloni, M. Friesen, S. Li, V. Souw, P. Metcalf, and M. McElfresh, Phys. Rev. B 56, 14784 (1997)
- <sup>56</sup> M. V. Feigel'man, V. B. Geshkenbein, A. I. Larkin, and V. M. Vinokur, Phys. Rev. Lett. 63, 2303 (1989)
- <sup>57</sup> T. Higuchi, S. I. Yoo, and M. Murakami, Phys. Rev. B 59, 1514 (1999) and references therein.
- <sup>58</sup> M. P. A. Fisher, P. B. Weichmann, G. Grinstein, and D. S. Fisher, Phys. Rev. B 40, 546 (1989)
- <sup>59</sup> D. R. Nelson and V. M. Vinokur, Phys. Rev. Lett. 68, 2398 (1992); Phys. Rev. B 48, 13060 (1993); U. C. Täuber and D. R. Nelson, Phys. Rev. B 52, 16106 (1995)
- <sup>60</sup> D. Grier, C. A. Murray, C. A. Bolle, P.L. Gammel, D. J. Bishop, D. B. Mitzi, and A. Kapitulnik, Phys. Rev. Lett. 66, 2270 (1991)
- <sup>61</sup> R. Cubit, E. M. Forgan, G. Yang, S. L. Lee, D. McK. Paul, H. A. Mook, M. Yethiraj, P. H. Kes, T. W. Li, A. A. Menovsky, Z. Tarnawski, and K. Mortensen, Nature (London) 365, 407 (1993)
- <sup>62</sup> K. Harada, T. Matsuda, H. Kasai, J. E. Bonevich, T. Yoshida, U. Kawabe, and A. Tonomura, Phys. Rev. Lett. 71, 3371 (1993)
- <sup>63</sup> T. Nattermann, Phys. Rev. Lett. 64, 2454 (1990)
- <sup>64</sup> S. E. Korshunov, Phys. Rev. B 48, 3969 (1993)
- <sup>65</sup> T. Giamarchi and P. Le Doussal, Phys. Rev. Lett. 72, 1530 (1994); Phys. Rev. B 52, 1242 (1995); *ibid.* 55, 6577 (1997)
- <sup>66</sup> D. Ertas and D. R. Nelson, Physica C272, 79 (1996)
- <sup>67</sup> V. M. Vinokur, B. Khaykovich, E. Zeldov, M. Konczykowski, R. A. Doyle, and P. H. Kes, Physica C295, 209 (1998)

- <sup>68</sup> J. Kierfeld, T. Nattermann, and T. Hwa, Phys. Rev. B 55, 626 (1997)
- <sup>69</sup> D. S. Fisher, Phys. Rev. Lett. 78, 1964 (1997)
- <sup>70</sup> A. E. Koshelev and V. M. Vinokur, Phys. Rev. B 57, 8026 (1998)
- <sup>71</sup> M. J. P. Gingras and D. A. Huse, Phys. Rev. B 53, 15193 (1996); S. Ryu, A. Kapitulnik, and S. Doniach, Phys. Rev. Lett. 77, 2300 (1996); A. van Otterlo, R. T. Scalettar, and G. T. Zimányi, Phys. Rev. Lett. 81, 1497 (1998)
- <sup>72</sup> E. J. Brandt, J. R. Clem, and D. G. Walmsley, J. Low Temp. Phys. 37, 43 (1979); T. Hwa, P. Le Doussal, D. R. Nelson, and V. M. Vinokur, Phys. Rev. Lett. 71, 3545 (1993)
- <sup>73</sup> D. Carpentier, P. Le Doussal, and T. Giamarchi, Europhys. Lett. 35, 379 (1996)
- <sup>74</sup> T. Giamarchi and P. Le Doussal, Phys. Rev. Lett. 76, 3408 (1996); P. Le Doussal and T. Giamarchi, Phys. Rev. B 57, 11356 (1998)
- <sup>75</sup> K. H. Fischer and J. A. Hertz, *Spin Glasses* (Cambridge University Press, Cambridge, 1991)
- <sup>76</sup> R. Wördenweber, P. H. Kes and C. C. Tsuei, Phys. Rev. B 33, 3172 (1986)
- <sup>77</sup> M. Steingart, A. G. Putz and E. J. Kramer, J. Appl. Phys. 44, 5580 (1973); H. Küpfer and W. Gey, Philos. Mag. 36, 859 (1977)
- <sup>78</sup> S. B. Roy and P. Chaddah, Physica C 279, 70 (1997); J. Phys.: Condens. Matter 9, L625 (1997); S. B. Roy, P. Chaddah and S. Chaudhary, *ibid.* 10, 4885 (1998)
- <sup>79</sup> W. Henderson, E. Y. Andrei, M. J. Higgins, and S. Bhattacharya, Phys. Rev. Lett. 77, 2077 (1996); W. Henderson, E. Y. Andrei and M. J. Higgins, Phys. Rev. Lett. 81, 2352 (1998)
- <sup>80</sup> A. C. Marley, M. J. Higgins and S. Bhattacharya, Phys. Rev. Lett. 74, 3029 (1995); S. Bhattacharya and M. J. Higgins, Phys. Rev. B 52, 64 (1995)
- <sup>81</sup> G. Ravikumar, V. C. Sahni, P. K. Mishra, T. V. Chandrasekhar Rao, S. S. Banerjee, A. K. Grover, S. Ramakrishnan, S. Bhattacharya, M. J. Higgins, E. Yamamoto, Y. Haga, M. Hedo, Y. Inada, Y. Onuki, Phys. Rev. B 57, R11069 (1998); S. S. Banerjee, N. G. Patil, S. Saha, S. Ramakrishnan, A. K. Grover, S. Bhattacharya, G. Ravikumar, P. K. Mishra, T. V. C. Rao, V. C. Sahni, M. J. Higgins, E. Yamamoto, Y. Haga, M. Hedo, Y. Inada, and Y. Onuki, Phys. Rev. B 58, 995 (1998); S. S. Banerjee, S. Saha, N. G. Patil, S. Ramakrishnan, A. K. Grover, S. Bhattacharya, G. Ravikumar, P. K. Mishra, T. V. C. Rao, V. C. Sahni, C. V. Tomy, G. Balakrishnan, D. McK. Paul, and M. J. Higgins, Physica C 308, 25 (1998); S. S. Banerjee, N. G. Patil, S. Ramakrishnan, A. K. Grover, S.

- Bhattacharya, P. K. Mishra, G. Ravikumar, T. V. C. Rao, V. C. Sahni, M. J. Higgins, C. V. Tomy, G. Balakrishnan, and D. McK. Paul, Phys. Rev. B 59, 6043 (1999)
- <sup>82</sup> B. Khaykovich, E. Zeldov, D. Majer, T. W. Li, P. H. Kes, and M. Konczykowski, Phys. Rev. Lett. 76, 2555 (1996)
- <sup>83</sup> K. Deligiannis, P. A. J. de Groot, M. Oussena, S. Pinfold, R. Langan, R. Gagnon, and L. Taillefer, Phys. Rev. Lett. 79, 2121 (1997)
- <sup>84</sup> T. Nishizaki, T. Naito, and N. Kobayashi, Phys. Rev. B 58, 11169 (1998)
- <sup>85</sup> H. K pfer, Th. Wolf, C. Lessing, A. A. Zhukov, X. Lan on, R. Meier-Hirmer, W. Schauer, and H. W hl, Phys. Rev. B 58, 2886 (1998)
- <sup>86</sup> S. Kokkaliaris, P. A. J. de Groot, S. N. Gordeev, A. A. Zhukov, R. Gagnon, and L. Taillefer, Phys. Rev. Lett. 82, 5116 (1999)
- <sup>87</sup> S. Kokkaliaris, A. A. Zhukov, P. A. J. de Groot, R. Gagnon, L. Taillefer, and T. Wolf, Phys. Rev. B 61, 3655 (2000)
- <sup>88</sup> S. Kokkaliaris, A. A. Zhukov, S. N. Gordeev, P. A. J. de Groot, R. Gagnon, and L. Taillefer, J. Low Temp. Phys. to be published; S. Kokkaliaris, A. A. Zhukov, P. A. J. de Groot, R. Gagnon, L. Taillefer, and T. Wolf, Physica C to be published.
- <sup>89</sup> D. J. L. Hong and D. M. Smyth, J. Am. Ceram. Soc. 74, 1751 (1991)
- <sup>90</sup> R. Kershaw, M. Vlasse, and A. Wold, Inorg. Chem. 6, 1599 (1967)
- <sup>91</sup> E. H. Brandt, Phys. Rev. B 58, 6506 (1998)
- <sup>92</sup> R. L. Peterson, J. Appl. Phys. 67, 6930 (1990)
- <sup>93</sup>  $R$  was calculated at 0.3 T below  $B_{\max}$  or above  $B_{\min}$ . This value was chosen rather large to avoid any possible influence of the remagnetization process when reversing the field. The same procedure was also applied for the calculation of  $\Delta M_{\text{suc}}$ .
- <sup>94</sup> S. N. Gordeev, (unpublished)
- <sup>95</sup> M. Oussena, P. A. J. de Groot, R. Gagnon, and L. Taillefer, Phys. Rev. Lett. 72, 3606 (1994); S. N. Gordeev, P. A. J. de Groot, M. Oussena, A. V. Volkozub, S. Pinfold, R. M. Langan, R. Gagnon, and L. Taillefer, Nature 385, 324 (1997)
- <sup>96</sup> M. A. Angadi, D. A. Caplin, J. R. Lavery, and Z. X. Shen, Physica C 177, 479 (1991)
- <sup>97</sup> The lines in the phase diagrams of Fig. 5.15 do not extend to even lower temperatures since the field of full penetration attains high values (above 0.1 T) and consequently due to the influence of the reversal of the Bean profile the point where successive PLs deviate from the universal line cannot be determined accurately. In addition with decreasing

temperature  $R$  attains low values close to our experimental resolution that makes the determination of  $B_{p1}$  rather ambiguous.

<sup>98</sup>  $B_{on}$  is taken as the point where the absolute value of the magnetization in the ascending branch of the CL attains a minimum before its increase towards the peak.

<sup>99</sup> A. van Otterlo, R. T. Scalettar, G. T. Zimányi, R. Olsson, A. Petrean, W. K. Kwok, and V. M. Vinokur, preprint (submitted to Phys. Rev. Lett.)

<sup>100</sup> S. L. Lee, P. Zimmermann, H. Keller, M. Warden, I. M. Savić, R. Schauwecker, D. Zech, R. Cubitt, E. M. Forgan, P. H. Kes, T. W. Li, A. A. Menovsky, and Z. Tarnawski, Phys. Rev. Lett. 71, 3862 (1993)

<sup>101</sup> L. I. Glazman and A. E. Koshelev, Phys. Rev. B 43, 2835 (1991)

<sup>102</sup> A. A. Zhukov, S. Kokkaliaris, P. A. J. de Groot, M. J. Higgins, S. Bhattacharya, R. Gagnon, and L. Taillefer, Phys. Rev. B 61, R886 (2000)

<sup>103</sup> P. L. Gammel, U. Yaron, A. P. Ramirez, D. J. Bishop, A. M. Chang, R. Ruel, L. N. Pfeiffer, E. Bucher, G. D'Anna, D. A. Huse, K. Mortensen, M. R. Eskildsen, and P. H. Kes, Phys. Rev. Lett. 80, 833 (1998)

<sup>104</sup> W. K. Kwok, U. Welp, G. W. Crabtree, K. G. Vandervoort, R. Hulscher, and J. Z. Liu, Phys. Rev. Lett. 64, 966 (1990); J. N. Li, A. A. Menovsky, and J. J. M. Franse, Phys. Rev. B 48, 6612 (1993); A. A. Zhukov, H. Küpfer, G. K. Perkins, L. F. Cohen, A. D. Caplin, S. A. Klestov, H. Claus, V. I. Voronkova, T. Wolf, and H. Wühl, Phys. Rev. B 51, 12704 (1995)

<sup>105</sup> C. A. Duran, P. L. Gammel, R. Wolfe, V. J. Fratello, D. J. Bishop, J. P. Rice, and D. M. Ginsberg, Nature (London) 357, 474 (1992); M. Oussena, P. A. J. de Groot, S. J. Porter, R. Gagnon, and L. Taillefer, Phys. Rev. B 51, 1389 (1995); A. A. Zhukov, H. Küpfer, H. Claus, H. Wühl, M. Kläser, and G. Müller-Vogt, Phys. Rev. B 52, R9871 (1995)

<sup>106</sup> L. Civale, A. D. Marwick, T. K. Worthington, M. A. Kirk, J. R. Thompson, L. Krusin-Elbaum, Y. Sun, J. R. Clem, and F. Holtzberg, Phys. Rev. Lett. 67, 648 (1991)

<sup>107</sup> M. Konczykowski, F. Rullier-Albenque, E. R. Yacoby, A. Shaulov, Y. Yeshurun, and P. Lejay, Phys. Rev. B 44, 7167 (1991)

<sup>108</sup> C. J. van der Beek, M. Konczykowski, V. M. Vinokur, G. W. Crabtree, T. W. Li, and P. H. Kes, Phys. Rev. B 51, 15492 (1995)

---

# Chapter 6

---

## The peak effect in pure $\text{YBa}_2\text{Cu}_3\text{O}_{7-\delta}$ single crystals

### 6.1 Introduction

The competition between the intervortex interactions and pinning by disorder in a type-II superconductor can lead to a remarkable phenomenon, which is generally described by the term “peak effect”. The peak effect (PE) refers to a maximum in the measured current density in the superconductor and can be observed by varying either the temperature or the applied magnetic field. In transport studies this phenomenon corresponds to a dip in the resistivity temperature and field dependencies, whereas in magnetization measurements manifests itself as a peak in the magnetic hysteresis far above the self-field dominated region.

The PE has been studied experimentally in conventional superconductors for over forty years.<sup>1-5</sup> In this case the PE occurs as the upper critical field line,  $B_{c2}(T)$ , is approached. Theoretically, an early understanding of this phenomenon attributed the observed enhancement in the current near  $B_{c2}$  to the reduction in the rigidity of the lattice, which falls more rapidly than the pinning strength of inhomogeneities.<sup>6</sup> This enables better adjustment of the vortex lattice to the underlying pinning potential, enhancing pinning.<sup>6</sup> Following this seminal work, Larkin and Ovchinnikov<sup>7</sup> gave more quantitative arguments for the increase of the current near the superconducting to normal phase boundary, as arising from either the dispersion of the tilt modulus  $c_{44}$ , in the case of a large density of weak pinning centres, or the reduction in both the dispersive tilt modulus and the shear modulus when pinning centres are sufficiently strong so as to define individual coherence volumes in this region. (For a more extended discussion on this

topic see also Chapter 2). The subsequent decrease of the current is then accounted by either the field dependence of parameters such as the elementary pinning force and the effective tilt modulus on approaching  $B_{c2}$ ,<sup>7</sup> or the onset of plastic deformations due to shearing of the vortex lattice.<sup>8</sup>

The peak effect has been found to be present in the high temperature superconductors as well. The extreme interest in these compounds has stimulated a remarkable number of experimental investigations dedicated to the study of this phenomenon, providing with a plethora of nominated interpretations. By means of magnetization measurements on  $\text{YBa}_2\text{Cu}_3\text{O}_{7-\delta}$  single crystals, Däumling et al.,<sup>9</sup> except proving its presence, also demonstrated that in contrast to the low- $T_c$  compounds, in these systems the magnetization peak is located far below the  $B_{c2}(T)$  line. In this study it was proposed that the PE can be attributed to the presence of precipitates of a second superconducting phase that become normal with raising field, thus being transformed to efficient pinning sites.<sup>9</sup> Under these conditions, the decrease of the current above the peak was attributed to granularity of the sample that is produced by overlapping of normal zones.<sup>9</sup> In a similar approach, Klein et al.<sup>10</sup> proposed that in  $\text{YBa}_2\text{Cu}_3\text{O}_{7-\delta}$  the enhancement of the current density with raising the field is due to the increasing interaction energy of vortices with oxygen deficient regions. When the field exceeds the irreversibility field of these regions, a percolationlike network of reversible regimes is formed, resulting in a reduction of the irreversible magnetization.<sup>10</sup>

The models introduced in Refs. 9 and 10 are “static” models, in the sense that they postulate the presence of a peak in the unrelaxed current. In contrast, Krusin-Elbaum et al.<sup>11</sup> suggested a dynamic model, conjecturing that in  $\text{YBa}_2\text{Cu}_3\text{O}_{7-\delta}$  single crystals the peak is actually absent in the critical current  $J_c$ , but it is seen in the experimentally measured relaxed current values due to the influence of dynamic effects. In particular, they associated the shape of the magnetization versus field curves with different relaxation regimes as these are determined by the collective creep theory.<sup>12</sup> The observed increasing with field hysteresis was attributed to a transition from the single vortex to the small bundle collective pinning regimes, whilst the current relaxes in the course of the experiment. As the former regime is characterized by a higher relaxation rate than the latter, and considering that the current values corresponding to the crossover between these two regions increase with field,<sup>12</sup> the measured current could show a dip in the intermediate field region.<sup>11</sup> On the other hand, at high fields, one crosses over to the large

bundle regime where relaxation is weak and the field dependence of the observed current is determined by  $J_c$ , thus decreasing with field.<sup>11, 12</sup> However, the validity of this interpretation was disputed by Zhukov et al.<sup>13</sup> In this work it was also conjectured that the magnetization peak in  $\text{YBa}_2\text{Cu}_3\text{O}_{7-\delta}$  single crystals might be related to plastic deformations in the vortex lattice.

A peak effect in the current density was also seen with transport measurements on an  $\text{YBa}_2\text{Cu}_3\text{O}_{7-\delta}$  single crystal containing only two twin boundaries.<sup>14</sup> However, in contrast to the investigations outlined above, this peak was observed at quite high temperatures, just below the melting transition. Moreover, it was much sharper than the peak seen in magnetic studies. This PE was proposed to originate from the enhanced vortex pinning by the twin boundaries, owing to the softening of the shear modulus prior to melting. The subsequent drop of the current was associated with the onset of plastic flow.<sup>14</sup> In a similar way, the sharp peak in the current observed in untwinned single crystals at elevated temperatures using ac susceptibility measurements, was attributed to the pre-melting softening of the lattice.<sup>15</sup> The interpretation for the PE proposed in Refs. 14 and 15 was subsequently supported by analytical calculations, appropriate for the high temperature superconductors.<sup>16</sup> In addition, these results indicated that the low and high temperature peaks seen in  $\text{YBa}_2\text{Cu}_3\text{O}_{7-\delta}$  single crystals with magnetization and transport or ac susceptibility measurements respectively might be of different nature.

In more anisotropic systems, such as BSCCO or the TI-based compounds, the magnetization peak has been demonstrated to be rather sharp and to occur at much lower field values as compared with  $\text{YBa}_2\text{Cu}_3\text{O}_{7-\delta}$ . Several mechanisms have also been suggested. In Ref. 17 a matching effect between the decoupled two-dimensional pancake vortices and the dislocation networks present in the sample was discussed. Tamegai et al.<sup>18</sup> attributed the PE in BSCCO to a better adaptation of the vortex lattice to the pinning sites due to a crossover from a three- to a two-dimensional lattice. A similar scenario was also proposed by Hardy et al.<sup>19</sup> for TI-based materials. In contrast, Kopylov et al.<sup>20</sup> attributed the PE in BSCCO to an interplay between bulk and surface-barrier pinning. Similarly to the case of  $\text{YBa}_2\text{Cu}_3\text{O}_{7-\delta}$ ,<sup>11</sup> Yeshurun et al.<sup>21</sup> supported the dynamic scenario, whereas using a miniature Hall probe, Chikumoto et al.<sup>22</sup> speculated a possible interplay between a collective flux-creep barrier that increases with field and the melting or softening of the vortex lattice. On the other hand, more recent studies have conjectured that the increase in the current in pure BSCCO single crystals is due to a disorder-induced

phase transition in the vortex system,<sup>23</sup> as was proposed theoretically in Refs. 24-26. A similar mechanism has also been postulated for the case of  $\text{Nd}_{1.85}\text{Ce}_{0.15}\text{CuO}_{4-\delta}$ ,<sup>27</sup> that is a compound with intermediate to high anisotropy, thus supporting the notion of a universal behaviour of the vortex system in the layered high- $T_c$  compounds.

Another interesting issue is the defect structure responsible for the PE. It is mentioned that in the case of  $\text{YBa}_2\text{Cu}_3\text{O}_{7-\delta}$  the magnetization PE is present in twinned, untwinned and single crystals with modest increase in the density of defects by irradiation, as well as in ceramics, thick films, and melt textured samples. However, it is absent in thin films. For pure, twin-free  $\text{YBa}_2\text{Cu}_3\text{O}_{7-\delta}$  single crystals, it has been demonstrated that in the fully oxidised state the current decreases monotonously with field without exhibiting a peak.<sup>28</sup> Nevertheless, a small oxygen reduction results in a pronounced peak, suggesting that in these samples the PE is caused by oxygen vacancies. This observation is in contrast to the behaviour of less pure crystals, where the peak is mainly due to defects other than oxygen vacancies. This is clearly illustrated by the fact that in this case variations in the oxygen stoichiometry do not affect significantly the irreversible behaviour in the peak region.<sup>28</sup>

Finally, it was recently demonstrated that in high quality  $\text{YBa}_2\text{Cu}_3\text{O}_{7-\delta}$  single crystals, the second magnetization peak also depends on the distribution of oxygen defects. In particular, it was found that at relatively high temperatures ( $T = 70$  K) the PE can be suppressed by high pressure sample annealing.<sup>29-31</sup> As shown in Ref. 31, the latter treatment leads to a more uniform distribution of oxygen vacancies as compared to low pressure annealing and the elimination of oxygen vacancy clusters. Accordingly, it was alleged that the disappearance of the peak is due to reduced pinning by a more homogeneous distribution of oxygen deficient regions.<sup>29-31</sup>

## 6.2 Studies of the second magnetization peak in pure $\text{YBa}_2\text{Cu}_3\text{O}_{7-\delta}$ single crystals

From the above discussion it becomes clear that at the time the present work commenced three years ago, as far as the topic second magnetization peak in  $\text{YBa}_2\text{Cu}_3\text{O}_{7-\delta}$  is concerned, there were two important problems to be addressed. First and

foremost, the origin of the PE was rather contentious with researchers supporting completely different scenarios. An important factor impeding a widely accepted interpretation was the low quality of available  $\text{YBa}_2\text{Cu}_3\text{O}_{7-\delta}$  single crystals that led to irreproducible observations. However, with the development of better growing techniques, this quality has been significantly improved, eliminating ambiguities stemming from sample inhomogeneity and allowing for a more consistent study of this effect. A second issue needed elucidation was the dependence of the PE on the distribution of oxygen defects. Although the Geneva group had demonstrated that high pressure annealing can lead to the suppression of the peak at  $T = 70$  K and fields below  $5.5$  T,<sup>29-31</sup> the understanding of this phenomenon was rather poor. Moreover, the influence of the distribution of oxygen vacancies on the magnetization peak in a broad range of temperatures, fields and oxygen concentrations remained unquestioned.

A step towards clarifying these issues is made in this chapter, by presenting an extended investigation of the second magnetization peak in pure  $\text{YBa}_2\text{Cu}_3\text{O}_{7-\delta}$  single crystals. We demonstrate that for samples characterized by low densities of pinning centres, the magnetization peak shows several new features that are inconsistent with both the static and dynamic models outlined in the previous section. Thus in contrast to the conventional “fishtail” behaviour seen in crystals with a relatively high level of background impurities,<sup>9-11</sup> the position of the magnetization peak shows a non-monotonous temperature dependence.<sup>32-34</sup> In addition, with increasing temperature in the vicinity of the melting transition line, the initially broad peak transforms to a rather sharp one. In this temperature range, the magnetization peak is further found to be correlated with the resistivity dip (or equivalently current peak) observed in transport measurements, indicating that both features might originate from the same mechanism. These measurements also reveal that the position of the magnetization peak is extremely sensitive to variations in the oxygen content, shifting to lower field values with increasing oxygen deficiency. Based on the insight provided by the results presented in Chapter 5, we suggest that these features can be qualitatively understood by regarding the PE as being determined by the interplay between plastic deformations in the vortex lattice, that dominate the irreversibility above the peak, and pinning by a temperature dependent concentration of effective pinning sites.

In order to obtain a complete picture about the effect of oxygen ordering on the second magnetization peak, we have investigated two sets of pure  $\text{YBa}_2\text{Cu}_3\text{O}_{7-\delta}$  single

crystals with several oxygen contents in the region near optimal doping ( $6.91 < 7-\delta < 6.98$ ) and different degrees of oxygen vacancy ordering, as achieved by low (1 bar) and high (100 bar) oxygen pressure annealing. Measurements have been performed in a broad temperature range and for fields up to 12 T.<sup>35</sup> We demonstrate that for temperatures below  $\sim 70$  K the peak is present even after high pressure annealing. In addition, although for both treatments the position of the peak changes drastically with oxygen stoichiometry, no dependence on the distribution of oxygen vacancies has been found at these temperatures. For  $T > 70$  K, however, ordering effects become important, as illustrated by the suppression of the peak in the high pressure annealed samples. These results suggest that while at low temperatures pinning of the vortex system by clusters or a more homogeneous distribution of oxygen vacancies is similar, at elevated temperatures the former are more robust against thermal depinning leading to larger hysteresis and the presence of the peak.

## 6.2.1 Experimental details

### A. Samples

Experiments have been performed on  $YBa_2Cu_3O_{7-\delta}$  single crystals grown at McGill University using a conventional self-flux method as described more extensively in Chapter 3. We have studied two sets of single crystals annealed under 1 bar and 100 bar pressure of oxygen respectively. The 1 bar annealed samples were two detwinned single crystals (DT1 and DT2). After growth, they were initially annealed at 500 °C for 6 days in oxygen atmosphere and subsequently detwinned by applying a uniaxial pressure of  $\sim 50$  MPa at 550 °C in air for 15 min. After detwinning they were reoxygenated for 1 day at 500 °C in flowing  $O_2$ . This treatment results in  $7-\delta = 6.934$ . DT1 was then reannealed twice. The first annealing was performed at 485 °C for 8 days and the second at 450 °C for another 8 days, which should give oxygen contents of  $7-\delta = 6.946$  and 6.970 respectively. The sample was studied in each of these states, to which we refer as DT1B and DT1C respectively. For the 100 bar annealing studies we used one single crystal (T1). The crystal had a uniform twin structure and it was fractured into three pieces with rectangular shape and similar size. These samples were subsequently annealed in 100 bar of oxygen at 625, 650 and 700 °C for 72 hours. With this treatment the crystals, called hereafter T1A, T1B, and T1C, attained oxygen concentrations of 6.960, 6.948 and 6.918

Sample	$7-\delta$	$l \times w \times t$ (mm <sup>3</sup> )	$T_c$ (K)	P(O <sub>2</sub> ) (bar)	Defect Status
DT2	6.934	$1.52 \times 0.85 \times 0.065$	92.5	1	detwinned
DT1B	6.946	$1.04 \times 0.80 \times 0.052$	92.7	1	detwinned
DT1C	6.970	$1.04 \times 0.80 \times 0.052$	92.3	1	detwinned
DT6	6.946	$1.44 \times 0.75 \times 0.055$	92.8	1	detwinned
T1C	6.918	$0.74 \times 0.66 \times 0.090$	92.5	100	twinned
T1B	6.948	$1.03 \times 0.77 \times 0.090$	92.7	100	twinned
T1A	6.960	$0.77 \times 0.66 \times 0.090$	92.9	100	twinned

Table 6.1. Oxygen content, dimensions, transition temperature, annealing pressure and the defect status of the samples under study.

respectively.

In order to demonstrate the crucial role of sample purity for a consistent study of the second magnetization peak, in this chapter we also present data acquired on a detwinned  $YBa_2Cu_3O_{7-\delta}$  single crystal (DT6) that was grown in alumina crucibles, as described in Ref. 36. Samples produced in this way are known to be of low purity, as far as background impurity level is concerned, due to strong contamination by the crucible material.<sup>36,37</sup> DT6 was annealed in 1 bar of oxygen at a temperature of  $\sim 450$  °C and had an oxygen content of  $7-\delta \approx 6.946$ .

In all cases, oxygen contents were determined from eq. (6) of Ref. 38 that relates the oxygen concentration with the annealing pressure and temperature. The details of the investigated samples, that had rectangular shape, are summarized in table 6.1.

## B. Measuring procedure

Magnetization measurements were performed using our *Oxford Instruments* vibrating sample magnetometer for applied fields up to 12 T and a sweep rate of 20 mT/sec. Studies of the detwinned single crystals were carried out for the usual

configuration of fields applied along the  $c$ -axis. On the other hand, in the case of the high-pressure annealed samples the field was applied at an angle  $\theta = 15^\circ$  away from the  $c$ -axis direction. This angle exceeds well the trapping angle,<sup>39, 40</sup> and therefore the influence of twin boundaries is expected to be eliminated. Indeed, as shown recently in this geometry a twinned crystal behaves as though it is detwinned,<sup>39-41</sup> with the field replaced by the effective field  $B_{\text{eff}} = B \cos\theta$ .<sup>42</sup> Moreover, the peak lines in the  $B - T$  plane are independent of whether the crystal is twinned or detwinned.<sup>32</sup>

The transport results presented in this chapter were obtained by S. N. Gordeev using a conventional four probe technique. Narrow silver epoxy pads were painted onto the crystal surface to which gold wires with a diameter of 25  $\mu\text{m}$  were attached. The contact pads were annealed in an oxygen atmosphere at a temperature equal to the annealing temperature of the sample, so as to avoid any changes in the oxygen concentration. After curing for 1 hour the sample was quenched to room temperature. The resulting contact resistances were about 1  $\Omega$ . The current pads were placed on the sides of the sample so as to provide a uniform current flow along the  $ab$ -plane. In this direction square wave currents with a frequency of 88 Hz and maximum magnitude of 38.8 mA were applied. Measurements were performed for fields up to 12 T. Finally, the data were collected via a Stanford SR530/830 lock-in amplifier.

## 6.2.2 Results and discussion

### 6.2.2.1 The second magnetization peak in pure $YBa_2Cu_3O_{7-\delta}$ single crystals

Figure 6.1 illustrates magnetization loops for DT1B at various temperatures. The magnetization curves show a peak at fields far beyond the self-field dominated region, in accordance with other reports.<sup>9-11, 13</sup> However, an interesting and previously unobserved feature depicted in Fig. 6.1, is that the position of the peak varies non-monotonously with temperature. This behaviour has been revealed as a consequence of the improved quality of available single crystals and is absent in samples characterized by strong disorder.<sup>9-11</sup> This becomes obvious from Fig. 6.2, which illustrates magnetization loops for sample DT6 that as discussed in the previous section contains a large amount of background

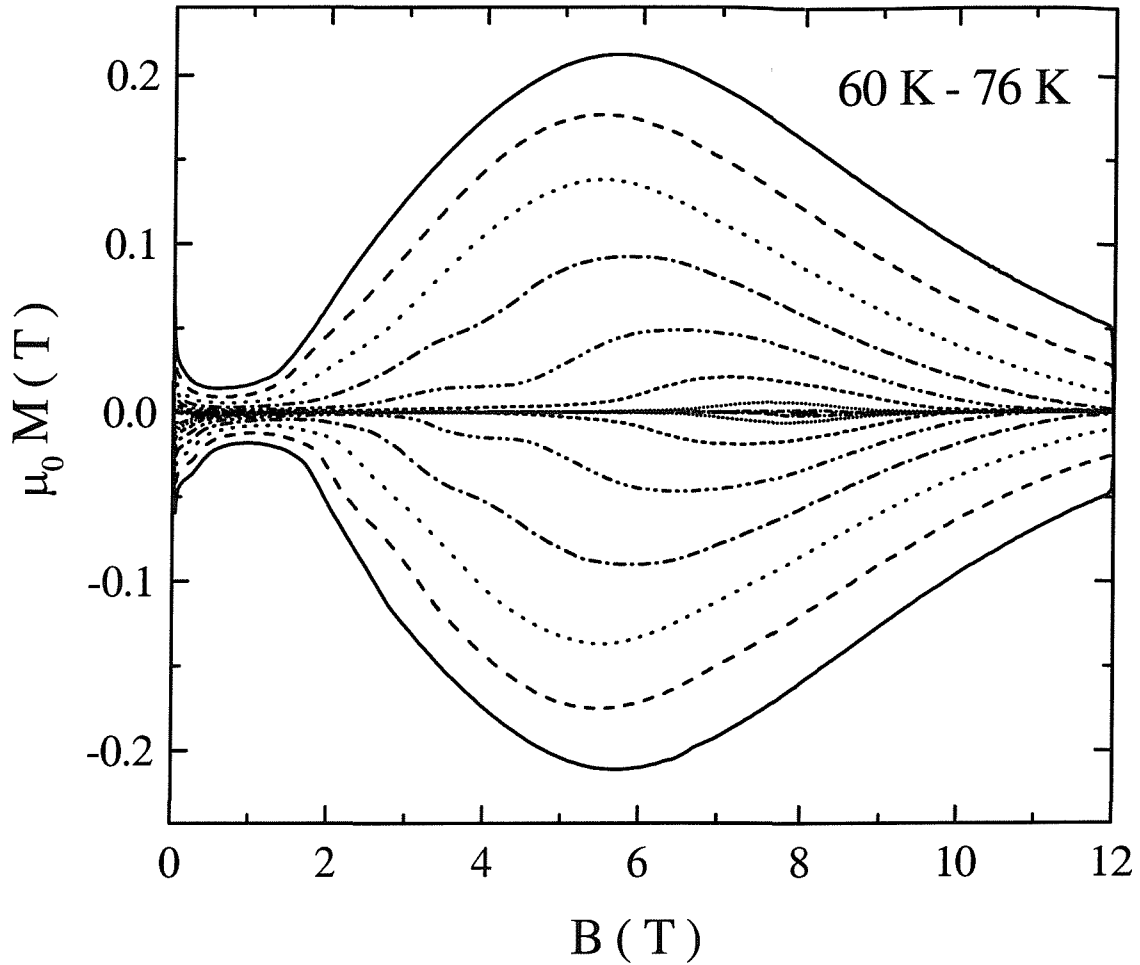


Fig. 6.1. Magnetic hysteresis loops for sample DT1B ( $7-\delta = 6.946$ ) for several temperatures in the range 60 K – 76 K. Temperature increases with a step of 2 K from the outer to the inner curves.

impurities.<sup>43</sup> Indeed, for this sample a monotonous decrease of the peak position with temperature is seen.

The second magnetization peak is additionally found to be strongly influenced by variations in the oxygen stoichiometry. More specifically, with increasing oxygen deficiency the peak shifts to lower field values. This behaviour is depicted in Fig. 6.3, where the peak position,  $B_p$ , is plotted as a function of temperature for several oxygen concentrations near optimal doping. In the range of oxygen contents under study,  $B_p$  increases by as much as 8 T, pointing out the importance of oxygen vacancies as pinning

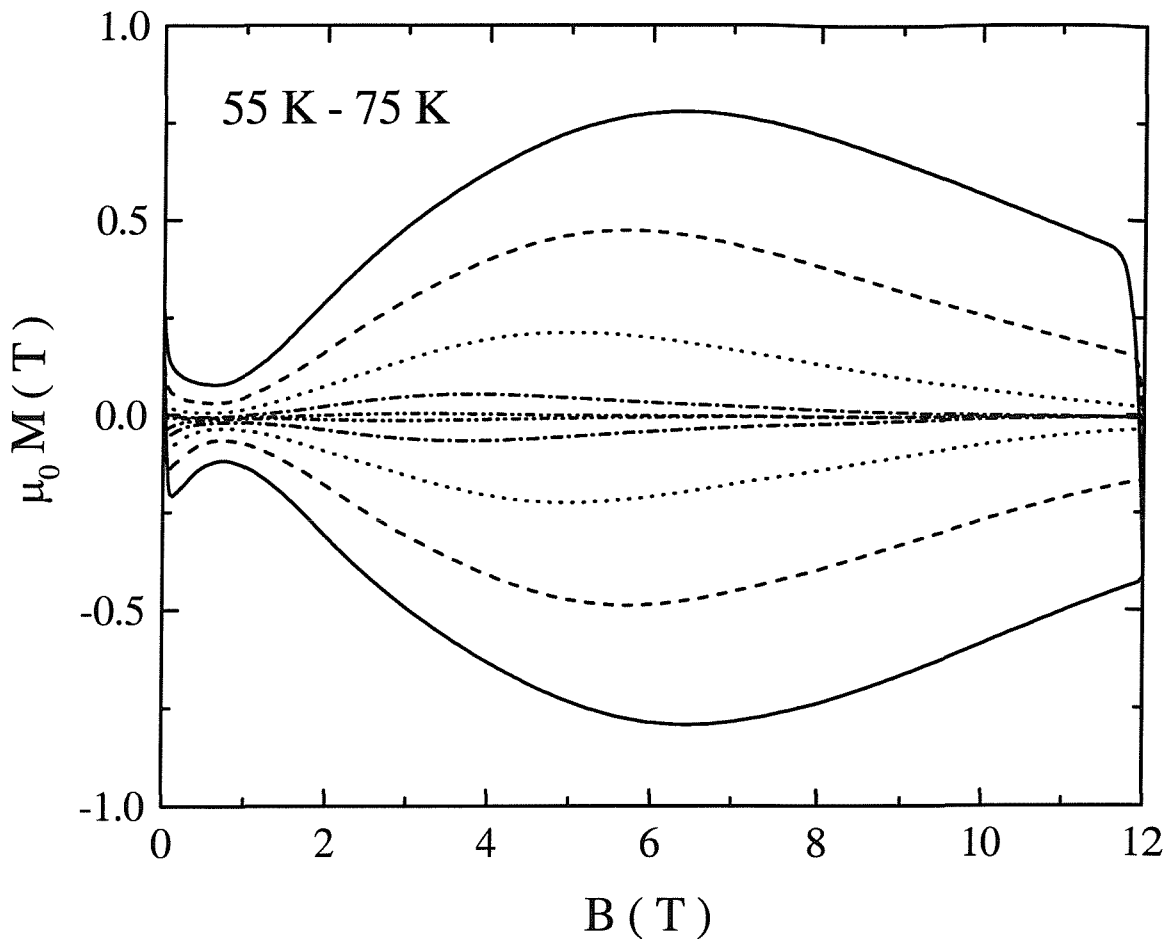


Fig. 6.2. Magnetization versus field curves for DT6 ( $7-\delta \approx 6.946$ ). Data are shown for several temperatures in the range 55 K – 75 K with temperature increasing with a step of 5 K from the outer to the inner loops.

centres in our crystals. This is in contrast to observations in less pure samples, where  $B_p$  is only weakly affected by similar variations in  $\delta$ ,<sup>44</sup> illustrating the dominant role of extrinsic defects other than oxygen vacancies on the magnetic hysteresis in this case.

There are a few more interesting features marking the behaviour of the second magnetization peak in pure  $YBa_2Cu_3O_{7-\delta}$  single crystals. In Fig. 6.4 we present a closer view of the high temperature magnetization loops shown in Fig. 6.1. As can be seen, in this temperature range the peak becomes remarkably sharp. For instance, in the region  $T > 72$  K the difference  $B_p - B_{on}$  falls below 1 T. This value is the smallest ever reported for

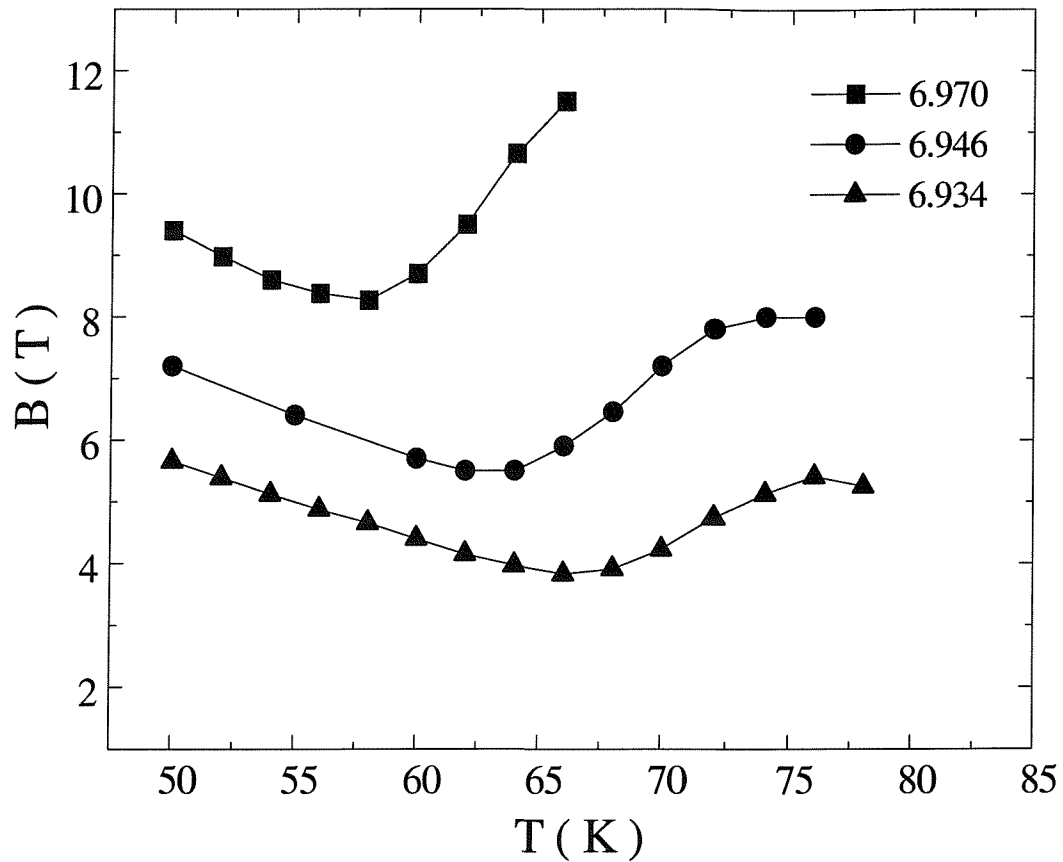


Fig. 6.3. The position of the second magnetization peak is plotted as a function of temperature for the indicated oxygen contents.

$YBa_2Cu_3O_{7-\delta}$ . Furthermore, as firstly observed in our laboratory,<sup>32, 45</sup> at these elevated temperatures the magnetization peak line approaches the first order melting transition line in agreement with recent reports by other groups.<sup>28, 46</sup> This finding is illustrated in Fig. 6.5, where we show for sample DT2 the  $B_p(T)$  line together with the melting line as this has been determined by transport measurements.<sup>47</sup>

The evolution of the magnetization peak starting at elevated temperatures near the melting line, urges for a comparison of this peak with the one seen in transport measurements, which is similarly located close to the solid-to-liquid phase boundary.<sup>14, 48</sup> Therefore, in Fig. 6.5 we have also included the temperature dependence of the transport PE, i.e., the dip seen in the resistivity versus temperature ( $T > 80$  K) or field ( $T < 80$  K) curves. It is stressed that all data are for the same sample. At elevated temperatures (low

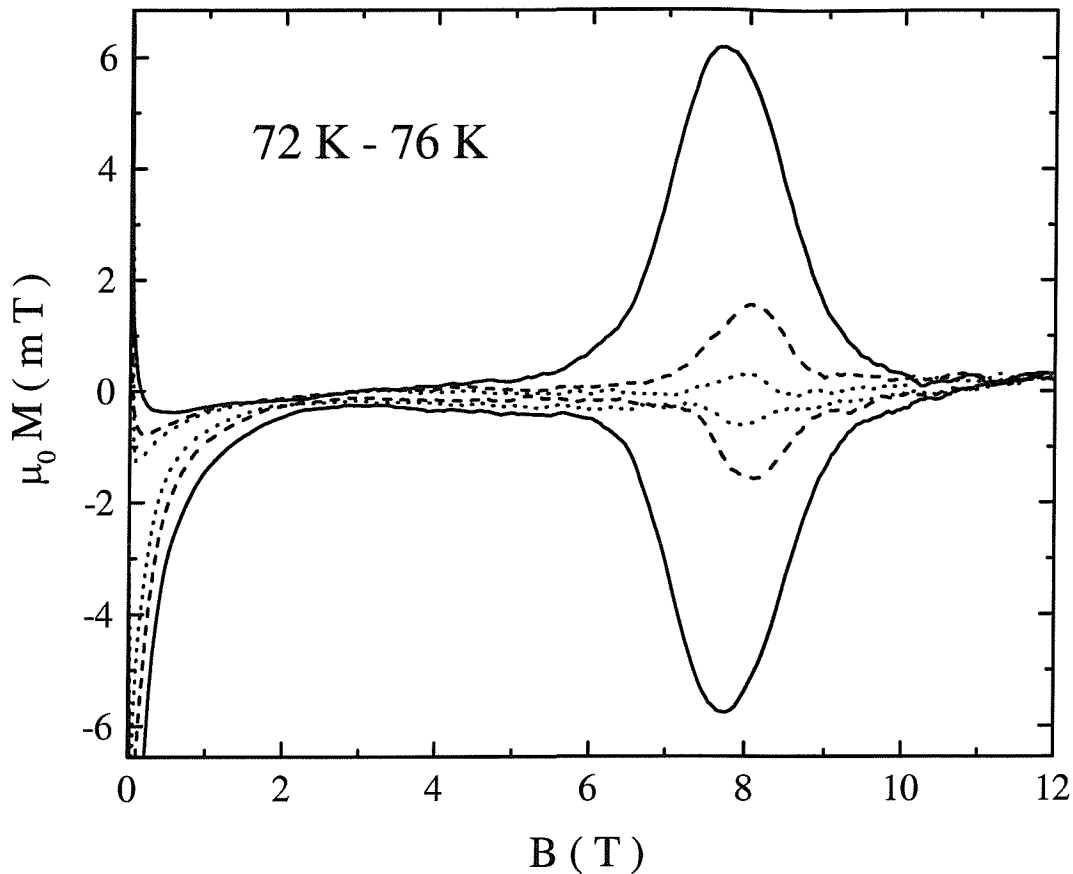


Fig. 6.4. Magnetization loops for sample DT1B ( $7-\delta = 6.946$ ) at temperatures 72 K – 76 K. Temperature increases with a step of 2 K towards the inner curves.

applied fields) the transport peak effect is attributed to a pre-melting softening of the vortex lattice.<sup>14-16</sup> Its temperature dependence defines a boundary that falls just below the first order melting transition line (see Fig. 6.5). However, at lower temperatures the transport peak moves away from this line and as depicted in Fig. 6.5, it eventually splits up into two parts, in agreement with other reports.<sup>49</sup> The physical mechanism underlying the origin of these two peaks has not been understood yet. The high field branch shows a stronger temperature dependence and is located in the vicinity of the second order melting transition line. On the other hand, the low field transport PE moves to smaller fields with decreasing temperature and is in good correspondence with the magnetization peak. This result is also obvious from Fig. 6.6, where magnetic and transport data are compared directly, and indicates strongly that these two peaks are closely related to each other.

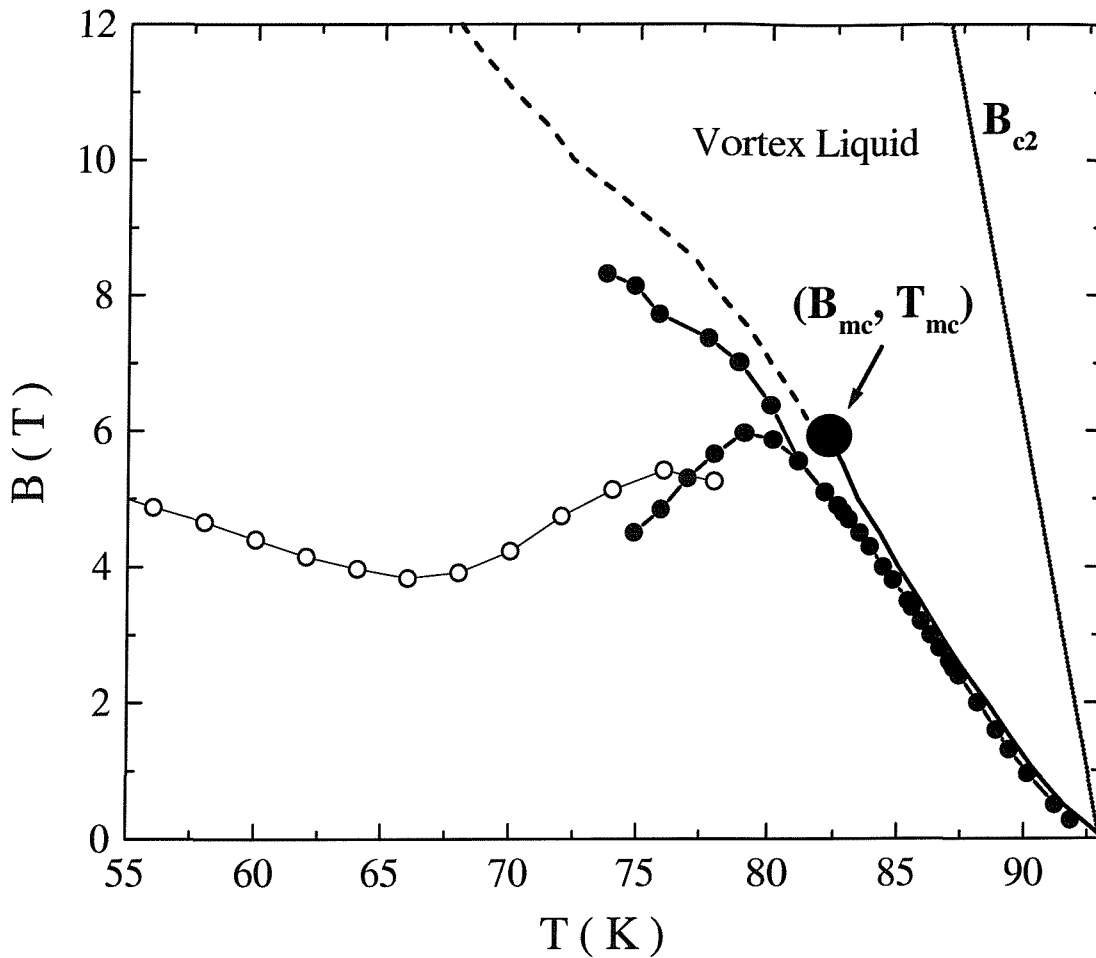


Fig. 6.5. The second magnetization peak line (open circles) is shown in the  $B - T$  plane together with the transport peak line (closed circles) for sample DT2 ( $7-\delta = 6.934$ ) (see text). The continuous line represents the first order melting transition that terminates at the multicritical point  $(B_{mc}, T_{mc})$ . It follows the relation  $B_m(T) = B_0 (1-T/T_c)^a$ , with  $B_0 = 127$  T and  $a = 1.45$ .<sup>50</sup> Above  $B_{mc}$  the melting transition is continuous and can be described using the scaling vortex glass approach of Ref. 51 where the resistivity is given by  $\rho \sim (T-T_g)^s$ . The dashed line represents the vortex glass temperature  $T_g$ , which was obtained by plotting  $\rho^{1/s}$  as a function of  $T$  for  $s = 6$ , at each field.  $T_g$  corresponds to the point where the linear part of  $\rho^{1/s}$  intersects the temperature axis. The upper critical field line is also indicated (dotted line).

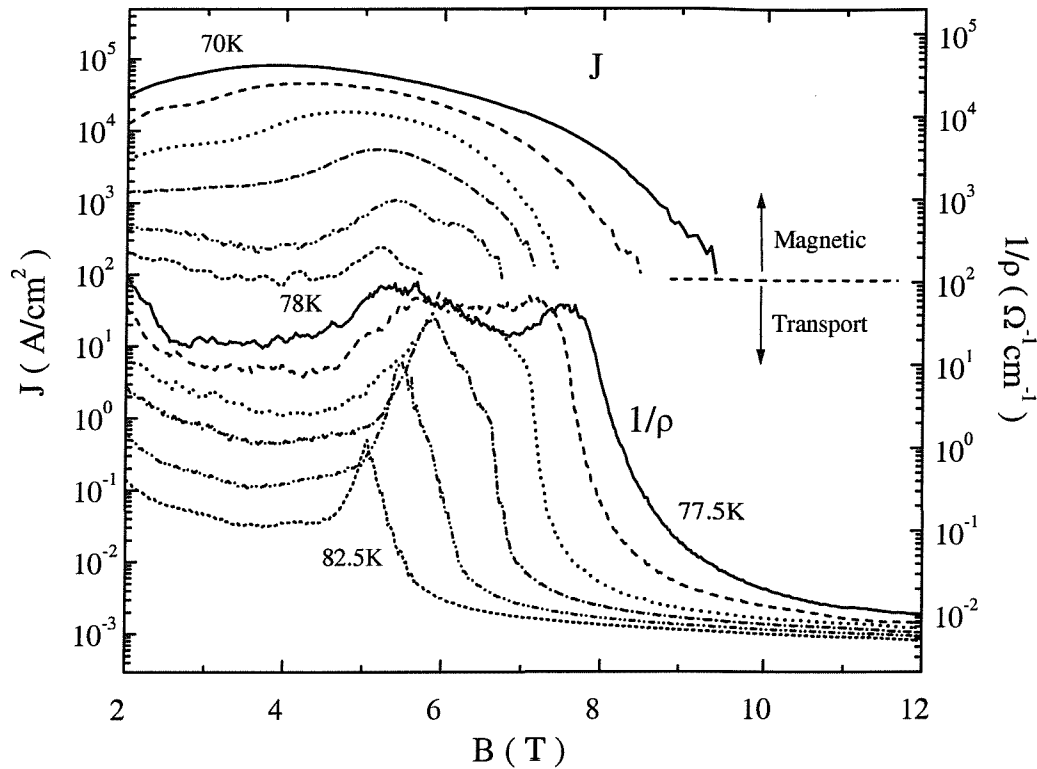


Fig. 6.6. The upper part of the graph shows the field dependence of the current density in  $DT_2$  for temperatures  $70\text{ K} \leq T \leq 78\text{ K}$ , as calculated from the magnetic hysteresis widths using the Bean formula.<sup>52</sup> Temperature increases with a step of 2 K. The lower part represents the inverse resistivity,  $1/\rho$ , as a function of the field for the same sample, in the range  $77.5\text{ K} \leq T \leq 82.5\text{ K}$ , with temperature increasing with a step of 1 K.

The temperature dependence of the peak position illustrated in Figs. 6.1 and 6.3-6.6 is inconsistent with the explanation of the magnetization PE as resulting from granularity of the sample, induced by the intersection of either normal or reversible regions as proposed in Refs. 9 and 10. Indeed, according to this model the peak position must follow the temperature dependence of the irreversibility or upper critical field, and accordingly, it should decrease monotonously with temperature, in obvious contradiction with our results. It is also noted that the significance of granularity was rejected by transport measurements.<sup>53</sup> In addition, the fact that the peak is present at elevated temperatures near the melting line far above the single vortex collective pinning regime, together with our

observation that the elastic region is restricted below the onset of the PE (see Chapter 5) disprove the dynamic scenario.<sup>11</sup>

Hence, in order to understand the behaviour of the magnetization PE in  $\text{YBa}_2\text{Cu}_3\text{O}_{7-\delta}$ , one has to consider other possible mechanisms causing this phenomenon. Significant new insight regarding the origin of the PE has been provided by our results outlined in Chapter 5. As we demonstrated there, the onset of the peak in pure  $\text{YBa}_2\text{Cu}_3\text{O}_{7-\delta}$  single crystals is closely related to a phase transition from a quasi-ordered Bragg glass to a highly disordered vortex phase.<sup>33, 34, 54, 55</sup> With raising the field above the Bragg glass stability region, vortex entanglement takes place, leading to the introduction of dislocations in the vortex lattice.<sup>24-26</sup> Due to entanglement, firmly pinned vortex lines will hold others in place, thus increasing the effectiveness of pinning because of flux cutting barriers.<sup>56-58</sup> As a result the critical current density will be enhanced.<sup>25</sup> However, the proliferation of dislocations will have an additional effect on the hysteretic response of the superconductor. In particular, an immediate consequence of the introduction of topological defects in the vortex lattice will be the reduction of  $c_{66}$ .<sup>4, 51, 59</sup> Therefore, in view of older predictions,<sup>6, 7</sup> the dislocation-induced softening of the lattice will result in a better adaptation of vortices to the underlying random pinning landscape, increasing pinning further. There are two factors that will eventually limit the enhancement of the current. First, when the density of dislocations is high, vortex crossing angles will become large. At this point, flux line cutting will be easier,<sup>56-58</sup> and the current will drop with field.<sup>25</sup> Second, with increasing field shearing of the lattice will ultimately be favoured and will also lead to a reduction in the current. In other words, in one way or another, the magnetic hysteresis will show a peak in the region where the pinning force overcomes the force required for breaking up the flux line lattice.

There has been an increasing number of experimental reports supporting the idea that the location of the magnetization PE in  $\text{YBa}_2\text{Cu}_3\text{O}_{7-\delta}$  is determined by an interplay between pinning and the rigidity of the vortex lattice. Local relaxation measurements in  $\text{YBa}_2\text{Cu}_3\text{O}_{7-\delta}$  single crystals have indicated that above the peak, plastic motion governs the vortex dynamics.<sup>60</sup> Furthermore, in Ref. 28 it was shown that, unlike below, above  $B_p$  the current is insensitive to the growing strength of the defect structure, which is consistent with a plastic deformation of the vortex lattice in this region (see also Ref. 8). In addition, the presence of a peak in the field dependence of the critical current following

the Bragg glass – disordered phase transition, was recently confirmed by numerical simulations of the vortex system.<sup>61</sup>

Finally, it is reminded that a similar scenario based on a lattice-softening mechanism has been successfully employed to account for the PE observed close to the melting line in transport and ac susceptibility measurements of  $YBa_2Cu_3O_{7-\delta}$  single crystals.<sup>14, 15</sup> The difference in this case, however, is that the softening of the lattice is expected to be mainly thermally-driven.<sup>16</sup>

In the absence of a firm theoretical description of the entangled disordered phase, the dislocation-mediated mechanism for the PE cannot be quantified at the moment. Nevertheless, from the above discussion it is clear that the position of the peak can be generally considered as being determined by a competition between the pinning force and the force required to induce plastic motion of the flux line lattice. Therefore, for simplicity in the following we will refer to such plastic distortions using the general term “lattice-breaking”, knowing that, in principle, both effects mentioned above (i.e., flux line cutting and shearing of the lattice) might be involved.

In the case of weak random point disorder, pinning of the vortex lattice is determined by fluctuations in the density and force of the defects.<sup>7, 59</sup> The randomness of the pinning landscape results in a distribution of pinning energies that in a simple approach can be regarded as a Gaussian, as is schematically illustrated in Fig. 6.7.<sup>62</sup> In such a situation, at a finite temperature  $T$ , pinning energies  $U_p < k_B T$  will be thermally smeared out and the corresponding pinning sites will not contribute to the irreversibility. Obviously, the higher the temperature the smaller the concentration of effective pinning centres and accordingly the total pinning force. On the other hand, with increasing temperature the force required for “lattice-breaking” will be reduced as well.<sup>56-58, 63</sup> Therefore, coming back to our results, in order to understand the temperature dependence of the magnetization peak, the relative influence of the varying temperature on these two parameters must be considered.

A key insight was provided in Ref. 28: For a certain density of pinning centres, there will be a characteristic temperature  $T_{\min}$ , below which  $k_B T$  will be located at the low energy tail of the pinning energy distribution (see Fig. 6.7). Accordingly, in this temperature range the density of effective pinning centres will be very weakly temperature dependent (note that this idea is also supported theoretically in Ref. 59). As a result, following the reduction in the “lattice-breaking” force, the peak position will

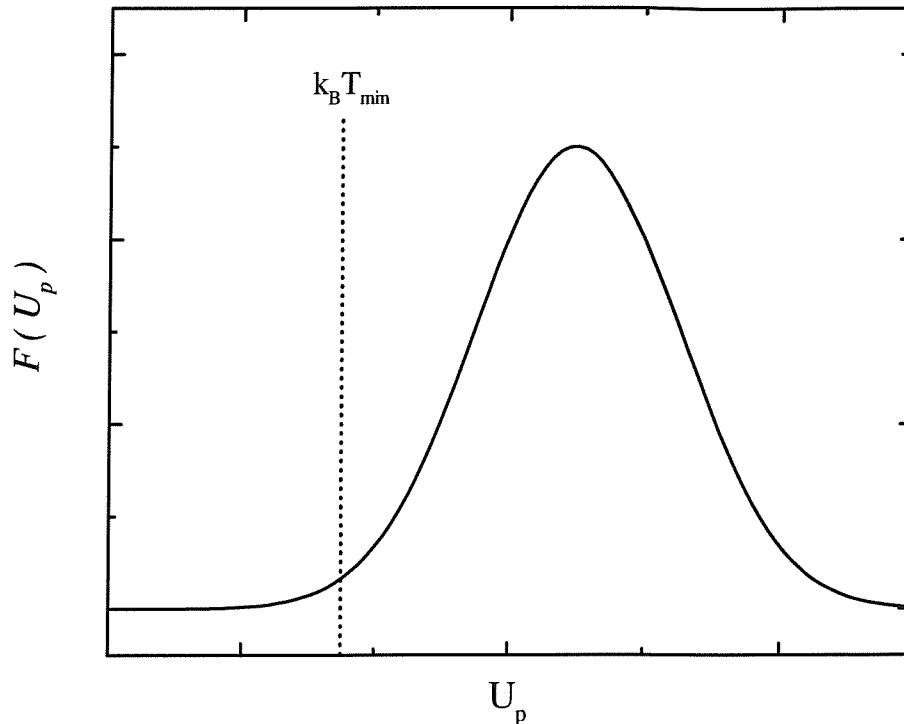


Fig. 6.7. The solid line represents a schematic illustration of the distribution of the pinning energies. The vertical axis represents the function  $F(U_p) = dn/dU_p$ , where  $n$  is the density of pinning centres with pinning energy  $U_p$ , and the horizontal axis the pinning energy  $U_p$ . For simplicity  $n$  is taken as a continuous variable, whereas the temperature dependence of the distribution is neglected. For illustration purposes a possible location for  $T_{min}$  (discussed in the text) is also indicated.

decrease with temperature. On the other hand, when the temperature increases above  $T_{min}$ ,  $k_B T$  enters the pinning energy distribution and  $n$  starts to be considerably reduced. Consequently, with increasing temperature in this region, the reduction in the pinning force will eventually become stronger than the one in the “lattice-breaking” force, leading to an increase in the peak position with temperature. Thus from this discussion it is clear that  $T_{min}$  corresponds to the minimum in the  $B_p(T)$  dependencies illustrated in Fig. 6.3.

In a similar manner, the increase in the density of oxygen vacancies with  $\delta$ , shifts the pinning energy distribution to higher values. Moreover, since as discussed in Chapter 3, with decreasing oxygen content both  $\lambda_{ab}$  and  $\xi_{ab}$  tend to increase (but only slightly in the region under study<sup>41</sup>), from eq. (2.5) and the energy scale  $U_{cut} \sim \lambda_{ab}^{-2}$  involved in flux

line cutting,<sup>56, 63</sup> one can see that at lower oxygen concentrations “lattice-breaking” will be easier. Consequently, at a certain temperature, for higher oxygen deficiencies plastic motion of the lattice will be favoured at lower fields, thus shifting the location of the peak to lower values (it is reminded that  $B_{\text{on}}$  also decreases with  $\delta$ , see Fig. 5.15). Notice that as illustrated in Fig. 6.3,  $T_{\text{min}}$  increases with the density of pinning centres as one would anticipate by the above arguments.

### 6.2.2.2 Peak effect and oxygen ordering in pure $\text{YBa}_2\text{Cu}_3\text{O}_{7-\delta}$ single crystals

As already mentioned in section 6.1, it was recently shown that, at  $T = 70$  K, the magnetization peak in pure  $\text{YBa}_2\text{Cu}_3\text{O}_{7-\delta}$  single crystals can be reversibly produced and removed by proper oxygenation methods.<sup>29-31</sup> These methods differ in the oxygen pressure used for the annealing treatment. Utilising high pressures allows for the use of higher temperatures to obtain a certain oxygen content.<sup>38</sup> Accordingly, considering the almost exponential dependence of the oxygen diffusion coefficient on the inverse temperature,<sup>64, 65</sup> for a given annealing time, a larger oxygen diffusion distance will be succeeded.<sup>66</sup> In this way, for high pressure annealing a more homogeneous oxygenation of the sample is achieved as contrasted to the low pressure treatment where oxygen deficient regions tend to form clusters.<sup>30, 31, 66</sup> Consequently, it was proposed in Refs. 29-31, that the elimination of oxygen vacancy clustering is the reason for the observed suppression of the second magnetization peak after high pressure annealing.

However, in these studies the disappearance of the peak was demonstrated only for a single temperature of 70 K. Moreover, they were constrained to magnetic fields below 5.5 T. As a result, the question concerning the effect of high pressure annealing upon the magnetic hysteresis of pure  $\text{YBa}_2\text{Cu}_3\text{O}_{7-\delta}$  single crystals for other temperatures and higher fields, as well as the influence of variations in the density of oxygen vacancies remains open. In order to clarify this issue, we have investigated several pure single crystals with oxygen contents in the region near optimal doping ( $0.02 < \delta < 0.09$ ) and different degrees of oxygen vacancy ordering, in a broad temperature range and for fields up to 12 T.<sup>35</sup>

Figure 6.8 illustrates magnetization loops for the high pressure annealed sample T1B at several temperatures ranging from 56 K to 76 K. In accordance with the results for

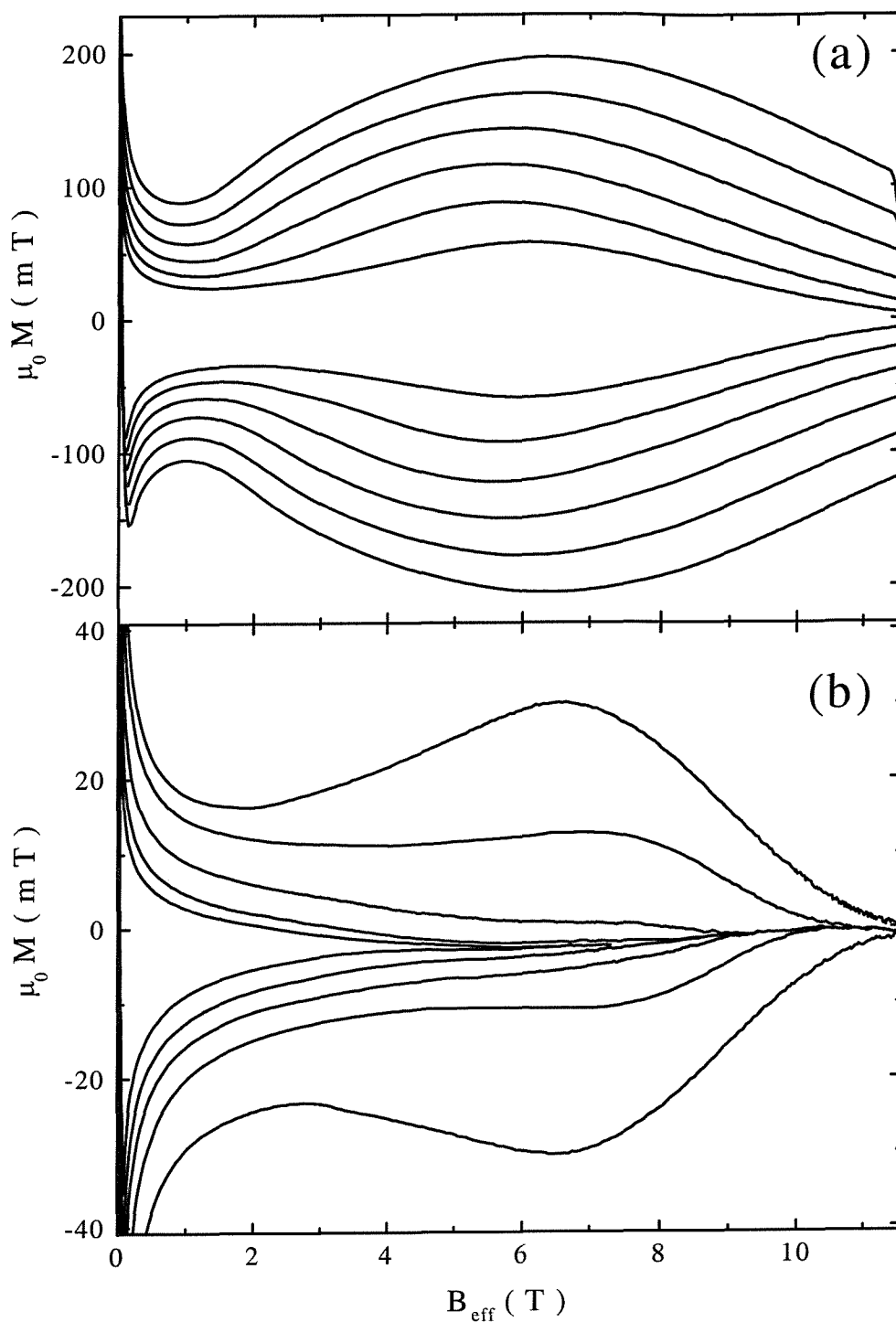


Fig. 6.8. Magnetization loops for crystal T1B ( $7-\delta = 6.948$ ) for temperatures in the range (a) 56 K – 66 K and (b) 68 K – 76 K. Temperature increases with a step of 2 K from the outer to the inner curves.

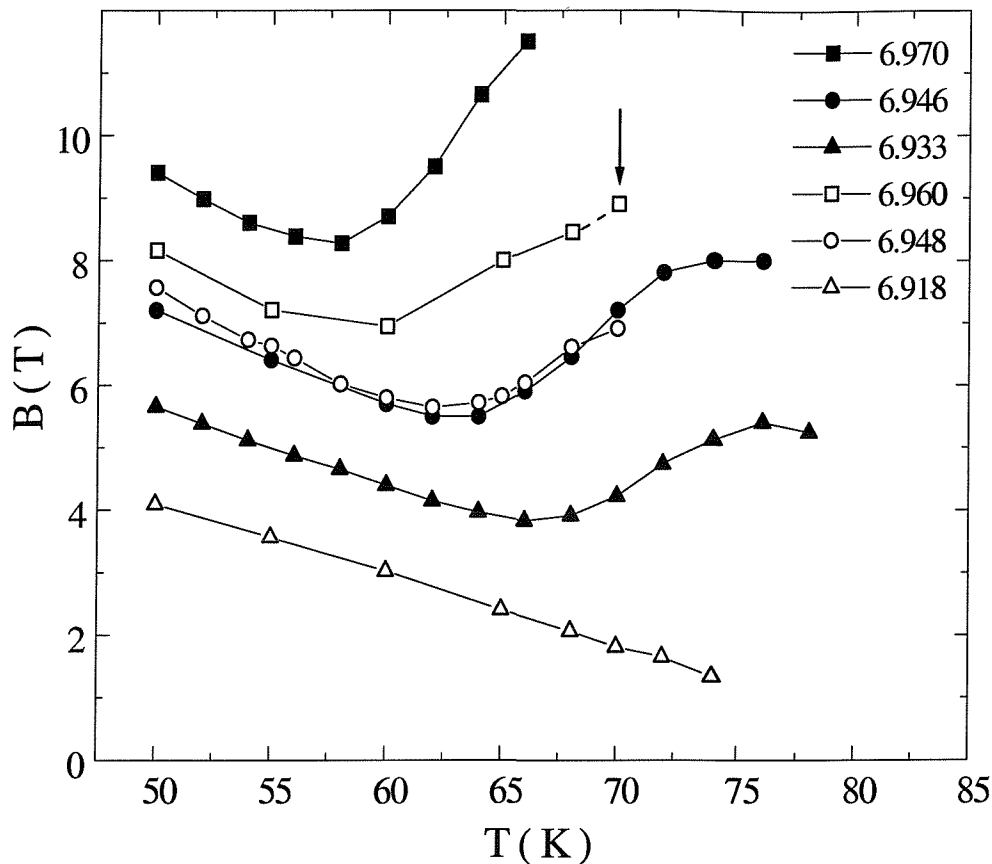


Fig. 6.9. Position of the magnetization peak in the  $B - T$  plane for various oxygen contents and for single crystals annealed at 100 bar (open symbols) and 1 bar (closed symbols) of oxygen. The arrow indicates the position of the peak for T1A at 70 K after ageing as discussed in the text.

DT1B, the magnetic hysteresis in this sample exhibits a peak below 70 K, and although with increasing temperature its position initially shifts to lower fields, at high temperatures the opposite behaviour is observed.

The evolution of the peak lines in the  $B - T$  plane with oxygen content for the high pressure annealed samples is illustrated with the open symbols in Fig. 6.9. For comparison, on the same graph we have also included the  $B_p(T)$  lines for the 1 bar annealed samples (closed symbols) as taken from Fig. 6.3. A non-monotonic temperature dependence of the peak position is seen that disappears for  $7-\delta < 6.92$ .

An important observation from Figures 6.8 and 6.9 is that below 70 K the magnetization curves of the high pressure annealed crystals display a peak. Therefore, high pressure annealing does not result in the suppression of the peak in this temperature range. Furthermore, the main features of the peak for the 100 bar annealed samples (i.e., the non-monotonic temperature dependence and the shift to higher fields with increasing oxygen content) are similar with the ones observed for the 1 bar annealed crystals (see Fig. 6.3). However, as illustrated in Fig. 6.8 (b), for temperatures above 70 K the peak is absent in T1B and is substituted by only a monotonous decrease of the magnetization with field, in agreement with the results by Erb et al.<sup>29-31</sup>

The suppression of the peak is shown more clearly in Fig. 6.10 below, where we

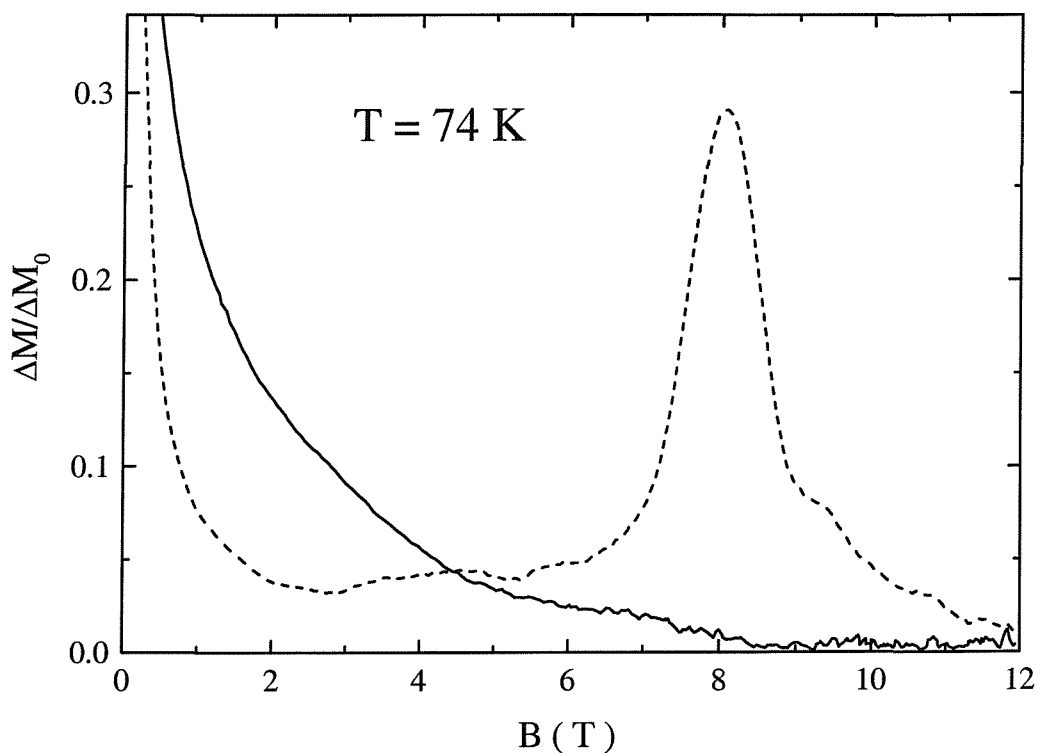


Fig. 6.10. The field dependence of the magnetization widths,  $\Delta M$ , normalised by their values  $\Delta M_0$  at  $B = 0$  T, for the low and high pressure annealed DT1B ( $7-\delta = 6.946$ , dashed line) and T1B ( $7-\delta = 6.948$ , solid line) respectively, at  $T = 74$  K. As can be seen at this temperature the magnetization peak can be suppressed by high pressure annealing.

present the field dependence of the normalized magnetization widths for DT1B and T1B at  $T = 74$  K. As can be seen, the sharp magnetization peak seen in the high field region for DT1B, has been replaced by a monotonously decreasing and almost reversible magnetic response in the case of T1B. The same result has been obtained for all the high pressure annealed crystals studied. This is obvious from Fig. 6.9, where one can discern that the  $B_p(T)$  lines of the high pressure annealed crystals always terminate at temperatures lower than the ones corresponding to the 1 bar annealed samples. For example, for the two crystals with oxygen content of almost 6.95, the temperatures above which the peak cannot be further observed differ by almost 6 K. Hence, we conclude that high pressure annealing can lead to the suppression of the magnetization peak but only at high enough temperatures.

Another significant result depicted in Fig. 6.9, is that for  $7-\delta \approx 6.95$  the peak positions for DT1B and T1B almost coincide. Since the intrinsic parameters of the superconductor depend only on the oxygen content, then considering that, as demonstrated in Ref. 31 by several independent techniques, the high and low pressure treatments result in different distributions of oxygen vacancies, this observation implies that the peak is independent of the precise configuration formed by these pinning centres. To further investigate such an implication, we have performed the following analysis. If the peak depended only on the density and not the distribution of oxygen vacancies, then at a certain temperature, a plot of the peak position as a function of oxygen content would result in a single line for both treatments. Remarkably, this is exactly what we observe in Fig. 6.11, where  $B_p$  is plotted versus the oxygen concentration for both high and low pressure annealed samples, for temperatures of 50 K and 60 K.

As discussed in more detail in the previous section, the position of the magnetization peak is considered as being determined by the competition between the rigidity of the vortex lattice and the pinning strength. However, in the region of oxygen contents under study ( $6.91 < 7 - \delta < 6.97$ ) intrinsic parameters of the superconductor, such as the anisotropy, penetration depth and coherence length are almost unaffected by variations in the oxygen stoichiometry.<sup>41, 67</sup> Hence, the elastic properties of the lattice do not vary considerably in the investigated samples and the peak position should be mainly determined by the temperature and field dependencies of the pinning force. In this sense, the large variation of  $B_p$  with oxygen content shown in Fig. 6.9 demonstrates that the peak position is very sensitive to changes in pinning. Moreover, it shows that the peak is

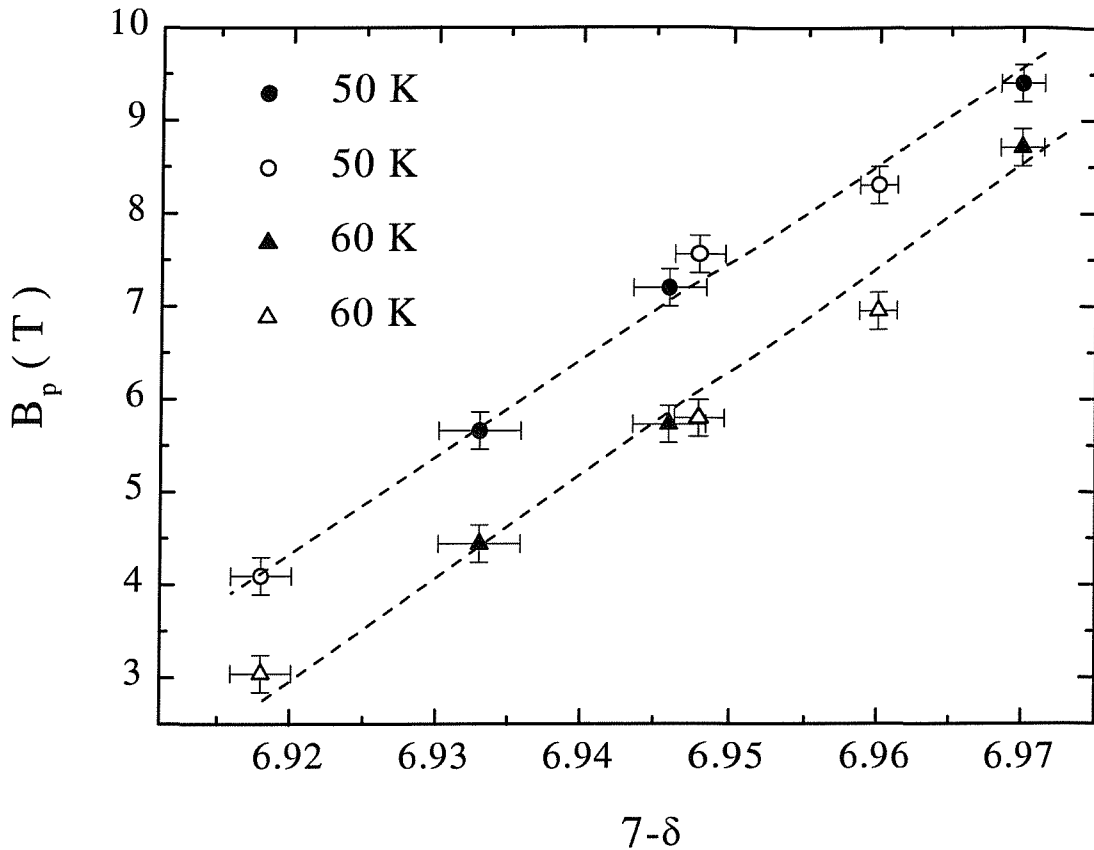


Fig. 6.11.  $B_p$  plotted as a function of oxygen content at the indicated temperatures for single crystals annealed at 1 bar (closed symbols) and 100 bar (open symbols) of oxygen. The dashed lines are guides to the eye.

mainly determined by oxygen vacancies, thus excluding the possibility that for  $T < 70$  K the peak might be produced by pinning by other defects, such as background impurities. Therefore, considering the strong dependence of the peak position on pinning and that samples annealed under high and low pressures are characterized by different distributions of oxygen vacancies,<sup>31</sup> the results depicted in Fig. 6.11 suggest that for temperatures below 70 K, pinning does not depend significantly on the formation or not of oxygen vacancy clusters.

To additionally elucidate the above statement we have performed the following experiment.  $\text{YBa}_2\text{Cu}_3\text{O}_{7-\delta}$  has been shown to be characterized by relatively high oxygen mobility.<sup>68</sup> Hence, short scale diffusion of oxygen can take place even at room

temperature leading to an ordering process (ageing) that occurs in the absence of compositional changes.<sup>69</sup> The result of ageing is the formation of oxygen vacancy clusters.<sup>69</sup> To accelerate the ordering process, after studying sample T1A we heated it at 50 °C for 24 hours and subsequently studied it again. Figures 6.12 (a) and (b) show the field dependence of the current density for this sample before and after ageing, at 65 K and 70 K respectively. The current density has been calculated from the magnetization widths using the Bean formula.<sup>52</sup> Remarkably, we observe that at 70 K ageing leads to the reappearance of the peak as well as a doubling of the current density in the peak region, illustrating clearly that ordering effects become very important at these elevated temperatures. The position of this peak has been included in the  $B - T$  plane of Fig. 6.9 and is indicated by the arrow. Interestingly, it is found to follow the line defined by the other points. On the other hand, as can be seen from Fig. 6.12 (a), at 65 K ageing does not affect significantly the irreversibility. This is a general behaviour for  $T < 70$  K, where oxygen ordering is seen to lead to a change in the current density by not more than  $\sim 10$  %. This becomes more clear from Fig. 6.13, where the ratio,  $R$ , of the current density values at the peak, after and before ageing is plotted versus temperature. No larger variation of the current is observed in the whole field range, whereas the peak position is almost unaltered after ageing. Since both the current density and  $B_p$  depend on the pinning strength, from the above results one can conclude that the induced formation of clusters (or increase in the size of clusters already present in the sample) due to ageing does not affect significantly the pinning properties for temperatures below 70 K.

The similarity in the low temperature behaviour of high and low pressure annealed samples is not surprising. In both cases the elementary pinning centres are the same (oxygen vacancies) and pinning is collective (i.e., each vortex line interacts with many pins). As already discussed, in these systems pinning is generally determined by “fluctuations” in the density of the pinning sites that for the case at hand are determined by the distribution (statistics) of the oxygen vacancies.<sup>42</sup> This, however, is different in the high and low pressure annealed samples: In the former, due to the high annealing temperatures oxygen vacancies are expected to be distributed more uniformly, whereas in the latter they are less randomly distributed and tend to form clusters.<sup>31</sup> This means that for the 1 bar annealed crystals the size of such “fluctuations” should be larger; however, their overall density must be smaller.

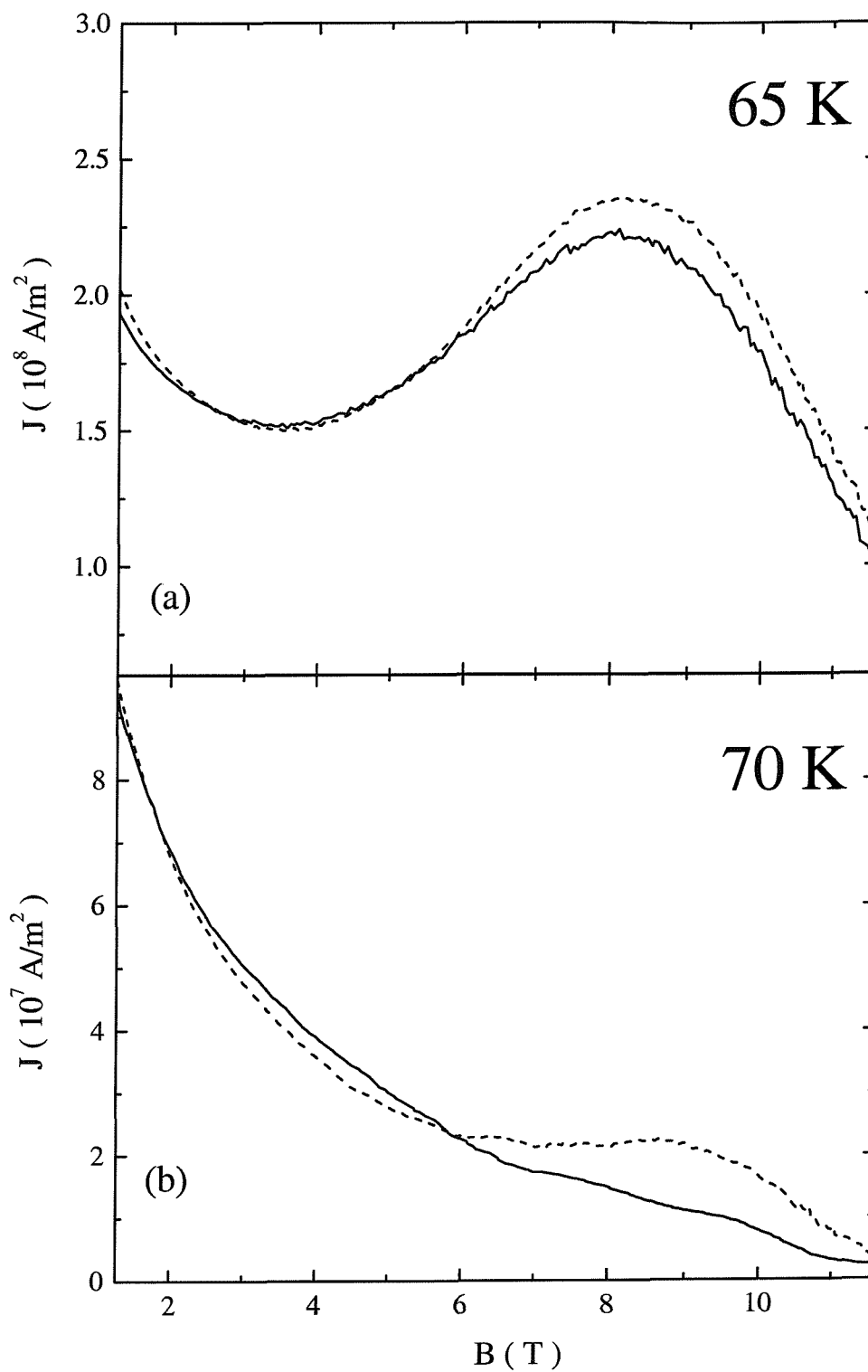


Fig. 6.12. Current versus field curves for crystal T1A ( $7-\delta = 6.96$ ) at 65 K (a) and 70 K (b), before (solid lines) and after (dashed lines) ageing at  $50^\circ\text{C}$  (see text).

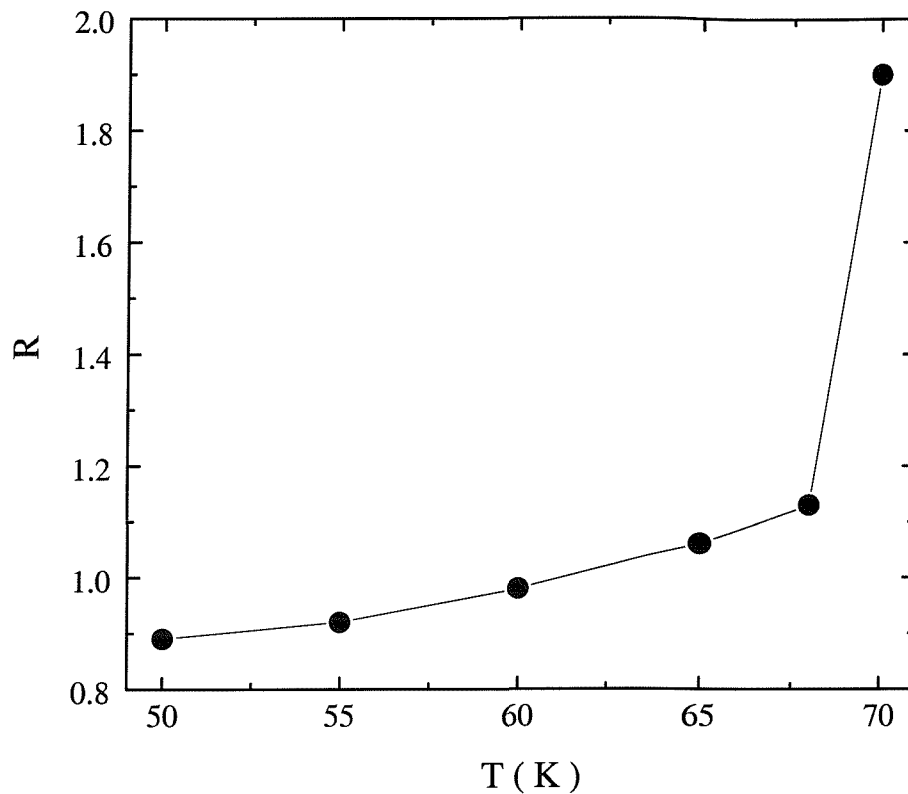


Fig. 6.13. The temperature dependence of the ratio  $R$  of the shielding currents at the peak for crystal T1A after and before ageing at  $50^\circ\text{C}$ .

Quantitative analysis of vortex pinning in such complex environments requires a detailed knowledge of the spatial distribution of oxygen defects and is not available at the moment. Nevertheless, our experimental results clearly demonstrate that at sufficiently low temperatures ( $T < 70\text{ K}$ ), for both types of samples pinning is determined by the integral concentration of oxygen defects and that the distribution of these defects is not of great importance. This effect could be attributed to a compromise in this temperature range between the higher density and smaller size of “fluctuations” in the pinning energy for the case of high pressure annealing, and the smaller density and larger size of such “fluctuations” for the low pressure treatment, resulting in similar pinning properties. At higher temperatures, however, small-size “fluctuations” are thermally smeared out.<sup>12</sup> This effect has the strongest influence on the high-pressure annealed samples, where the

fraction of small “fluctuations” in the pinning landscape is greater, leading to reduced currents and the suppression of the peak.

### 6.2.3 Conclusions

In summary, in this chapter we investigated the second magnetization peak in pure  $\text{YBa}_2\text{Cu}_3\text{O}_{7-\delta}$  single crystals. It was demonstrated that for low densities of point defects, the peak shows a non-monotonous temperature dependence, a behaviour that is distinctly different from observations on less pure samples. At high temperatures the peak was found to become rather sharp and to approach the melting line. In addition, in this region the magnetization peak was in correspondence with the one seen in transport studies, suggesting that both features might originate from the same physical mechanism. Finally, the effect of decreasing oxygen concentration was shown to be the shift of the location of the peak to lower fields. These findings were accounted by considering a model where the peak is determined by a competition between pinning and plastic deformations in the vortex lattice.

We have also studied the influence on the second magnetization peak of different distributions of oxygen vacancies. By comparing high quality  $\text{YBa}_2\text{Cu}_3\text{O}_{7-\delta}$  single crystals annealed under different conditions, we have shown that in a large temperature range ( $T < 70$  K) the position of the peak does not depend significantly on the oxygenation treatment and hence on the distribution of oxygen deficient sites. These results suggested that at these temperatures point and cluster defect configurations of oxygen vacancies are characterized by similar pinning properties. Above 70 K, however, clusters were found to be more robust against thermal depinning resulting into the presence of the peak and higher current densities for the low pressure annealed samples.

## References

- <sup>1</sup> T. Belincourt, Phys. Rev. 114, 969 (1959)
- <sup>2</sup> M. Steingart, A. G. Putz, and E. J. Kramer, J. Appl. Phys. 44, 5580 (1973); H. K pfer and W. Gey, Philos. Mag. 36, 859 (1977)
- <sup>3</sup> H. R. Kerchner, J. Low Temp. Phys. 50, 337 (1983)
- <sup>4</sup> R. W rdenweber, P. H. Kes, and C. C. Tsuei, Phys. Rev. B 33, 3172 (1986)
- <sup>5</sup> S. Bhattacharya and M. J. Higgins, Phys. Rev. Lett. 70, 2617 (1993)
- <sup>6</sup> A. B. Pippard, Philos. Mag. 19, 217 (1969)
- <sup>7</sup> A. I. Larkin and Yu. N. Ovchinnikov, J. Low Temp. Phys. 34, 409 (1979)
- <sup>8</sup> K. E. Osborne and E. J. Kramer, Philos. Mag. 29, 685 (1974); E. J. Kramer, J. Appl. Phys. 44, 1360 (1973). For an extension of this approach to  $\text{YBa}_2\text{Cu}_3\text{O}_{7-\delta}$  epitaxial films see R. W rdenweber, Phys. Rev. B 46, 3076 (1992).
- <sup>9</sup> M. D umling, J. M. Seuntjens, and D. C. Larbalestier, Nature 346, 332 (1990)
- <sup>10</sup> L. Klein, E. R. Yacoby, Y. Yeshurun, A. Erb, G. M ller-Vogt, V. Breit, and H. W hl, Phys. Rev. B 49, R4403 (1994)
- <sup>11</sup> L. Krusin-Elbaum, L. Civale, V. M. Vinokur, and F. Holtzberg, Phys. Rev. Lett. 69, 2280 (1992)
- <sup>12</sup> M. V. Feigel'man, V. B. Geshkenbein, A. I. Larkin, and V. M. Vinokur, Phys. Rev. Lett. 63, 2303 (1989); M. V. Feigel'man and V. M. Vinokur, Phys. Rev. B 41, 8986 (1990); M. V. Feigel'man, V. B. Geshkenbein, and V. M. Vinokur, *ibid.* 43, 6263 (1991)
- <sup>13</sup> A. A. Zhukov, H. K pfer, G. K. Perkins, L. F. Cohen, A. D. Caplin, S. A. Klestov, H. Claus, V. I. Voronkova, T. Wolf, and H. W hl, Phys. Rev. B 51, 12704 (1995)
- <sup>14</sup> W. K. Kwok, J. A. Fendrich, C. J. van der Beek, and G. W. Crabtree, Phys. Rev. Lett. 73, 2614 (1994)
- <sup>15</sup> G. D'Anna, M. V. Indenbom, M.-O. Andr , W. Benoit, and E. Walker, Europhys. Lett. 25, 225 (1994)
- <sup>16</sup> A. I. Larkin, M. C. Marchetti, and V. M. Vinokur, Phys. Rev. Lett. 75, 2992 (1995)
- <sup>17</sup> G. Yang, P. Shang, I. P. Jones, J. S. Abell, and C. E. Gough, Phys. Rev. B 48, 4054 (1993)
- <sup>18</sup> T. Tamegai, Y. Iye, I. Oguro, and K. Kishio, Physica C 213, 33 (1993)

- <sup>19</sup> V. Hardy, A. Wahl, A. Ruyter, A. Maignan, C. Martin, L. Couldrier, J. Provost, and Ch. Simon, *Physica C* 232, 347 (1994)
- <sup>20</sup> V. N. Kopylov, A. E. Koshelev, I. F. Schegolev, and T. G. Togonidze, *Physica C* 170, 291 (1990)
- <sup>21</sup> Y. Yeshurun, N. Bontemps, L. Burlachkov, and A. Kapitulnik, *Phys. Rev. B* 49, R1548 (1994)
- <sup>22</sup> N. Chikumoto, M. Konczykowski, N. Motohira, and A. P. Malozemoff, *Phys. Rev. Lett.* 69, 1260 (1992)
- <sup>23</sup> B. Khaykovich, M. Konczykowski, E. Zeldov, R. A. Doyle, D. Majer, P. H. Kes, and T. W. Li, *Phys. Rev. B* 56, R517 (1997)
- <sup>24</sup> T. Giamarchi and P. Le Doussal, *Phys. Rev. Lett.* 72, 1530 (1994); *Phys. Rev. B* 52, 1242 (1995); *ibid.* 55, 6577 (1997)
- <sup>25</sup> D. Ertas and D. R. Nelson, *Physica C* 272, 79 (1996)
- <sup>26</sup> V. M. Vinokur, B. Khaykovich, E. Zeldov, M. Konczykowski, R. A. Doyle, and P. H. Kes, *Physica C* 295, 209 (1998)
- <sup>27</sup> D. Giller, A. Shaulov, R. Prozorov, Y. Abulafia, Y. Wolfus, L. Burlachkov, Y. Yeshurun, E. Zeldov, V. M. Vinokur, J. L. Peng, and R. L. Greene, *Phys. Rev. Lett.* 79, 2542 (1997)
- <sup>28</sup> H. K pfer, Th. Wolf, C. Lessing, A. A. Zhukov, X. Lan on, R. Meier-Hirmer, W. Schauer, and H. W hl, *Phys. Rev. B* 58, 2886 (1998)
- <sup>29</sup> M. D umling, A. Erb, E. Walker, J.-Y. Genoud, and R. Fl kiger, *Physica C* 257, 371 (1996)
- <sup>30</sup> A. Erb, J. Y. Genoud, F. Marti, M. D umling, E. Walker, and R. Fl kiger, *J. of Low Temp. Phys.* 105, 1023 (1996)
- <sup>31</sup> A. Erb, A. A. Manuel, M. Dhalle, F. Marti, J.-Y. Genoud, B. Revaz, A. Junod, D. Vasumathi, S. Ishibashi, A. Shukla, E. Walker, O. Fisher, and R. Fl kiger, *cond-mat/9805222* (submitted to *Phys. Rev. Lett.*)
- <sup>32</sup> K. Deligiannis, P. A. J. de Groot, M. Oussena, S. Pinfold, R. Langan, R. Gagnon, and L. Taillefer, *Phys. Rev. Lett.* 79, 2121 (1997)
- <sup>33</sup> S. Kokkaliaris, P. A. J. de Groot, S. N. Gordeev, A. A. Zhukov, R. Gagnon, and L. Taillefer, *Phys. Rev. Lett.* 82, 5116 (1999)

- <sup>34</sup> S. Kokkaliaris, A. A. Zhukov, P. A. J. de Groot, R. Gagnon, L. Taillefer, and T. Wolf, *Phys. Rev. B* 61, 3655 (2000)
- <sup>35</sup> S. Kokkaliaris, S. N. Gordeev, P. A. J. de Groot, R. Gagnon, L. Taillefer, P. F. Henry, and M. T. Weller, *Physica C* 320, 161 (1999)
- <sup>36</sup> C. Changkang, A. J. S. Chowdhury, H. Yongle, M. Spears, J. W. Hodby, and B. M. Wanklyn, *Supercond. Sci. Technol.* 7, 795 (1994)
- <sup>37</sup> A. Erb, E. Walker, J.-Y. Genoud, and R. Flükiger, *Physica C* 282-287, 89 (1997)
- <sup>38</sup> D. J. L. Hong and D. M. Smyth, *J. Am. Ceram. Soc.* 74, 1751 (1991)
- <sup>39</sup> M. Oussena, P. A. J. de Groot, K. Deligiannis, A. V. Volkozub, R. Gagnon, and L. Taillefer, *Phys. Rev. Lett.* 76, 2559 (1996)
- <sup>40</sup> A. A. Zhukov, G. K. Perkins, J. V. Thomas, A. D. Caplin, H. Küpfer, and T. Wolf, *Phys. Rev. B* 56, 3481 (1997)
- <sup>41</sup> R. M. Langan, S. N. Gordeev, P. A. J. de Groot, R. Gagnon, and L. Taillefer, *Phys. Rev. B* 58, 14548 (1998)
- <sup>42</sup> G. Blatter, D. B. Geshkenbein, and A. I. Larkin, *Phys. Rev. Lett.* 68, 875 (1992); Z. Hao and J. R. Clem, *Phys. Rev. B* 46, 5853 (1992)
- <sup>43</sup> The lower purity of this sample is directly reflected upon the critical current. For instance, at  $T = 70$  K, the critical current density at the peak for DT6 is more than two and a half times higher than the one corresponding to DT1B.
- <sup>44</sup> J. G. Ossandon, J. R. Thompson, D. K. Christen, B. C. Sales, H. R. Kerchner, J. O. Thompson, Y. R. Sun, K. W. Lay, and J. E. Tkaczyk, *Phys. Rev. B* 45, 12534 (1992)
- <sup>45</sup> S. Kokkaliaris, K. Deligiannis, P. A. J. de Groot, R. Gagnon and L. Taillefer, *Proceedings of CMD17-JMC6*, Grenoble, France, 1998; S. N. Gordeev, R. M. Langan, K. Deligiannis, D. Bracanovic, A. P. Rassau, S. Kokkaliaris, P. A. J. de Groot, R. Gagnon and L. Taillefer, *Bulletin of the American Physical Society*, Vol. 43, No. 1, 584 (1998)
- <sup>46</sup> T. Nishizaki, T. Naito, and N. Kobayashi, *Phys. Rev. B* 58, 11169 (1998)
- <sup>47</sup> R. M. Langan, S. N. Gordeev, M. Oussena, P. A. J. de Groot, A. G. M. Jansen, R. Gagnon, and L. Taillefer, *Physica C* 313, 294 (1999)
- <sup>48</sup> S. N. Gordeev, (unpublished)
- <sup>49</sup> H. Safar, P. L. Gammel, D. A. Huse, G. B. Alers, D. J. Bishop, W. C. Lee, J. Giapintzakis, and D. M. Ginsberg, *Phys. Rev. B* 52, 6211 (1995)
- <sup>50</sup> R. M. Langan, Ph.D. thesis (University of Southampton, 1999)

- <sup>51</sup> D. S. Fisher, M. P. A. Fisher, and D. A. Huse, *Phys. Rev. B* 43, 130 (1991)
- <sup>52</sup> R. L. Peterson, *J. Appl. Phys.* 67, 6930 (1990)
- <sup>53</sup> S. N. Gordeev, W. Jahn, A. A. Zhukov, H. K upfer, and T. Wolf, *Phys. Rev. B* 49, 15420 (1994)
- <sup>54</sup> S. Kokkaliaris, A. A. Zhukov, S. N. Gordeev, P. A. J. de Groot, R. Gagnon, and L. Taillefer, *J. Low Temp. Phys.* to be published; S. Kokkaliaris, A. A. Zhukov, P. A. J. de Groot, R. Gagnon, L. Taillefer, and T. Wolf, *Physica C* to be published.
- <sup>55</sup> A. A. Zhukov, S. Kokkaliaris, P. A. J. de Groot, M. J. Higgins, S. Bhattacharya, R. Gagnon, and L. Taillefer, *Phys. Rev. B* 61, R886 (2000)
- <sup>56</sup> E. J. Brandt, J. R. Clem, and D. G. Walmsley, *J. Low Temp. Phys.* 37, 43 (1979)
- <sup>57</sup> D. R. Nelson and H. S. Seung, *Phys. Rev. B* 39, 9153 (1989)
- <sup>58</sup> T. Hwa, P. Le Doussal, D. R. Nelson, and V. M. Vinokur, *Phys. Rev. Lett.* 71, 3545 (1993)
- <sup>59</sup> G. Blatter, M. V. Feigel'man, V. B. Geshkenbein, A. I. Larkin, and V. M. Vinokur, *Rev. Mod. Phys.* 66, 1125 (1994)
- <sup>60</sup> Y. Abulafia, A. Shaulov, Y. Wolfus, R. Prozorov, L. Burlachkov, Y. Yeshurun, D. Majer, E. Zeldov, H. W uhl, V. B. Geshkenbein, and V. M. Vinokur, *Phys. Rev. Lett.* 77, 1596 (1996)
- <sup>61</sup> A. van Otterlo, R. T. Scalettar, G. T. Zim anyi, R. Olsson, A. Petrean, W. K. Kwok, and V. M. Vinokur, preprint (submitted to *Phys. Rev. Lett.*)
- <sup>62</sup> Note that we consider a Gaussian distribution only for the sake of simplicity. As becomes clear from the following discussion our approach is not qualitatively affected by the exact form of the function describing the distribution of the pinning energies.
- <sup>63</sup> E. H. Brandt, *Physica C* 195, 1 (1992)
- <sup>64</sup> S. J. Rothman, J. L. Routbort, and J. E. Baker, *Phys. Rev. B* 40, 8852 (1989); 44, 2326 (1991)
- <sup>65</sup> A. P. Mozhaev, S. V. Chernyaev, T. I. Udal'tsova, and N. M. Kotov, *Russ. J. Inorg. Chem.* 37, 1111 (1992)
- <sup>66</sup> The oxygen diffusion distance,  $d_{\text{diff}}$ , is usually estimated using the formula:<sup>29</sup>  
 $d_{\text{diff}} \approx \sqrt{6D(T)t}$ , with  $D(T)$  the oxygen diffusion coefficient and  $t$  the annealing time. To illustrate the difference between the high and low pressure annealing treatments, we consider the special case of e.g.  $7-\delta \approx 6.95$ . Based on the  $D(T)$  values estimated in Ref.

65, a 72 hour treatment with the former procedure [ $P(O_2) = 100$  bar,  $T_{\text{anneal}} \approx 650$  °C] results in  $d_{\text{diff}} \approx 1.5$  mm. Therefore, a quite homogeneous oxygenation of a typical single crystal with size of  $\sim 1$  mm is achieved. On the other hand, to obtain the same diffusion distance with the low pressure treatment [ $P(O_2) = 1$  bar,  $T_{\text{anneal}} \approx 485$  °C], an annealing period of almost thirty times longer (i.e.  $\sim 90$  days) is required. Hence, for the experimentally feasible annealing time of 1-2 weeks, samples annealed in low pressure of oxygen will be less homogeneously oxygenated.

<sup>67</sup> S. Kokkaliaris, K. Deligiannis, M. Oussena, A. A. Zhukov, P. A. J. de Groot, R. Gagnon, and L. Taillefer, *Supercond. Sci. Technol.* 12, 690 (1999)

<sup>68</sup> S. J. Rothman, J. L. Routbort, and J. E. Baker, *Phys. Rev. B* 40, 8852 (1989)

<sup>69</sup> B. W. Veal, H. You, A. P. Paulikas, H. Shi, Y. Fang, and J. W. Downey, *Phys. Rev. B* 42, 4770 (1990)

---

# Chapter 7

---

## Commensurability effects induced by the layered structure of $\text{YBa}_2\text{Cu}_3\text{O}_{7-\delta}$

### 7.1 Vortices in layered superconductors

#### 7.1.1 Theoretical approach

The high- $T_c$  cuprates are layered compounds consisting of stacks of weakly coupled superconducting  $\text{CuO}_2$  planes, separated by buffer layers that serve as charge reservoirs. The layered arrangement confers on them a large electronic anisotropy and affects directly the structure and pinning of the vortex lattice.<sup>1</sup> In general, the anisotropy is accounted by introducing an electronic mass anisotropy constant, defined as  $\gamma \equiv (m_c/m_{ab})^{1/2}$ , with  $m_c$  and  $m_{ab}$  the effective masses across and along the layers respectively (for simplicity we ignore for the moment the possibility of an in-plane anisotropy).

In the case that the anisotropy of the layered system is not too large, for the description of the physical properties of the superconductor one can apply the approach provided by the three-dimensional anisotropic Ginzburg-Landau (GL) or London theories (see Chapter 1). In both models the superconductor is regarded as anisotropic but uniform.<sup>2-6</sup> The GL formulation describes variations in the superconducting order parameter,  $\Psi(\mathbf{r}) = |\Psi(\mathbf{r})|\exp[i\varphi(\mathbf{r})]$ , and gives the free energy of the superconductor in the form:<sup>2,7</sup>

$$F = \int d^3r \left[ \alpha(T) |\Psi|^2 + \frac{1}{2} \beta(T) |\Psi|^4 + \frac{\hbar^2}{4m_{ab}} \left| (i\nabla_{//} + \frac{2e}{\hbar} \mathbf{A}_{//}) \Psi \right|^2 + \frac{\hbar^2}{4m_c} \left| (i\nabla_z + \frac{2e}{\hbar} A_z) \Psi \right|^2 \right] + \int d^3r \frac{B^2}{2\mu_0} \quad (7.1)$$

where  $\alpha(T)$  and  $\beta(T)$  are temperature dependent parameters,  $\mathbf{A}$  the vector potential ( $\mathbf{B} = \text{curl } \mathbf{A}$ ) with components  $A_{//} = (A_x, A_y, 0)$  and  $A_z$ , parallel and perpendicular to the layers respectively (in the following  $(x, y)$  and  $z$  will denote the coordinates in the layers and along the  $c$ -axis respectively). The London model is obtained by assuming a nearly constant order parameter ( $|\Psi| = \Psi_0$ ) at length scales much larger than the coherence lengths, an approximation appropriate for fields far from the upper critical field (note that another requirement for the applicability of this approach is  $\kappa \gg 1$ , so that the core contribution can be ignored). In this case the free energy can be related to experimentally measurable quantities, namely:<sup>3, 7</sup>

$$F = -\frac{B_c^2}{2\mu_0} + \frac{1}{2\mu_0} \int d^3r \left[ B^2 + \lambda_{ab}^2 |(\text{curl } \mathbf{B})_{//}|^2 + \lambda_c^2 |(\text{curl } \mathbf{B})_z|^2 \right], \quad (7.2)$$

with  $B_c$  the thermodynamical critical field and  $\lambda_{ab}, \lambda_c$  the penetration depths for currents flowing parallel and normal to the planes respectively.

On the other hand, for very large anisotropies the discreteness of the layered structure becomes relevant and the above models fail to completely capture the physics of the system. Under such conditions, the Lawrence-Doniach (LD) model,<sup>8</sup> or its generalizations<sup>9</sup> are more appropriate, since they provide with a more realistic description of the superconductor in terms of alternating insulator and superconducting layers that are weakly coupled together by Josephson tunnelling. The LD model assumes a two dimensional order parameter that is zero between the superconducting layers and equal to  $\Psi_n(x,y)$  on the  $n$ th layer. In this way, in order to account for both the fact that the order parameter does not vary smoothly in the  $c$ -axis direction and the Josephson coupling between the layers, eq. (7.1) is replaced by the LD free energy functional:<sup>7, 8</sup>

$$\begin{aligned}
 F = d \cdot \sum_n \int d^2r \left[ \alpha(T) |\Psi_n|^2 + \frac{1}{2} \beta(T) |\Psi_n|^4 + \frac{\hbar^2}{4m_{ab}} \left| (i\nabla_{\parallel} + \frac{2e}{\hbar} A_{\parallel}) \Psi_n \right|^2 \right. \\
 \left. + f_J \left| \Psi_{n+1} - \Psi_n \exp\left( \frac{2ie}{\hbar} \int_{nd}^{(n+1)d} dz A_z \right) \right|^2 \right] + \int d^2r dz \frac{B^2}{2\mu_0}.
 \end{aligned} \tag{7.3}$$

The parameter  $f_J$  characterizes the weak Josephson coupling between the layers and can be expressed in terms of an effective mass  $m_c$ , as  $f_J = \hbar^2/4m_c d^2$ , with  $d$  the interlayer distance. Although in simple cases  $m_c$  can be derived from microscopic parameters,<sup>4</sup> in real systems, that usually possess a complicated electronic structure, this is not trivial and  $m_c$  must be regarded as a phenomenological parameter.<sup>7</sup> Also note that the LD model matches the GL model at high enough temperatures, where the layered structure becomes inessential.<sup>1</sup>

The range of applicability of the *continuous* and *discrete* descriptions is usually determined by the dimensionless parameter  $r = 2\xi_c^2(0)/d^2$ , with  $\xi_c$  the coherence length along the  $c$ -axis at  $T = 0$  K. For  $r \gg 1$ , i.e., coherence lengths  $\xi_c(0) \gg d$ , the *continuous* three-dimensional approach is always valid. However, in the opposite limit of  $r \ll 1$ ,  $\xi_c(0) \ll d$  and the system behaves in a quasi-two-dimensional manner; hence the LD model should be used.<sup>1, 10</sup> If  $r < 1$ , then supposing a GL variation of  $\xi_c$ , the crossover between three- and two-dimensional behaviour takes place at a characteristic temperature  $T_{cr} = (1-r)T_c$ , which is defined by the condition  $\xi_c(T_{cr}) = d/\sqrt{2}$ .<sup>1, 8</sup> For parameters appropriate for  $YBa_2Cu_3O_{7-\delta}$ , one finds that  $T_{cr}$  is of the order of 80 K.<sup>11</sup>

Compared to an uniform anisotropic superconductor, in a strongly layered superconductor the structure of both the individual vortices and the vortex lattice can be modified significantly. In particular, in the latter the vortex lines generally differ from the usual Abrikosov vortices in the sense that they are not uniform objects. Instead, they are composed of two-dimensional vortices (usually called ‘‘pancake’’ vortices), which are situated in the superconducting planes.<sup>12</sup> The pancakes have a normal core, are directed along the  $c$ -axis and are connected by Josephson vortices (see below) that thread through the junctions between the superconducting layers.<sup>12</sup> This unusual vortex structure leads to new physical effects that are absent in an uniform three dimensional superconductor, such as the disintegration of a vortex line into independent pancakes,<sup>13</sup> the lock-in

transition,<sup>10, 14, 15</sup> and the transition from a tilted to a combined vortex lattice, consisting of two crossing lattices of Josephson and Abrikosov vortices.<sup>16</sup>

## 7.1.2 Josephson vortices

The LD model predicts that a magnetic field applied parallel to the ab-plane, penetrates a layered superconductor in the form of the so-called “Josephson vortices”. A Josephson vortex (JV) differs from the Abrikosov one mainly in the structure of its core. In a JV the usual normal core of dimensions  $\xi_c$  and  $\xi_{ab}$  is absent and it is replaced by a “Josephson” or “phase” core of dimensions  $d$  and  $\lambda_J = \gamma d$  along the c-axis and the ab-plane respectively.<sup>4, 17-19</sup> The phase core does not correspond to a region of a strongly depressed order parameter. Instead, it is the region where the phase of the order parameter changes rapidly and in which the magnitude of the Josephson current varies from zero to its maximum value. For instance, the suppression of the order parameter caused by a JV placed between two superconducting layers, on them, is estimated to be of the order of  $(\xi_{ab}/\lambda_J)^2$ .<sup>12</sup> It is mentioned that the absence of a normal core in the JVs is due to the fact that the screening currents are cutoff by the Josephson-coupling current density between the layers. In contrast, in an Abrikosov vortex such a cutoff is absent and the screening currents flowing in distances less than  $\xi_{ab}$  attain high values of the order of the depairing current, resulting in a complete suppression of the order parameter.<sup>12</sup>

On the other hand, the region outside the phase core is roughly equivalent to the corresponding regime in the Abrikosov vortices, with screening currents extending to distances  $\lambda_{ab}$  and  $\gamma\lambda_{ab}$  along the c-axis and ab-plane respectively.<sup>4, 17-19</sup> Some differences in this region are mainly restricted to the current flow and magnetic field patterns due to the presence of the layered structure.<sup>17</sup> Clem et al.<sup>20</sup> have calculated the line energy of a JV and found it to be equal to:

$$\varepsilon_J = \frac{\varepsilon_0}{\gamma} \left( \ln \frac{\lambda_{ab}}{d} + 1.12 \right) \quad (7.4)$$

with  $\varepsilon_0 = \left( \frac{\Phi_0^2}{4\pi\mu_0\lambda_{ab}^2} \right)$ . Eq. (7.4) can be compared to the standard expression giving the line energy of an Abrikosov vortex:<sup>5,21</sup>

$$\varepsilon_A = \frac{\varepsilon_0}{\gamma} \left( \ln \frac{\lambda_{ab}}{\xi_c} + 0.50 \right). \quad (7.5)$$

As can be seen, the main difference between the two results is that the coherence length in the logarithm of eq. (7.5) has been replaced in eq. (7.4) by the interlayer distance, yielding a slightly different temperature dependence.<sup>20</sup> Nevertheless, the energy values obtained by both expressions are very close (see Fig. 3 of Ref. 20), demonstrating the similar behaviour of the Josephson and Abrikosov vortex lines at distances far from the core region. Indeed, as has been pointed out by several workers, at these length scales the continuous and LD descriptions are equivalent.<sup>10, 12, 22-24</sup>

Another important consequence of the discrete structure is the “intrinsic pinning” of vortices due to the superconducting layers acting as natural extended pinning centres.<sup>25</sup> A force exerted on the vortices perpendicular to the layers (e.g. by a current flowing parallel to the planes) will be opposed by a strong pinning force. The latter originates from the modulation of the order parameter perpendicular to the planes that results in maximum loss of superconducting cohesive energy when the vortices try to move across them.<sup>25</sup> The intrinsic pinning energy is rather high, and can be as large as one tenth of the total vortex energy thus providing with strong pinning along the full length of a vortex line.<sup>7</sup> On the other hand, vortices can move easily parallel to the layers thus resulting in small critical current densities in the transverse direction.<sup>12, 26</sup>

### 7.1.3 The lock-in transition

In an uniform three-dimensional anisotropic superconductor, vortices cannot run along a certain crystallographic direction unless the field is applied in this direction. However, such a behaviour is not always true for layered superconductors. Indeed, for this case it has been demonstrated that when the applied field,  $B_a$ , makes an angle  $\vartheta_a$  with the ab-plane that is smaller than a critical value  $\vartheta_{cr}$ , it is energetically more favourable for

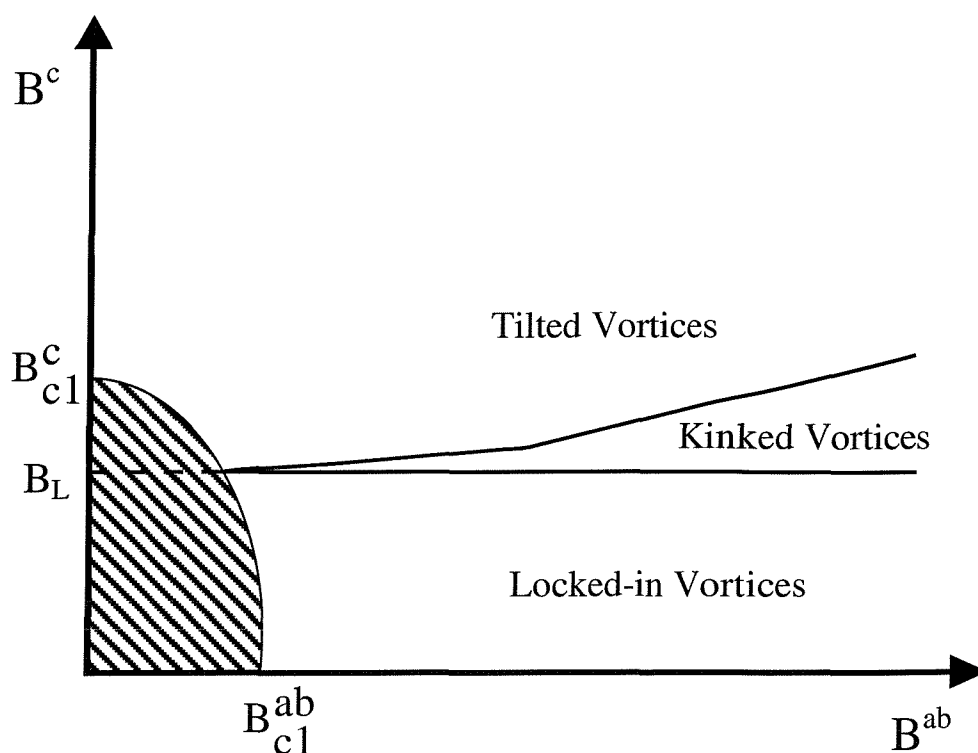


Fig. 7.1. Diagram showing the region of the vortex lock-in state in the plane defined by the components  $B^{ab}$  and  $B^c$  of the applied field parallel and perpendicular to the  $ab$ -plane respectively.<sup>7</sup> The regimes corresponding to the other two possible vortex configurations discussed in the text are also indicated. The dashed region corresponds to the Meissner state, whereas the field  $B_L$  is defined in the text. Note that this diagram is appropriate for the quasi-two-dimensional regime and is not drawn to scale.

the flux lines to “lock-in” and run strictly parallel to the planes.<sup>10, 14, 15</sup> This is the so-called lock-in transition that corresponds to a second order phase transition, with the angle  $\vartheta$  of the vortices with respect to the  $ab$ -plane going continuously from  $\vartheta = 0$  for  $\vartheta_a < \vartheta_{cr}$ , to finite values  $\vartheta = \vartheta_a - \vartheta_{cr}$  for  $\vartheta_a > \vartheta_{cr}$ .<sup>10, 12</sup> In the locked-in state the perpendicular component of the magnetic induction is zero, and the macroscopic tilt modulus  $[c_{44} \propto \left( \frac{\partial B_{\perp}}{\partial B_{a\perp}} \right)^{-1}]$  infinite.<sup>12, 14, 27</sup> This ideal transverse shielding state of the vortex system

is destroyed only when the component of the applied field along the  $c$ -axis exceeds a characteristic threshold value  $B_L$  that is found to be of the order of the lower critical

field,  $B_{cl}^c$ , along the c-axis (see Fig. 7.1).<sup>7, 24</sup> It is noted that the lock-in phenomenon is not peculiar to the present situation. Similar effects can also occur when vortices interact with other extended defects, such as twin boundaries and columns.<sup>12, 28</sup>

In the absence of demagnetization effects, the lock-in angle is found to decrease with the field according to the relation:<sup>12</sup>

$$\vartheta_{cr} \approx \frac{B_{cl}^c}{B_a} \frac{\ln\left(\frac{\eta\lambda_J}{\xi_{ab}}\right)}{\ln\left(\frac{\lambda_{ab}}{\xi_{ab}}\right)}, \quad (7.6)$$

with  $\eta$  a constant of order unity. Nevertheless, in the more realistic situation where demagnetization effects are present, the directions of  $B_a$  and the internal field  $B_{in}$  do not coincide. In this case eq. (7.6), with  $B_{in}$  substituted for  $B_a$ , gives the lock-in angle,  $\vartheta_{incr}$ , corresponding to the internal field. For a sample in the form of a rotational ellipsoid with demagnetization factors  $v_a = v_b = v \ll 1$  and  $v_c = 1-2v$ ,  $\vartheta_{cr}$  is estimated to be equal to:<sup>12</sup>

$$\vartheta_{cr} \approx (1-v_c) \frac{B_{cl}^c}{B_a} \frac{\ln\left(\frac{\eta\lambda_J}{\xi_{ab}}\right)}{\ln\left(\frac{\lambda_{ab}}{\xi_{ab}}\right)}. \quad (7.7)$$

Eq. (7.7) shows clearly that the lock-in angle is quite sensitive to demagnetizing fields, making the experimental observation of the lock-in transition difficult even at low fields.

For typical  $YBa_2Cu_3O_{7-\delta}$  single crystals ( $v \sim 0.1$ ) and  $\frac{B_{cl}^c}{B_a} \sim 0.1$ , the estimated lock-in angles are of the order  $0.1^\circ$ - $1^\circ$ , in agreement with experimental observations.<sup>29</sup>

Experimentally, there have been several reports indicating the presence of the lock-in transition. By performing torque magnetometry studies on  $YBa_2Cu_3O_{7-\delta}$  single crystals, Farrell et al.<sup>11</sup> demonstrated that the three dimensional theory fails to describe the data for fields close to the  $CuO_2$  planes and temperatures below 80 K, which was attributed to a crossover to quasi-two-dimensional behaviour. Subsequently, it was shown theoretically that this torque anomaly could be accounted by the LD model and be considered as a

fingerprint of the lock-in transition.<sup>10</sup> In the same sense, torque studies of BSCCO and  $(La_{1-x}Sr_x)_2CuO_4$  single crystals have shown a torque increasing linearly with the perpendicular component of the internal field (up to values  $\sim B_{c1}^c$ ), supporting the notion of a transverse Meissner effect at low fields.<sup>30, 31</sup> A similar result has also been obtained by means of magnetization measurements, where the magnetic induction was found to be directed nearly parallel to the ab-plane for fields applied in a certain angular range away from this direction.<sup>32</sup> The observation of the locked-in state has also been conjectured with SQUID magnetometry studies.<sup>33</sup> Additional experimental support has been provided by Kwok et al.,<sup>34</sup> who have studied the angular dependence of the resistivity at temperatures above 88 K. For field directions close to the ab-plane and the Lorentz force nearly perpendicular to the  $CuO_2$  planes, they observed a sharp drop in the resistivity in an angular region of  $\sim 0.5^\circ$ . This drop was attributed to the onset of intrinsic pinning due to the lock-in transition of the vortex lines.<sup>34</sup> However, the most unambiguous observation of the lock-in transition has been given in Ref. 35. In this work, complications arising from thermal fluctuations, surface barriers, electrodynamic and sample shape effects were overcome by studying at low fields and temperatures a  $La_{1.9}Sr_{0.1}CuO_4$  single crystal cut in the form of a disk, with the c-axis along the disk plane. Using a vector magnetometer with high angular resolution, it was illustrated that for applied fields within a threshold angle, the remanent moment was strictly parallel to the ab-plane and the magnetization component along the c-axis reversible.<sup>35</sup> Moreover, the threshold angle was found to scale with temperature in the same manner as  $B_{c1}^c$ , thus providing with indisputable evidence for the presence of a vortex lock-in transition.<sup>35</sup>

The structure of the vortex lines beyond the locked-in state depends on the angle  $\vartheta$ . Three different angular regimes exist.<sup>7, 12, 24</sup> When  $\tan\vartheta < 1/\gamma$  a kinked vortex structure is realized with pancake vortices in the planes being connected with strings of JVs as shown in Fig. 7.2 (a) (see also Fig. 7.1). In the range  $1/\gamma < \tan\vartheta < d/\xi_{ab}$ , the two dimensional vortex cores are displaced by more than their width. This is the region where with decreasing  $\vartheta$  the kinked structure starts to develop and the screening currents shift from predominantly planar to Josephson. Finally, in the large angle regime,  $\tan\vartheta > d/\xi_{ab}$  the normal cores of the pancakes overlap, generating tilted vortex lines (see Figs. 7.1 and 7.2 (b)). In this situation, the physics of the system is well described by the GL and, provided that  $B \ll B_{c2}$ ,  $\kappa \gg 1$ , London models.

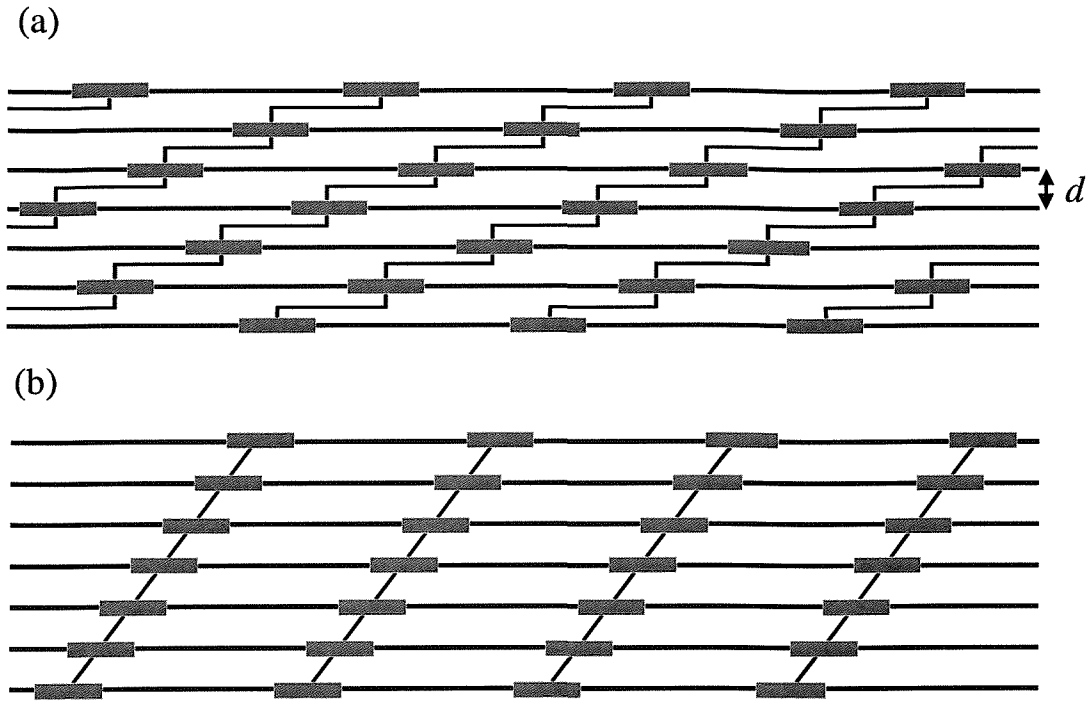


Fig. 7.2. Different vortex line configurations for tilted magnetic fields in the quasi-two-dimensional regime and for (a)  $\vartheta < \arctan(1/\gamma)$  (kinked vortices) and (b)  $\vartheta > \arctan(d/\xi_{ab})$  (tilted vortices).

The above results have been deduced for the quasi-two-dimensional regime ( $\xi_c(T_{cr}) < d/\sqrt{2}$ ). However, some reminiscent features of two-dimensionality can be present even in the temperature region where  $\xi_c(T_{cr}) > d/\sqrt{2}$ . In this case, for fields along the  $ab$ -plane, the vortex core consists of the usual anisotropic normal core extending to distances  $\xi_c > d$  and  $\xi_{ab} > \lambda_J$ , but also of a phase core of dimensions  $d$  and  $\lambda_J$  located in the central part of this region.<sup>7, 24</sup> Due to the presence of the phase core, some locations in the direction along the  $c$ -axis become more favourable than others. Indeed, it can be shown that the stable position of an individual vortex is the one with the phase core situated between the layers.<sup>7, 24</sup> The peculiar structure of this vortex core has also led to the prediction that the lock-in transition can persist even above  $T_{cr}$ .<sup>7, 24</sup> Moreover, for a vortex lattice slightly tilted from the layer direction a kinked structure can possibly still develop.<sup>7, 24</sup>

Finally, another interesting consequence of a strongly layered structure for tilted fields, is the formation of a combined lattice, i.e., the coexistence of an Abrikosov and Josephson lattices that run parallel to the c-axis and ab-plane respectively.<sup>16, 36</sup> With increasing  $\vartheta_a$  above  $\vartheta_{cr}$ , the combined lattice becomes energetically favourable for applied fields in the range  $B_{c1} < B_a < B_0 = \sqrt{3} \Phi_0 / 2\gamma d^2$ , provided that  $\lambda_J > \lambda_{ab}$ . The transition parallel – combined lattice is a second order one.<sup>12</sup> On the other hand, with further increasing angle, the crossing lattices transform into the conventional tilted lattice via a first order transition at an angle below  $\arctan(d/\xi_{ab})$ . The combined lattice is also favoured in the high field region ( $B_a > B_0$ ), for small angles ( $\tan\vartheta < 1/\gamma$ ) irrespective of the ratio  $\lambda_J/\lambda_{ab}$ .<sup>16</sup> Note that as shown recently by Koshelev,<sup>37</sup> in the case of a combined lattice, the in-plane lattice can affect the melting temperature and field of the pancake lattice in correspondence with experimental observations.<sup>38</sup>

## 7.2 Signature of Josephson vortices in pure YBa<sub>2</sub>Cu<sub>3</sub>O<sub>7-δ</sub> single crystals

### 7.2.1 Introduction

As discussed in the previous section, when a field is applied away from the ab-plane at angles smaller than the lock-in angle, JVs running parallel to the ab-direction penetrate the superconductor. The anisotropic London model predicts that vortices will form a hexagonal lattice that is compressed along the crystal c-axis and expanded in the plane direction. The ratio  $a/l$  of the lattice spacings  $a$  and  $l$  perpendicular and parallel to the c-axis respectively is predicted to be field independent and equal to  $2\gamma/\sqrt{3}$ .<sup>7, 12, 39</sup> The structure of this equilibrium lattice is shown schematically in Fig. 7.3. Since the superconducting cohesive energy is maximum in the CuO<sub>2</sub> planes, in order to minimize the energy of the system, JVs will be preferably positioned in the interlayer space.<sup>40</sup>

The equilibrium and pinning properties of the Josephson vortex lattice is an exciting topic that up to now has not been extensively explored theoretically and mainly experimentally. Therefore, by means of magnetization measurements, in this chapter we present a detailed experimental study of the hysteretic behaviour of the vortex system in pure detwinned YBa<sub>2</sub>Cu<sub>3</sub>O<sub>7-δ</sub> single crystals for this field configuration. We demonstrate

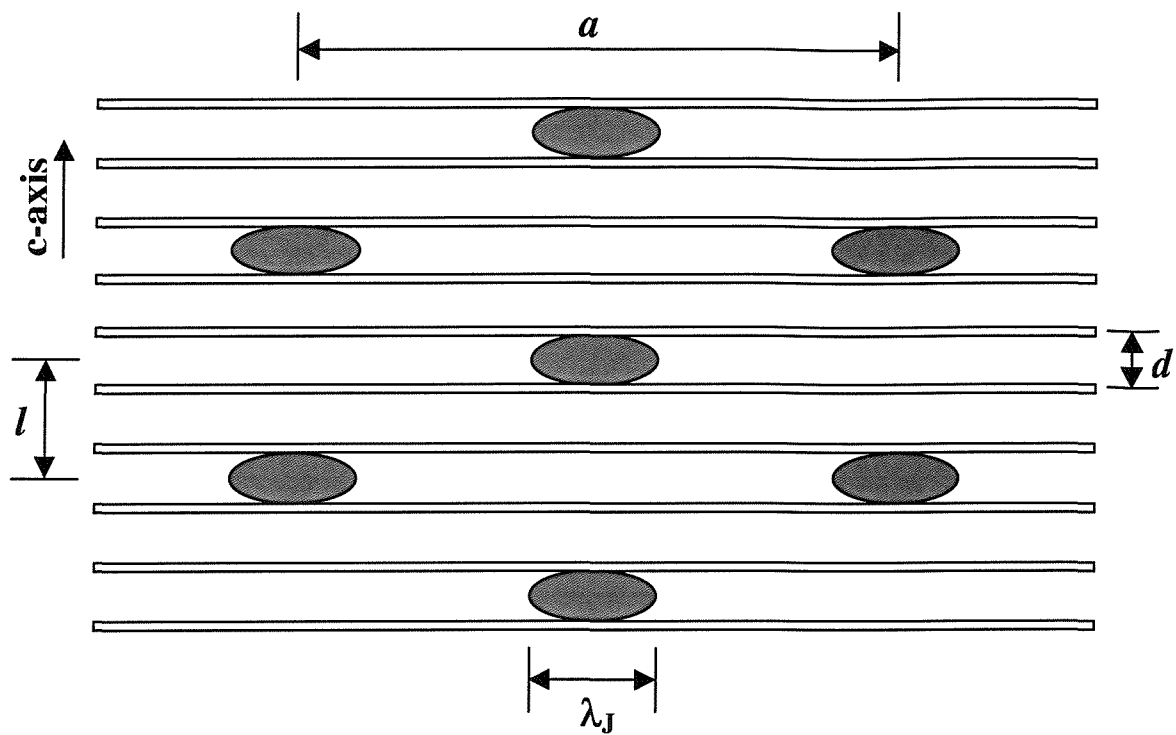


Fig. 7.3. Structure of the equilibrium Josephson vortex lattice for a magnetic field parallel to the superconducting layers. The dark areas represent the cross sections of the Josephson cores that are placed between the planes. The various lengths shown on the diagram are discussed in the text.

that for applied fields parallel to the planes the magnetic hysteresis shows an oscillatory behaviour.<sup>41, 42</sup> These oscillations, called henceforth “lock-in” or “commensurability” oscillations, are a direct consequence of intrinsic pinning of JVs and are induced by a succession of transitions between states for which the vortex lattice is commensurate with the crystal lattice periodicity along the c-axis.<sup>41, 42</sup> We give a complete analysis of the mechanism responsible for the lock-in oscillations and study the influence of variations in the oxygen stoichiometry.<sup>42, 43</sup> The interplay between intrinsic pinning, pinning by point disorder and thermal fluctuations is found to result in the suppression of the commensurability oscillations at low and high temperatures and in a bizarre non-monotonous temperature dependence of the current in the intermediate temperature range, where the oscillations are prominent. Finally, it is demonstrated that the lock-in oscillations are a useful tool for extracting intrinsic parameters of the superconductor, such as the anisotropy. We find that for a variation in the oxygen deficiency,  $\delta$ , by as

much as 300 %, the out-of-plane anisotropy,  $\gamma_{ck} \equiv (m_c/m_k)^{1/2}$  ( $k$  denotes either  $a$  or  $b$ ) decreases but only slightly ( $\sim 14$  %) with increasing oxygen content.<sup>43</sup> Comparison of these results with the ones obtained using torque magnetometry and transport studies on similar crystals points out the possibility of a temperature dependent anisotropy.

## 7.2.2 Experimental details

### A. Samples

Three detwinned YBa<sub>2</sub>Cu<sub>3</sub>O<sub>7-δ</sub> single crystals from the same batch have been studied. They were grown at McGill University by a conventional self-flux method using yttria-stabilised zirconia crucibles as discussed in detail in Chapter 3. The crystals, called hereafter D1, D2 and D3, were initially annealed at 500 °C for 6 days in oxygen atmosphere under a pressure of 1 bar. They were subsequently detwinned by applying a uniaxial pressure of  $\sim 50$  MPa at 550 °C in air for 15 min. After detwinning they were reoxygenated for 1 day at 500 °C in flowing O<sub>2</sub>. This treatment results in  $7-\delta = 6.934$ .<sup>44</sup> D1 and D3 were then reannealed for a further 8 days in 1 bar of oxygen at 525 °C and 450 °C respectively, which should give oxygen contents of  $7-\delta = 6.908$  and  $6.970$  respectively.<sup>44</sup> The details of the investigated samples, that had rectangular shape, are summarized in table 7.1.

Sample	$7-\delta$	$l \times w \times t$ (mm <sup>3</sup> )	T <sub>c</sub> (K)	$\Delta T_c$ (K)
D1	6.908	$1.07 \times 0.86 \times 0.08$	92.7	0.25
D2	6.934	$1.69 \times 1.08 \times 0.09$	92.8	0.10
D3	6.970	$1.29 \times 1.25 \times 0.08$	91.7	0.35

*Table 7.1. Oxygen content, dimensions, transition temperature and the width of the superconducting transition for the samples under study.*

## B. Measuring procedure

Magnetization measurements were performed using our *Oxford Instruments* vibrating sample magnetometer (model 3001) for applied fields up to 12 T, in collaboration with K. Deligiannis. The magnetization loops were measured by remagnetizing from a negative field several times the full penetration field. The sweep rate of the applied magnetic field was 5 mT/sec. For the studies of the commensurability oscillations the samples were rotated away from the magnetic field in a plane containing the c-axis and either the a- or b-axis of the crystal. The angle  $\vartheta$  of the applied field with the ab-plane could be determined with an accuracy better than  $1^\circ$ .

Torque measurements were carried out in a 4 T torque magnetometer at the University of Paris-Sud in Orsay. A capacitive method was used as described in more detail in Chapter 4. The torque was measured by rotating the magnetic field in a plane defined by either the a- or b-axis of the superconductor and the normal to the ab-plane. After each run the sample was heated to a temperature of 99 K and measured again at the same field. This signal was then subtracted from the low temperature data in order to eliminate the contribution arising from both the sampleholder and the sample above  $T_c$ .

### 7.2.3 Results and Discussion

Figure 7.4 illustrates magnetization loops for D2 at several temperatures as obtained for the usual configuration of fields applied along to the c-axis. The  $M(B)$  curves exhibit a peak in the high field region whose position,  $B_p$ , varies non-monotonously with temperature. As discussed in detail in the previous chapter, this behaviour is typical for pure  $\text{YBa}_2\text{Cu}_3\text{O}_{7-\delta}$  single crystals.<sup>45-47</sup> The characteristic shape of the  $M(B)$  curves depicted in Fig. 7.4, however, changes dramatically when the field is applied along the ab-direction. This becomes clear from Fig. 7.5 (a), where we show magnetization loops for two different runs and for magnetic fields aligned with the ab-plane (with the accuracy of our setup  $\vartheta_1, \vartheta_2 < 1^\circ$ ). As can be seen the hysteretic magnetization exhibits an oscillatory behaviour with the period of the oscillations increasing with field.<sup>41-43</sup> On the other hand, when the field is intentionally rotated away from the ab-plane by an angle  $\vartheta_3 = \vartheta_2 + 2^\circ$  the oscillations disappear (see Fig. 7.5 (b)).

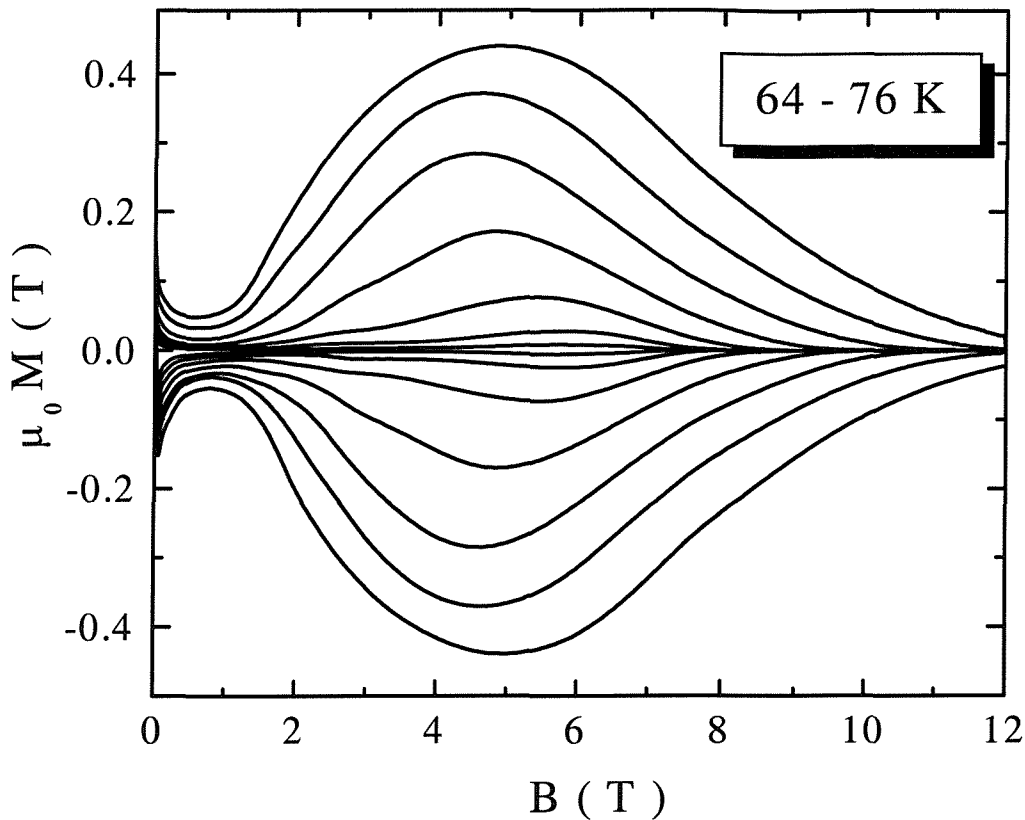


Fig. 7.4. Magnetization loops for sample D2 for fields along the  $c$ -axis and temperatures in the range 64 K - 76 K. Temperature increases with a step of 2 K from the outer to the inner curves.

An important observation from Fig. 7.5 (a), is that within an angular range of less than  $1^\circ$  the positions of the peaks and dips of the oscillations are independent of the magnetic field orientation. Moreover, as can be seen from Fig. 7.6, where we show magnetization curves at several temperatures for D2, they are also found to be temperature independent. This observation indicates that the oscillations are due to matching of the vortex lattice constant to a regular pinning structure. Therefore, taking into account the existence of a critical angle above which the oscillatory features of the hysteresis loop are suppressed, the oscillations can be explained in terms of states of the “locked-in” lattice that are commensurate with the layered structure of the superconductor.<sup>41, 42</sup> For this reason they have been named “lock-in” or “commensurability oscillations”.<sup>41, 42, 48</sup>

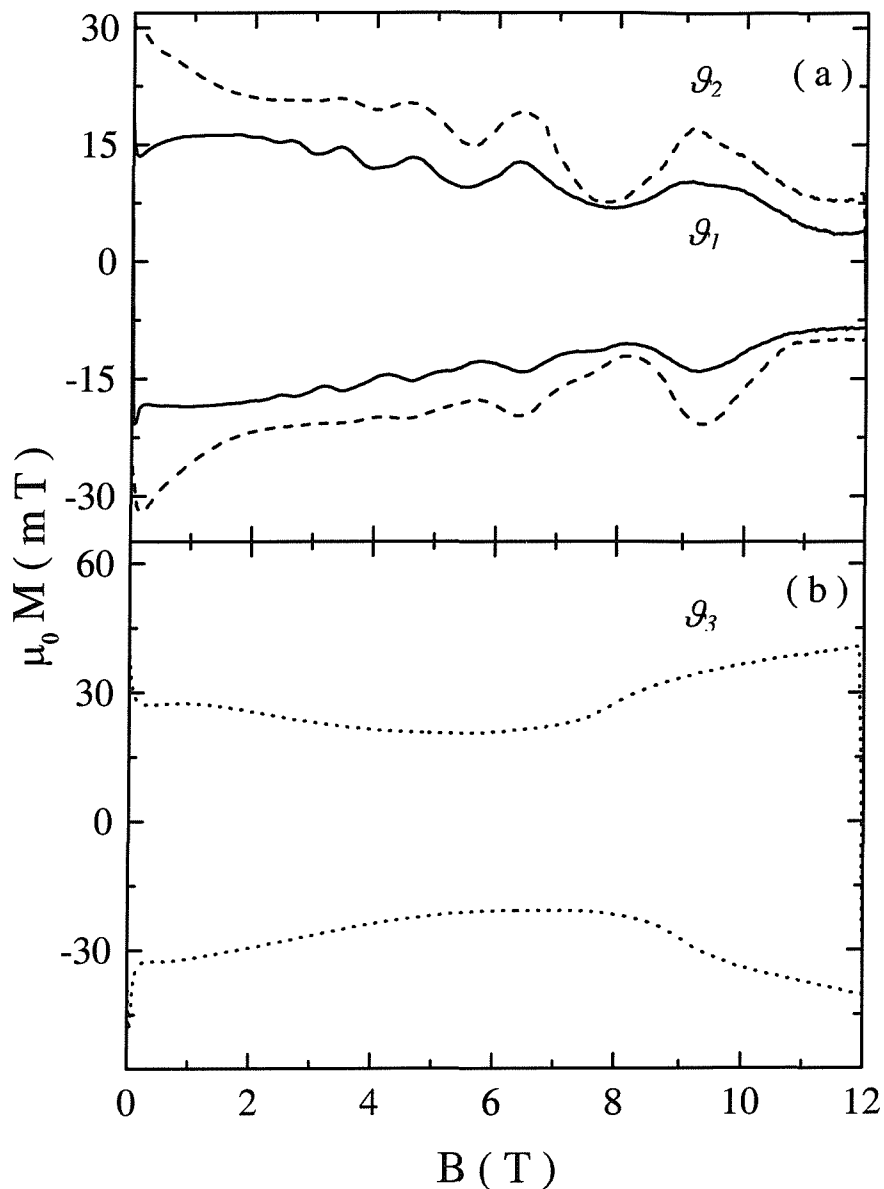


Fig. 7.5. Irreversible magnetization loops for sample D2 at 64 K. Data are shown for three different orientations  $\vartheta_1$ ,  $\vartheta_2 < 1^\circ$  (a) and  $\vartheta_3 = (\vartheta_2 + 2^\circ) \pm 0.1^\circ$  (b) of the magnetic field with respect to the  $a$ -axis.

In more detail, the mechanism producing the lock-in oscillations can be understood in the following way.<sup>42, 43</sup> As already mentioned, for fields along the  $ab$ -plane the anisotropic London model predicts a compressed hexagonal vortex lattice with longitudinal and transverse constants of ratio  $a/l = 2\gamma_{ck}/\sqrt{3}$ . This configuration corresponds to a state of minimum vortex-vortex interaction energy. This lattice will be

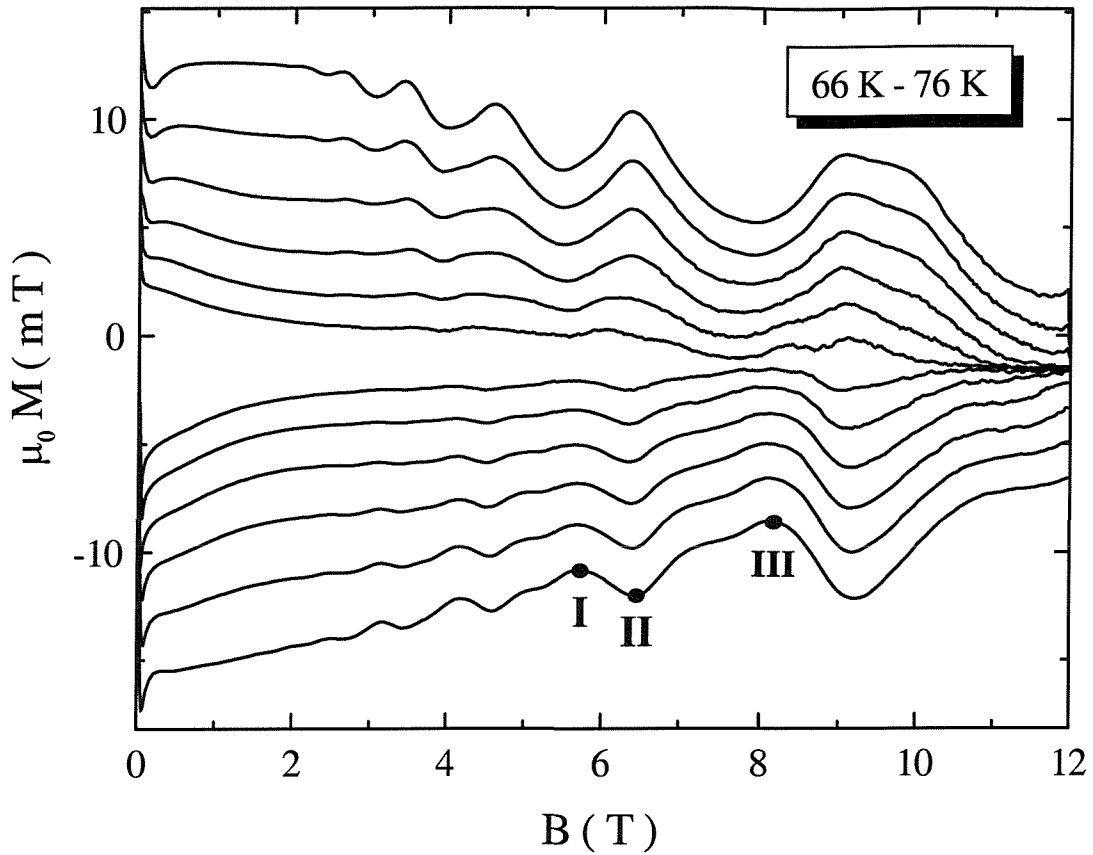


Fig. 7.6. Commensurability oscillations for crystal D2 in the temperatures range 66 K – 76 K for the case of fields along the  $a$ -axis. Temperature increases with a step of 2 K from the outer to the inner loops.

commensurate with the layered structure of the superconductor for certain field values  $B_n$  (see Fig. 7.3).<sup>49</sup> For such a commensurate state, the vortex lattice period  $l$  perpendicular to the  $ab$ -planes will be equal to an integer number  $n = 1, 2, 3, \dots$  of interlayer spacings  $d$ , i.e., at  $B = B_n$ ,  $l = nd$ .

In this situation, the magnetic hysteresis is determined by pinning of JVs by extrinsic defects. In the absence of a normal core, however, JVs cannot be pinned effectively. Indeed, as shown by Blatter et al.,<sup>12</sup> the elementary pinning force acting on a single JV, for both  $\delta T_c$  and  $\delta l$  pinning, is reduced by a factor  $\sim (\xi_{ab}/\lambda_J)^3$  as compared with the force acting on an Abrikosov vortex. Therefore, vortex motion along the  $ab$ -planes should be easy and the current density will be minimum corresponding to a magnetization

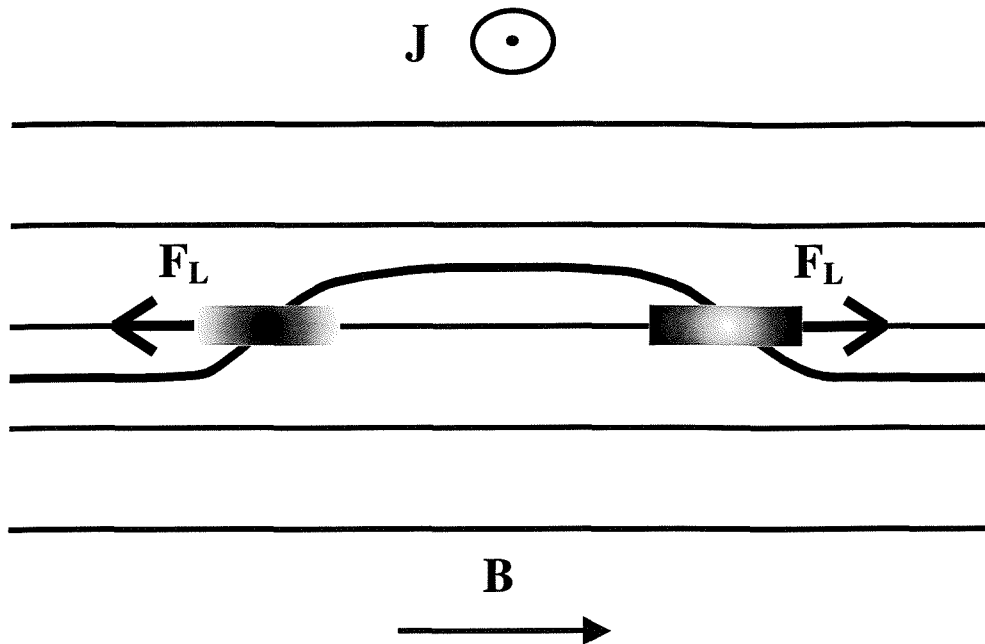


Fig. 7.7. Kink and antikink pair nucleated on a Josephson vortex line. The direction of the Lorentz force  $F_L$  exerted on the pancakes by a current  $J$  parallel to the layers and the magnetic induction  $B$  are also shown.

dip (such as points I and III in Fig. 7.6).

When the field increases above  $B_n$ , due to the presence of intrinsic pinning changes in the vortex density will be initially accommodated by accumulation of vortices in the ab-planes.<sup>22, 23</sup> Hence,  $a$  starts to decrease while  $l$  remains constant. Nevertheless, under these conditions the vortex-vortex interaction energy is enhanced significantly. As a consequence, in order to eliminate this excess energy gain vortices will eventually attempt to cross the  $\text{CuO}_2$  planes in order to bring the system to the next commensurate state at  $B_{n-1}$  that is characterized by  $l = (n-1)d$ . Nevertheless, the vortex lines do not pass rigidly from one interlayer spacing to another. Instead, vortex motion in the c-axis direction proceeds through the nucleation and motion of pairs of kinks and antikinks that for  $T < T_{cr}$  consist of pairs of two-dimensional Abrikosov vortices and antivortices as shown schematically in Fig. 7.7.<sup>7</sup> In order to minimize the compressional energy such pairs might form coherently in several layers.<sup>7</sup> However, the vortex disks in the  $\text{CuO}_2$  planes have a normal core and can be pinned strongly. As a result, pinning of vortices is enhanced and the hysteresis in this field range will increase (region between points I and

II in Fig. 7.6), finally attaining a maximum for the highest density of kinks (point II in Fig. 7.6). On the other hand, from the geometry of the problem it is obvious that once nucleated the kinks and antikinks experience a force parallel to the layers but in opposite directions (see Fig. 7.7). By moving in this way, they eventually “transfer” vortex lines to subsequent interlayer spacings, thus increasing the number of JVs that can slide easily along the ab-direction. In this way, as more and more lines are transported to neighbouring layers, the density of kinks is gradually reduced and pinning will decrease, leading to a reduction in the irreversible magnetization (region above point II in Fig. 7.6). This behaviour continues until the commensurate state at  $B_{n-1}$  is reached (point III in Fig. 7.6). With further increasing the field from this point, the same process is repeated towards the next commensurate state at  $B_{n-2}$ .

Before going further, it is stressed that this mechanism is expected to be valid for fields not too close to the characteristic field  $B_0$ , which corresponds to the commensurate state with  $n = 1$ .<sup>7, 22, 23</sup> For fields near  $B_0$  the nonlinear Josephson cores of vortices overlap strongly and the problem requires a different approach.<sup>22, 23</sup> For parameters pertinent to  $\text{YBa}_2\text{Cu}_3\text{O}_{7-\delta}$ ,  $B_0$  is estimated to be about 210 T,<sup>23</sup> and therefore, for the range of fields under consideration the description outlined above should be appropriate.

From this discussion one also anticipates that, for the present field configuration, the measured irreversible magnetization must be mainly dominated by the easier vortex motion parallel to the  $\text{CuO}_2$  planes or equivalently by currents flowing along the c-axis. As was demonstrated recently by Zhukov et al.,<sup>50</sup> this is indeed the case realized experimentally. Accordingly, using the Bean formula,<sup>51</sup> from the magnetic hysteresis widths obtained for the transverse ( $B \parallel c$ -axis) and longitudinal ( $B \perp c$ -axis) geometries, we find that for our samples, the currents corresponding to the former configuration can be as much as thirty times higher than the currents flowing parallel to the c-axis in the latter case.

In Fig. 7.8 we have plotted as a function of  $B^{-1/2}$ , the magnetization on the ascending branches of the loops depicted in Fig. 7.6. For illustration purposes the curves have been shifted along the vertical axis, which obviously does not affect the periodicity of the signal. Remarkably, we observe that the oscillations are periodic in  $B^{-1/2}$ , with a period  $\Delta B^{-1/2}$  that is found to be temperature independent. The same result is illustrated in a different way in Fig. 7.9, by the obtained linear relation between  $B^{-1/2}$  and the serial number  $n$  of the magnetization dips (i.e., the order  $n$  of the commensurate state). Similar

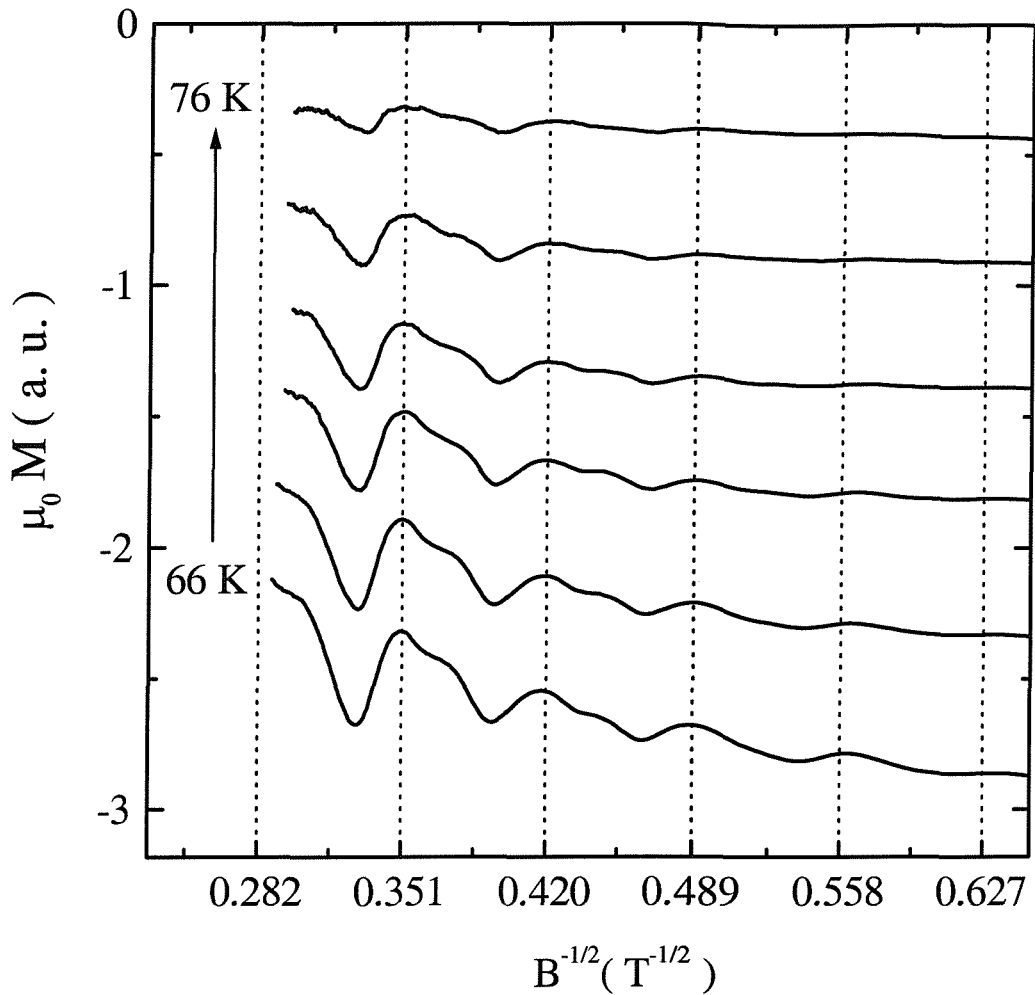


Fig. 7.8. The magnetization on the ascending branches of the curves shown in Fig. 7.6 is plotted versus  $B^{-1/2}$ . Temperature increases with a step of 2 K in the direction of the arrow. Note that for a better presentation of the results the curves have been shifted vertically.

results have been obtained and for the other samples (see Fig. 7.11 below).

The observed periodicity supports firmly our interpretation that the oscillations are due to a succession of transitions between commensurate and incommensurate states of the vortex lattice. Indeed, according to the anisotropic London model, for magnetic fields parallel to the  $ab$ -planes, at a commensurate state  $n$  the vortex spacing along the  $c$ -axis can be written as:<sup>22</sup>

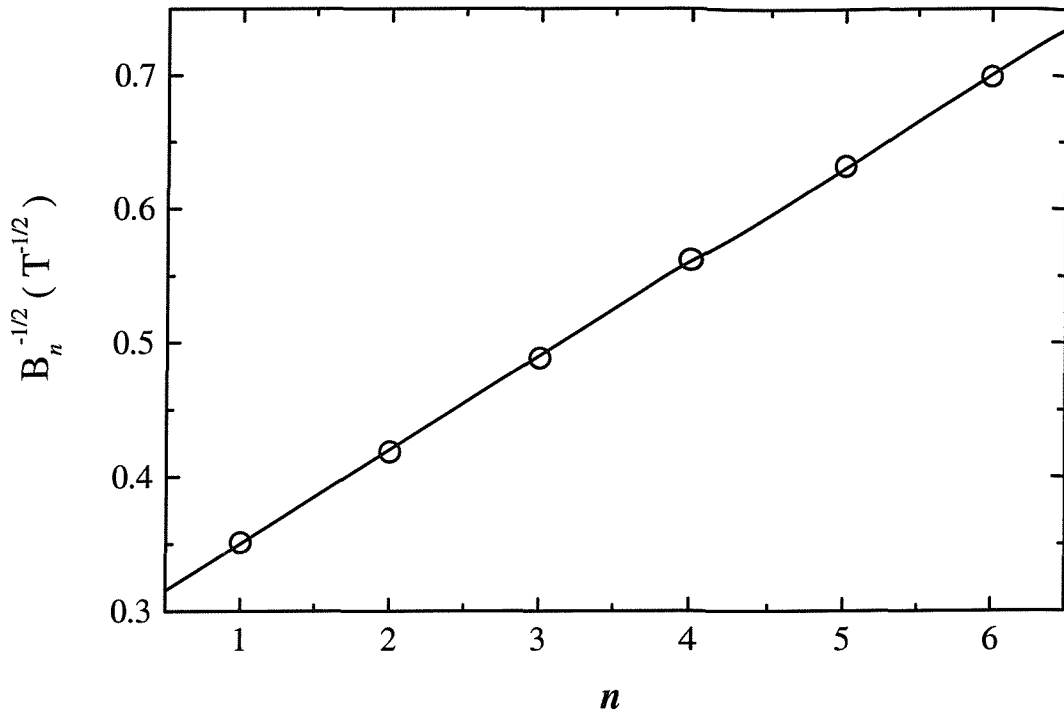


Fig. 7.9. The circles show the positions of the commensurability oscillation dips in  $B^{-1/2}$  space for sample D2 at 66 K plotted versus the serial number of the dip. The solid line is a linear fit of the data.

$$l = \left( \frac{\sqrt{3}\Phi_0}{2\gamma_{ck}} \right)^{1/2} B_n^{-1/2}. \quad (7.8)$$

Since between successive commensurate states  $l$  changes always by a constant value  $d$ , eq. (7.8) points out that with varying field, every feature pertinent to the commensurate state, such as the dips in the magnetic hysteresis, should be periodic in the  $B^{-1/2}$  space in agreement with our results. From eq. (7.8) one can show straightforwardly that the oscillation period,  $\Delta(B^{-1/2})$ , will be equal to:

$$\Delta(B^{-1/2}) = d \left( \frac{2\gamma_{ck}}{\sqrt{3}\Phi_0} \right)^{1/2} = \left( \frac{1}{B_0} \right)^{1/2}. \quad (7.9)$$

From this relation and the experimental result  $\Delta(B^{-1/2}) \approx 0.069$  (see Fig. 7.8), we find that for D2,  $B_0 \approx 210$  T in accordance with independent estimations.<sup>23</sup>

Finally, the validity of our interpretation concerning the origin of the commensurability oscillations is additionally confirmed by the following estimations. Considering that in the commensurate state corresponding to the field  $B_n$ ,  $l = nd$ , and that  $B_0 = \sqrt{3} \Phi_0 / 2\gamma_{ck} d^2$ , from eq. (7.8) one can obtain the commensurability condition:

$$\left( \frac{B_0}{B_n} \right)^{1/2} = n. \quad (7.10)$$

Therefore, if the dips in the magnetization curves corresponded indeed to a commensurate state, substitution of the experimentally observed  $B_n$  values in eq. (7.10) would give numbers very close to an integer. Remarkably, this is exactly what we observe. For instance, from the lock-in oscillations shown in Fig. 7.6 for D2, we find that at a temperature of e.g. 66 K the experimental  $B_n$  values are 2.05, 2.52, 3.19, 4.22, 5.70, and 8.14 T. Then for  $B_0 \approx 210$  T, the estimated values for the ratio  $(B_0/B_n)^{1/2}$  are 10.12, 9.12, 8.11, 7.05, 6.06, and 5.08 respectively.

Theoretically, commensurability effects due to the discrete nature of layered anisotropic superconductors have been studied analytically and numerically within the framework of both the LD and London models.<sup>22, 23, 52</sup> It has been argued that in the absence of extrinsic pinning, the transition between successive commensurate states of the lattice is of the first order and is accompanied by a jump in the equilibrium magnetization,<sup>22, 23</sup> which is predicted to be periodic in  $B^{-1/2}$  for  $n > 4$ .<sup>23</sup> The magnitude of these jumps is maximum near  $B_0$  (of the order of  $B_{c1}^{ab}/\mu_0$ ), but drops rapidly with  $n$ , becoming negligible far below  $B_0$ .<sup>22</sup> This fact, together with the small size of our samples in the c-direction (less than 100  $\mu\text{m}$ ), which limits significantly our experimental resolution, has not allowed us to confirm the presence of such first order magnetization jumps in the high temperature, reversible region. On the other hand, at lower temperatures, the presence of extrinsic pinning complicates the situation and it is not obvious whether such first order jumps would still persist. As a fact, in this regime the shape of the theoretically predicted (equilibrium) magnetization curves<sup>23</sup> are not in correspondence with the experimental data. This is because the oscillatory behaviour of

the magnetization is dominated by the irreversible contribution as discussed in the previous paragraphs. However, the possibility that tiny magnetization jumps are still present but masked due to the presence of pinning cannot be excluded.

The commensurability oscillations are not qualitatively affected by variations in the oxygen stoichiometry in the region near optimal doping. As can be seen from Fig. 7.10, that shows magnetization loops for samples D1 and D3 at several temperatures and for fields applied along the b-axis, the lock-in oscillations are present for both samples. Moreover, as illustrated in Fig. 7.11 they show a periodic behaviour when plotted versus  $B^{-1/2}$ . On the other hand, comparison of Figures 7.11 (a) and 7.11 (b) demonstrates that the period of the oscillations shows a slight decrease with the oxygen concentration.<sup>43</sup>

Careful examination of Figs. 7.6 and 7.11 also reveals that, in the high field region and between successive dips, the magnetization curves often exhibit some additional features, such as a shoulder or even extra tiny dips. These characteristics were first reported by Oussena et al.<sup>41</sup> and have not been elucidated yet. We now know that they are not induced by the interaction of JVs with the one-dimensional Cu-O chains, since they are observed for any orientation of the applied field in the ab-plane.<sup>42</sup> A possible explanation could be that in order to avoid unnecessary energy gain, for these high fields the reorganisation of the vortex system from one commensurate state to another takes place in more than one steps.

Fig. 7.12 illustrates magnetization loops for sample D2 in a broad temperature range. Fields are applied along the ab-plane (at an angle  $\vartheta_a$  of less than  $1^\circ$  as determined with the accuracy of our set-up) in the direction of the a-axis. At temperatures above  $\sim 20$  K the magnetization exhibits the characteristic oscillatory behaviour, indicating that  $\vartheta_a$  is below the lock-in angle  $\vartheta_{cr}$ . However, for  $T \leq 20$  K no oscillations are discerned in the magnetization curves, implying a destruction of the ideal vortex lock-in state. According to theoretical predictions<sup>12</sup> and experimental observations<sup>35</sup>  $\vartheta_{cr}$  increases weakly with decreasing temperature. Therefore, considering that during our experiment the field orientation is kept constant, the absence of the lock-in oscillations in this temperature range cannot be attributed to a possible field misalignment. In fact, at these reduced temperatures another important factor comes into play. This is the enhanced influence of point disorder that can lead to the nucleation of kinks at defect sites.<sup>7, 53</sup> As a consequence, vortices do not run parallel to the ab-planes anymore and the lock-in oscillations are suppressed. The formation of a kinked structure at these temperatures is

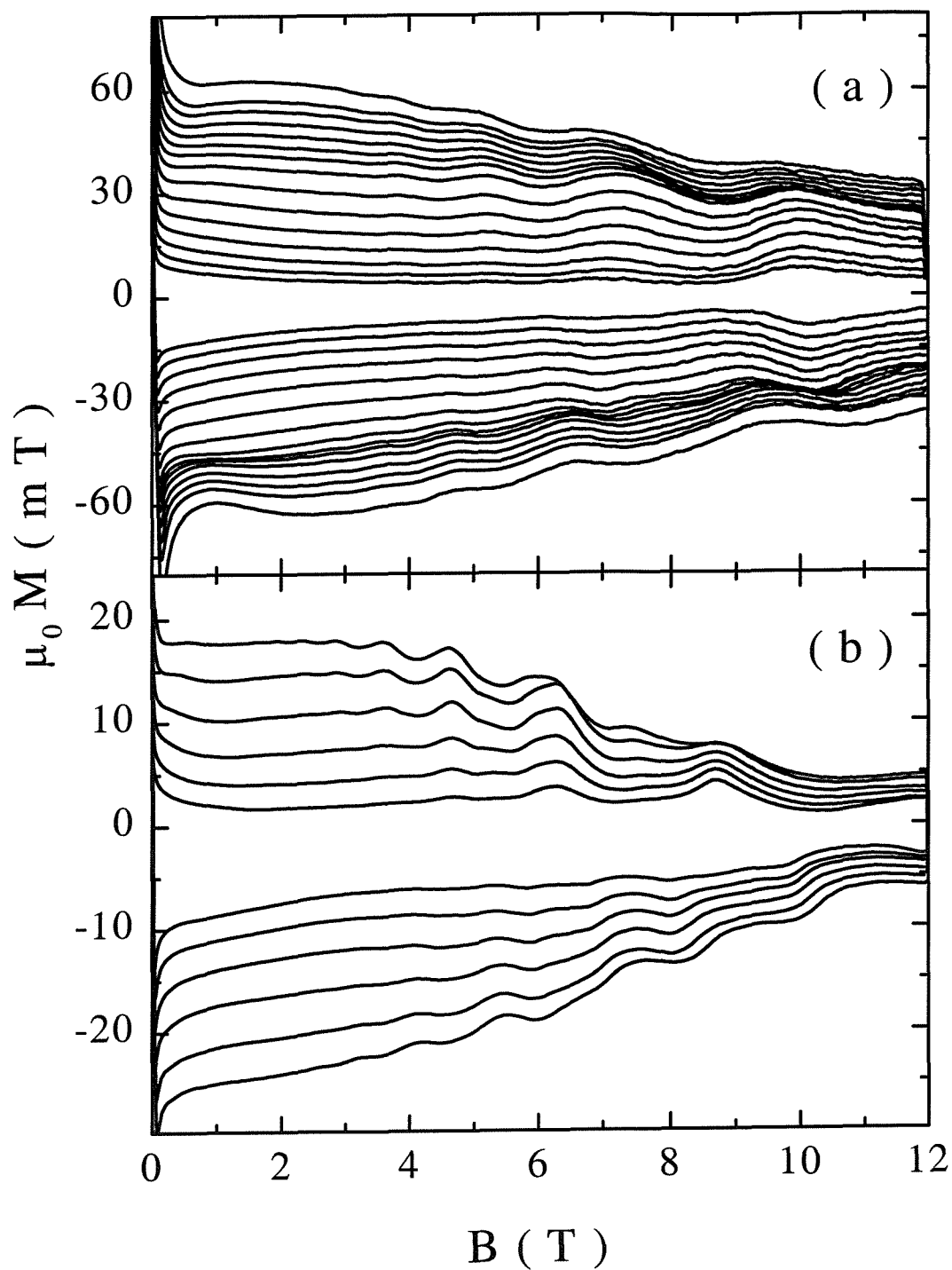


Fig. 7.10. Lock-in oscillations for fields along the  $b$ -axis for samples (a) D1 ( $7-\delta = 6.908$ ) and  $44\text{ K} \leq T \leq 74\text{ K}$  and (b) D3 ( $7-\delta = 6.970$ ) for temperatures in the range  $60\text{ K} - 70\text{ K}$ . The temperature increases from the inner to the outer curves with a step of  $2\text{ K}$ .

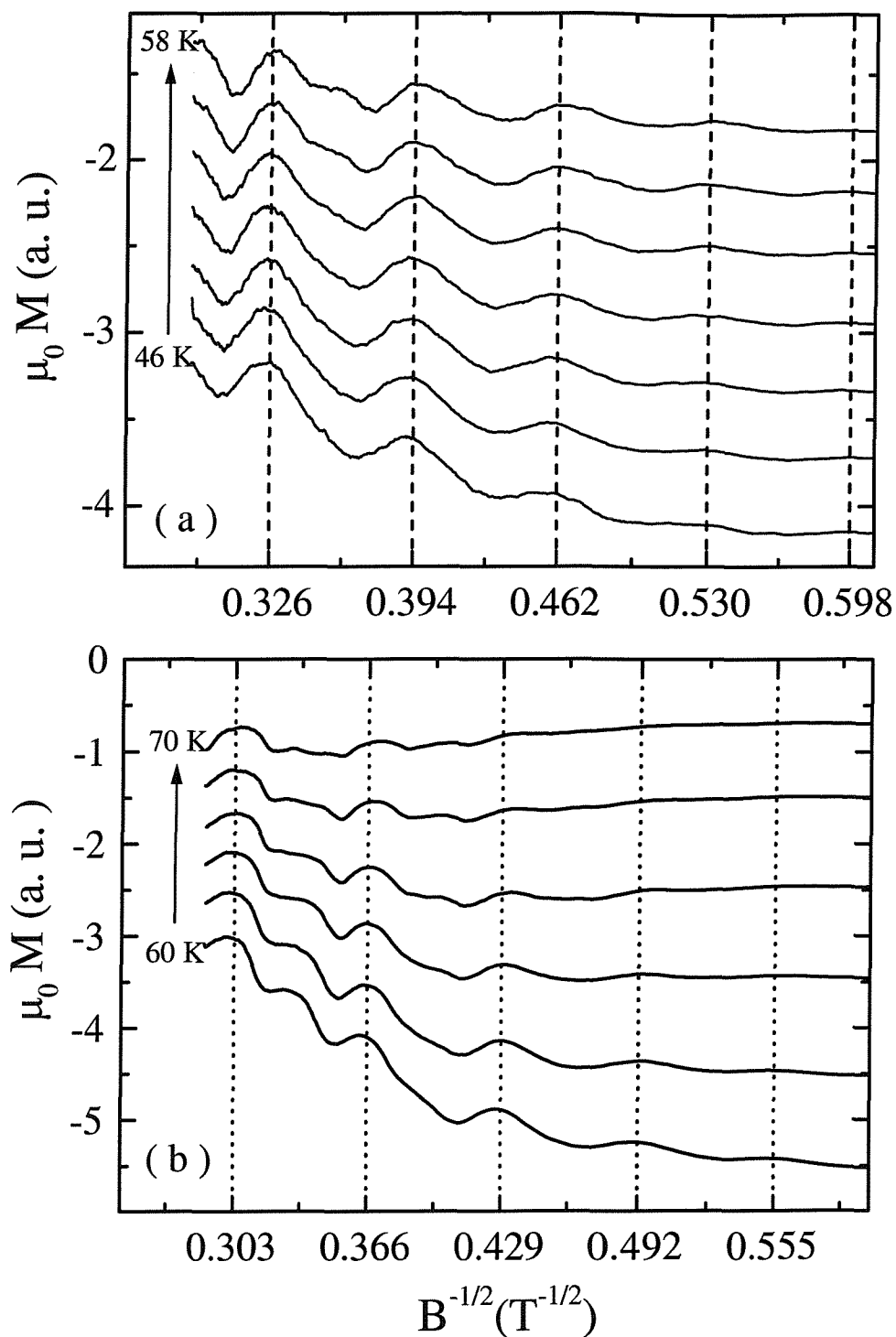


Fig. 7.11. Magnetization on the ascending branches of hysteresis loops is plotted versus  $B^{-1/2}$  for (a) sample D1 ( $7-\delta = 6.908$ ) and (b) sample D3 ( $7-\delta = 6.970$ ) at several temperatures. Temperature increases with a step of 2 K in the direction of the arrows. Note that for clarity the curves have been shifted vertically.

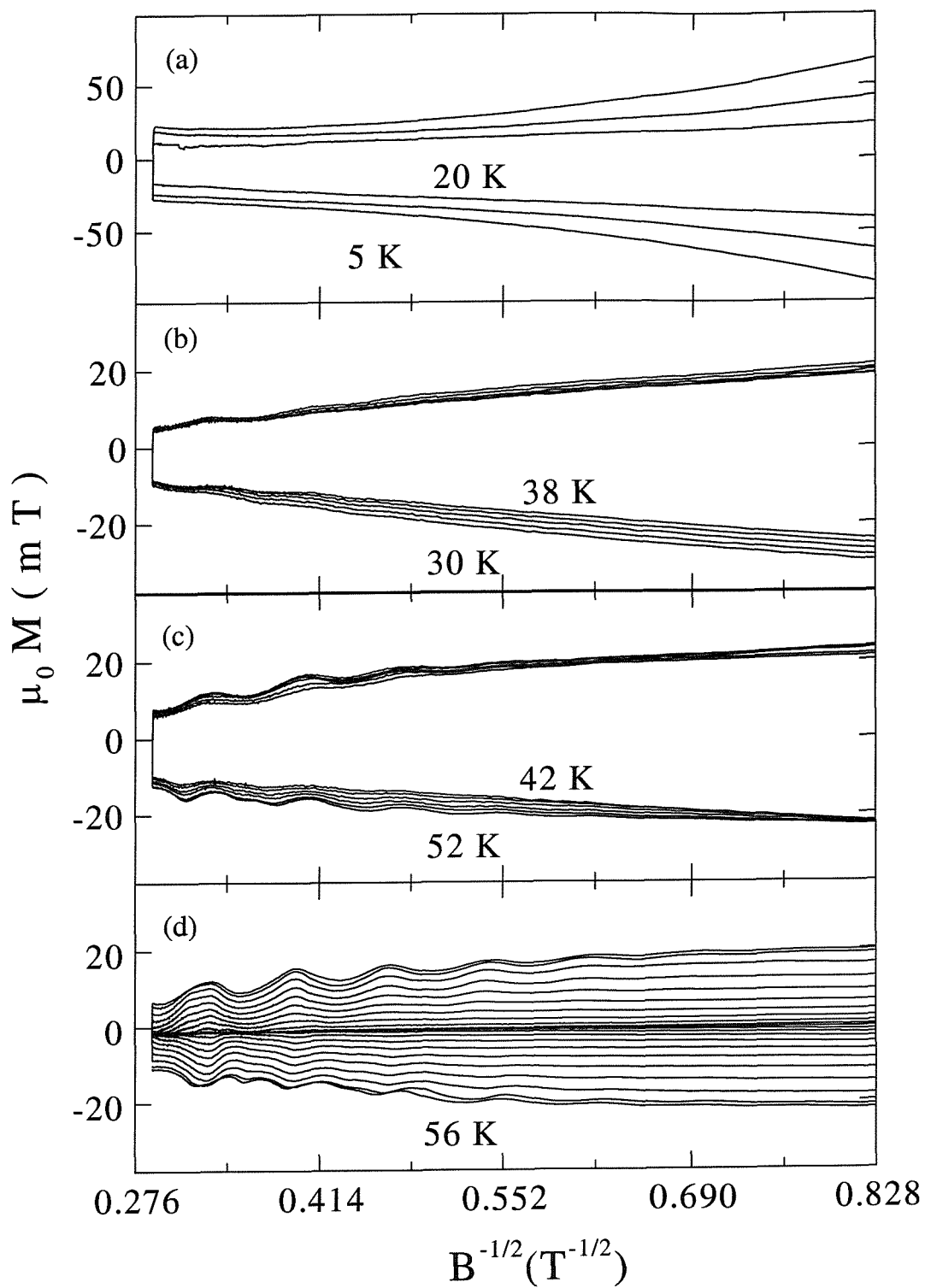


Fig. 7.12. Magnetization loops for sample D2 for fields along the  $a$ -axis in the temperature range 5 K – 80 K

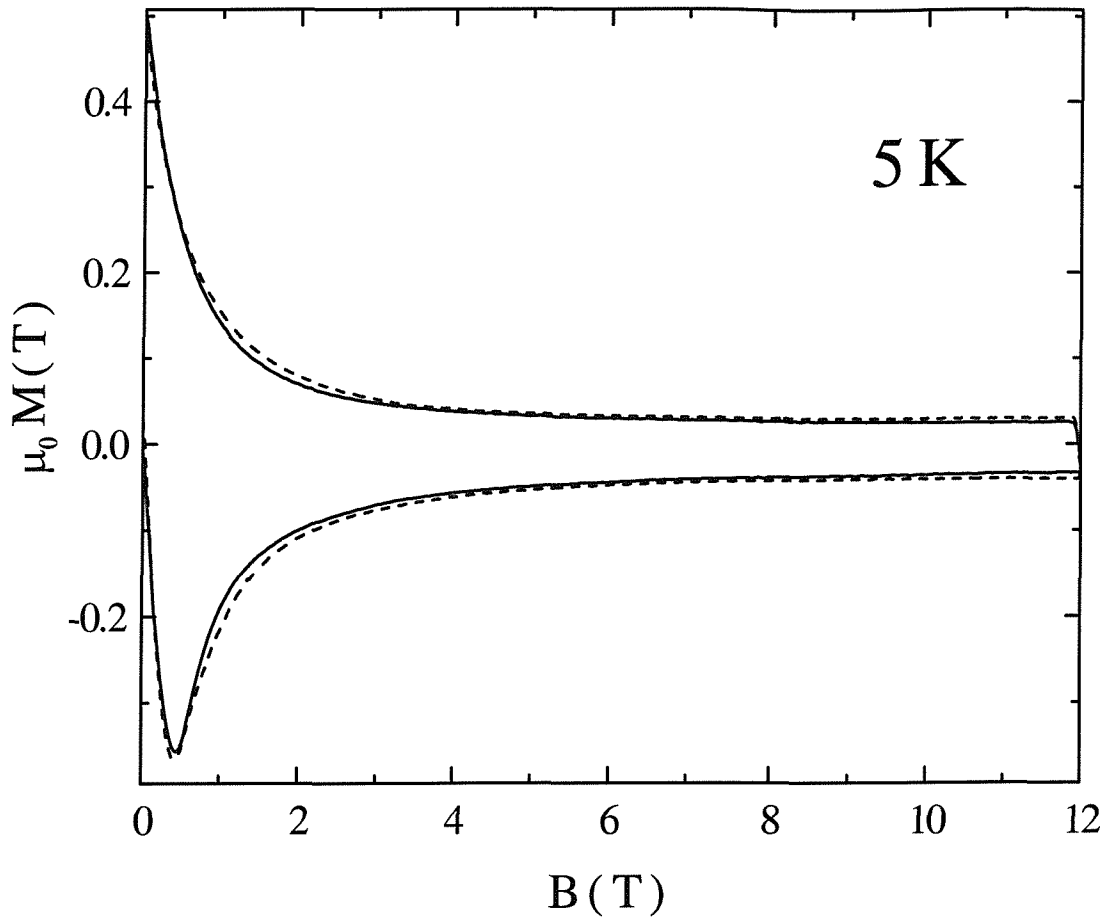


Fig. 7.13. Field dependence of the magnetization for D2 at 5 K and for the field applied at an angle  $\vartheta_a < 1^\circ$  (solid line) and  $(\vartheta_a + 2^\circ) \pm 0.1^\circ$  (dashed line) away from the  $a$ -axis.

further supported by the following observation: The hysteresis is almost unaffected when the field is deliberately applied at an angle  $\vartheta_a + 2^\circ$ , i.e., near but above  $\vartheta_{cr}$ , as illustrated in Fig. 7.13.<sup>42</sup> In addition, the presence of kinks at low temperatures was clearly demonstrated recently by an independent experimental study.<sup>54</sup> This result also points out that the purity of the sample is a crucial factor for the observation and investigation of the lock-in oscillations.

In the temperature region  $20 \text{ K} < T < 40 \text{ K}$  (Fig. 7.12 (b)), although present, the lock-in oscillations are still rather weak. This implies that even though reduced, the influence of quenched disorder is still considerable resulting in a partial destruction of the perfectly aligned vortex state. Following the usual behaviour, for temperatures below

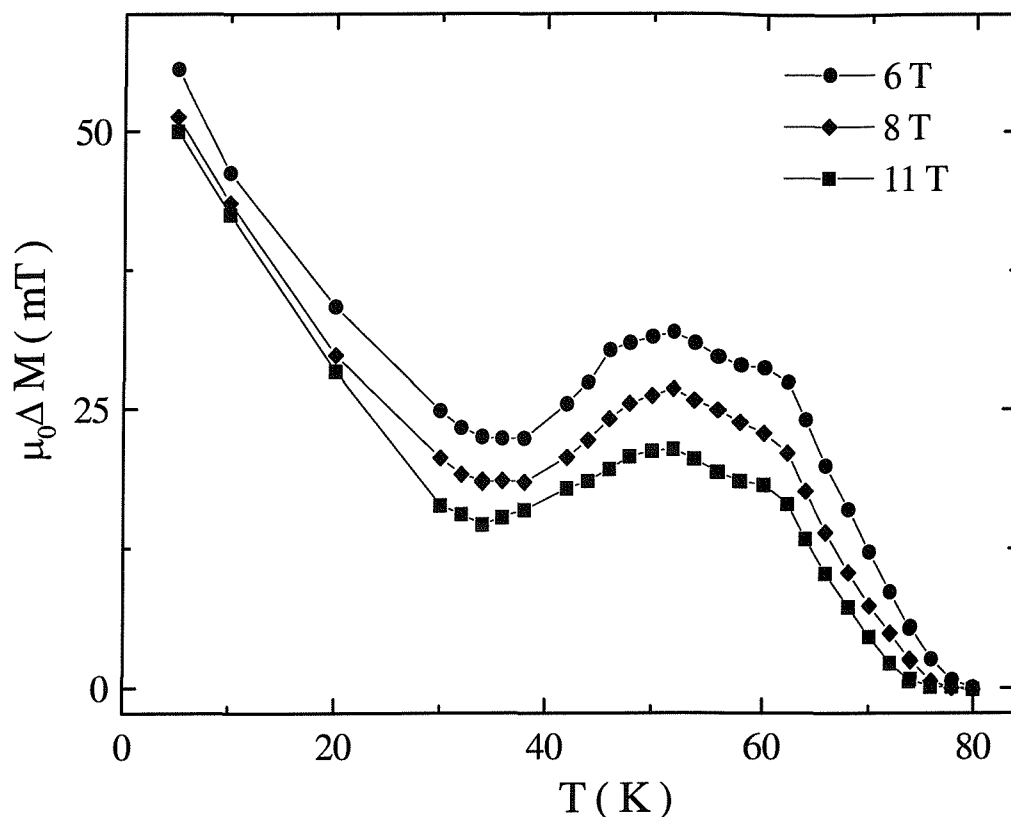


Fig. 7.14. The temperature dependence of the magnetic hysteresis width for sample D2 at the indicated fields. The field is applied along the *a*-axis.

~ 38 K the width of the magnetization loops decreases with temperature as characteristically depicted in Figures 7.12 (a) and (b).

With further increasing temperature (Fig. 7.12 (c)) the efficiency of disorder in nucleating kinks is reduced and the lock-in state better preserved. For this reason one would expect the amplitude of the commensurability oscillations to eventually become larger, in agreement with our results (see Fig. 7.12 (c)). However, the most unexpected and previously unreported finding in the temperature range  $36 \text{ K} < T < 55 \text{ K}$ , is that the magnetization width, and therefore, the critical current density increases with temperature. This observation becomes more obvious in Fig. 7.14 where we have plotted the temperature dependence of the hysteresis width  $\Delta M$ , for several fields. The same result has been obtained for all the investigated samples and for fields along both the *a*- and *b*-directions.

Such a behaviour is distinctly different from the usual monotonous decrease with temperature seen in the magnetic hysteresis for fields applied away from the *ab*-plane and can be explained as follows.<sup>42</sup> As mentioned above, in the case of magnetic measurements with fields parallel to the superconducting layers, the irreversibility does not reflect the intrinsic pinning but is rather determined by pinning of JVs between the  $\text{CuO}_2$  planes. Theoretical work by Blatter et al.<sup>12</sup> has shown that the suppression of the order parameter in a Josephson core is proportional to  $\xi_{ab}^2(T)$  and it should therefore increase with temperature, thus leading to an enhancement of pinning of JVs. The same conclusion was also drawn independently by Feinberg.<sup>7</sup> Consequently, in the case that the hysteresis is mainly determined by pinning of JVs the current should increase with temperature, in correspondence with our findings.

On the other hand, as can be seen from Figures 7.12 (d) and 7.14, for temperatures greater than almost 55 K, the usual trend of a hysteresis width that decreases with temperature is recovered. Moreover, the lock-in oscillations become gradually weaker and finally disappear above  $\sim 80$  K. At these elevated temperatures the effect of thermal fluctuations in reducing pinning of JVs by smearing of the pinning wells<sup>55</sup> becomes essential. This mechanism will gradually dominate the temperature dependence of the current, leading to an irreversibility that decreases with temperature according to the usual behaviour. In addition, at these temperatures the density of thermally-induced kinks increases,<sup>7</sup> spoiling the perfect alignment of vortices and gradually suppressing the lock-in oscillations. Also note that since for  $\text{YBa}_2\text{Cu}_3\text{O}_{7-\delta}$ ,  $T_{cr} \sim 80$  K, the eventual elimination of the oscillations could also result from the increase of  $\xi_c$  above  $d$ .<sup>7, 24</sup>

Note that a non-monotonous temperature dependence of the magnetic hysteresis width similar to the one depicted in Fig. 7.14, was recently reported and by Zhukov et al.<sup>50</sup> In this study it was proposed that the peak in the  $\Delta M$  versus  $T$  curves could also be related to a second order phase transition from a three-dimensional solid phase below the peak to a smectic phase above. In the latter, although vortices remain periodically arranged in the transverse direction they are disordered within the layers, as in usual smectic liquid crystals.<sup>56</sup> Nevertheless, this suggestion is still speculative and awaits firmer direct confirmation from, for example, structural studies.

Since the observed oscillations are a direct consequence of the interaction of the locked-in lattice with the periodic pinning structure, that the layers represent, it is natural to expect that their measurement would allow one to extract useful information about the

anisotropic properties of the superconductor.<sup>42, 43, 50</sup> Indeed, as can be seen from eq. (7.9), the out-of-plane anisotropy  $\gamma_{ck}$  can be directly related to the period  $\Delta(B^{-1/2})$  of the commensurability oscillations, namely:

$$\gamma_{ck} = \frac{\sqrt{3}}{2} \Phi_0 \left[ \frac{\Delta(B^{-1/2})}{d} \right]^2. \quad (7.11)$$

Substituting  $\Phi_0 = 2.067 \times 10^{-15}$  Wb,  $d = 1.164$  nm,<sup>57</sup> and the experimentally observed values for  $\Delta(B^{-1/2})$  for fields along the b- and a-axis, the estimated  $\gamma_{ca}$  and  $\gamma_{cb}$  values respectively for all the studied oxygen contents are shown in table 7.2. On the same table we also show the in-plane anisotropy  $\gamma_{ab} = \gamma_{cb}/\gamma_{ca}$ , which results from a difference in the sizes of the a- and b-axis lattice parameters of the order of 1 %.

As can be seen from table 7.2,  $\gamma_{ck}$  increases with oxygen deficiency. The enhancement, however, is not very large (not more than 14 % considering the change in  $\delta$  by almost 300 %). This result is in agreement with recent anisotropy estimations from transport measurements on highly oxygenated  $YBa_2Cu_3O_{7-\delta}$  single crystals of the same origin and quality.<sup>58</sup> On the other hand, the in-plane anisotropy is found to be almost unaffected by variations in the oxygen content in the region under investigation.

The out-of-plane anisotropy values given in table 7.2 are consistent with the results by Zhukov et al.,<sup>50</sup> who, by using the lock-in oscillation technique and a crystal of similar

$7 - \delta$	$\gamma_{ca}$	$\gamma_{cb}$	$\gamma_{ab}$
6.908	$6.11 \pm 0.05$	$6.47 \pm 0.11$	$1.06 \pm 0.02$
6.934	$5.76 \pm 0.05$	$6.18 \pm 0.07$	$1.07 \pm 0.01$
6.970	$5.36 \pm 0.10$	$5.76 \pm 0.13$	$1.07 \pm 0.03$

Table 7.2. Values of the anisotropy parameters for the three  $YBa_2Cu_3O_{7-\delta}$  single crystals as found from the period of the magnetization commensurability oscillations.

quality, found  $\gamma \approx 5.5$  for  $7-\delta = 6.97 \pm 0.02$ . In addition, they are in good correspondence with recent anisotropy estimations from specific heat ( $\gamma = 5.9 \pm 0.5$  for  $7-\delta = 6.96 \pm 0.01$ ),<sup>59</sup> and magnetization measurements ( $\gamma = 6.5$  for  $7-\delta = 6.92$ ).<sup>60</sup>

According to structural studies, the unit cell of  $\text{YBa}_2\text{Cu}_3\text{O}_{7-\delta}$  contains two  $\text{CuO}_2$  layers separated by a distance  $\sim 0.34$  nm; these bilayers are spaced by  $\sim 0.83$  nm.<sup>57</sup> For our anisotropy estimations, we have considered just a single minimum energy well in the middle of the bilayer spacing (see Fig. 7.3). The correspondence of our results with Refs. 59 and 60, where the details of the layered structure were not essential, leads to the important conclusion that the spatial period of the intrinsic pinning potential, effectively coincides with the length of the crystal unit cell in the *c*-direction.

Although the anisotropy values found from the commensurability oscillations are in good agreement with the ones reported by other groups, for consistency, and in order to avoid ambiguities stemming from possible differences in the properties of samples prepared by different workers, we have performed one more check. We have tried to compare the anisotropy estimations from the commensurability oscillations directly with the ones obtained by another technique, namely torque magnetometry, on the same samples. Therefore we have performed torque measurements on one of our samples, the single crystal D2.

It is well established that when a field is applied at an angle  $\theta$  away from the anisotropy axis (*c*-axis) of an anisotropic superconductor, the equilibrium orientation of vortices is not parallel to the applied field, i.e., the magnetization has a component normal to the applied magnetic field.<sup>1, 4, 5</sup> Under such conditions, a finite torque  $\tau(\theta)$  is exerted on the superconductor that is given by:

$$\frac{\tau(\theta)}{V} = \mathbf{M} \times \mathbf{B}_a \quad (7.12)$$

with  $V$  the volume of the sample,  $\mathbf{M}$  and  $\mathbf{B}_a$  the magnetization and applied magnetic field vectors respectively. Eq. (7.12) can be written in an analytical form using the three-dimensional anisotropic London model, which gives for the equilibrium torque:<sup>61</sup>

$$\frac{\tau(\theta_{ck})}{V} = \frac{\Phi_0 B_a}{16\pi\mu_0\lambda_{ab}^2} \frac{(\gamma_{ck}^2 - 1) \sin(2\theta_{ck})}{\gamma_{ck} \varepsilon(\theta_{ck})} \ln \left[ \frac{\gamma_{ck} \eta B_{c2}^c}{B_a \varepsilon(\theta_{ck})} \right] \quad (7.13)$$

where  $\theta_{ck}$  is the angle between the c-axis and the applied field,<sup>62</sup>  $\varepsilon(\theta_{ck}) = (\sin^2\theta_{ck} + \gamma_{ck}^2 \cos^2\theta_{ck})^{1/2}$ ,  $\eta$  a constant of order unity and  $B_{c2}^c$  the upper critical field parallel to the c-axis. It is stressed that this result is restricted by the applicability of the London model, and is therefore valid in the range  $B_{c1} \ll B \ll B_{c2}$  and  $T > T_{cr}$ , provided that  $\kappa \gg 1$ . Indeed, as shown by Farrell et al.,<sup>11</sup> for  $YBa_2Cu_3O_{7-\delta}$  this formula works well only for temperatures above  $T_{cr} \sim 80$  K and moderate fields. In order to satisfy these conditions, we have performed our studies at temperatures  $T > 87$  K and applied fields  $B_a \geq 1$  T. Moreover, in order to avoid the influence of fluctuation effects near the  $B_{c2}(T)$  line, our temperature range was restricted below 91 K. For these temperatures the torque signal was completely reversible.

The angular dependence of the torque for sample D2 is illustrated in Figures 7.15 (a) and 7.15 (b) for a field of 1 T rotated in the ca- and cb-plane respectively. Data are shown for several temperatures. Also included are the theoretical fits using eq. (7.13) with fitting parameters  $\gamma_{ck}$ ,  $\lambda_{ab}$  and  $\eta B_{c2}^c$ . As can be seen, the fitting is rather good. The average values for  $\gamma_{ca}$  and  $\gamma_{cb}$  are  $6.51 \pm 0.22$  and  $7.56 \pm 0.14$  respectively. This gives  $\gamma_{ab} = 1.16 \pm 0.05$ . Comparison of these results with the anisotropy values obtained from the lock-in oscillations for the same sample (see table 7.2), demonstrates that although both studies are in reasonable agreement, the values given by torque are slightly higher. The maximum deviation of approximately 18 % is seen for  $\gamma_{cb}$ . Similarly, increased anisotropy values were obtained in Ref. 58 using transport measurements. For example, for a crystal with the same oxygen content as D2, the out-of-plane anisotropy was estimated to be equal to 7.46.<sup>58</sup> If it is remembered that in the last two techniques measurements are performed at temperatures close to 90 K whereas the commensurability oscillation method is employed at  $T < 80$  K, this result could be explained by a temperature dependent anisotropy in this regime. For layered superconductors, such a possibility was pointed out by Feinberg et al.,<sup>9</sup> as a consequence of nonzero values of the order parameter between the superconducting layers due to their coupling with proximity effects. In  $YBa_2Cu_3O_{7-\delta}$  such effects can be of importance, since the  $CuO_2$  layers are coupled with the Cu-O chains that

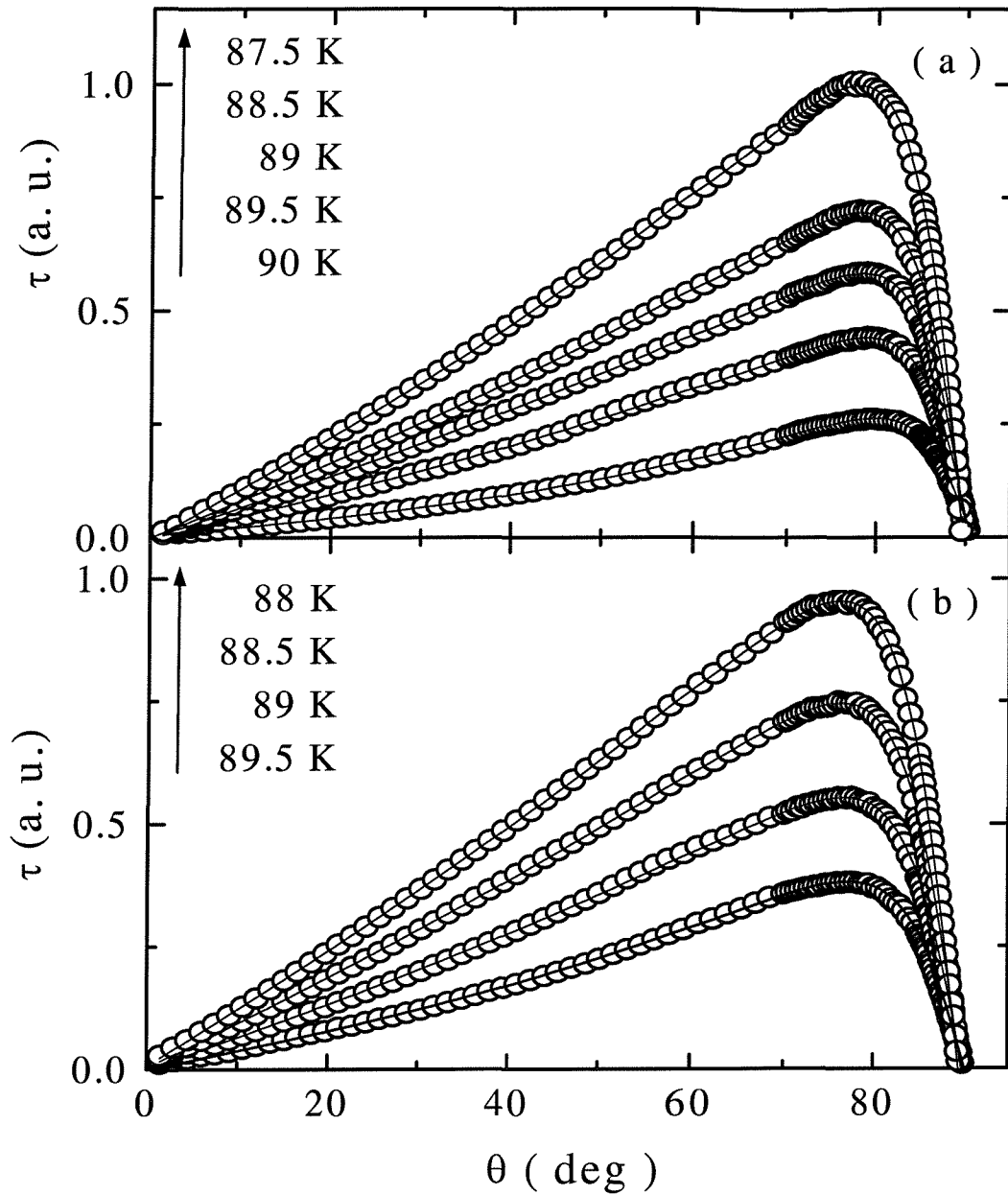


Fig. 7.15. Angular dependence of the equilibrium torque for sample D2 at the indicated temperatures and for an applied field of 1 T rotated in the  $ca$ -plane (a) and  $cb$ -plane (b).

have metallic character.<sup>9</sup> As a fact, an increase in the out-of-plane anisotropy with temperature of similar magnitude with the one observed in our experiments was recently seen in  $\text{YBa}_2\text{Cu}_3\text{O}_{7-\delta}$  single crystals using equilibrium magnetization measurements in the range  $76 \text{ K} < T < 92 \text{ K}$ .<sup>33</sup> An additional source of the temperature variation of  $\gamma_{ck}$  might be the increase in the distance between the  $\text{CuO}_2$  planes with temperature. Although for

the range of temperatures under consideration this change is rather small (less than 0.1 %),<sup>57, 63</sup> our recent work on thallium based cuprates has demonstrated that its influence on  $\gamma_{ck}$  should not be underestimated.<sup>64</sup>

Finally, the lower anisotropy values calculated from the commensurability oscillations could also partially result from a limited applicability of eq. (7.11) that was derived for the case of a hexagonal vortex lattice. As was shown recently, under certain conditions, such as in the case of an anisotropic Fermi surface or d-wave nature of pairing, at high enough fields a square lattice becomes energetically favourable.<sup>65</sup> For the anisotropic superconductor under study this lattice should transform to a rectangular with aspect ratio  $\gamma_{ck}$ . In such a case, the coefficient  $\sqrt{3}/2$  in eq. (7.11) should be dropped out leading to higher anisotropy values. For instance, for D2 one would then obtain  $\gamma_{ca} = 6.65$  and  $\gamma_{cb} = 7.14$ , values that although still slightly lower are closer to the transport and torque results.<sup>43</sup>

## 7.2.4 Summary

Summarizing, in this chapter we have presented a detailed study of the hysteretic behaviour of the vortex system in pure detwinned  $\text{YBa}_2\text{Cu}_3\text{O}_{7-\delta}$  single crystals for fields along the superconducting planes. It has been demonstrated that for this field configuration the shape of the magnetic hysteresis curves alters dramatically, showing an oscillatory behaviour. The latter results from vortex order and the discrete nature of the superconductor, and can be accounted by considering the commensurability of the vortex lattice with the layered arrangement. Indeed, the observed oscillations are periodic in  $B^{-1/2}$  space in quantitative agreement with the predictions of the three-dimensional anisotropic London model. The effect of variations in the oxygen stoichiometry in the region near optimal doping has also been studied and found to be a slight increase of the oscillation period with oxygen deficiency. The temperature dependence of the commensurability oscillations has revealed some unique features, resulting from the competition between intrinsic pinning, quenched disorder and thermal fluctuations. Thus at low ( $T < 30$  K) and high temperatures ( $T > 80$  K) the lock-in oscillations are absent due to the existence of a great number of disorder- or thermally-nucleated kinks respectively that destroy the ideal parallel vortex lattice. On the other hand, in the intermediate temperature range the lock-

in state is better preserved and the oscillations are prominent. We have found that remarkably enough in this region the current density varies non-monotonously with temperature. This strange behaviour has been attributed to the suppression of the order parameter in the Josephson cores that increases with temperature, resulting in stronger pinning at higher temperatures. Finally, it has been illustrated that lock-in oscillations are a useful tool for extracting the anisotropy parameters of the superconductor in a direct and easy way. Comparison of the anisotropy values derived using this method with techniques employed in a higher temperature range, such as torque magnetometry and transport, has pointed out the possibility of a temperature dependent anisotropy, which had been anticipated by theory.

## References

---

- <sup>1</sup> M. Tinkham, *Introduction to Superconductivity*, (McGraw-Hill, Singapore, 1996)
- <sup>2</sup> V. L. Ginzburg, Zh. Eksp. Teor. Fiz. 14, 134 (1944); L. Landau and V. L. Ginzburg, Zh. Eksp. Teor. Fiz. 20, 1064 (1950); V. L. Ginzburg, Zh. Eksp. Teor. Fiz. 23, 236 (1952)
- <sup>3</sup> P. G. de Gennes, *Superconductivity of Metals and Alloys*, (Benjamin, 1966)
- <sup>4</sup> L. N. Bulaevskii, Zh. Eksp. Teor. Fiz. 64, 2241 (1973) [Sov. Phys. JETP 37, 1133 (1973)]
- <sup>5</sup> R. A. Klemm and J. R. Clem, Phys. Rev. B 21, 1868 (1980); R. A. Klemm, Phys. Rev. B 38, 6641 (1988)
- <sup>6</sup> V. G. Kogan, Phys. Rev. B 24, 1572 (1981)
- <sup>7</sup> D. Feinberg, J. Phys. III 4, 169 (1994)
- <sup>8</sup> W. Lawrence and S. Doniach, *Proceedings of the Twelfth International Conference on Low Temperature Physics*, edited by E. Kanda (Academic Press of Japan, Kyoto, 1970), p. 361
- <sup>9</sup> D. Feinberg, S. Theodorakis, and A. M. Ettouhami, Phys. Rev. B 49, 6285 (1994) and references therein.
- <sup>10</sup> L. N. Bulaevskii, Phys. Rev. B 44, R910 (1991)
- <sup>11</sup> D. E. Farrell, J. P. Rice, D. M. Ginsberg, and J. Z. Liu, Phys. Rev. Lett. 64, 1573 (1990)
- <sup>12</sup> G. Blatter, M. V. Feigel'man, V. B. Geshkenbein, A. I. Larkin, and V. M. Vinokur, Rev. Mod. Phys. 66, 1125 (1994)
- <sup>13</sup> D. S. Fisher, M. P. A. Fisher, and D. A. Huse, Phys. Rev. B 43, 130 (1991); L. I. Glazman and A. E. Koshelev, Phys. Rev. B 43, 2835 (1991)
- <sup>14</sup> D. Feinberg and C. Villard, Phys. Rev. Lett. 65, 919 (1990)
- <sup>15</sup> B. I. Ivlev, Yu. N. Ovchinnikov, and V. L. Pokrovsky, Mod. Phys. Lett. B 5, 73 (1991)
- <sup>16</sup> L. N. Bulaevskii, M. Ledvij, and V. G. Kogan, Phys. Rev. B 46, 366 (1992)
- <sup>17</sup> J. R. Clem and M. W. Coffey, Phys. Rev. B 42, 6209 (1990)
- <sup>18</sup> K. B. Efetov, Zh. Eksp. Teor. Fiz. 76, 1781 (1979) [Sov. Phys. JETP 49, 905 (1979)]
- <sup>19</sup> J. P. Carton, J. Phys. I (Paris) 1, 113 (1991)
- <sup>20</sup> J. R. Clem, M. W. Coffey, and Z. Hao, Phys. Rev. B 44, 2732 (1991)
- <sup>21</sup> C. R. Hu, Phys. Rev. B 6, 1756 (1972)
- <sup>22</sup> L. N. Bulaevskii and J. R. Clem, Phys. Rev. B 46, 366 (1992)

- <sup>23</sup> M. Ichioka, Phys. Rev. B 51, 9423 (1995)
- <sup>24</sup> D. Feinberg and A. M. Ettouhami, Int. J. Mod. Phys. B 11, 2085 (1993); Phys. Scr. T49, 159 (1993)
- <sup>25</sup> M. Tachiki and S. Takahashi, Solid State Commun. 70, 291 (1989)
- <sup>26</sup> P. Berghuis, E. Di Bartolomeo, G. A. Wagner, and J. E. Evetts, Phys. Rev. Lett. 79, 2332 (1997)
- <sup>27</sup> L. Balents and D. R. Nelson, Phys. Rev. Lett. 73, 2618 (1994); Phys. Rev. B 52, 12951 (1995)
- <sup>28</sup> E. B. Sonin, Phys. Rev. B 48, 10487 (1993)
- <sup>29</sup> A. A. Zhukov, Yu. V. Bugoslavsky, G. K. Perkins, J. V. Thomas, A. D. Caplin, H. K pfer, and T. Wolf, Physica C 282-287, 2151 (1997)
- <sup>30</sup> J. C. Martinez, S. H. Brongersma, A. Koshelev, B. Ivlev, P. H. Kes, R. P. Griessen, D. G. de Groot, Z. Tarnavski, and A. A. Menovsky, Phys. Rev. Lett. 69, 2276 (1992); F. Steinmeyer, R. Kleiner, P. Muller, H. Muller, and K. Winzer, Europhys. Lett. 24, 459 (1994)
- <sup>31</sup> V. Vulcanescu, G. Collin, H. Kojima, I. Tanaka, and L. Fr chter, Phys. Rev. B 50, 4139 (1994)
- <sup>32</sup> S. Kole nik, T. Sko kiewicz, J. Igalsen, and Z. Tarnawski, Phys. Rev. B 54, 13319 (1996)
- <sup>33</sup> P. Pugn t, G. Fillion, H. Noel, and B. Barbara, Europhys. Lett. 35, 49 (1996)
- <sup>34</sup> W. K. Kwok, U. Wlep, V. M. Vinokur, S. Flesher, J. Downey, and G. W. Crabtree, Phys. Rev. Lett. 67, 390 (1991)
- <sup>35</sup> Yu. V. Bugoslavsky, A. A. Zhukov, G. K. Perkins, A. D. Caplin, H. Kojima, and I. Tanaka, Phys. Rev. B 56, 5610 (1997)
- <sup>36</sup> M. Benkraouda and M. Ledvij, Phys. Rev. B 51, 6123 (1995)
- <sup>37</sup> A. E. Koshelev, Phys. Rev. Lett. 83, 187 (1999)
- <sup>38</sup> B. Schmidt, M. Konczykowski, N. Morozov, and E. Zeldov, Phys. Rev. B 55, R8705 (1997); S. Ooi, T. Shibauchi, N. Okuda, and T. Tamegai, Phys. Rev. Lett. 82, 4308 (1999)
- <sup>39</sup> L. J. Campbell, M. M. Doria, and V. G. Kogan, Phys. Rev. B 38, 2439 (1988)
- <sup>40</sup> R. A. Klemm, A. Luther, and M. R. Beasley, Phys. Rev. B 12, 877 (1975)
- <sup>41</sup> M. Oussena, P. A. J. de Groot, R. Gagnon, and L. Taillefer, Phys. Rev. Lett. 72, 3606 (1994)

- <sup>42</sup> K. Deligiannis, S. Kokkaliaris, M. Oussena, P. A. J. de Groot, L. Früchter, R. Gagnon, and L. Taillefer, *Phys. Rev. B* 59, 14772 (1999)
- <sup>43</sup> S. Kokkaliaris, K. Deligiannis, M. Oussena, A. A. Zhukov, P. A. J. de Groot, R. Gagnon, and L. Taillefer, *Supercond. Sci. Technol.* 12, 690 (1999)
- <sup>44</sup> D. J. L. Hong and D. M. Smyth, *J. Am. Ceram. Soc.* 74, 1751 (1991)
- <sup>45</sup> K. Deligiannis, P. A. J. de Groot, M. Oussena, S. Pinfold, R. Langan, R. Gagnon, and L. Taillefer, *Phys. Rev. Lett.* 79, 2121 (1997)
- <sup>46</sup> H. Küpfer, Th. Wolf, C. Lessing, A. A. Zhukov, X. Lançon, R. Meier-Hirmer, W. Schauer, and H. Wühl, *Phys. Rev. B* 58, 2886 (1998)
- <sup>47</sup> S. Kokkaliaris, P. A. J. de Groot, S. N. Gordeev, A. A. Zhukov, R. Gagnon, and L. Taillefer, *Phys. Rev. Lett.* 82, 5116 (1999)
- <sup>48</sup> H. Küpfer, A. A. Zhukov, A. Will, W. Jahn, R. Meier-Hirmer, T. Wolf, V. I. Voronkova, M. Kläser, and K. Saito, *Phys. Rev. B* 54, 644 (1996)
- <sup>49</sup> This study is concentrated on the high field region where the condition  $B_a \gg \mu_0 M$  always holds (e.g. at  $B_a \sim 1$  T,  $\frac{B_a}{\mu_0 M} > 10^6$ ). Therefore, the magnetic flux and the applied field are considered as identical. For the same reason demagnetization effects are inessential and need not be taken into account.
- <sup>50</sup> A. A. Zhukov, H. Küpfer, G. K. Perkins, A. D. Caplin, T. Wolf, K. I. Kugel, A. L. Rakhmanov, M. G. Mikheev, V. I. Voronkova, M. Kläser, and H. Wühl, *Phys. Rev. B* 59, 11213 (1999)
- <sup>51</sup> R. L. Peterson, *J. Appl. Phys.* 67, 6930 (1990)
- <sup>52</sup> S. E. Burkov, *Phys. Rev. B* 44, R2850 (1991)
- <sup>53</sup> M. Tachiki and S. Takahashi, *Solid State Commun.* 72, 1083 (1989)
- <sup>54</sup> A. A. Zhukov, H. Küpfer, P. A. J. de Groot, and T. Wolf, *Phys. Rev. Lett.* 83, 5110 (1999)
- <sup>55</sup> M. V. Feigel'man and V. M. Vinokur, *Phys. Rev. Lett.* 41, 8986 (1990)
- <sup>56</sup> L. Balents and D. R. Nelson, *Phys. Rev. Lett.* 73, 2618 (1994); *Phys. Rev. B* 52, 12951 (1995)
- <sup>57</sup> R. M. Hazen, *Physical Properties of High Temperature Superconductors II*, edited by D. M. Ginsberg, (World Scientific, Singapore, 1990), p.121.

- <sup>58</sup> R. M. Langan, S. N. Gordeev, P. A. J. de Groot, A. G. M. Jansen, R. Gagnon, and L. Taillefer, *Phys. Rev. B* 58, 14548 (1998)
- <sup>59</sup> M. Roulin, A. Junod, A. Erb, and E. Walker, *Phys. Rev. Lett.* 80, 1722 (1998)
- <sup>60</sup> D. Babić, J. R. Cooper, J. W. Hodby, and C. Changkang, *Phys. Rev. B* 60, 698 (1999)
- <sup>61</sup> V. G. Kogan, *Phys. Rev. B* 38, 7049 (1988)
- <sup>62</sup> Note that in the field and temperature range of our measurements, corrections due to demagnetization effects are negligible (B. Janossy, R. Hergt, and L. Früchter, *Physica C* 170, 22 (1990))
- <sup>63</sup> J. J. Capponi, C. Chaillout, A. W. Hewat, P. Lejay, M. Marezio, N. Nguyen, B. Raveau, J. L. Soubeyrou, J. L. Tholence, and R. Tournier, *Europhys. Lett.* 3, 1301 (1987)
- <sup>64</sup> S. Kokkaliaris, S. N. Gordeev, P. A. J. de Groot, X. M. Yang, and M. T. Weller, *Physica C* 209, 46 (1998)
- <sup>65</sup> K. Park and D. A. Huse, *Phys. Rev. B* 58, 9427 (1998) and references therein.

---

# Chapter 8

---

## Summary

In this thesis we have presented a detailed investigation of the vortex phase diagram and pinning in pure  $\text{YBa}_2\text{Cu}_3\text{O}_{7-\delta}$  single crystals. In order to obtain a complete picture of the behaviour of the vortex system in this compound in the region of the magnetic phase diagram below the melting line, we have carried out experiments under various conditions. Thus we have studied numerous samples that were characterized by different types, densities as well as distributions of pinning sites. Measurements have been performed using mainly vibrating sample magnetometry and in a lesser degree equilibrium torque magnetometry, for a broad range of experimental parameters, such as the temperature, the field magnitude, orientation and sweep rate. These results have provided with significant new insight into several current issues in the field of high temperature superconductivity and can be summarized briefly as follows.

### 8.1 The vortex phase diagram of $\text{YBa}_2\text{Cu}_3\text{O}_{7-\delta}$

By employing a partial magnetization loop technique, we have studied in detail history effects in the magnetic hysteresis of pure  $\text{YBa}_2\text{Cu}_3\text{O}_{7-\delta}$  single crystals with various kinds and densities of pinning centres. These measurements have enabled the detection of the point where topological disorder first invades the vortex system. Accordingly, studies of detwinned single crystals with very low densities of point defects have revealed a transition in the mixed state of the superconductor that separates a dislocation-free Bragg glass from a highly disordered vortex phase. The transition line has been mapped in the

field-temperature phase diagram and found to lie in the vicinity of the onset of the second magnetization peak. In addition, the form of this line has been in quantitative correspondence with theoretical predictions.

We went even further and investigated the dependence of this boundary on the density of point defects. It has been demonstrated that, in the range of oxygen concentrations under study ( $6.550 \leq 7-\delta \leq 6.999$ ), the Bragg glass stability region shrinks with decreasing the oxygen stoichiometry and is eventually completely suppressed for high values of the oxygen deficiency ( $7-\delta = 6.550, 6.750$ ). This result is in agreement with theoretical predictions and can be understood by considering the enhanced role of quenched disorder in promoting wandering of vortices from their equilibrium positions, destroying long range order in the vortex lattice at lower fields for larger densities of pinning defects.

With increasing the magnetic field above the Bragg glass phase boundary, topological defects, such as dislocations that exhibit metastable behaviour, proliferate in the vortex system, resulting in a prominent dependence of the critical current density on the formation history of the flux line lattice. Nevertheless, for low oxygen concentrations near optimal doping, the memory effects diminish at high fields, a finding that has been attributed to a saturation in the density of dislocations. Such saturation, however, is absent for detwinned crystals close to the stoichiometric state, due to the reduced efficiency of disorder in this case in promoting vortex entanglement.

Finally, we have studied the influence on the Bragg glass – disordered phase transition of correlated pinning centres, such as twin planes and columns. It has been illustrated that a low density of twin boundaries does not affect the Bragg glass significantly. This is because in this case the magnetic response is dominated mainly by the contribution of vortices in the broad inter-twin boundary space that are negligibly affected by the presence of the twin planes. In contrast, a high concentration of twins as well as even low densities of columnar defects have been found to be very efficient pinning centres, destroying the Bragg glass and eliminating the memory effects. Under these conditions, the vortex system is expected to most probably form a Bose glass.

## 8.2 The peak effect in pure $\text{YBa}_2\text{Cu}_3\text{O}_{7-\delta}$ single crystals

We have performed extensive measurements in order to study the second magnetization peak in high quality  $\text{YBa}_2\text{Cu}_3\text{O}_{7-\delta}$  single crystals. These experiments have revealed that for specimens with low densities of pinning centres, the magnetization peak shows several new features that are absent in less pure samples. Thus it has been demonstrated that in contrast to the conventional “fishtail” behaviour, the position of the peak in the  $B - T$  plane shows a non-monotonous temperature dependence. In addition, with increasing temperature this peak approaches the vortex lattice melting transition line. At these elevated temperatures the magnetization peak becomes rather sharp, and is in good correspondence with the peak seen in transport measurements. Finally, with increasing oxygen deficiency the location of the peak has been found to shift to lower field values. These findings are in contradiction with several existing scenaria proposed in order to explain this phenomenon in  $\text{YBa}_2\text{Cu}_3\text{O}_{7-\delta}$ , and have urged for a more realistic interpretation. Hence, in view of our work on the vortex phase diagram outlined in the last section, which has demonstrated clearly that the onset of the peak is closely related to the destruction of the ideal lattice and the onset of vortex entanglement, we proposed that these results can be accounted by considering a mechanism where the peak effect is determined by the interplay between pinning and plastic distortions of the flux line lattice.

The effect of oxygen ordering on the second magnetization peak has also been investigated. By choosing appropriate oxygen annealing conditions we have prepared and studied samples with different densities as well as distributions of oxygen vacancies. These experiments have disclosed that below a threshold temperature of the order of 70 K, the position of the peak and the hysteresis in general, are not affected significantly by the oxygenation treatment and therefore by the exact configuration formed by the oxygen deficient sites. This result indicates that in this temperature range the pinning properties of clusters and a more homogeneous distribution of oxygen vacancies are very similar. On the other hand, for temperatures above  $\sim 70$  K, oxygen ordering becomes very important. This is demonstrated by the suppression of the magnetization peak and the rather lower critical currents for the high pressure annealed samples, illustrating that oxygen vacancy clusters are much more efficient pinning centres in this temperature region.

### 8.3 Commensurability effects induced by the layered structure of $\text{YBa}_2\text{Cu}_3\text{O}_{7-\delta}$

The hysteretic response of  $\text{YBa}_2\text{Cu}_3\text{O}_{7-\delta}$  single crystals for fields along the ab-plane has exhibited a very interesting behaviour. Thus for this field configuration, the presence of a peculiar feature in the hysteretic magnetization curves has been divulged, namely oscillations. Angular studies have demonstrated that the oscillations are present only in a small angular range close to the  $\text{CuO}_2$  planes. Furthermore, when plotted versus  $B^{-1/2}$ , the oscillations are periodic, with a temperature independent period. These observations, in conjunction with the anisotropic London model have established that the oscillations, which have been termed lock-in or commensurability oscillations, are a consequence of the discrete nature of the superconductor and are induced by a succession of transitions between states for which the locked-in vortex lattice is commensurate with the layered structure. Therefore, they consist an extremely useful tool for studying pinning of Josephson vortices in the so-called quasi-two dimensional regime.

In general, the lock-in oscillations are only weakly affected by variations in the oxygen stoichiometry in the region near optimal doping. The main effect has been found to be a small increase in their periodicity with oxygen deficiency. On the other hand, variations in temperature have disclosed a richer variety of phenomena. At low and elevated temperatures the commensurability oscillations are either very weak or absent. This has been attributed to the formation of a kinked vortex structure, due to the influence of either pinning (low temperatures) or thermal fluctuations (high temperatures) that results in the destruction of the perfectly aligned vortex state. However, the commensurability oscillations are prominent at intermediate temperatures, where the ideal lock-in state is better preserved. In this temperature range, our experiments have further revealed that the critical current density exhibits a remarkable non-monotonous temperature dependence. This finding confirms recent theoretical reports, which conjectured the possibility of an enhancement in the pinning of Josephson vortices with temperature, as a consequence of the increasing suppression of the order parameter in the Josephson cores.

Finally, the lock-in oscillations have been used to extract the anisotropy parameters of this compound. We have found that the anisotropy is only slightly affected by changes in the oxygen concentration in the region near optimal doping. In addition, we have compared the anisotropy estimations from the commensurability oscillations with the ones obtained using another technique, namely equilibrium torque magnetometry, on the same samples. A small deviation between these two methods has been obtained, supporting the notion of a temperature dependent anisotropy as anticipated in various theoretical works.